

Southern Methodist University

SMU Scholar

Chemistry Theses and Dissertations


Chemistry

Fall 12-21-2019

Hypervalent Iodine Compounds with Carboxylate and Tetrazolate Ligands

Avichal Vaish
avaish@smu.edu

Follow this and additional works at: https://scholar.smu.edu/hum_sci_chemistry_etds

 Part of the [Analytical Chemistry Commons](#), [Inorganic Chemistry Commons](#), [Materials Chemistry Commons](#), [Organic Chemistry Commons](#), and the [Polymer Chemistry Commons](#)

Recommended Citation

Vaish, Avichal, "Hypervalent Iodine Compounds with Carboxylate and Tetrazolate Ligands" (2019). *Chemistry Theses and Dissertations*. 15.
https://scholar.smu.edu/hum_sci_chemistry_etds/15

This Dissertation is brought to you for free and open access by the Chemistry at SMU Scholar. It has been accepted for inclusion in Chemistry Theses and Dissertations by an authorized administrator of SMU Scholar. For more information, please visit <http://digitalrepository.smu.edu>.

HYPervalent IODINE COMPOUNDS WITH CARBOXYLATE
AND TETRAZOLATE LIGANDS

Approved by:

Advisor: Dr. Nicolay V. Tsarevsky
Associate Professor of Chemistry

Dr. Isaac Garcia-Bosch
Assistant Professor of Chemistry

Dr. David Y. Son
Professor of Chemistry

Dr. Brian D. Zoltowski
Associate Professor of Chemistry

Dr. Mihaela C. Stefan
Professor of Chemistry (UT Dallas)

HYPervalent IODINE COMPOUNDS WITH CARBOXYLATE
AND TETRAZOLATE LIGANDS

A Dissertation Presented to the Graduate Faculty of

Dedman College

Southern Methodist University

in

Partial Fulfillment of the Requirements

for the degree of

Doctor of Philosophy

with a

Major in Chemistry

by

Avichal Vaish

B.S. – M.S., Chemical Sciences, Indian Institute of Science Education and Research, Kolkata

December 21st, 2019

Copyright © 2019

Avichal Vaish

All Rights Reserved

ACKNOWLEDGEMENTS

The experience of graduate school provided me with the widest range of personal and professional experience. Although, this journey was full of ups and downs, it taught me valuable lessons and certainly prepared me for the life to come. I could not have achieved my goals without the support of several people, and I would now like to thank them and recognize their support with utmost sincerity.

First of all, I would like to express my deepest appreciation to my research advisor, Dr. Nicolay V. Tsarevsky, for giving me an opportunity to pursue a Ph.D. degree under his guidance. I have always been encouraged and supported by him to explore new techniques and ideas. He has been essential in my growth as a scientist by allowing me to express my creativity and giving me the freedom to solve the challenges that I encountered in my research in my own way. I am grateful that he encouraged me to work outside my comfort zone which made me a better and confident chemist.

I am extremely grateful to Dr. Priyadarsi De, my master's thesis advisor, who introduced me to polymer chemistry and gave me an opportunity to join his lab early in my career which paved a path for me to pursue Ph. D. in chemistry.

I would like to thank all my fellow present and past group members, specially Rajesh and Yakun, for frequent discussion related to my research. I would also like to thank National Science

Foundation and Department of Chemistry (SMU) for financial support to conduct my research. SMU's Department of Chemistry provided excellent study and research atmosphere. I am extremely grateful to Dr. Michael Lattman for guiding me through the course work. Particularly, I would like to give my sincere thanks to my committee members, Dr. Mihaela C. Stefan (UT Dallas), Dr. David Son, Dr. Isaac Garcia-Bosch, and Dr. Brian D. Zoltowski for their precious time and assistance in reviewing, criticizing, and improving my work. There were several occasions where the required instrument for my research was not available at SMU. Therefore, I reached out to the neighboring universities to find an instrument. I would like to thank Dr. Danieli Rodrigues and Mr. Danyal Siddiqui from University of Texas at Dallas for providing help with the rheological measurements. I am also grateful to Mr. Meciej Kukula and Dr. Eric Weaver from University of Texas at Arlington for trusting me with the LCMS-IT-ToF and MALDI-ToF instrument, respectively.

I am grateful to Dr. Alan Humason for clarifying all my doubts and helping me with instruments. I am grateful to Dr. Isaac Garcia Bosch for allowing me to use his cyclic voltammeter and glove box. Thanks to Khashayar and Rachel for teaching me to operate the cyclic voltammeter and glove box. I would also like to thank Dr. Alexander Lippert for allowing me to use his ESI-MS instrument and thanks to Luke for running the samples for me. I am thankful to Dr. Tomče Runčevski, John, and Christina for helping me with the TGA, DSC, and powder XRD measurements.

Finally, and most importantly, I would like to thank my family and friends, especially my parents Vijai Kumar Vaish & Sarla Vaish, my brother Aviral Vaish, my sister Virla Vaish, and my brother-in-law Akhil Mudgal for providing their unwavering support and unceasing love they have given me while I have pursued my education for which I will always be in debt to them. A special

thanks to Sumanjani Vinnakota for helping me throughout my career and always motivating and steering me in the correct direction. I am grateful to my friends Stephen Budy, Caleb Bunton, Weiwei An, Jian Cao, Ashutosh Pudasaini, Sandra Plunkett Pudasaini, Bibek Ranjan Samanta, Chiranjit Mitra, Saswata Roy, Harsh Vardhan Gaur, Krupal Desai, and Nikhil Katiyar for their unconditional support.

Reproduced by permission of the John Wiley & Sons, Inc. (Hypervalent Iodine Compounds in Polymer Science and Technology. In Main Group Strategies towards Functional Hybrid Materials eds T. Baumgartner and F. Jäkle, [10.1002/9781119235941.ch19](https://doi.org/10.1002/9781119235941.ch19)), the Royal Society of Chemistry (Polym. Chem., 2019, 10, 3943-3950, [10.1039/C9PY00664H](https://doi.org/10.1039/C9PY00664H)), the American Chemical Society (J. Org. Chem., 2018, 83, 12496-12506, [10.1021/acs.joc.8b01715](https://doi.org/10.1021/acs.joc.8b01715)), and the Elsevier Publishing Company (Tetrahedron Lett., 2019, 60, 150995, [10.1016/j.tetlet.2019.150995](https://doi.org/10.1016/j.tetlet.2019.150995)).

Avichal Vaish

B.S.-M.S. Dual Degree, Chemical Sciences, Indian Institute of Science

Education and Research, Kolkata

Hypervalent Iodine Compounds with Carboxylate and Tetrazolate Ligands

Adviser: Professor Nicolay V. Tsarevsky

Doctor of Philosophy conferred December 21, 2019

Dissertation completed October 29, 2019

In modern organic chemistry, hypervalent (HV) iodine(III) compounds are frequently used as oxidizing agents but application of λ^3 -iodanes in polymer and material chemistry is still underexplored. This dissertation describes the preparation of dynamic and self-healing materials by employing ligand exchange reactions involving HV iodine(III) compounds of the type ArIL_2 (Ar = Aryl, L = ligand, e.g., carboxylate or (pseudo)halide). These compounds can undergo ligand exchange reactions in presence of nucleophiles (Nu^-) to form ArINu_2 . Diacetoxyiodo benzene was successfully employed as a crosslinker to prepare dynamic and self-healing gels derived from carboxylate-containing polymers. Furthermore, advantage was taken of the ability of diacetoxyiodo benzene to generate radicals upon UV light irradiation in order to convert the dynamic crosslinked structures to permanent (set) networks. Star polymers were prepared by mixing block copolymers Sty/MMA and AA with diacetoxyiodo benzene solution. The star polymers were characterized by dynamic light scattering and diffusion ordered NMR spectroscopy. Besides that, oligomeric and μ -oxo- HV iodine(III) compounds with two I-N bonds, containing 5-substituted tetrazoles as the ligands $\text{PhI}(\text{N}_4\text{CR})_2$ (R = C_6H_5 , and 4- $\text{CH}_3\text{C}_6\text{H}_4$) were synthesized using PhIO. The crystal structure of one representative compound (an oligomer with

three I atoms in the backbone and 5-phenyltetrazole end groups) was solved and refined from synchrotron powder X-ray diffraction. The novel compounds were characterized by cyclic voltammetry and were found to be strong oxidants. An attempt was made to prepare tetrazole based polymer networks. After synthesizing tetrazole containing oligomeric HV iodine(III) compounds, *N*-heterocycle-stabilized pseudocyclic λ^3 -iodane with tetrazole as the stabilizing group was synthesized and its thermal stability and redox activity were studied. The oxidative power of the polyvalent iodine compound with a tetrazole ligand was demonstrated by conducting oxidation of thioanisole to sulfoxide and dimerization of thiobenzamide to 3,5-diphenyl-1,2,4-thiadiazole.

TABLE OF CONTENTS

LIST OF FIGURES	XIII
LIST OF SCHEMES.....	XVIII
LIST OF TABLES	XXI
LIST OF ABBREVIATIONS	XXII
CHAPTER I INTRODUCTION	1
I.1 Introduction to Polymer Chemistry	1
I.1.1 Introduction and Historical Development	1
I.1.2 Definitions	3
I.1.3 Controlled/"Living" Radical Polymerization	8
I.2 Introduction to Hypervalent Iodine Chemistry	15
I.2.1 History	15
I.2.2 Bonding in Hypervalent Iodine Compounds	18
I.2.3 Nomenclature and Structure of HV Iodine Compounds	19
I.2.4 Reactivity of HV Iodine Compounds Relevant to Applications in Polymer Science....	20
I.2.5 Applications of HV Iodine Compounds in Polymer Science	22
I.3 Self-Healing Polymers.....	41
I.4 Characterization Techniques.....	45
I.4.1 Size Exclusion Chromatography (SEC) or Gel Permeation Chromatography (GPC)...	45

I.4.2 Rheology	47
I.4.3 Diffusion Ordered NMR Spectroscopy (DOSY NMR)	50
I.5 References.....	51
CHAPTER II HYPERVALENT IODINE BASED DYNAMIC NETWORK AND STAR POLYMERS.....	55
II.1 Introduction.....	55
II.2 Results and Discussion	57
II.2.1 HV Iodine Based Network Polymers	57
II.2.2 HV Iodine-Based Star Polymers	71
II.3 Experimental Section	79
II.3.1 Materials.....	79
II.3.2 Analyses and characterization methods.....	80
II.3.3 Synthetic procedures.....	81
II.4 Conclusions.....	87
II.5 Acknowledgements	88
II.6 References	88
CHAPTER III SYNTHESIS, CHARACTERIZATION AND REACTIVITY OF OLIGOMERIC HYPERVALENT IODINE(III) COMPOUNDS WITH TETRAZOLE LIGANDS.....	93
III.1. Introduction	93

III.2. Results and Discussion.....	97
III.2.1. Tetrazole Containing Oligomeric HV Iodine(III) Compounds.....	97
III.2.2. Preparation of Network Polymers Using Tetrazole Containing HV Iodine(III) Compounds.....	112
III.3. Experimental Section.....	117
III.3.1. Materials.....	117
III.3.2. Analytical Procedures.....	118
III.3.3. Synthetic Procedures.....	122
III.4. Conclusions.....	127
III.5. Acknowledgments.....	127
III.6. References.....	127
III.7. Appendix.....	133
III.7.1. Crystallographic Data.....	133
III.7.2. NMR Spectra.....	135
CHAPTER IV N-HETEROCYCLE (TETRAZOLE)-STABILIZED PSEUDOCYCLIC Λ^3-IODANE: SYNTHESIS, STRUCTURE, AND REACTIVITY.....	139
IV.1. Introduction.....	139
IV.2. Results and Discussion.....	141
IV.3. Experimental Section.....	150
IV.3.1. Materials.....	150

IV.3.2. Analytical Procedures.....	151
IV.4. Synthetic Procedures	152
IV.4.1. Synthesis of 2-iodophenyl tetrazole (13).....	152
IV.4.2. Synthesis of (2-(1H-tetrazol-5-yl)phenyl)(hydroxy)iodonium tosylate (12).....	153
IV.4.3. Oxidation of thioanisole	154
IV.4.4. Oxidative dimerization of thiobenzamide	154
IV.4.5. Synthesis of compound 16.....	155
IV.4.6. Synthesis of compound 18.....	156
IV.5. Conclusions	156
IV.6. Acknowledgements.....	157
IV.7. References	157
IV.8. Appendix	160
IV.8.1. HRMS Spectra	160
IV.8.2. NMR Spectra	161
IV.8.3. Crystallographic Data.....	167

LIST OF FIGURES

Figure I-1 Representation of a homopolymer and various types of copolymers. A and B represent two different monomers.	4
Figure I-2 Schematic representation of polymer architectures: (a) linear, (b) branched and (c) network polymers.....	5
Figure I-3 Distribution of molecular weights in a typical polymer sample.	7
Figure I-4 General structure of CTAs used in RAFT polymerization.	13
Figure I-5. Bernard Courtois - chemist who discovered Iodine in 1811.....	15
Figure I-6. Formation of a linear fragment L^i-X-L^{ii} via 3c-4e HV bonds between a central atom X and ligands $L^i\bullet$ and $L^{ii}\bullet$, and energy diagram of the formed molecular orbitals.	19
Figure I-7. Most common classes of HV iodine compounds.	20
Figure I-8. Structures diaryliodonium salts used as photoinitiators of the polymerization of various monomers (shown at the bottom).	23
Figure I-9. Structures of symmetric and asymmetric diaryliodonium hexafluorophosphates used as photoinitiators.	27
Figure I-10. Diaryliodonium butyltriphenylborate photoinitiators.....	28
Figure I-11 Categories of supramolecular chemistries utilized in self-healing functional materials.	42
Figure I-12 Dynamic reactions used to prepare self-healing materials.	43
Figure I-13 A) Associative exchange and B) dissociative exchange of dynamic covalent bonds.	44
Figure I-14 Process of SEC. (A) Schematic picture of a bead with an electron microscopic enlargement. (B) Schematic drawing of sample molecules diffusing into bead pores. (C) the	

smallest molecule (yellow) is more delayed than the largest molecule (red); the largest molecule is eluted first from the column. V_o is void volume, V_e is elution volume, and V_t is total liquid volume (Adapted from GE-Healthcare (2010b)).....46

Figure I-15 Example of the Two-Plate Model, specifically Cone Plate (d is the truncation gap, R is the radius, and α is the cone angle).47

Figure I-16 Shear stress (on left) and shear strain (on right) using the Two-Plate Model with shear area A , shear force F , deflection path S , and shear gap h48

Figure I-17 Vector diagram illustrating the relation between complex shear modulus (G^*), storage modulus (G'), and loss modulus (G'') using the phase shift angle δ49

Figure II-1 Kinetics of RAFT copolymerization of Sty and tBA (a); evolution of $M_{n,app}$ and M_w/M_n with monomer conversion (b).....58

Figure II-2 Evolution of SEC traces of the polymers obtained using feed molar ratios of Sty and tBA equal to 1:3 (a), 1:1 (b), and 3:1 (c). The reaction times and monomer conversions are shown at each curve.59

Figure II-3 1H NMR spectra of poly(Sty-co-tBA) (bottom) and poly(Sty-co-AA) (top) in acetone- d_6 and DMSO- d_6 , respectively. The peaks marked with asterisks belong to residual solvents.60

Figure II-4 Dynamic gel 15 min after mixing copolymer Sty₁AA_{0.9} (300 μ L, 0.73 M with respect to carboxylate groups) and PhI(O₂CCH₃)₂ (200 μ L, 0.15 M) solutions (a), gel immediately after addition of DMAc and CH₃CO₂H (600 μ L, 5:1 (v/v)) (b), and degraded gel 12 h after the addition of CH₃CO₂H (c). The precipitate on the bottom of the tube consists of Co Blue.62

Figure II-5 Gels with (diacyloxyiodo)benzene-type groups at the crosslinks treated with NaN₃ solution (a, b) or Bu₃P (c, d). The first picture in each case shows the gel right after the addition of the reagent, and the second picture shows the degraded gel after the specified time.63

Figure II-6 Gels prepared by mixing solutions of Sty₁AA_{0.7} (400 μ L, 0.73 M with respect to carboxylate groups) and PhI(O₂CCH₃)₂ (100 μ L, 0.15 M) in DMAc with trace amount of indigo carmine present in one of the gels (a); the gels cut into two pieces (b); reattached semicircular segments taken from the two pieces of gels after 30 min (c); and effect of stretching on the self-healed gel (d).64

Figure II-7 G' and G'' values of a gel prepared by using Sty₁AA_{0.7} and PhI(O₂CCH₃)₂ in DMAc (a) on strain amplitude sweep; (b) on angular frequency sweep; (c) in time-dependent strain sweep measurement, in which, strain was gradually increased from 0.1% to 1300% and then back to 1% strain for 300 s; (d) in continuous step strain measurement, gel was subjected to 1300% strain for 30 s, then go back to 1% strain in the linear regime for 120 s, and 3 cycles were carried out.....66

Figure II-8 a) Gel 15 mins after mixing of Sty ₁ AA _{0.9} (300 μL, 0.73 M with respect to carboxylate groups) and PhI(O ₂ CCH ₃) ₂ (200 μL, 0.15 M) solutions in DMAc. b) Gel after 30 mins of UV curing and addition of CH ₃ CO ₂ H in DMAc (600 μL, 1:5 (v/v)). c) Washed gel 24 h after the addition of CH ₃ CO ₂ H and DMAc, and d) the same swollen gel after 1 week.....	68
Figure II-9 Set gel prepared by microwave heating of dynamic gel just after the addition of CH ₃ CO ₂ H (a) and 72 h later (b).....	69
Figure II-10 Continuous step-strain measurement of the UV cured gel, in which, gel was subjected to 1300% strain for 30 s, then go back to 1% strain in the linear regime for 120 s, and 3 cycles were done.....	71
Figure II-11 Schematic representation of star polymers prepared by mixing solutions of block copolymers and PhI(O ₂ CCH ₃) ₂	72
Figure II-12 Kinetics of homopolymerization of Sty and MMA.	74
Figure II-13 Evolution of GPC traces during the synthesis of block copolymers.....	75
Figure II-14 DLS measurement of star polymers.....	76
Figure II-15 . DOSY spectra of Sty ₂₀₀ AA ₁₀₀ . Δ = 0.2 s; δ = 2 ms; g was varied from 27 mT/m to 0.27 T/m.	77
Figure II-16 DOSY spectra of star polymer prepared by using Sty ₂₀₀ AA ₁₀₀ . Δ = 0.2 s; δ = 3 ms; g was varied from 27 mT/m to 0.27 T/m,	77
Figure II-17 DOSY spectra of MMA ₂₈₀ AA ₁₀₀ . Δ = 0.2 s; δ = 2 ms; g was varied from 27 mT/m to 0.27 T/m.	78
Figure II-18 DOSY spectra of star polymer prepared by using MMA ₂₈₀ AA ₁₀₀ . Δ = 0.2 s; δ = 3 ms; g was varied from 27 mT/m to 0.27 T/m,	78
Figure III-1 ¹ H NMR spectra of mixture of compound 3c (20 mM) and (n-Bu) ₄ NPF ₆ (400 mM) on regular interval.	98
Figure III-2 Cyclic voltammogram of ferrocene (1 mM) in anhydrous DMF containing 0.1 M (n-Bu) ₄ NPF ₆ (vs. AgNO ₃ /Ag) at different scan rates using glassy carbon electrode.....	99
Figure III-3 Cyclic voltammogram of PhI(O ₂ CCH ₃) ₂ (1 mM) in anhydrous DMF containing 0.1 M (n-Bu) ₄ NPF ₆ (vs. AgNO ₃ /Ag) at different scan rates using glassy carbon electrode.....	100

Figure III-4 Cyclic voltammogram of $\text{PhI}(\text{N}_4\text{CC}_6\text{H}_5)_2$ (1 mM, on left) and $\text{PhI}(\text{N}_4\text{C}(4\text{-CH}_3\text{C}_6\text{H}_4))_2$ (1 mM, on right) in anhydrous DMF containing 0.1 M $(\text{n-Bu})_4\text{NPF}_6$ (vs. AgNO_3/Ag) at different scan rates using glassy carbon electrode.	101
Figure III-5 Voltammogram for $\text{PhI}(\text{N}_4\text{CCH}_3)_2$ (vs. AgNO_3/Ag) in anhydrous DMF (1mM) + 0.1 M $(\text{n-Bu})_4\text{NPF}_6$, glassy carbon electrode at different scan rates.	102
Figure III-6 DOSY NMR spectrum of PhI in CD_3OD	104
Figure III-7 DOSY NMR spectrum of 1c in CD_3OD	105
Figure III-8 DOSY NMR spectrum of 3c in CD_3OD	106
Figure III-9 DOSY NMR spectrum of 2c in CD_3OD	106
Figure III-10 ^1H NMR spectra of compound 1c (80 mM) in DMSO-d_6 after adding 4 eq, 12 eq, and 36 eq of CH_3OH	107
Figure III-11 a) One molecule of 2b featuring three HV iodine (III) atoms, linked by bridging oxygen atoms and terminal nitrogen (N_2) atoms of the 5-phenyltetrazole units in a zigzag motif. b) Intermolecular I---N interactions between two neighbouring molecules in the crystal packing of 2b	109
Figure III-12 Molecular weight evolution with time (on top) and kinetics of polymerization of Sty and AN (bottom).	113
Figure III-13 FT-IR spectra of SAN and SVT.	115
Figure III-14 Rietveld refinement plot of 2b . Measured scattered intensity is presented with blue dots; the best fit with red line and the corresponding difference plot with gray line. The Bragg reflections are given with blue bars.	121
Figure III-15 Thermal ellipsoid plot for compound 2b	122
Figure IV-1 O- and N-stabilized pseudocyclic λ^3 -iodanes.	140
Figure IV-2 Simultaneous TGA and DSC analysis of compounds 10 (solid lines) and 11 (dashed lines).	142
Figure IV-3 Cyclic voltammograms of 1 mM solutions of compound 10 , 11 , and TsOH in anhydrous DMSO containing 0.1 M $(\text{n-Bu})_4\text{NPF}_6$ at scan rate of 0.02 V/s using a glassy carbon electrode.	143

Figure IV-4 ORTEP drawing of the X-ray crystal structure of compound 14 at 50% ellipsoid probabilities.	147
Figure IV-5 ORTEP drawing of the X-ray crystal structure of compound 15 at 50% ellipsoid probabilities.	148
Figure IV-6 Secondary interactions found in the crystal structure of 15 (at the 50% probability level).....	149

LIST OF SCHEMES

Scheme I-1 General reaction mechanism of conventional radical polymerization.....	9
Scheme I-2 General mechanisms for controlled radical polymerization technique. k_{act} , k_{deact} , k_p , k_t , and k_{tr} represents rate constant of activation, deactivation, propagation, termination, and transfer, respectively.	10
Scheme I-3 Mechanism of RAFT polymerization.	14
Scheme I-4. Early examples of preparation of polyvalent iodine(III) and iodine(V) compounds.	17
Scheme I-5. Bond homolysis and ligand-exchange reactions with HV iodine(III) compounds with applications in the synthesis of polymeric materials.	21
Scheme I-6. Photochemistry of diaryliodonium salts.....	24
Scheme I-7. Mechanism of photopolymerization of 1,2-cyclohexane oxide initiated by diaryliodonium salts.	26
Scheme I-8. Direct versus sensitized photolysis of diaryliodonium salts.	29
Scheme I-9. Photodecomposition of (diacetoxy)iodo benzene.....	30
Scheme I-10. Iniferter capability of (diacetoxy)iodo benzene under UV light.	31
Scheme I-11. Proposed mechanism for the formation of linear and branched polymers in radical copolymerizations initiated by HV iodine(III) compound, in which the same compounds served also as chain transfer agents.	32
Scheme I-12. Polymerization of vinyl monomers initiated by the iodossylbenzene-pseudohalide system and formation of pseudohalide-capped polymers	34
Scheme I-13. Exchange of acetoxy groups in (diacetoxy)iodo arenes with polymerizable carboxylic acid and its radical decomposition in presence of light or heat.....	35

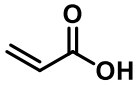
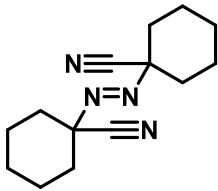
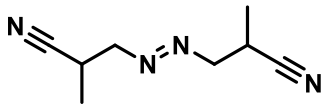
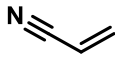
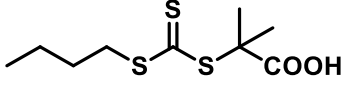
Scheme I-14. Branching via incorporation into the polymer chain of a hypervalent iodine-containing mono- or difunctional monomer. The I–O bonds in the inimers formed in situ can serve as initiating sites. R [•] represents any low molecular weight or macro-radical able to propagate..	36
Scheme I-15. Ligand-exchange of the acetoxy groups in (diacetoxyiodo)benzene with azide anions to form HV iodine-based precursors of azide (and methyl) radicals. Formation of highly branched multiazidated polymers via one-pot procedures and their functionalization with alkenes (for instance, the fluorescent pyrenyl 4-pentyonate) under “click” chemistry conditions.....	37
Scheme I-16. Synthesis of branched polymers with HV iodine(III) groups at the branching points. Degradation mechanisms of branched polymers with HV iodine(III)-based crosslinks in the presence of reducing agents or carboxylic acids.	38
Scheme I-17. Direct azidation of polystyrene using ligand-exchange reaction between (diacetoxy)iodobenzene and trimethylsilyl azide and preparation of graft copolymers using click reaction between the multiazidated product and poly(ethylene oxide) monomethyl ether 4-pentynoate. ...	40
Scheme II-1 Synthesis of carboxylate group-containing copolymers by copolymerization of Sty and tBA under RAFT polymerization conditions, followed by deprotection of the tert-butyl ester groups in the presence of CF ₃ CO ₂ H.	58
Scheme II-2 Preparation of dynamic gels via carboxylate ligand-exchange reactions with PhI(O ₂ CCH ₃) ₂ , curing of the gels using light or heat, and conversion of the dynamic to permanent network following the coupling of some of the radicals formed during the curing step.	61
Scheme II-3 Synthesis of block copolymers Sty ₂₀₀ AA ₁₀₀ and MMA ₂₈₀ AA ₁₀₀	73
Scheme III-1 Synthesis of PhI(N ₄ CR) ₂ using PhIL ₂ and RCN ₄ H (or RCN ₄ K ⁺) at room temperature in different solvents.....	97
Scheme III-2 Reaction of RCN ₄ H (R = C ₆ H ₅ , 4-CH ₃ C ₆ H ₅) with PhIO.....	102
Scheme III-3 ARGET ATRP of Sty and AN.	113
Scheme III-4 Conversion of SAN to SVT.....	114
Scheme III-5 Preparation of polymer network using SVT.....	115
Scheme III-6 Deprotonation of SVT.....	116
Scheme III-7 Preparation of network polymers using SVT ⁻ K ⁺	116
Scheme IV-1 Synthesis of (2-(1H-tetrazol-5-yl)phenyl)(hydroxy)iodonium tosylate 10	141

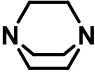
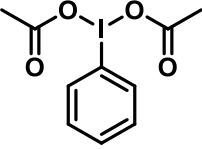
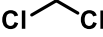
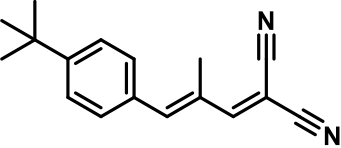
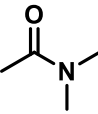
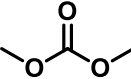
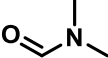
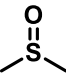
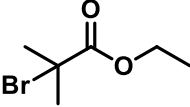
Scheme IV-2 Proposed pathway of electrochemical reduction of 11	144
Scheme IV-3 (i) Oxidation of thioanisole, (ii) oxidative rearrangement of thiobenzamide in the presence of λ^3 -iodane 10	145
Scheme IV-4 Tautomerism in compound 11	146
Scheme IV-5 Synthesis of compound 14	146
Scheme IV-6 Synthesis of compound 15	148

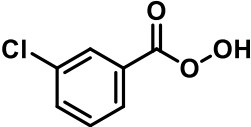
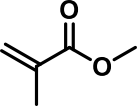
LIST OF TABLES

Table II-1 Diffusion coefficients of block and star polymers.	79
Table III-1 Redox potential of ferrocene at different scan rates	99
Table III-2 Reduction potential of various HV iodine(III) compounds (1 mM) in anhydrous DMF containing 0.1 M (n-Bu) ₄ NPF ₆ (vs. AgNO ₃ /Ag) at different scan rates using glassy carbon electrode.	100
Table III-3 Diffusion coefficients of PhI and various tetrazole containing HV iodine(III) compounds.....	104
Table III-4 Iodotetrazolylolation reaction of cyclohexene.....	111

LIST OF ABBREVIATIONS

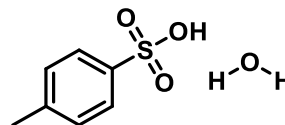
A	Shear Area	
AA	Acrylic Acid	
ACHN	1,1'-Azobis(cyclohexanecarbonitrile)	
AIBN	Azobisisobutyronitrile	
AN	Acrylonitrile	
ARGET	Activators Regenerated by Electron Transfer	
ATRP	Atom Transfer Radical Polymerization	
BMP	(2-(((butylthio)carbonothioyl)thio)-2-methylpropanoic acid	
CRP	Controlled Radical Polymerization	
CTA	Chain Transfer Agent	
CV	Cyclic Voltammetry	
D	Diffusion Coefficient	

DABCO	1,4-Diazabicyclo[2.2.2]octane	
DAIB	(Diacetoxyiodo)benzene	
DCM	Dichloromethane	
DCTB	trans-2-[3-(4-tert-Butylphenyl)-2-methyl-2-propenylidene]malononitrile	
DLS	Dynamic Light Scattering	
DMAc	Dimethylacetamide	
DMC	Dimethyl Carbonate	
DMF	Dimethylformamide	
DMSO	Dimethyl sulfoxide	
DOSY	Diffusion Ordered Spectroscopy	
DP	Degree of Polymerization	
DSC	Differential Scanning Calorimetry	
EBiB	Ethyl α -bromoisobutyrate	
F	Shear Force	
FT-IR	Fourier Transfer Infrared Spectroscopy	

g	Gradient Strength	
G	Shear Modulus	
G*	Complex Shear Modulus	
G'	Storage Modulus	
G''	Loss Modulus	
GC-MS	Gas Chromatography Mass Spectrometer	
GPC	Gel Permeation Chromatography	
h	Shear Gap	
HV	Hypervalent	
k	Boltzmann Constant	
MALDI-ToF	Matrix Assisted Laser Desorption/Ionization – Time of Flight	
mCPBA	meta-Chloroperoxybenzoic acid	
MMA	Methyl Methacrylate	
M _n	Number Average Molecular Weight	
M _w	Weight Average Molecular Weight	
MWD	Molecular Weight Distribution	
NMR	Nuclear Magnetic Resonance	
ORTEP	The Oak Ridge Thermal Ellipsoid Plot	
PDI or Đ	Polydispersity Index	

pTsOH.H₂O

p-Toluenesulfonic acid monohydrate



RAFT

Radical Addition-Fragmentation Chain Transfer Polymerization

r_s

Hydrodynamic Radius

S

Deflection Path

SEC

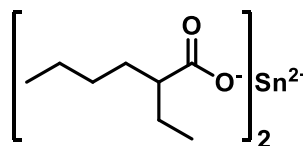
Size Exclusion Chromatography

SFRP

Stable Free Radical Polymerization

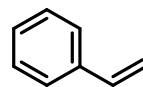
Sn(EH)₂

Tin(II) 2-ethylhexanoate



Sty

Styrene

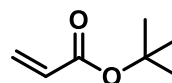


T

Temperature

tBA

Tert-Butyl Acrylate

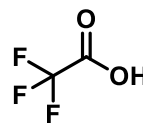


T_d

Onset Degradation Temperature

TFA

Trifluoroacetic Acid



TGA

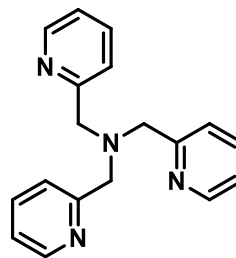
Thermogravimetry Analysis

THF

Tetrahydrofuran



TPMA Tris(2-pyridylmethyl)amine



UV Ultraviolet

XRD X-ray Diffraction

γ Shear Strain

Δ Diffusion Time

δ Length of Gradient

ΔH_d Enthalpy of Degradation

η Viscosity

τ Shear Stress

Dedicated to my beloved parents

CHAPTER I

INTRODUCTION

I.1 Introduction to Polymer Chemistry

I.1.1 Introduction and Historical Development

In this era, polymers are ubiquitous. Plastics, fibers, elastomers, coatings, adhesives, rubber, protein, cellulose – these are all part of the fascinating world of polymer chemistry. Polymers are large molecules made up of simple repeating units. The name is derived from the Greek words *poly* and *mer*, meaning “many” and “part”, respectively. Polymers are also known as *macromolecules* which means “large molecules”. Polymers are synthesized from simple molecules called *monomers* (“single part”) by a process called *polymerization*.

The word “polymer” was first used by the Swedish chemist Berzelius in 1833.¹ In nineteenth century, polymers were used by chemists without any clear understanding of their structure. For example, nitrated cellulose (known as the misnomer of nitrocellulose) was marketed as Celluloid and guncotton. In 1839, polymerization of styrene was reported for the first time,² and during 1860s, the synthesis of poly(ethylene glycol)³ and poly(ethylene succinate)⁴ was published with correct structures. At about the same time, isoprene was isolated as the degradation product of natural rubber, although incorporation of isoprene into the polymer was not understood.⁵

The first truly synthetic and commercial polymer, phenolformaldehyde resin (commercially known as Bakelite), was developed by Belgian born chemist Leo Baekeland in early 1900s.⁶ Other

polymers like alkyd (polyester) paints and polybutadiene rubber were introduced at about the same time. These polymers found their way into a wide spectrum of consumer products. Yet, despite such commercial success, most scientists had no clear concept of polymer structures.

The prevailing theory was that polymers were aggregates of small molecules much like colloids but held together by some mysterious secondary forces. This theory was soon rejected by German scientist Hermann Staudinger, who stated that the intermolecular forces between the molecules having large molecular weights are responsible for the remarkable properties of polymers. Staudinger also introduced the term *mackromolekül*.⁷ In the 1930s, work of an American chemist Wallace Hume Carothers placed the theories of Staudinger on a firm experimental basis which led to the commercial development of neoprene rubber and polyamide (nylon) fibers.⁸ In recognition to his contribution, Staudinger was awarded the Nobel Prize in Chemistry in 1953.

World War II was responsible for significant advancement of polymer chemistry. Amongst the significant developments of the post-war era, one of the most important discoveries was that of a new coordination catalyst for the initiation of polymerization reaction by German scientist Karl Ziegler.⁹ Italian scientist Giulio Natta applied this catalyst to develop polymers with controlled stereochemistry and superior mechanical properties.¹⁰ This work revolutionized the polymer industry and Ziegler and Natta were awarded Nobel Prize in 1963 for their contribution. After that, several commercially useful polymers like engineering plastics, high-strength aromatic fibers, nonflammable polymer, degradable polymer, conducting polymers, and polymers having excellent thermal and oxidative stability were developed, illustrating that polymer chemistry is an exciting field with almost limitless possibilities.

I.1.2 Definitions

As mentioned earlier, the term *polymer* refers to a large molecule – macromolecule – whose structure depends on the monomer or monomers used in the synthesis. If only a few monomer units were joined together to make a low-molecular weight polymer, it is called an *oligomer*, which is originated from Greek work “*oligos*” meaning “few”. The structural unit closed by brackets or parentheses is called *repeating unit* (or *monomeric unit*).

End groups are the structural unit that terminates the polymer chain and are always shown outside the brackets or parentheses.

Polymers formed by alkene addition reactions are called *homochain* polymers because the polymer chain, or *backbone*, as it is commonly known, consists of a single atom type – carbon – with other atoms or group of atoms attached. *Heterochain* polymers such as polyesters or polyamides contain more than one atom type in the backbone.

The *degree of polymerization (DP)* represents total number of repeating units in a polymer chain, including end groups, thus, also representing the molecular weight and chain length of a polymer. Since, the different polymer chains in a polymer sample have varying chain lengths (except certain natural polymers like proteins), the DP of a polymer sample is normally referred to as *average degree of polymerization (\overline{DP})*.

A polymer prepared by polymerizing a single monomer is called *homopolymer*. If two or more monomers are used to synthesize a polymer, the product is called *copolymer*. In copolymers, the monomeric units may be distributed randomly (*random copolymer*), in alternating fashion (*alternating copolymer*), or in blocks (*block copolymer*). A *graft polymer* consists of one polymer

chain branching from the backbone of the other. These various possibilities are shown in Figure I-1.

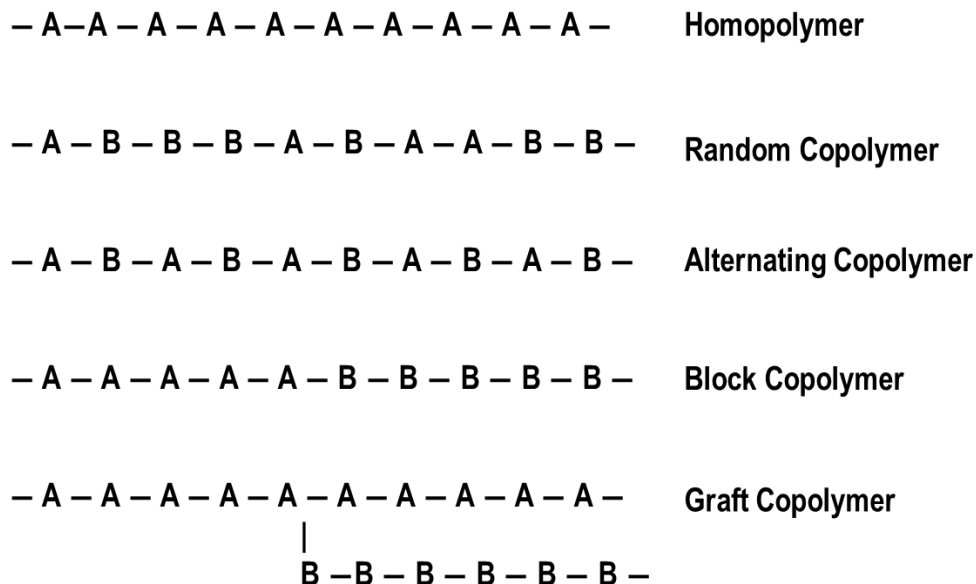


Figure I-1 Representation of a homopolymer and various types of copolymers. A and B represent two different monomers.

Although, there are several different type of polymer architectures, the following three architectures are most common: (a) *linear*, (b) *branched*, and (c) *network* as shown in Figure I-2. While a linear polymer has no branching other than the pendant groups associated with the monomer, branched polymers have branches at irregular intervals along the polymer backbone. All graft copolymers are branched polymers, but not all branched polymers are graft copolymers. For example, low density polyethylene is a common example of branched polymer (but not a graft copolymer) where, chain branching arises as a result of side reaction during the polymerization.

Network polymers are formed by a process called *crosslinking* where, linear or branched polymer chains are joined by a covalent bond. Usually, a small molecule, called *crosslinker*, is

used to connect or crosslink two polymer chains. All the terms defined in this section will be frequently used in this dissertation.

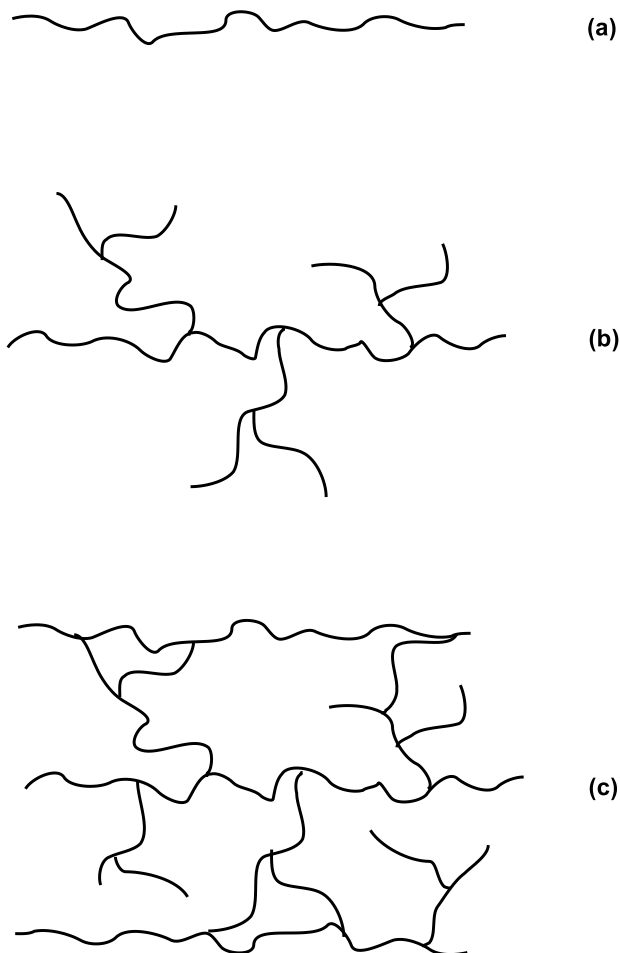


Figure I-2 Schematic representation of polymer architectures: (a) linear, (b) branched and (c) network polymers.

I.1.2.1 Molecular Weight

Molecular weight of a polymer is defined quite differently from the molecular weight of a small-sized molecule. Polymers differ from small-sized molecules in terms of molecular weight,

i.e. they are polydispersed or heterogeneous in nature. Even if a polymer is synthesized free from contaminants and impurities, it is still not a pure substance in the usually accepted sense. Polymers, in their purest form, are a mixture of large molecules with different molecular weights. The reason for the polydispersity of polymers lies in the statistical variation present in the polymerization process. The molecular weight of a polymer involves its average molecular weight. Both the average molecular weight and the exact distribution of different molecular weights within a polymer sample are required to fully characterize the polymer sample. The control of molecular weight and molecular weight distribution (MWD) is often used to obtain and improve certain desired properties in a polymer product.

The *number average molecular weight* (M_n) is determined by experimental methods that counts number of polymer chains in a polymer sample. M_n is defined as the total weight w of all the molecules in a polymer sample divided by the total number of moles present. Thus, the number average molecular weight is

$$M_n = \frac{w}{\sum N_x} = \frac{\sum N_x M_x}{\sum N_x}$$

where the summations are over all the different sizes of polymer molecules from $x = 1$ to $x = \infty$ and N_x is the number of moles whose weight is M_x .

The *weight average molecular weight* (M_w) is obtained by light-scattering measurement and defined as

$$M_w = \sum w_x M_x$$

where w_x is the weight fraction of molecules whose weight is M_x . M_w can also be defined as

$$M_w = \frac{\sum c_x M_x}{\sum c_x} = \frac{\sum c_x M_x}{c} = \frac{\sum N_x M_x^2}{\sum N_x M_x}$$

where c_x is the weight concentration of M_x molecules, c is the total weight concentration of all the polymer molecules, and the following relationships hold:

$$w_x = \frac{c_x}{c}$$

$$c_x = N_x M_x$$

$$c = \sum c_x = \sum N_x M_x$$

For most practical purposes, molecular weight of a polymer is characterized by measuring M_n and M_w . The former is biased towards low-molecular weight fractions, while the latter is biased towards high-molecular weight fractions as shown in Figure I-3.

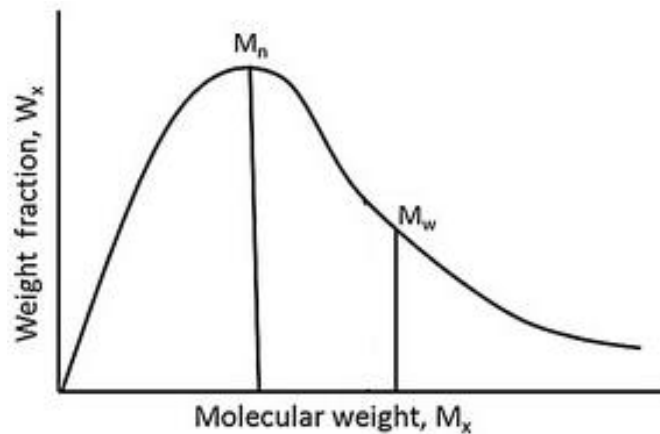


Figure I-3 Distribution of molecular weights in a typical polymer sample.

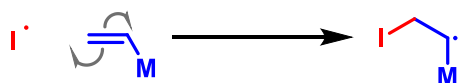
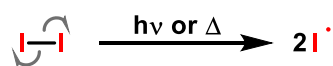
The ratio of two average molecular weights, M_w/M_n , depends on the breadth of the distribution curve and often referred as *polydispersity index* (\mathcal{D}). The value of \mathcal{D} would be 1 for a perfectly monodisperse polymer. The ratio is always greater than 1 for all actual polymers and increases with increasing dispersity.

I.1.3 Controlled/"Living" Radical Polymerization

Chain-termination reactions are part of a conventional radical chain polymerization systems due to the type of propagating centers and/or the reagent present. Bimolecular termination and chain transfer are ever present in the radical chain polymerization and limit the lifetime of a radicals as shown in Scheme I-1. The term *chain transfer* refers to a polymerization reaction by which the activity of a growing polymer chain is transferred to another molecule. Chain polymerization without chain-termination reactions, referred to as *living polymerization*, would be highly desirable because they would allow the synthesis of block copolymers by the sequential addition of different monomers.

Block copolymers have commercial potential for obtaining products that can incorporate the desirable properties of two or more homopolymers. This potential has led to an intense effort to find reaction systems that proceed as living polymerization. Some anionic chain polymerizations proceed as living polymerization under conditions where no viable chain termination reaction occurs, and this has resulted in useful block polymerization. This type of anionic polymerization is very sensitive to impurities and difficult to perform. Therefore, efforts were made to develop a relatively easy technique.

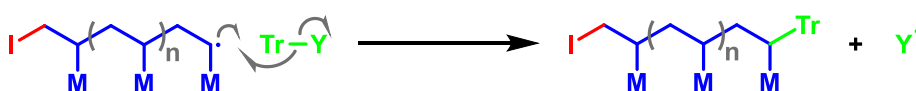
(A) Initiation



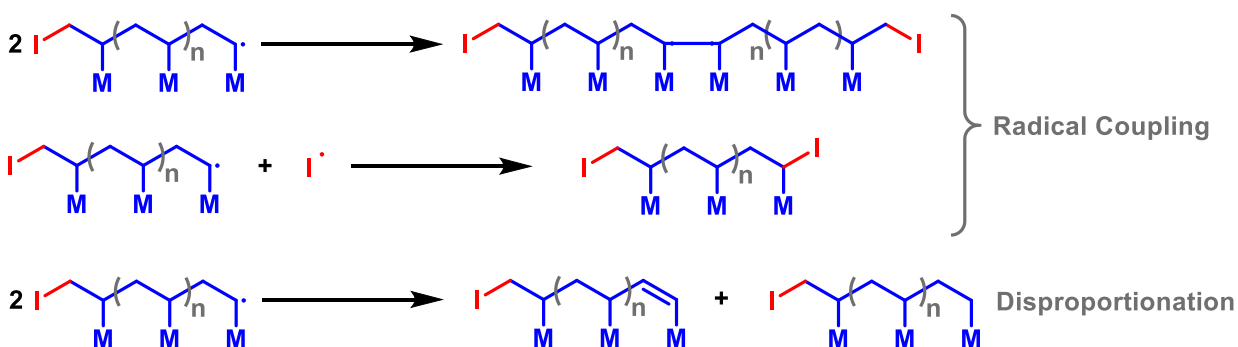
(B) Propagation



(C) Chain Transfer



(D) Termination

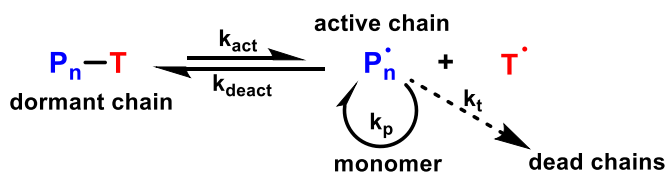


Scheme I-1 General reaction mechanism of conventional radical polymerization.

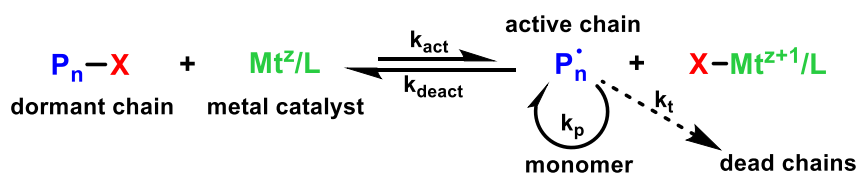
The situation is very different with conventional (nonliving) radical polymerization since the lifetime of propagating radicals in this system is very short because of ever present chain transfer and radical reactions (Scheme I-1). Controlled/Living radical polymerization have been achieved by minimizing the bimolecular radical coupling and prolonging the lifetime of propagating radical. This was attained by introducing dormant state for the propagating radicals through alternate modes of reaction for propagating radicals, specifically, by either *reversible*

termination or reversible transfer. A dynamic equilibrium is established between the dormant (reversibly deactivated or capped) and active (radical) species. Dormancy (deactivation) is favored, lowering the concentration of propagating radicals and thus the rates of irreversible termination and chain transfer. While some termination is unavoidable, this equilibrium allows for a significant increase in chain life (from ~ 1 s in radical polymerization to ≥ 1 h in controlled radical polymerization), making several polymer compositions and topologies, as well as predetermined molecular weights, possible.

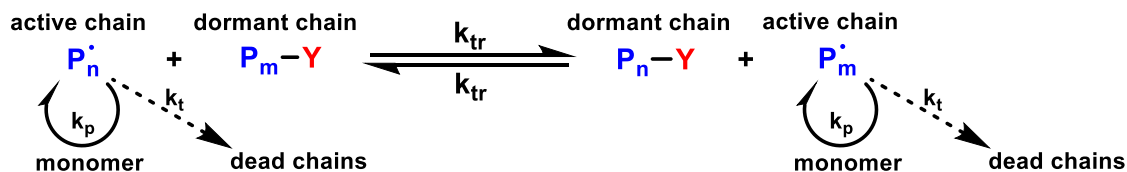
(A) Reversible Deactivation by Coupling



(B) Reversible Deactivation by Atom Transfer



(C) Reversible Deactivation by Degenerative Transfer



Scheme I-2 General mechanisms for controlled radical polymerization technique. k_{act} , k_{deact} , k_p , k_t , and k_{tr} represents rate constant of activation, deactivation, propagation, termination, and transfer, respectively.

Various methods have been described to test the “livingness” of polymerization process. All these tests have limitations. The radical polymerization should satisfy following conditions assessed by Quirk and Lee to be entitled as “living”.

- (a) Living polymerization proceed until all monomer is consumed and may continue growth if further monomer is added.
- (b) In a living polymerization molecular weight (M_n) increases linearly with monomer conversion (MC). This contrasts with observations for conventional radical polymerizations where molecular weights are initially high and decrease with conversion due to monomer depletion. However, molecular weights obtained in radical polymerizations with conventional transfer agents with transfer coefficient >1 will increase with conversion and may meet this test.
- (c) In a living radical polymerization, concentration of active species remains constant. If $[M]_0$ is initial concentration of monomer and $[M]$ is concentration at a time and a kinetic plot of $\ln([M]_0/[M])$ vs time, where $\ln([M]_0/[M]) = -\ln(1 - MC)$, is both linear (first order) and passes through the origin, then it can be deduced that the initiation step is relatively fast and efficient compared to propagation, and there are a constant number of propagating reactive centers. This plot alone, however, does not necessarily prove that the polymerization is free from chain-killing transfer events, which limit the MW that can be obtained.
- (d) Living polymerization provide narrow molecular distribution (MWD). An ideal living polymerization can provide a Poisson MWD and polydispersity in the range of 1.05 – 1.4. low dispersity alone does not imply the absence of side reactions.
- (e) Block copolymers can be prepared by sequential addition of monomers.
- (f) End groups are retained allowing end-functional polymers to be obtained in quantitative yield.

Quirk and Lee concluded, “there is no single criterion which is satisfactory for the determination of whether a given polymerization is living or not.”

A variety of controlled radical polymerization methods have been developed over the years with focus on robustness of conditions and optimizing control via reversibility of termination. The most widely used controlled radical polymerization methods can be categorized by the mechanism of their reversible deactivation: coupling, atom or group transfer, and degenerative transfer. The basic mechanisms of each process are outlined in Scheme I-2.

Reversible deactivation by coupling is the mechanism found in stable free radical polymerizations (SFRPs), which include iniferter, organocobalt, and nitroxide mediated polymerizations (NMP). The most widely known type of CRP involving the reversible transfer of an atom is atom transfer radical polymerization (ATRP). Reversible deactivation by degenerative transfer characterizes a few CRP techniques including reverse iodine transfer, telluride-mediated, organo- bismuthine mediated, and most notably reversible addition-fragmentation chain transfer (RAFT) polymerizations.

All the well-defined materials in the work discussed in subsequent chapters were prepared via RAFT. The following discussion will provide more information about this technique.

I.1.3.1 Reversible Addition-Fragmentation Chain Transfer (RAFT) Polymerization

RAFT is a reversible deactivation radical polymerization process which can possess the attributes of living or controlled radical polymerization with appropriate attention to reagents and reaction conditions. In RAFT, livingness is achieved by adding reagent that provide reversible deactivation by degenerate chain transfer, called chain transfer agent (CTA). The chain transfer

step has been termed degenerate because the process involves only exchange of functionalities and the only distinction between the species on the two sides of the equilibrium is their degree of polymerization (DP). Usually, in RAFT polymerization, dithiocarbamate or trithiocarbonate are used as chain transfer agents with different groups attached at both ends (Z and R) as shown in Figure I-4.



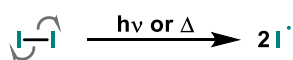
Figure I-4 General structure of CTAs used in RAFT polymerization.

The efficiency and reactivity of CTAs can be changed by altering Z and R groups. The addition and fragmentation rate of CTA can be modulated by modifying Z groups. While, R is a homolytic leaving group and must be able to reinitiate the polymerization. In general, trithiocarbonate have higher transfer rate than dithiocarbamate chain transfer agents.

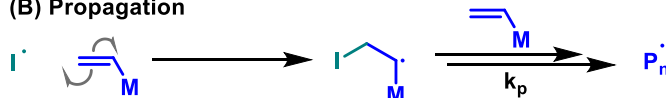
In RAFT, the polymerization reaction is initiated by a free-radical source or an initiator like azobisisobutyronitrile (AIBN) which decomposes to give two fragments (I^{\bullet}). One of the fragments reacts with a single monomer to yield an active radical (P_1^{\bullet}). P_1^{\bullet} further reacts with multiple monomer units to form propagating radical with 'n' monomer units (P_n^{\bullet}). This propagating radical reacts with chain transfer agent to form RAFT adduct radical **1** (Scheme I-3), which undergoes a fragmentation reaction in either direction to form either initial propagating radical (P_n^{\bullet}) or a polymeric chain transfer agent (**2**) and a radical (R^{\bullet}). This R^{\bullet} reinitiate the

polymerization to provide another propagation radical with 'm' number of monomer units (P_m^\bullet). This new propagating participates in main equilibrium with polymeric chain transfer agent **2** to provide polymeric RAFT adduct radical intermediate (**3**). The polymeric RAFT adducts radical **3** again undergoes fragmentation reaction to yield P_n^\bullet and macro CTA (**4**). The polymerization was terminated when propagating radicals couple with each other, R^\bullet or initiator fragment.

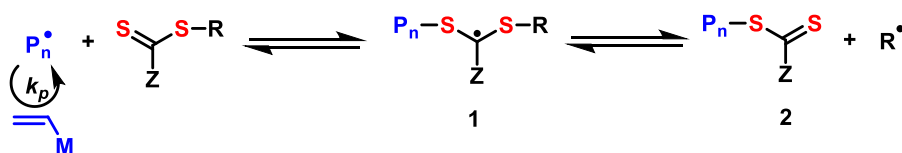
(A) Initiation



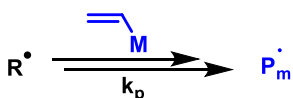
(B) Propagation



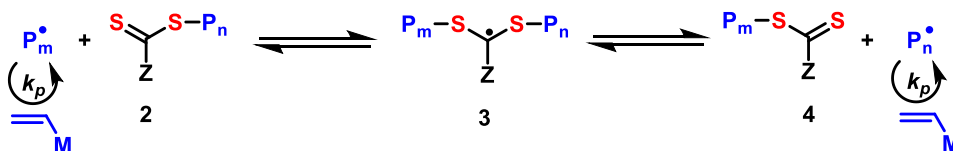
(C) Initialization



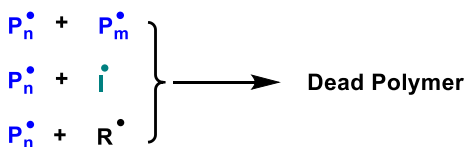
(D) Reinitiation



(E) Main Equilibrium



(F) Termination



Scheme I-3 Mechanism of RAFT polymerization.

I.2 Introduction to Hypervalent Iodine Chemistry

I.2.1 History

The 53rd element in the periodic table, Iodine, was accidentally discovered by a French chemist Bernard Courtois in 1811. Courtois served as a pharmacist in the French army and later joined his father's saltpeter business. In 1811, he added too much concentrated sulfuric acid to the ashes of seaweed (kelp), a major raw material in saltpeter production. The reaction led to evolution of purple vapors, which deposited dark lustrous crystals on the cooler walls of the vessel. The reaction was later understood as oxidation of iodide anions present in the ashes by sulfuric acid.



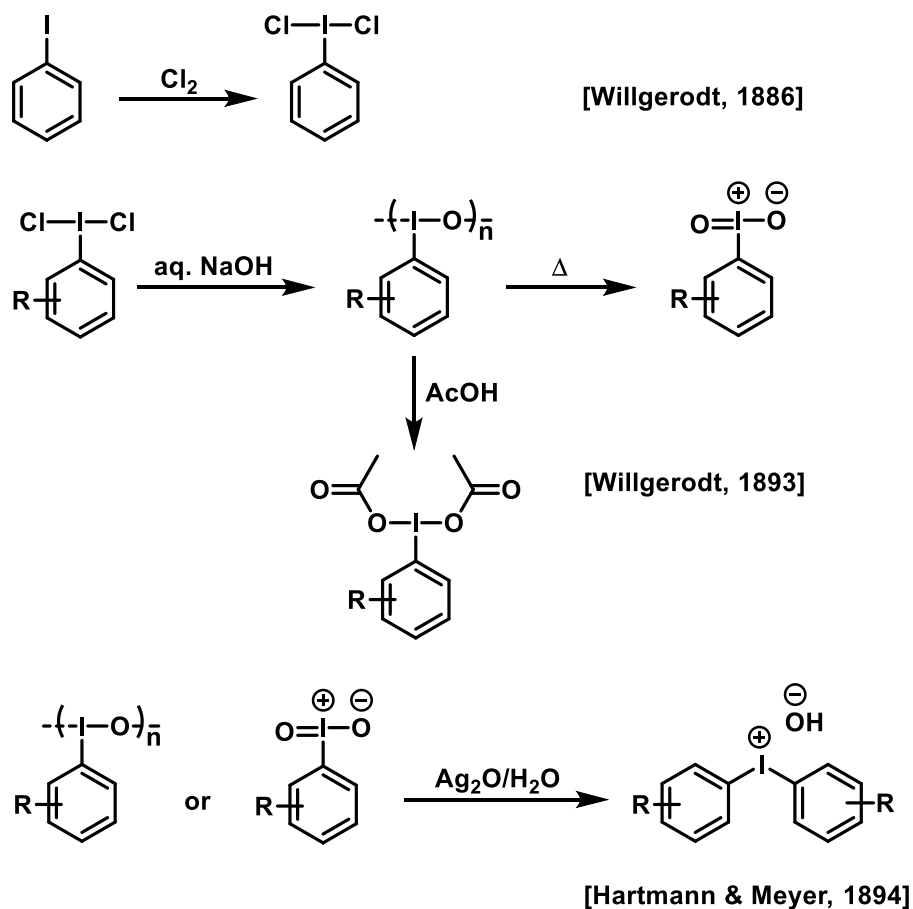
Figure I-5. Bernard Courtois - chemist who discovered Iodine in 1811.

He shared samples of this mysterious compound with his friends and colleagues. Joseph-Louis Gay-Lussac and Humphry Davy were among those who could analyze the samples. Davy was visiting France at the time with his portable laboratory and it was he who noted the similarities

of the substance with fluorine and chlorine. In 1813, Courtois¹¹, Gay-Lussac¹² and Davy¹³ reported discovery and properties of new substance, named *iode* (derived from Greek word $\iota\omicron\delta\eta\zeta$, meaning violet) for the color of its vapors. It was Davy who later suggested the name *iodine*.¹⁴ Immediately after discovery, large number of chemical properties of iodine were discovered, studied, and described within a year, including its reaction with starch, with ammonia and many others. The history of iodine has been summarized in several articles and book chapters.

The first naturally occurring (biogenic) iodine-containing organic compound, iodogorgonic acid (now known to be an amino acid derivative, 3,5-diiodotyrosine) was isolated in 1896 from the marine organism yellow gorgonia (*Eunicella cavolini*).¹⁵ After that, Kendall reported isolation of iodine-containing hormone of the thyroid gland (*S*)-thyroxine for the first time in 1915.¹⁶ The first synthetic organic compound of iodine, ethyl iodide, was reported by Gay-Lussac.¹⁷ It was soon realized that although inorganic iodine(III) and iodine(V) compounds were known (like ICl_3 , I_2O_5 , HIO_3 , and iodates), in its organic compounds, iodine was typically monovalent.

In 1862, first iodine(III) compound with organic groups, iodine(III) acetate, was reported by Schutzenberger.¹⁸ After almost quarter of the century, in 1886, Conard Willgerodt reported first iodine(III) compound with a C-I bond. In his paper, he reported that the reaction of iodobenzene with chlorine afforded a bright yellow crystalline solid characterized as (dichloroiodo)benzene (PhICl_2). After that, several organic polyvalent compounds were synthesized within a very short time, including iododisylarenes (ArIO)^{19, 20}, (diacyloxyiodo)arenes ($\text{ArI}(\text{O}_2\text{CR})_2$)²¹, iodoxyarenes (ArIO_2)²⁰, and diaryliodonium salts (both symmetric ($\text{Ar}_2\text{I}^+ \text{A}^-$) and asymmetric ($\text{Ar}^i\text{I}^+ \text{Ar}^{ii} \text{A}^-$) ones; A^- represents an anion)^{22, 23}. The synthetic methodologies used to prepare the first polyvalent iodine compounds are presented in Scheme I-4.



Scheme I-4. Early examples of preparation of polyvalent iodine(III) and iodine(V) compounds.

By 1914, several reports of synthetic methodology leading to preparation of various polyvalent iodine(III) and iodine(V) compounds, and describing their physical properties and reactivity were published which led to the publication of the first monograph on this subject by Willgerodt.²⁴ Since then, many detailed reviews²⁵⁻³⁸ and books³⁹⁻⁴² have been published which describe synthesis, physicochemical characterization, chemical reactivity, and applications of polyvalent iodine compounds.

I.2.2 Bonding in Hypervalent Iodine Compounds

Before the development of molecular orbital theory, bonding in compounds used to be explained by the octet rule, introduced by Lewis⁴³ and further developed by Langmuir⁴⁴. But, the existence of polyvalent iodine(III), iodine(V), and iodine(VII) seemed to contradict the octet rule. At first, bonding in these type of compound in which the “standard” valence number was exceeded, was conveniently described in terms of “promotion” of one or more p- or even s-electrons (total number of n) to one or more vacant d-orbitals, followed by formation of hybrid sp^3d^n orbitals⁴⁵. However, with the development of new bonding theories and in light of new structural data of polyvalent molecules, the participation of d-orbitals in the bond formation of such species became ambiguous. In 1951, a model was proposed^{46, 47} to account for the bonding in trihalide (e.g., triiodide) and pentaiodide anions, in which it was assumed that only p-orbitals of the halogen atoms participated in the bonding. Essentially, delocalized, multicenter-multielectron, specifically, 3-center-4-electron (3c-4e), bonds were proposed to exist in these species. This model was successfully employed to describe the bonding and the geometry of compounds of the noble gases, such as XeF_2 and XeF_4 ⁴⁸, and many others. By the end of the 1960s, several review articles^{49, 50} summarized the arguments against the involvement of d-orbitals in the formation of bonds of main group elements of “unusual” high valencies. In 1969, in a seminal work, Musher⁵¹ introduced the name *hypervalent (HV) bonds* for those formed using doubly occupied with lone pairs p- (or sometimes even s-) orbitals. The formation of 3c-4e HV bonds involving a main-group atom X having at least one lone pair and two atoms (or groups), typically dubbed *ligands*, each possessing a single electron on a p-orbital (L^{\bullet} and $L^{ii\bullet}$), is shown schematically in Figure I-6.

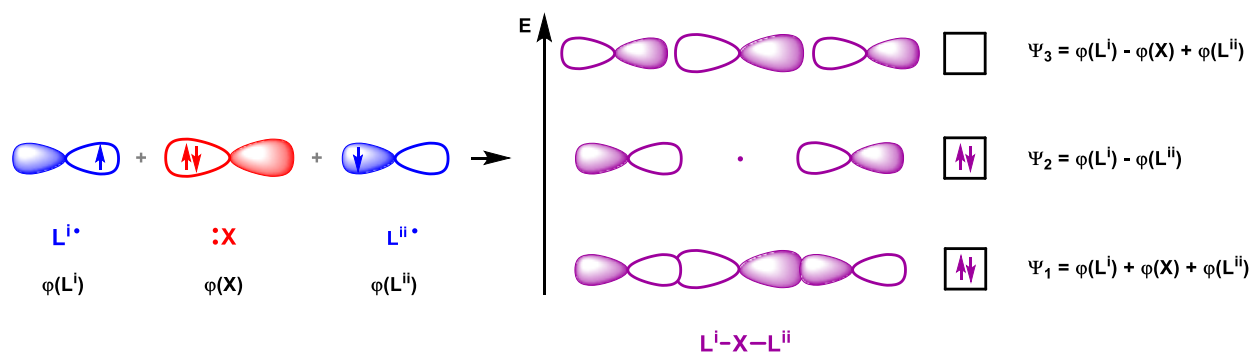


Figure I-6. Formation of a linear fragment L^i-X-L^{ii} via 3c-4e HV bonds between a central atom X and ligands $L^i•$ and $L^{ii}•$, and energy diagram of the formed molecular orbitals.

The three p atomic orbitals combine to form three molecular orbitals: bonding (Ψ_1 in Figure I-6), nonbonding (Ψ_2 , HOMO) and antibonding (Ψ_3 , LUMO). The four available bonding electrons populate the first two molecular orbitals and the net result is that the two ligands receive a partial negative charge, while the central atom becomes electrophilic due to partial positive charge. As could be expected, the ligands in most stable HV compounds contain an electronegative atom (F, Cl, O, N) directly bonded to the central HV atom. Several review papers⁵²⁻⁵⁴ and a monograph⁵⁵ were published on this subject.

I.2.3 Nomenclature and Structure of HV Iodine Compounds

To classify HV compounds, a convenient N-X-L nomenclature was proposed.⁵⁶ In the nomenclature, “N” represents total number of valence shell electrons surrounding the central atom (X), and “L” represents number of groups or atoms bonded with central atom via either conventional 2c-2e bonding or HV (3c-4e) bonding. According to this nomenclature, most of the HV iodine compounds belong to the classes 10-I-3 (iodine(III)) and 12-I-5 (iodine(V)), but representatives of other groups are also shown in Figure I-7.

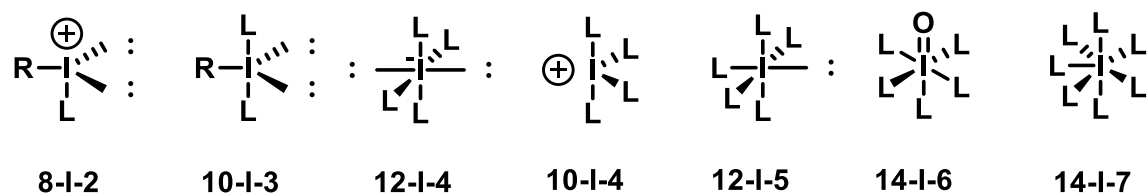


Figure I-7. Most common classes of HV iodine compounds.

In 10-I-3 compounds, the 5 electron pairs around the central iodine atom adopt a trigonal bipyramidal orientation, in which the electronegative ligands participating in the formation of the HV bonds occupy the axial positions while the third group connected to the central atom via a normal covalent bond (usually an aryl or less frequently a (perfluoro)alkyl group) is at the equatorial position. As a result, 10-I-3 compounds have a characteristic T-shaped geometry. The HV compounds of iodine(V), 12-I-5 compounds, contain two linear L-I-L HV bonding motifs, perpendicular to one another, at the base of a square pyramid, and the fifth, i.e., the least electronegative C-based group is perpendicular to the plane formed by the two HV bonds.

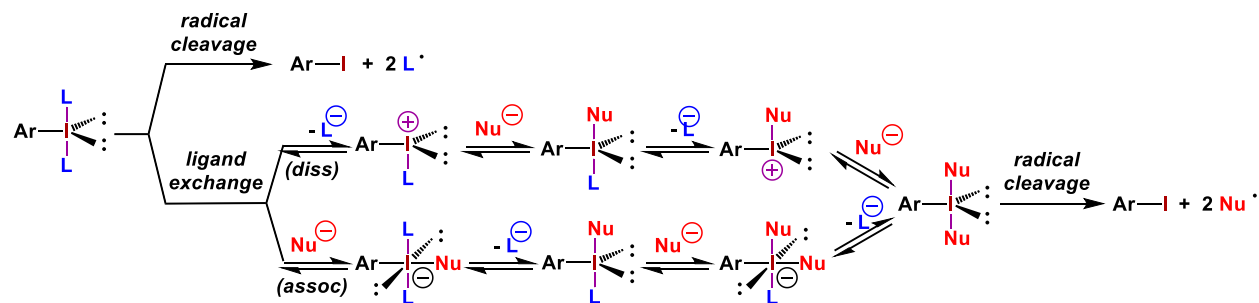
To assign names to compounds containing heteroatoms with nonstandard valence states (n), in 1983, IUPAC recommended names based on lambda convention. According to this convention, trivalent and pentavalent iodine with 10 and 12 electrons, respectively, were designated as λ^3 - and λ^5 -iodanes. λ^3 - and λ^5 -iodanes are also known as iodinanes and periodinanes, respectively.

I.2.4 Reactivity of HV Iodine Compounds Relevant to Applications in Polymer Science

HV bonds are weaker than typical 2c-2e covalent bonds and as a result they can be cleaved homolytically with the formation of the corresponding radicals. Several radical reactions involving

HV iodine compounds have found utility in synthetic organic chemistry.⁵⁷ The ability of HV iodine compounds to degrade upon heating or irradiation and yield radicals derived from the ligands in the fragment L-I-L makes these compounds particularly useful as radical initiators of polymerization (Scheme I-5). Heterolytic (ionic) reactions are also possible, especially with iodonium salts, which makes them suitable initiators for cationic polymerizations of vinyl and heterocyclic monomers. The ease of carrying out cleavage reactions of the HV iodine bonds that afford radicals and/or ions are the basis of the first group of uses of HV iodine compounds in polymer science, namely as radical or cationic thermal or photoinitiators.

The HV bonds are dynamic in nature⁵⁸ and ligand-exchange reactions with nucleophiles are not only possible but are rather efficient. These transformations can be employed to convert a nucleophile (Nu^-) into the corresponding functional radical (Nu^\cdot) by homolysis of the newly formed I-Nu HV bonds (Scheme I-5), which can be used to initiate polymerization or to modify chemically a pre-made polymer. There are a few reviews and book chapters describing the applications of HV iodine compounds in polymer chemistry.



Scheme I-5. Bond homolysis and ligand-exchange reactions with HV iodine(III) compounds with applications in the synthesis of polymeric materials.

I.2.5 Applications of HV Iodine Compounds in Polymer Science

I.2.5.1 HV Iodine Compounds as Initiators for Polymerization

I.2.5.1.1 Iodonium Salts

In a 1973 patent, diaryliodonium salts were reported to serve as efficient photoinitiators of polymerization of vinyl monomers in the presence of sensitizers. Within several years, in 1976, Crivello and Lam published a pioneering work describing preliminary studies indicating that diaryliodonium salts with complex halide anions could initiate the photoinduced polymerization of various cationically polymerizable monomers, including olefins (styrene, α -methylstyrene, vinyl ethers) and cyclic ethers (epoxides, tetrahydrofuran, 1,3,5-trioxane). A photolysis mechanism was also proposed, according to which the main initiator was a Brønsted acid containing the complex metal halide anion and proton generated by the reaction of one of the photolysis products (the radical cation $ArI^{+\bullet}$) with the solvent. Further details regarding the photodecomposition of diaryliodonium salts and the scope of the polymerization reaction (which now involved, in addition to the above-mentioned monomers, also lactones and thioethers) were provided in a follow-up work by Crivello and coworkers from 1977. Some of the synthesized iodonium salts used as photoinitiators are shown in Figure I-8, along with the structures of monomers that have been successfully polymerized.

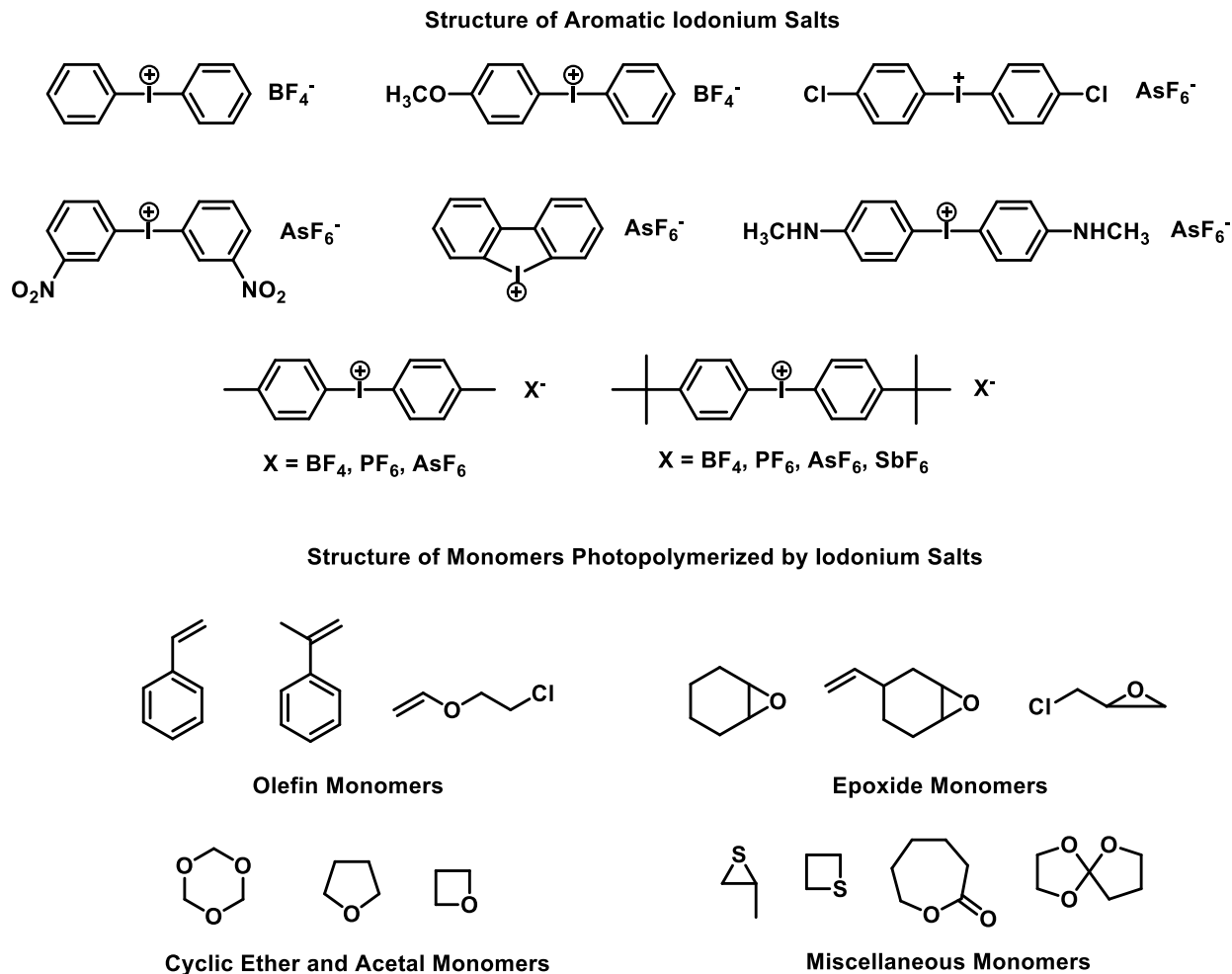
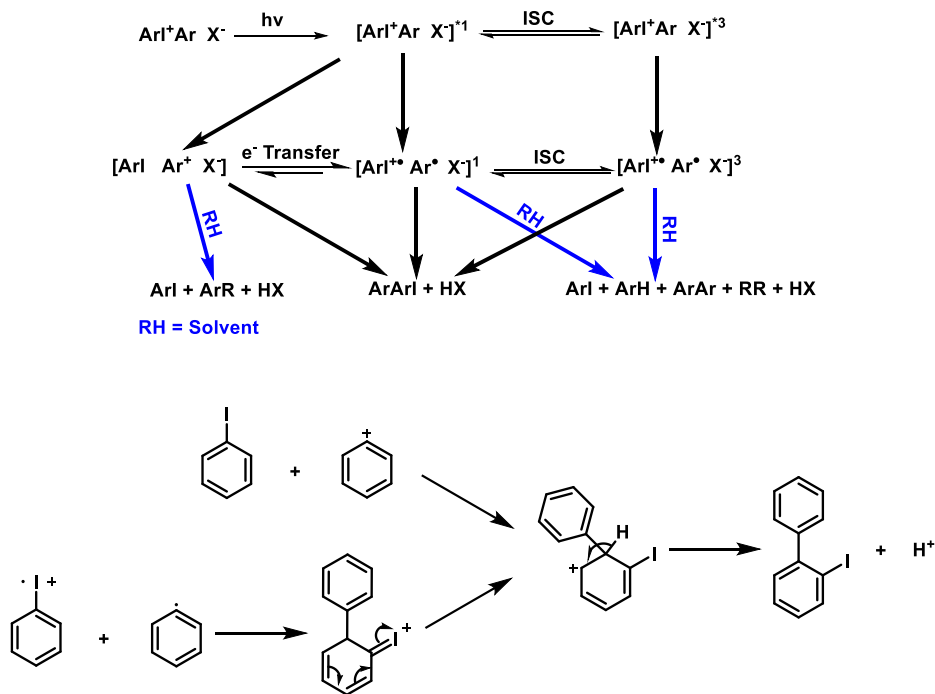


Figure I-8. Structures diaryliodonium salts used as photoinitiators of the polymerization of various monomers (shown at the bottom).

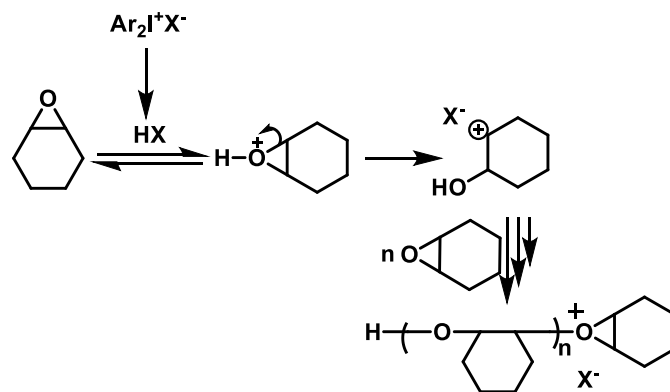
Dektar and Hacker suggested the mechanism for direct photolysis of diaryliodonium salts by compiling all the previous results. According to this paper, diaryliodonium salt absorbs a photon to go to a singlet excited state. This excited state may choose among three different pathways. First, it may dissociate heterolytically to form iodobenzene and phenyl cation. Second, it may dissociate homolytically to form iodobenzene radical cation and phenyl radical, or it can go to a triplet state by inter system crossing (ISC). Triplet excited state can undergo hemolysis to form triplet phenyl radical-iodobenzene radical cation pair. This ISC is reversible and it can probably

compete with the cleavage reaction because of spin-orbit coupling which favors heavy atoms like iodine. Since, both iodobenzene-phenyl cation pair and phenyl radical-iodobenzene radical cation pair has lower energy than singlet excited state, therefore the direct formation of both pairs from excited state is thermodynamically permitted. However, the formation of less stable iodobenzene-phenyl cation pair from the excited state may be followed by electron transfer to form more stable intermediate *i.e.* phenyl radical-iodobenzene radical cation pair. Furthermore, both iodobenzene-phenyl cation and phenyl radical-iodobenzene radical cation can recombine to form the starting iodonium salt or cyclohexadienyl cation which leads to iodobiphenyls along with free proton as shown in Scheme I-6. Additionally, all the intermediates can extract protons from the solvent. These protons can combine with the anions to give acid. This acid is considered as the true initiator of cationic polymerization when diaryliodonium salts are used in the cationic polymerization.



Scheme I-6. Photochemistry of diaryliodonium salts.

In the groundbreaking paper which Crivello and Lam published in 1977, they observed that neither cationic part of iodonium salt nor counter ions have any effect on photodecomposition of diaryliodonium salts. As a result of this observation, they suggested the amount of brønsted acid generated per unit time from different iodonium salts are identical. In contrast to this, Park and co-worker published a paper on photo-initiated cationic polymerization of epoxy monomers in 2006. In this detailed study of effect of anions and alkyl substituents of diaryliodonium salts on photo initiated cationic polymerization of epoxides, such as 3,4-Epoxyethylhexylmethyl 3,4-Epoxyethylhexane carboxylate and 1,2-Cyclohexane oxide, it was found that the diphenyliodonium cation substituted with bulky alkyl groups, such as bis(4-*tert*-butyl phenyl)iodonium and 4-cumenyl 4'-tolyliodonium salts, have higher efficiency in the photolysis reaction than unsubstituted iodonium salts. The difference in efficiency was explained by the inhibition of coupling reaction between highly reactive intermediate species due to stereoselectivity. The counter anions also play a decisive role in enhancing the polymerization rate despite their huge volume and low nucleophilic activity, with the general order of reactivity found to be $\text{PF}_6^- < \text{AsF}_6^- < \text{B}(\text{C}_6\text{F}_5)_4^-$. Bigger anions could not bind tightly to the end of the growing cationic chain, hence increasing the efficiency of the propagating cationic species in the polymerization (Scheme I-7).



Scheme I-7. Mechanism of photopolymerization of 1,2-cyclohexane oxide initiated by diaryliodonium salts.

Many papers have been published describing the use of iodonium salts as photoinitiators for the polymerization of various monomers. For example, photopolymerization of unsaturated cyclic ethers, photoinitiated polymerization of epoxide monomers like 1,2-cyclohexene oxide and 3,4-epoxycyclohexylmethyl 3,4-epoxycyclohexane carboxylate, photoinitiated cationic polymerization of tetrahydrofuran, cationic polymerization of 1,2-epoxy-6-(9-carbazoyl)-4-oxahexane, photopolymerization of various vinyl ethers, preparation of hydrogels based on 2-hydroxy methacrylate and N-vinyl-2-pyrrolidone and preparation of elastomers based on a cycloaliphatic diepoxide and poly(tetrahydrofuran).

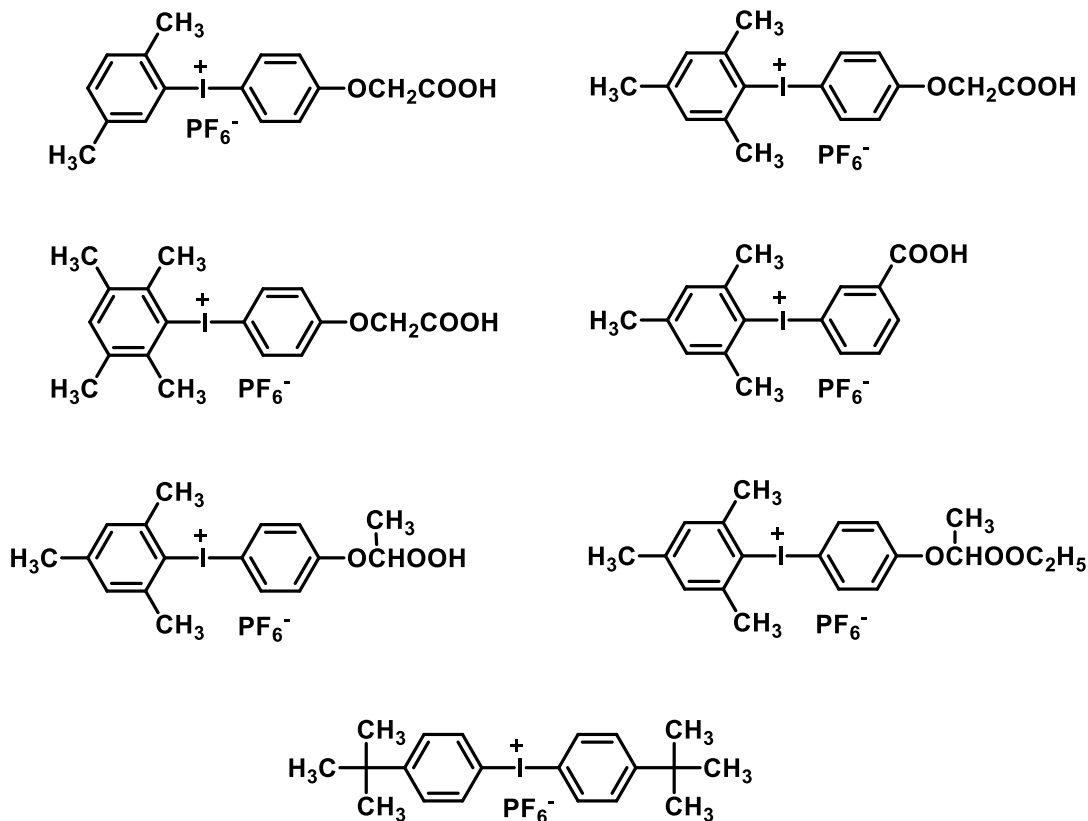


Figure I-9. Structures of symmetric and asymmetric diaryliodonium hexafluorophosphates used as photoinitiators.

A series of substituted diaryliodonium hexafluorophosphates (Figure I-9) were also prepared in order to improve the solubility and toxicity level of the photoinitiator. The combination of diaryliodonium hexafluorophosphate salts with 2-ethyl-9,10-dimethoxyanthracene shows higher photocuring than naphthyl-type sulfonium salt in the pigmented system containing titanium oxide.

Various iodonium butyltriphenylborates (Figure I-10) were synthesized by Necker and co-workers and found to be more effective than iodonium tetraphenylborate salts in the polymerization of acrylates. They were prepared by ion exchange between diphenyliodonium haloate salts and tetraammonium triphenylbutylborates. In a study of photoreaction of iodonium borate salts with methyl methacrylate, it was found that iodonium butyltriphenylborate salts

produce butyl radicals from the borate ions along with aryl radicals from the iodonium cation simultaneously upon irradiation. Iodonium borate salts strong absorption below 300 nm with a tail absorption above 400 nm. Hence, iodonium borate salts can be used as photoinitiators even in the visible light.

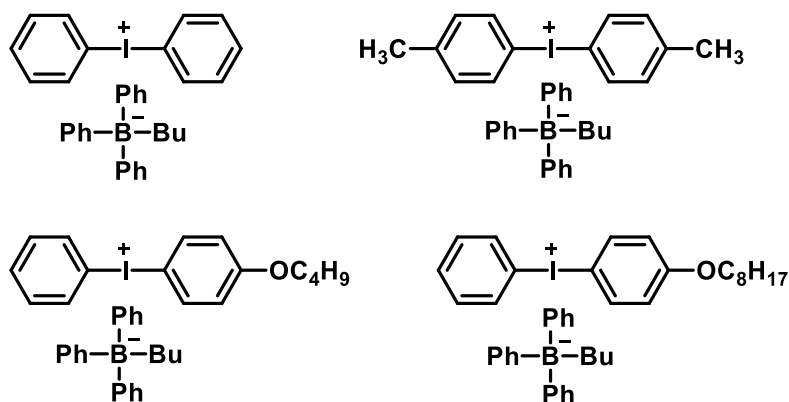
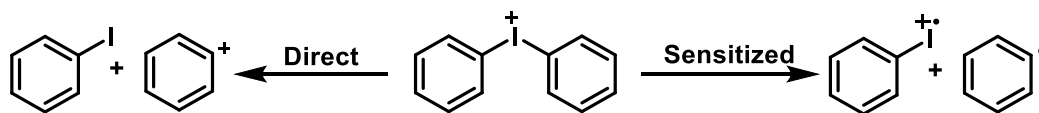


Figure I-10. Diaryliodonium butyltriphenylborate photoinitiators.

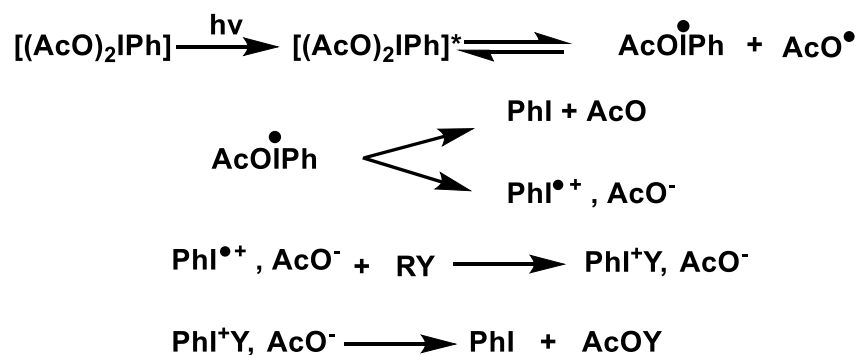
Many initiation techniques have been developed in order to increase the efficiency of diaryliodonium salt photoinitiators like visible laser irradiation, dual photo- and thermally induced cationic polymerization and use of photoinitiation system composed of a photosensitizer and diaryliodonium salt. Among these techniques, use of photosensitizer is most popular and effective. It was surmised that direct photolysis of the salt favors heterolytic cleavage to yield phenyl cation and iodobenzene (Scheme I-8), but sensitized decomposition leads to homolytic cleavage of I-O bond which produces phenyl radical and iodobenzene radical cation. This improves the efficiency of diaryliodonium salts as cationic photoinitiators.



Scheme I-8. Direct versus sensitized photolysis of diaryliodonium salts.

I.2.5.1.2 λ^3 -Iodanes

λ^3 -iodanes can be used as a photo- and thermal- initiator for (mostly) radical and cationic polymerization. The first report on the use of (diacetoxyiodo)benzene as thermal initiator for the radical polymerization of vinyl monomers was appeared in a patent in 1949.⁵⁹ In 1985, Georgiev and coworker⁶⁰ first proposed that diacetoxyiodo benzene and bis(trifluoroacetoxy) benzene can be used as photoinitiators for cationic polymerizations. In this paper, *i*-butyl vinyl ether was polymerized in presence of UV light by using diacetoxyiodo benzene and bis(trifluoroacetoxy) benzene as photoinitiators. After few years, Georgiev and coworker published a systematic study of homo- and copolymerization of methyl methacrylate, 2-(dimethylaminoethyl) methacrylate, styrene⁶¹ and established that diacetoxyiodo benzene and bis(trifluoroacetoxy) benzene can be used as a photoinitiator for cationic and radical polymerization. In this paper, they suggested that diacetoxyiodo benzene first get activated by light and this excited diacetoxyiodo benzene undergoes homolytic I-O bond cleavage to form iodonium and acetoxy radical as shown in Scheme I-9.

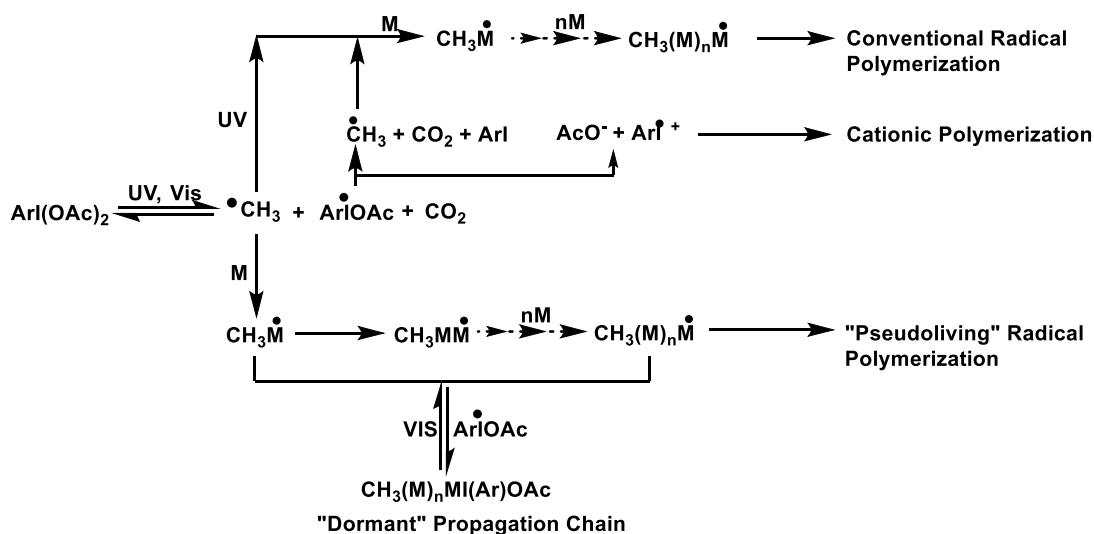


Scheme I-9. Photodecomposition of (diacetoxy)iodo benzene.

Acetoxy radicals can undergo decarboxylation to form carbon dioxide and methyl radicals. On the other hand, iodanyl radical can decompose either homolytically or heterolytically to form iodobenzene and acetoxy radical or iodobenzene cation radical-acetate ion pair, respectively. This iodobenzene cation radical-acetate ion pair can further react with either solvent or monomer to produce more radicals. At this point, it is important to notice the difference between diacetoxyiodo benzene and diaryliodonium salts. In diacetoxyiodo benzene, radical formation occurs in the primary dissociation reaction earlier than cation formation. Furthermore, in contrast to usual bulky anions of diaryliodonium salts, acetate ion has very high nucleophilicity which can combine with the iodonium radical cation to inhibit the cationic polymerization. Therefore, diacetoxyiodo benzene and bis(trifluoroacetoxy) benzene are more effective as radical photoinitiators instead of cationic photoinitiators.

Georgiev reported⁶² a photoiniferter ability of diaryliodanes established during the bulk polymerization of methyl methacrylate, styrene, and *N*-vinylpyrrolidone. The term ‘photoiniferter’ suggests that diaryliodanes can act as a free radical initiator, chain transfer agent, and terminator simultaneously in photopolymerization.⁶³ Diacetoxyiodo arenes initiate “pseudoliving” polymerization in presence of visible light, on the other hand, a conventional radical or cationic

polymerization are the results of the iodane decomposition under UV light (Scheme I-10). It is suggested that the spectral selectivity of 9-I-2 iodanyl radical decomposition and relative instability of the ends of the iodane macromolecules are the reasons of this unusual ability. As the modern concept of hypervalent bonds dictates, d-function provide orbital space at the central iodine atom to accept electron charge from ligands by back bonding. Due to this back-bonding, the resulting energy stabilization overcomes the strong ligand-ligand repulsion at the hypervalent iodine atom. Also, the overlap of sp hybrid orbital with the ligand orbitals is improved by the polarization functions of d-orbital.



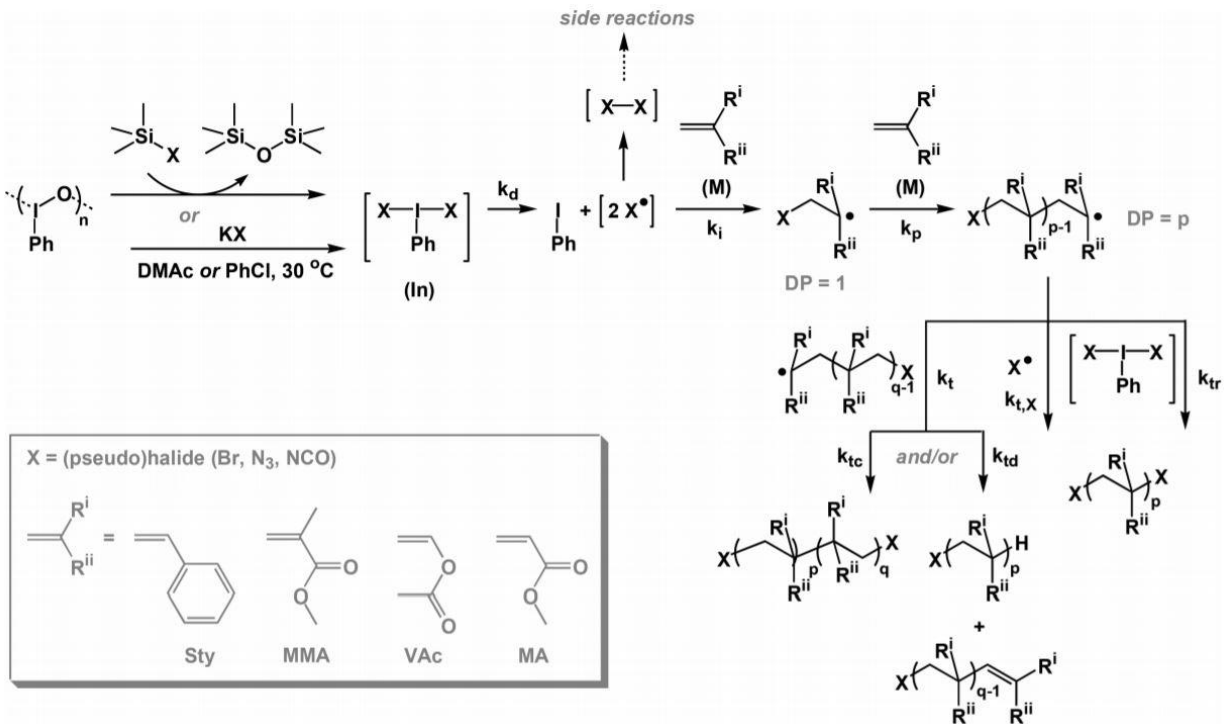
Scheme I-10. Iniferter capability of (diacetoxyl)iodo benzene under UV light.⁶³

Therefore, the stability of above mentioned 9-I-2 iodane radical intermediate increases and reactivity decreases because of negative hyperconjugation and the partially ionic character of I-O bond. Due to these reasons, the initiation efficiency of primary radical decreases considerably. However, this does not imply the exclusion of the possibility of the reaction between iodanyl radical and propagation ones. On the other hand, the stability of high molecular weight 10-I-3 with

compounds degrade homolytically upon heating and can initiate radical polymerization. For instance, 1-chloro-2-hexyl-1,2-benziodazol-3(2H)-one, is used in the polymerization of styrene, which yields low molecular weight polymers with alkyl chloride groups at the α - (initiation) and the ω -chain ends (transfer) as shown in Scheme I-11. The same initiator/chain transfer agent was successfully employed in the synthesis of highly branched polymers with multiple alkyl chloride-type chain ends when added to mixtures of styrene and 1,4-divinylbenzene containing 10–80 mol% of the divinyl crosslinker, or even pure crosslinker.

In 2001, Georgiev and coworkers showed that (diacetoxyiodo)benzene can also be used as thermo- and sono-initiator for the radical bulk polymerization of methyl methacrylate.⁶⁵ The polymerization kinetics and molecular mass characteristics suggest a combined polymerization mechanism including traditional bimolecular termination with chain transfer reaction and iniferter pseudo-living polymerization. After a year, Georgiev⁶⁶ *et al.* proved that (diacetoxyiodo)benzene is an effective iniferter in the bulk polymerization of methyl methacrylate and it has characteristics of “living” radical polymerization. In this paper, they showed that copper(I) salts can accelerate the diacetoxyiodo benzene initiated radical polymerization, while dipyridyl compounds do the opposite. Furthermore, they claimed that it is possible to control the speed of the process and molecular weight of the polymer to prepare well-defined polymers.

Asandei reported⁶⁷ photo(trifluoro)methylation and controlled radical polymerization of fluorinated alkenes using [bis(trifluoroacetoxy)iodo]benzene in the presence of visible light. [bis(trifluoroacetoxy)iodo]benzene is introduced as a precursor for triphenylmethyl radical and trifluoromethyl iodide. The radical polymer of vinylidene fluoride was controlled by using *in situ* generated trifluoromethyl iodide and externally added dodecafluoro-1,6-diiodohexane as chain transfer agent.

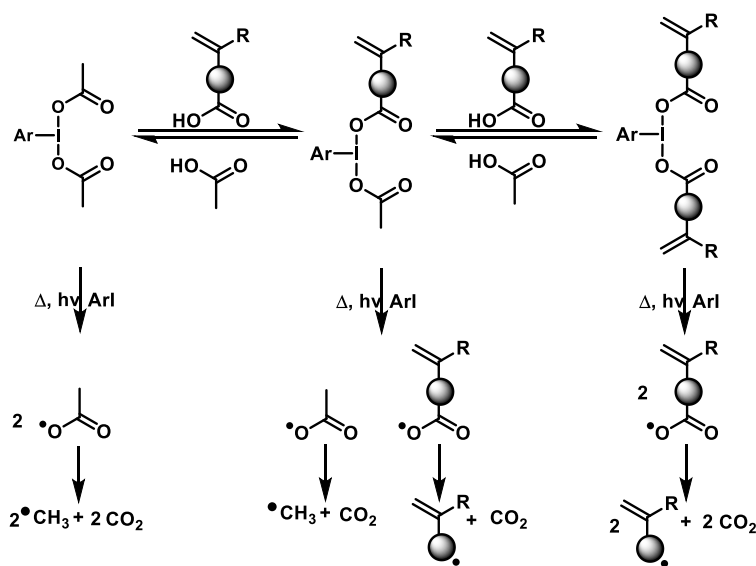


Scheme I-12. Polymerization of vinyl monomers initiated by the iododisilbenzene-pseudohalide system and formation of pseudohalide-capped polymers.⁶⁸

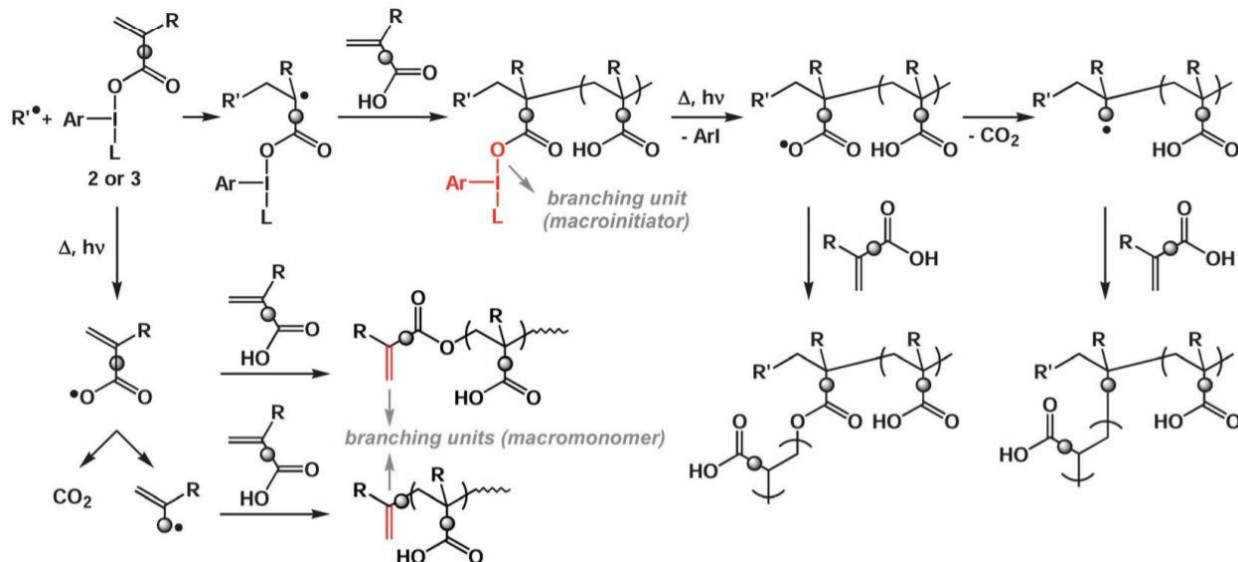
Recently, iododisilbenzene-pseudohalide based initiators were used to initiate the radical polymerization and introduce pseudohalide functionalities at α and ω chain ends.⁶⁸ The article reported that Iododisilbenzene reacts with various (pseudo)-halides (trimethylsilyl azide or isocyanate or potassium azide, cyanate, and bromide) to yield unstable hypervalent iodine(III) compounds, PhIX_2 ($\text{X} = (\text{pseudo})\text{halide}$), that undergo rapid homolysis of the hypervalent $\text{I}-\text{X}$ bonds and generate (pseudo)halide radicals, which can initiate the polymerization of styrene, (meth)acrylates, and vinyl esters. Polymers are formed containing (pseudo)halide functionalities at the α -chain end but, depending on the termination mechanism and the occurrence of transfer of (pseudo)halide groups from the initiator to the propagating radicals, also at the ω -chain end as shown in Scheme I-12.

I.2.5.2 Functional Radical Initiators Generated as a Result of Ligand-Exchange Followed by Homolysis

Most reactions of λ^3 -iodanes with general formula PhIL_2 , where L represents a ligand attached to central iodine atom, involves the initial exchange of ligands on the iodine atom with an external nucleophile. Taking advantage of this reaction, [(acetoxy methacryloyloxy)iodo]benzene and (dimethacryloyloxy)iodobenzene were prepared by exchanging acetoxy groups of (diacetoxyiodo)benzene with methacrylic acid in various solvent (Scheme I-13).⁶⁹ These two hypervalent iodine compounds can act as inimers due to presence of polymerizable moiety and easy generation of radicals upon thermal or light induced homolysis of the I-O bonds as shown in Scheme I-5. Branched and transiently crosslinked polymers were prepared by heating a mixture of (diacetoxyiodo)benzene, methacrylic acid and methyl methacrylate at 80 °C as shown in Scheme I-14. In homopolymerizations of methyl methacrylate initiated by $\text{PhI}(\text{OAc})_2$, i.e., in the absence of the monomer with carboxylic acid group, no branching or gelation was observed.



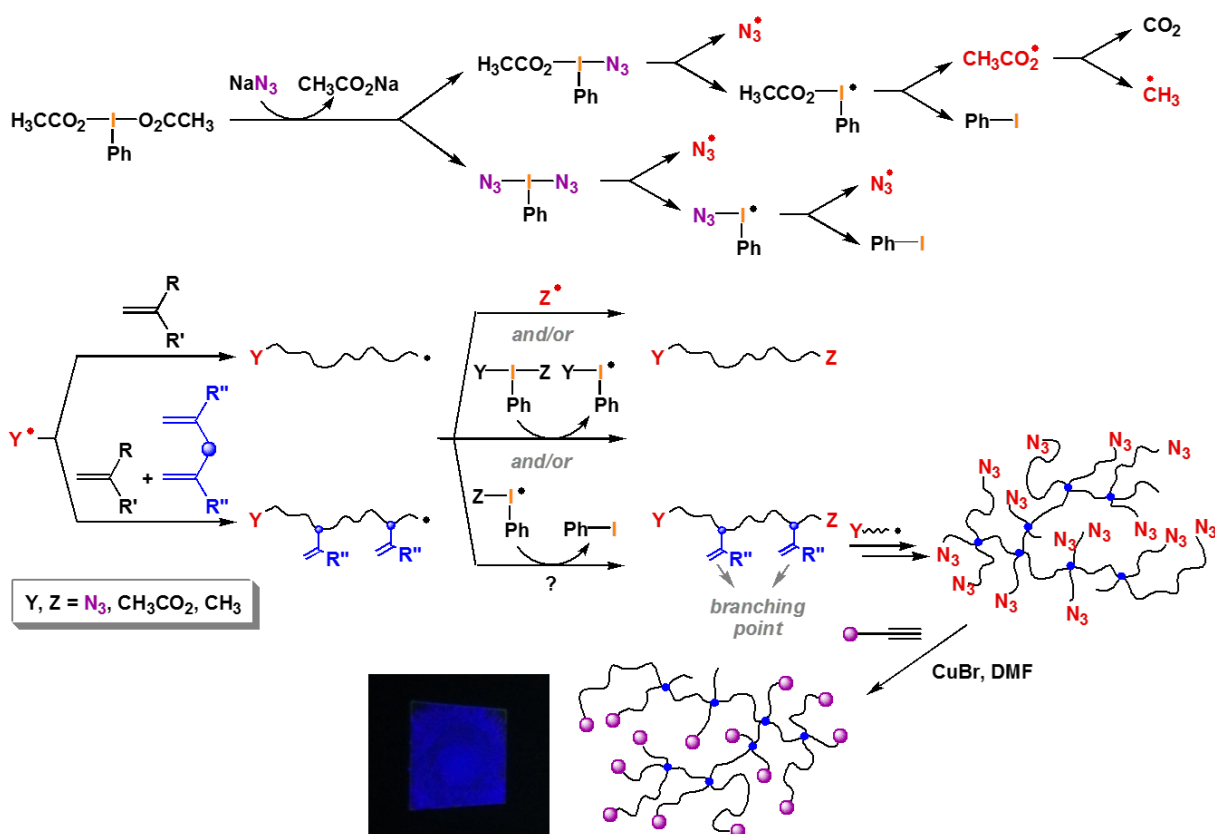
Scheme I-13. Exchange of acetoxy groups in (diacetoxy)iodo arenes with polymerizable carboxylic acid and its radical decomposition in presence of light or heat.⁶⁹



Scheme I-14. Branching via incorporation into the polymer chain of a hypervalent iodine-containing mono- or difunctional monomer. The I–O bonds in the inimers formed in situ can serve as initiating sites. R'• represents any low molecular weight or macro-radical able to propagate.⁶⁹

Using the same approach, a new method for the preparation of azide containing polymers that take advantage of the efficient exchange of acetoxy ligands in (diacetoxyiodo)benzene with azides, in this case, sodium azide.⁷⁰ The azide containing hypervalent iodine compounds $\text{PhI}(\text{N}_3)(\text{O}_2\text{CCH}_3)$ and $\text{PhI}(\text{N}_3)_2$ were generated in situ and due to poor stability, decomposed rapidly event at ambient temperature to yield monovalent iodobenzene and azide (and – in the former case – also acetoxy and methyl) radicals. Polymerization of methyl methacrylate was initiated by reactive azide radicals at 40-100 °C, yielding polymers with azide functionalities at the α -terminus along with low molecular weight linear polymers with an azide group at the ω -end (Scheme I-15). These low molecular weight polymers were formed due to fast termination of propagating radicals by coupling with azide radicals and azide transfer from $\text{PhI}(\text{N}_3)_x(\text{O}_2\text{CCH}_3)_{2-x}$ ($x = 1,2$). Highly branched polymers were formed when polymerization was done in the presence of divinyl compounds (crosslinker).

These highly functionalized branched polymers could be further functionalized using Cu(i)-catalyzed azide-alkyne “click” coupling reaction with functional alkynes; for instance, the reaction with pyrenyl 4-pentynoate afforded polymers with multiple fluorescent pyrene moieties at many of the chain ends (Scheme I-15).

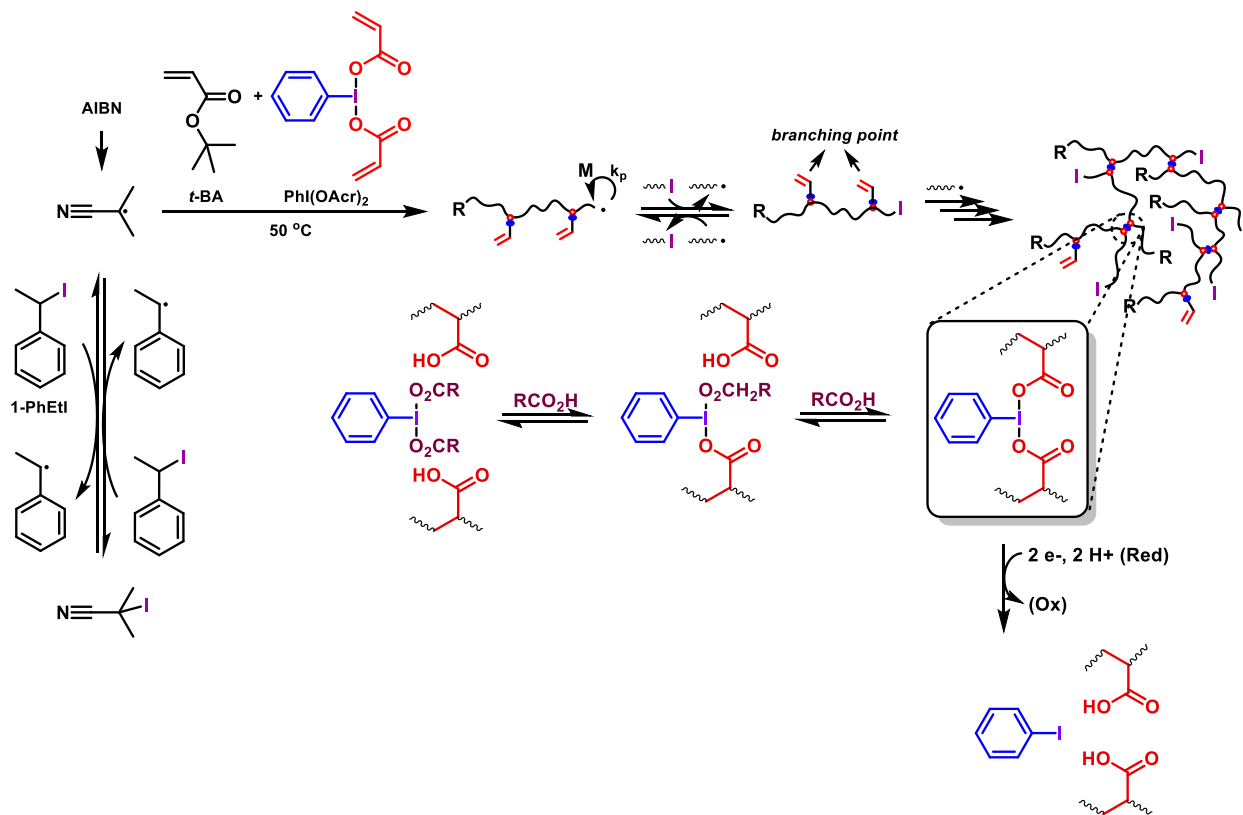


Scheme I-15. Ligand-exchange of the acetoxy groups in (diacetoxyiodo)benzene with azide anions to form HV iodine-based precursors of azide (and methyl) radicals. Formation of highly branched multi-azidated polymers via one-pot procedures and their functionalization with alkenes (for instance, the fluorescent pyrenyl 4-pentynoate) under “click” chemistry conditions.⁷⁰

I.2.5.3 Hypervalent Iodine Compound as Crosslinker

Recently, synthesis and crystal structure of a HV iodine(III)-containing crosslinker, (diacryloyloxyiodo)benzene ($\text{PhI}(\text{OAc})_2$), was reported.⁷¹ Highly branched polymers with HV

iodine(III) groups as the building blocks present at the branching points were synthesized by copolymerization of tert-butyl acrylate and the diacrylate crosslinker (up to 12 mol% vs the monovinyl monomer), under reversible deactivation radical polymerization (iodine transfer polymerization) conditions, which were employed to ensure that the incorporation of the crosslinker into the polymer chains was slow and gradual, that was, to limit the average number of pendant double bonds per chain and delay gelation (Scheme I-16).



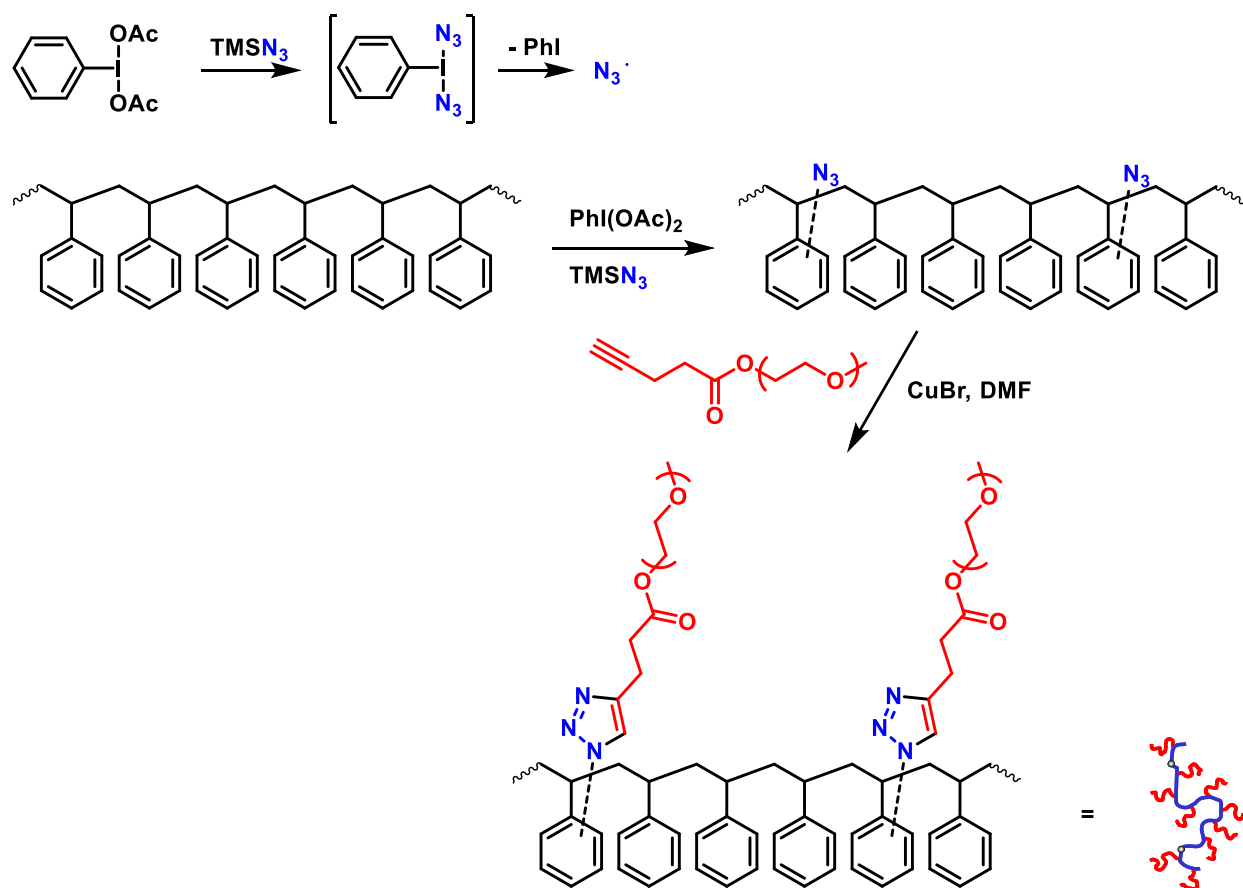
Scheme I-16. Synthesis of branched polymers with HV iodine(III) groups at the branching points. Degradation mechanisms of branched polymers with HV iodine(III)-based crosslinks in the presence of reducing agents or carboxylic acids.⁷¹

The branched polymers with (diacyloxyiodo)benzene-type linkers were responsive and react with monocarboxylic acids, for example, acetic acid, which participate in ligand-exchange reactions with the HV iodine(III) centers, and with reducing agents, for example, tributylphosphine, which reduce iodine(III) to iodine(I); both reactions lead to polymer degradation with the formation of random linear copolymers of tert-butyl acrylate and acrylic acid.

I.2.5.4 Post-Polymerization Modifications Using HV Iodine Compounds

HV iodine compounds are mainly considered as oxidizing agent in organic synthesis or thermo- and photoinitiator for radical or cationic polymerization but in 2010 Tsarevsky reported⁷² a reaction of polystyrene with a combination of diacetoxyiodo benzene and trimethylsilyl azide which led to direct azidation of polystyrene. Synthetic routes to polymers containing multiple azide functionalities are highly desirable because of “click” chemistry. Post-polymerization modification of polymer to introduce azide functionalities is an efficient and significantly less hazardous strategy as compared to the synthesis of polymers from azide containing monomers. As mentioned in this paper, approximately 1 in every 11 styrene units could be modified by using diacetoxyiodo benzene, trimethylsilyl azide and styrene with 1:2.1:1 ratio respectively at 0 °C for 4 hours followed by heating at 50 °C for 2 hours in chlorobenzene.

Modified polymers with azide groups were further used in copper-catalyzed click-type grafting-onto reactions using poly(ethylene oxide) monomethyl ether 4-pentynoate as the functional alkyne (Scheme I-17). This reaction produced polymeric brushes with hydrophobic backbone and a moderate density of hydrophilic sidechains.



Scheme I-17. Direct azidation of polystyrene using ligand-exchange reaction between (diacetoxy) iodobenzene and trimethylsilyl azide and preparation of graft copolymers using click reaction between the multi-azidated product and poly(ethylene oxide) monomethyl ether 4-pentynoate.⁷²

Recently, Bielawski and Liu reported⁷³ direct C-H azidation of isotactic polypropylene using azidoiodinane at 80-110 °C. If reaction was carried out at a lower temperature, it was necessary to add an initiator like di-*tert*-butylperoxyoxalate to obtain good yield. Furthermore, polypropylene-*graft*-poly(ethylene glycol) copolymers were also synthesized via azide-alkyne cycloaddition chemistry.

I.3 Self-Healing Polymers

Self-healing polymers are smart materials with the capability to repair themselves when damaged without any need for the detection or manual repair. The need for materials with extended lifetime is driven by the limited availability of petroleum feedstocks used to produce polymers and increasing demand for the polymeric materials with improved performance. The lifetime of a material can be extended by mitigating the mechanism leading to failure. In brittle polymers, failure occurs through crack formation and propagation and the ability to repair these cracks when they are still very small will prevent further propagation thus extending the lifetime of the material. Emerging self-healing technologies has provided the capability to restrict the crack propagation at an early stage, preventing catastrophic failure and increasing the scope of applications of polymeric materials.

The self-healing process is classified in the following four categories:

1. Embedding reactive encapsulated fluids which burst open upon damage to fill and repair damaged areas.
2. Chemical incorporation of dynamic bonds into existing materials' structures that upon cleavage reform.
3. Physically dispersing superparamagnetic or other nanomaterials, which remotely respond to magnetic or electromagnetic fields, thus enabling repairs.
4. Embedding living organisms capable of mending damaged structures.

The following discussion is based on the self-healing process in the soft matter, which mainly involved chemical incorporation of dynamic bonds since it is most relevant to this work. In soft matter, covalent bond reformations or secondary chemical interactions must be spatially and timely coordinated with the physical chain rearrangements to self-heal the materials since

mechanical damage may cause chain conformational changes with or without chain slippage or cleavage.

According to recent studies, two types of dynamic bonds/interactions are highly effective to achieve self-healing:

1. Supramolecular interactions
2. Reversible or dynamic covalent bonds

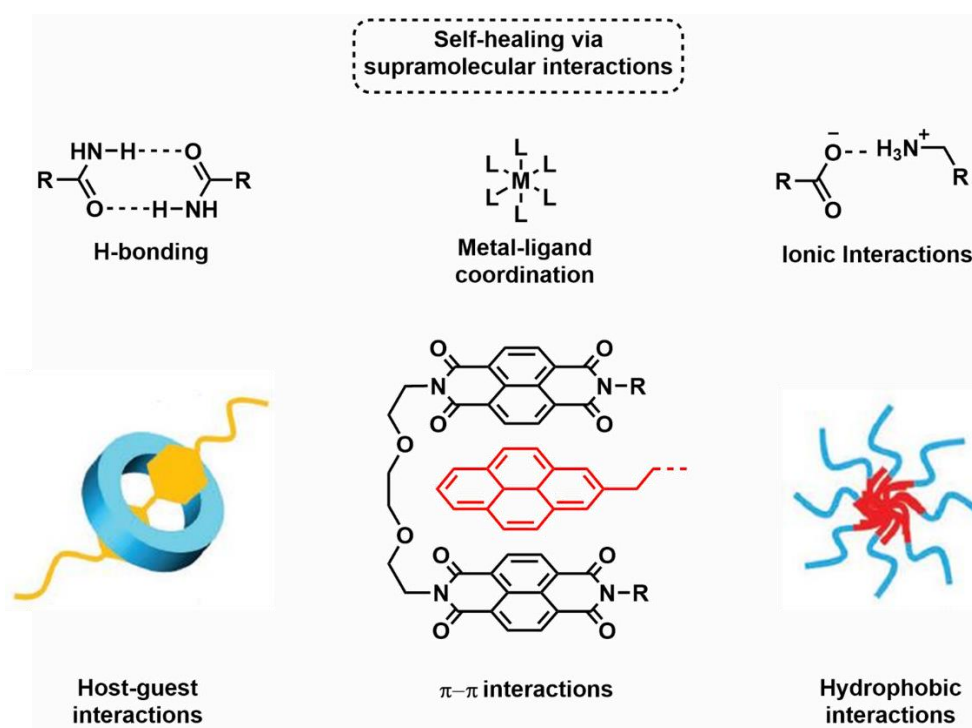
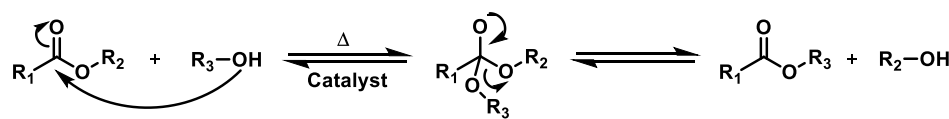


Figure I-11 Categories of supramolecular chemistries utilized in self-healing functional materials.

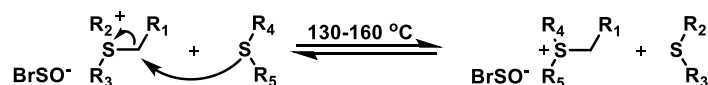
Self-healing involving dynamic dissociation/association using supramolecular chemistry offers fast reversibility under ambient conditions reaching exceptionally quickly equilibrium state, bonding directionality, and remarkable sensitivity. Since broad-range of network structures can be obtained via supramolecular interactions, applications in soft electronics, sensing, biomedical

technologies, 3D printing, and re-processable materials are highly attractive and may open many new technological opportunities. Mechanical integrity using supramolecular chemistry is achieved by the formation of multiple noncovalent interactions between multiple associative groups covalently attached to polymer side chain or chain ends of macromolecular building blocks. These interactions include H-bonding, metal–ligand complexation, host-guest, ionic interactions, π - π stacking, and hydrophobic interactions (Figure I-11).

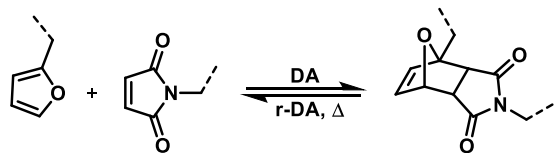
(a) Transesterification



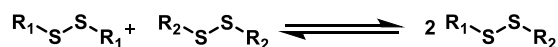
(b) Nucleophilic substitution



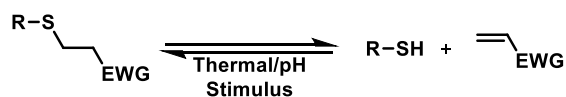
(c) Diels-Alder reaction



(d) Disulfide exchange reactions



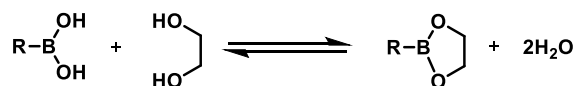
(e) Thiol-Michael reactions



(f) Transthioesterification



(g) Boronic esterification



(h) Si-O exchange reactions



Figure I-12 Dynamic reactions used to prepare self-healing materials.

Reversible or dynamic covalent bonds are also utilized to make self-healing materials. Dynamic covalent bonds can reversibly break and reform automatically or in response to a stimulus. To form these types of dynamic crosslinks, reactions (shown in Figure I-12) such as transesterification, nucleophilic substitution, Diels-Alder reaction, disulfide exchange reaction, Thiol-Michael reaction, transthioesterification, boronic esterification, Si-O exchange reactions, are frequently used. Generally, the exchange of these dynamic covalent bonds occurs by either associative or dissociative pathways. Associative pathway involves simultaneous breaking and reformation of bonds (Figure I-13). On the other hand, in dissociative pathway, some crosslinks dissociate first and then new linkages form after some time. Due to the loss in number of crosslinks, there is considerable change in the macromolecular structure.

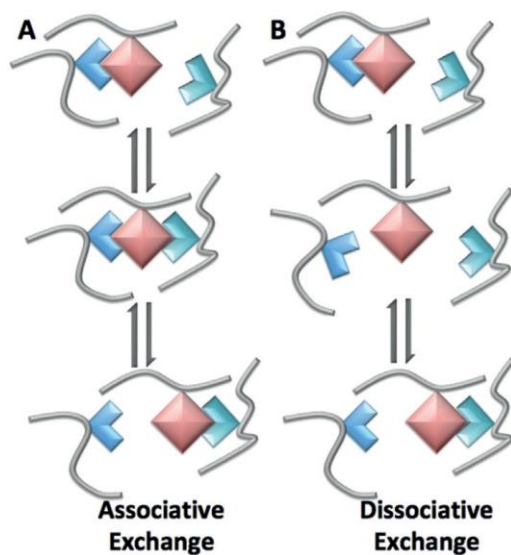


Figure I-13 A) Associative exchange and B) dissociative exchange of dynamic covalent bonds.

In this thesis, a ligand exchange reaction performed by HV iodine compounds, specifically (diacetoxyiodo)benzene (DAIB) was employed to prepare self-healing polymer network following the associative pathway. The detailed discussion can be found in the following chapter.

I.4 Characterization Techniques

I.4.1 Size Exclusion Chromatography (SEC) or Gel Permeation Chromatography (GPC)

Size exclusion chromatography involves separation of different sized polymers by passing the polymer solution through a column packed with microporous beads of crosslinked polystyrene. The column packs beads of different sized pore diameters (Figure I-14A). The polymer molecules pass through the column by a combination of transport into and through the beads and through the interstitial volume (volume between the beads) as shown in Figure I-14B.

Molecules that penetrate the beads are slowed down more in moving through the column than the molecules that do not penetrate the beads or transported through the interstitial volume is faster than through the pores. The smaller size polymer molecules penetrate all the beads since their molecular size (hydrodynamic radius) is smaller than the pore size of the beads with the smallest size pores. A polymer with larger hydrodynamic radius does not penetrate all the beads. The larger the molecular weight (or hydrodynamic radius), the fewer beads are penetrated and polymer moves faster in the column through interstitial space. The time (or volume) of elution of polymer through column decreases with increasing molecular weight or hydrodynamic radius (Figure I-14C). The use of an appropriate detector (refractive index, viscosity, UV, light scattering) measure the amount of polymer passing through the column as a function of time (or elution volume). This information and a calibration of the column with standard polymer samples of known molecular weight allow one to obtain the molecular weight distribution in the form of a plot as shown in Figure I-14D.

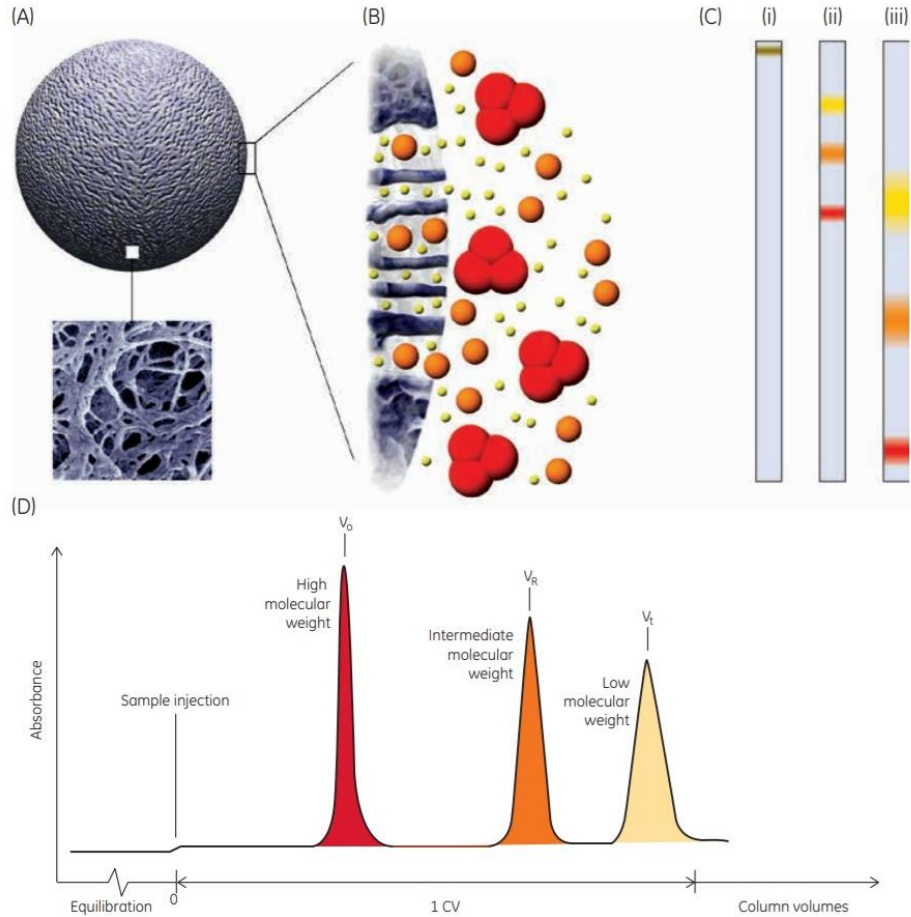


Figure I-14 Process of SEC. (A) Schematic picture of a bead with an electron microscopic enlargement. (B) Schematic drawing of sample molecules diffusing into bead pores. (C) the smallest molecule (yellow) is more delayed than the largest molecule (red); the largest molecule is eluted first from the column. V_0 is void volume, V_e is elution volume, and V_t is total liquid volume (Adapted from GE-Healthcare (2010b)).

I.4.2 Rheology

Rheology is a branch of physics which deals with deformation and flow behavior of any material. Therefore, it is a very important technique to study the mechanical properties of polymeric materials. The term rheology originates from the Greek word “rhei” meaning “to flow”. Rheometry is the measuring technology used to determine rheological properties. Modern rheometers can be used for shear and torsional tests. They operate with continuous rotation and rotational oscillation. Specific measuring systems can be used to carry out uniaxial tensile tests either in one direction of motion or as oscillatory tests. The Two-Plate Model is very popular and is used to define the rheological parameters needed for a scientific description of flow behavior. In these systems, shear is applied to a sample sandwiched between the two plates. The lower stationary plate is mounted on a very rigid support, and the upper plate can be moved parallel to the lower plate (Figure I-15).

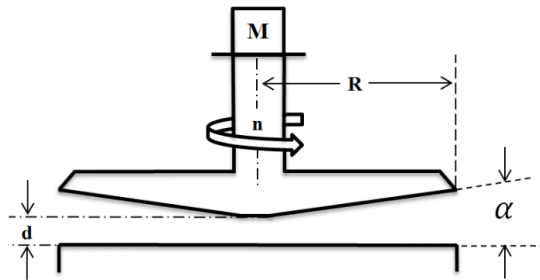


Figure I-15 Example of the Two-Plate Model, specifically Cone Plate (d is the truncation gap, R is the radius, and α is the cone angle).

Before discussing the viscoelastic properties, it is important to first define the shear stress and the shear rate.

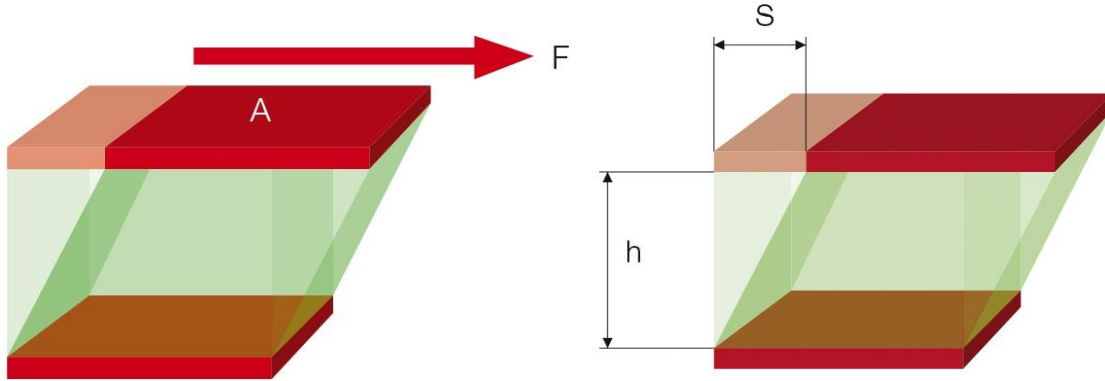


Figure I-16 Shear stress (on left) and shear strain (on right) using the Two-Plate Model with shear area A, shear force F, deflection path S, and shear gap h.

Shear stress (τ) is defined as the ratio of shear force (F, in Newton (N)) and shear area (A, in m^2) as shown in Figure I-16. A rheometer records the shear force via the torque at each measuring point and the size of the shear area for the measuring system is also known.

$$\tau = \frac{F}{A}$$

Shear strain (γ) is defined as the ratio of deflection path (S, in m) and shear gap (h, in m). The deflection path is recorded as deflection angle and the size of the shear gap is also known for the measuring system.

$$\gamma = \frac{S}{h}$$

Shear modulus (G) is the ratio of shear stress (τ) and shear strain (γ). This is the Law of Elasticity or Hooke's Law. According to this law, for solid matters, force is proportional to the deformation. The higher the G value, the stiffer the material.

$$G = \frac{\tau}{\gamma}$$

The complex shear modulus (G^*) describes entire viscoelastic behavior of a sample. G^* is a vector and can be divided into two components: storage modulus (G') and loss modulus (G'').

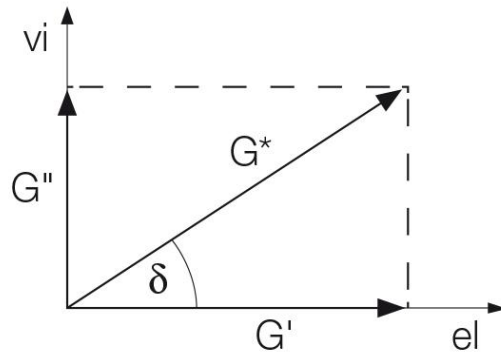


Figure I-17 Vector diagram illustrating the relation between complex shear modulus (G^*), storage modulus (G'), and loss modulus (G'') using the phase shift angle δ .

The G' value represents the elastic portion of the viscoelastic behavior, which quasi describes the solid-state behavior of the sample and G'' characterizes the viscous portion of the viscoelastic behavior, which can be seen as the liquid-state behavior of the sample. Phase shift angle (δ) is the time lag between the preset and the resulting sinusoidal oscillation determined for each measurement.

For viscoelastic solids, $G' > G''$ and on the other hand viscoelastic liquids will have $G'' > G'$.

I.4.3 Diffusion Ordered NMR Spectroscopy (DOSY NMR)

The molecules in liquid or solution state are always in rotational and translational motion. The translational motion is known as Brownian motion and is often simply referred as diffusion of self-diffusion. It depends on a lot of physical parameters like size and shape of molecules, temperature and viscosity. Assuming the spherical size of the molecule the diffusion coefficient D is described by the Stokes-Einstein equation

$$D = \frac{kT}{6\pi\eta r_s}$$

where k is Boltzmann constant, T is temperature, η is the viscosity of the liquid and r_s is hydrodynamic radius of the molecule.

Pulsed gradient NMR spectroscopy can be used to measure the translational diffusion of the molecules by using gradients, molecules can be spatially labeled, based on their position in the tube. If they move after the encoding, or ‘labeling’, during the diffusion time (Δ) that follows in the pulse sequence, their new position can be decoded with a second gradient. The measured signal was integrated over the whole sample volume and NMR signal intensity is attenuated depending on the diffusion time (Δ) and the gradient parameters (g and δ). The intensity change is described by

$$I = I_0 e^{-D(\gamma g \delta)^2 (\Delta - \frac{\delta}{3})}$$

where I is the observed intensity, I_0 is the reference intensity (unattenuated signal intensity), D is the diffusion coefficient, γ is the gyromagnetic ratio of the observed nucleus, g is the gradient strength, δ is the length of the gradient and Δ is the diffusion time.

I.5 References

- 1 Berzelius, J. J. *Jahresberichte* **1833**, 12, 63.
- 2 Simon, E. *Liebigs Ann. Chem.* **1839**, 31, 265.
- 3 Lourenco, A.-V. *Compt. Rend.* **1860**, 51, 365.
- 4 Lourenco, A.-V. *Ann. Chim. Phys.* **1863**, 3, 67.
- 5 Williams, C. G. *J. Chem. Soc.* **1862**, 15, 110.
- 6 Baekeland, L. H. *J. Ind. Eng. Chem. (Washington, D. C.)* **1913**, 5, 506.
- 7 Staudinger, H. B. H. *Berichte der Deutschen Chemischen Gesellschaft [Abteilung] B: Abhandlungen* **1924**, 57, 1203.
- 8 *Collected Papers of Wallace Hume Carothers on High Polymeric Substances*; Wiley-Interscience, New York, 1940.
- 9 Ziegler, K.; Holzkamp, E.; Breil, H.; Martin, H. *Angewandte Chemie* **1955**, 67, 541.
- 10 Natta, G.; Pino, P.; Corradini, P.; Danusso, F.; Mantica, E.; Mazzanti, G.; Moraglio, G. *Journal of the American Chemical Society* **1955**, 77, 1708.
- 11 Courtois, B. *Ann. Chim.* **1813**, 88, 304.
- 12 Gay-Lussac, J. L. *Ann. Chim.* **1813**, 88, 319.
- 13 Davy, H. *Ann. Chim.* **1813**, 88, 322.
- 14 Davy, H. *Phil. Trans. R. Soc. London* **1814**, 104, 74.
- 15 Drechsel, E. *Z. Biol.* **1896**, 33, 85.
- 16 Kendall, E. C. *J. Am Med. Assoc.* **1915**, 64, 2042.
- 17 Gay-Lussac, J. L. *Ann. Chim.* **1814**, 91, 5.
- 18 Schutzenberger, P. *Compt. Rend.* **1862**, 54, 1026.
- 19 Meyer, V.; Wachter, W. *Chem. Ber.* **1892**, 25, 2632.

- 20 Willgerodt, C. *Chem. Ber.* **1892**, 25, 3494.
- 21 Willgerodt, C. *Chem. Ber.* **1893**, 26, 1802.
- 22 Hartmann, C.; Meyer, V. *Chem. Ber.* **1894**, 27, 426.
- 23 Hartmann, C.; Meyer, V. *Chem. Ber.* **1894**, 27, 502.
- 24 Willgerodt, C. *Die Organischen Verbindungen mit Mehrwertigem Jod*; Ferdinand Enke, Stuttgart, 1914.
- 25 Sandin, R. B. *Chem. Rev.* **1943**, 32, 249.
- 26 Banks, D. F. *Chem. Rev.* **1966**, 66, 243.
- 27 Varvoglis, A. *Synthesis* **1984**, 709.
- 28 Moriarty, R. M.; Prakash, O. *Acc. Chem. Res.* **1986**, 19, 244.
- 29 Stang, P. J.; Zhdankin, V. V. *Chem. Rev.* **1996**, 96, 1123.
- 30 Zhdankin, V. V.; Stang, P. J. *Chem. Rev.* **2002**, 102, 2523.
- 31 Moriarty, R. M. *J. Org. Chem.* **2005**, 70, 2893.
- 32 Wirth, T. *Angew. Chem. Int. Ed.* **2005**, 44, 3656.
- 33 Zhdankin, V. V.; Stang, P. J. *Chem. Rev.* **2008**, 108, 5299.
- 34 Dohi, T.; Kita, Y. *Chem. Commun.* **2009**, 2073.
- 35 Zhdankin, V. V. *J. Org. Chem.* **2011**, 76, 1185.
- 36 Yoshimura, A.; Zhdankin, V. V. *Chem. Rev.* **2016**, 116, 3328.
- 37 Vaish, A.; Tsarevsky, N. V. In *Hypervalent Iodine Compounds in Polymer Science and Technology*; Wiley, 2017. pp 483.
- 38 Varvoglis, A. *Tetrahedron* **2010**, 66, 5739.
- 39 Varvoglis, A. *Organic Compounds of Polycoordinated Iodine*; Wiley-VCH, Weinheim, 1992.

- 40 Varvoglis, A. *Hypervalent Iodine in Organic Synthesis*; Academic Press, San Diego, 1997.
- 41 Wirth, T. *Hypervalent Iodine Chemistry: Modern Developments in Organic Synthesis*; Springer, Berlin, 2003.
- 42 Zhdankin, V. V. *Hypervalent Iodine Chemistry: Preparation, Structure and Synthetic Applications of Polyvalent Iodine Compounds*; Wiley, Chichester, 2014.
- 43 Lewis, G. N. *J. Am. Chem. Soc.* **1916**, 38, 762.
- 44 Langmuir, I. *J. Am. Chem. Soc.* **1916**, 41, 868.
- 45 Pauling, L. *The Nature of the Chemical Bond*; Cornell University Press, Ithaca, 1950.
- 46 Hach, R. J.; Rundle, R. E. *J. Am. Chem. Soc.* **1951**, 73, 4321.
- 47 Pimentel, G. C. *J. Chem. Phys.* **1951**, 19, 446.
- 48 Rundle, R. E. *J. Am. Chem. Soc.* **1963**, 85, 112.
- 49 Hudson, R. F. *Angew. Chem. Int. Ed.* **1967**, 6, 749.
- 50 Mitchell, K. A. R. *Chem. Rev.* **1969**, 69, 157.
- 51 Musher, J. I. *Angew. Chem. Int. Ed.* **1969**, 8, 54.
- 52 Martin, J. C. *Science* **1983**, 221, 509.
- 53 Kutzelnigg, W. *Angew. Chem. Int. Ed. Engl.* **1984**, 23, 272.
- 54 McGrady, G. S.; Steed, J. W. In *Hypervalent Compounds*; Wiley, Chichester, 2005; Vol. 3. pp 1.
- 55 Akiba, K.-y. In *Chemistry of Hypervalent Compounds*; Wiley-VCH, New York, 1999. pp xvi + 414.
- 56 Perkins, C. W.; Martin, J. C.; Arduengo, A. J., III; Law, W.; Alegria, A.; Kochi, J. K. *J. Am. Chem. Soc.* **1980**, 102, 7753.
- 57 Muraki, T.; Togo, H.; Yokoyama, M. *Rev. Heteroatom Chem.* **1997**, 17, 213.

- 58 Akiba, K.-y.; Yamamoto, Y. *Heteroatom Chem.* **2007**, *18*, 161.
- 59 Richards, L. M. In *Iodoso diacylate catalysis of addition polymerization processes*; E. I. du Pont de Nemours & Co. . 1949.
- 60 Georgiev, G.; Spyroudis, S.; Varvoglis, A. *Polym. Bull. (Berlin)* **1985**, *14*, 523.
- 61 Georgiev, G.; Kamenska, E.; Khristov, L.; Sideridou, K.; Karayannidis, G.; Varvoglis, A. *Eur. Polym. J.* **1992**, *28*, 207.
- 62 Georgiev, G. S. *Polym. Bull. (Berlin)* **1999**, *43*, 223.
- 63 Otsu, T.; Yoshida, M.; Kuriyama, A. *Polym. Bull. (Berlin)* **1982**, *7*, 45.
- 64 Cao, Y.; Kumar, R.; Tsarevsky, N. V. *Macromol. Chem. Phys.* **2019**, *220*, n/a.
- 65 Georgiev, G. S.; Kamenska, E. B.; Tsarevsky, N. V.; Christov, L. K. *Polym. Int.* **2001**, *50*, 313.
- 66 Georgiev, G.; Kamenska, E.; Tsarevsky, N.; Christov, L.; Koseva, N.; Proynov, D. *God. Sofii. Univ. "Sv. Kliment Okhridski", Khim. Fak.* **2002**, *95*, 27.
- 67 Asandei, A. D.; Adebolu, O. I.; Simpson, C. P.; Kim, J.-S. *Angew. Chem., Int. Ed.* **2013**, *52*, 10027.
- 68 Kumar, R.; Cao, Y.; Tsarevsky, N. V. *J. Org. Chem.* **2017**, *82*, 11806.
- 69 Han, H.; Tsarevsky, N. V. *Polym. Chem.* **2012**, *3*, 1910.
- 70 Han, H.; Tsarevsky, N. V. *Chem. Sci.* **2014**, *5*, 4599.
- 71 Han, H.; Kumar, R.; Tsarevsky, N. V. *Macromol. Rapid Commun.* **2019**, *40*, n/a.
- 72 Tsarevsky, N. V. *J. Polym. Sci., Part A: Polym. Chem.* **2010**, *48*, 966.
- 73 Liu, D.; Bielawski, C. W. *Polym. Int.* **2017**, *66*, 70.

CHAPTER II

HYPERVALENT IODINE BASED DYNAMIC NETWORK AND STAR POLYMERS

II.1 Introduction

The design and preparation of dynamic polymer gels that are formed based on reversible covalent interactions is of great interest¹⁻¹⁶ since these types of materials possess unique property like self-healing.¹⁷⁻²⁶ Self-healing is described as the property that enables a material to restore itself to normality by healing the damages automatically and intrinsically.²⁷⁻³¹ This phenomenon usually occurs without any intervention of external stimulus to promote the extent of self-healing and the material regains its associated mechanical strength depending on the self-healing efficiency.³²⁻³⁶ Self-healing mandates the re-formation of covalent bonds or re-bonding to material to its indigenous state, *e.g.*, cutting a gel in half and then allowing it to bond back together again.^{33, 37} Development of self-healing materials has the potential to extend the life-time of a material. Additionally, self-healing property increases the durability and reliability of a material. In certain applications, it reduces the safety risks by avoiding the failures caused by the accumulation of cracks or breaks.

In this work, we took advantage of ligand exchange reactions performed by HV iodine(III) compounds to prepare dynamic and self – healing polymer networks. HV iodine compounds are primarily used as oxidizing agents³⁸⁻⁴¹ and initiators for cationic⁴²⁻⁴⁴ and radical⁴⁵⁻⁴⁸ polymerizations. Due to the high polarity of the 3-center-4-electron HV bond,⁴⁹⁻⁵¹ L-I-L bonds in

a typical HV iodine(III) compound, ArIL_2 (where L is ligand, *e.g.* L = Cl, RCO_2 etc.) are dynamic in nature⁵² and “ligands”, L, which are directly connected to iodine(III) atom, can be replaced by nucleophiles.⁵³ These ligand exchange reactions are mainly used to synthesize new HV iodine compounds by interchanging the existing ligands with desired nucleophile. For example, several λ^3 -iodanes are prepared by exchanging the ligands of HV iodine(III) compounds like (diacetoxyiodo)benzene ($\text{PhI}(\text{OAc})_2$), (dichloroiodo)benzene (PhICl_2) or [bis(trifluoroacetoxy)iodo]benzene ($\text{PhI}(\text{OCOCF}_3)_2$) with desired nucleophilic compounds like various acids, azides and tetrazoles.^{38, 54} In the world of polymer chemistry, utilization of ligand exchange reaction is rather uncommon. Previously, our group reported that the acetoxy groups in $\text{PhI}(\text{OAc})_2$, can exchange with methacrylic acid in various solvents yielding [(acetoxy methacryloyloxy)iodo]benzene or (dimethacryloyloxyiodo)benzene and the last two HV iodine compounds can serve as inimers due to the presence of polymerizable moiety and the easy generation of radicals upon thermal or light-induced homolysis of the I–O bonds.⁵⁵ Subsequently, similar ligand exchange reaction was employed to develop azide-containing linear and branched polymers.⁵⁶

Herein we report preparation of dynamic polymer networks by mixing solutions of $\text{PhI}(\text{OAc})_2$ and copolymers containing pendant carboxylic acid groups and the dynamic nature of the gel comes from the ligand – exchange between the HV crosslinked bonds and available nucleophiles or the ligand exchange between the two HV crosslinks itself. The advantage of using HV iodine compound as a crosslinker is the dynamic nature of HV bond which provides quick self-healing ability to the gel.

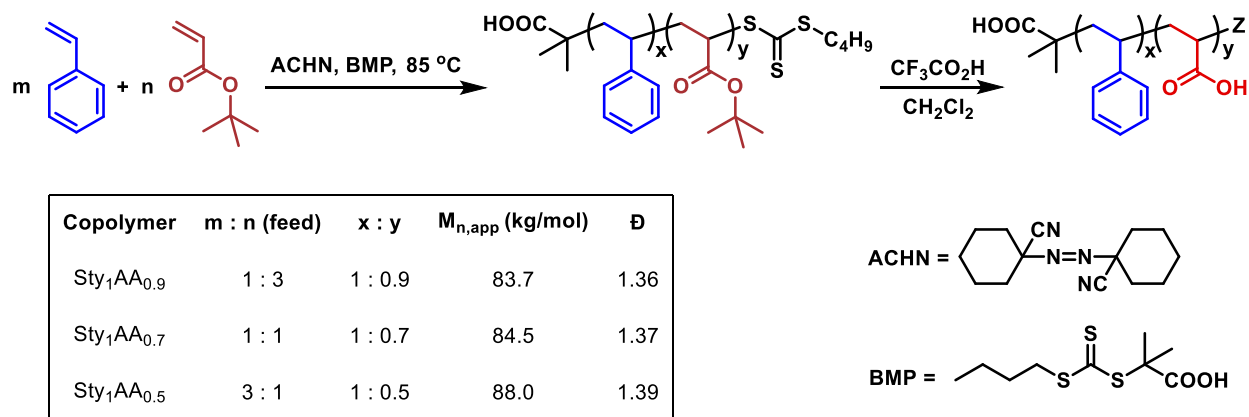
Due to the 3c-4e HV bond which is weaker than traditional 2-center-2-electron bond, HV iodine(III) compound, ArIL_2 , can also dissociate homolytically upon heating or irradiation and

yield iodoarene and the radicals $L\cdot$.^{39, 47, 57-61} For example, $\text{PhI}(\text{OAc})_2$ can yield acetoxy radicals ($\text{CH}_3\text{CO}_2\cdot$) upon heating or irradiation which can in turn further decarboxylate into $\text{CH}_3\cdot$ and the newly formed radical can couple with another $\text{CH}_3\cdot$ to form a coupling product in a closed systems. Following similar phenomenon, the HV crosslink bonds in the dynamic gel can dissociate in presence of heat or light to generate radicals in the pedant chains of polymers. These radicals, in turn, couple with each other and form a permanent crosslink bond to convert a dynamic and self-healing gel to a permanently crosslinked gel. This unique property gives flexibility to use the same polymer gel for different applications. Herein, we report the preparation of dynamic gels using $\text{PhI}(\text{OAc})_2$ and their conversion to permanent gels using UV light.

II.2 Results and Discussion

II.2.1 HV Iodine Based Network Polymers

The reversible addition–fragmentation chain transfer (RAFT) polymerization⁶²⁻⁶⁵ of Sty and tBA (Scheme II-1) was performed to prepare three different random copolymers – $\text{Sty}_1\text{tBA}_{0.9}$, $\text{Sty}_1\text{tBA}_{0.7}$, and $\text{Sty}_1\text{tBA}_{0.5}$, where the numbers indicate the molar ratios of the monomer units in the final isolated copolymers, determined by ^1H NMR spectroscopy. tBA was chosen as monomer instead of acrylic acid to get better control on the polymerization over a long time period. The polymerizations were carried out in bulk at 85 °C for 40-50 h depending on the monomer feed ratio. ACHN was chosen as initiator because of its relatively long half-life time at the conditions of the experiment (the reported value is 16 h at 85 °C in toluene⁶⁶). BMP was used as the chain transfer agent, which controls well the polymerization of both acrylates and styrenes. As the polymerizations proceeded, the number-average molecular weights ($M_{n,\text{app}}$) increased and the MWDs narrowed (Figure II-1).



Scheme II-1 Synthesis of carboxylate group-containing copolymers by copolymerization of Sty and tBA under RAFT polymerization conditions, followed by deprotection of the tert-butyl ester groups in the presence of CF_3CO_2H .

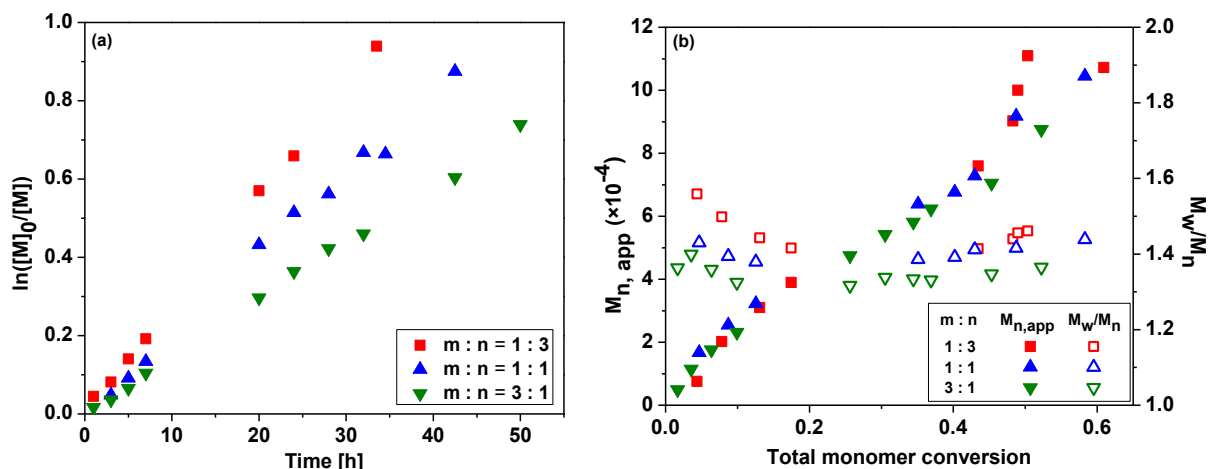


Figure II-1 Kinetics of RAFT copolymerization of Sty and tBA (a); evolution of $M_{n,app}$ and M_w/M_n with monomer conversion (b)

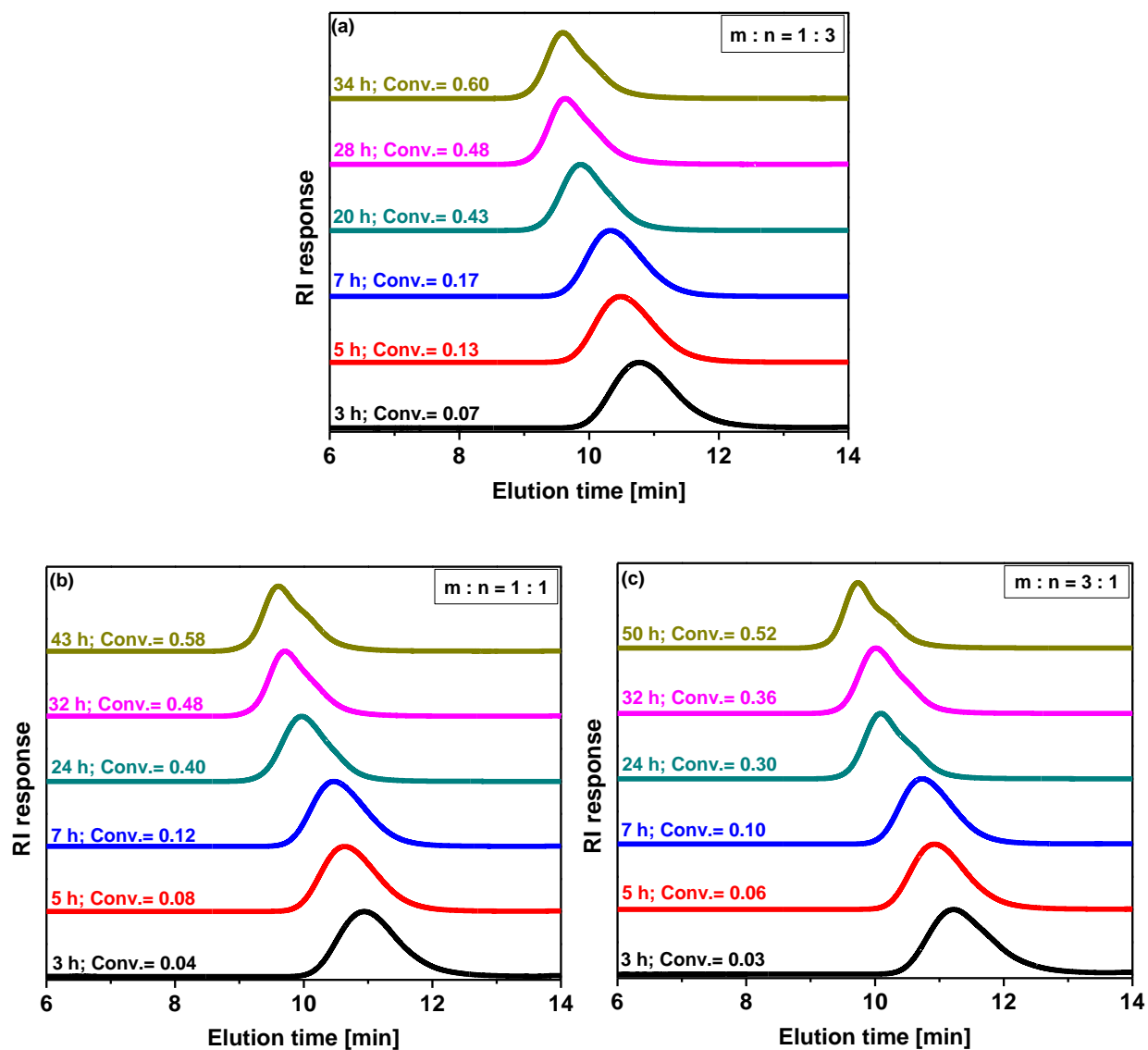


Figure II-2 Evolution of SEC traces of the polymers obtained using feed molar ratios of Sty and tBA equal to 1:3 (a), 1:1 (b), and 3:1 (c). The reaction times and monomer conversions are shown at each curve.

After preparing the random copolymers, the *tert*-butyl ester groups were removed using $\text{CF}_3\text{CO}_2\text{H}$. The apparent molecular weights of all three copolymers after the deprotection were similar (83,700-88,000 g/mol).

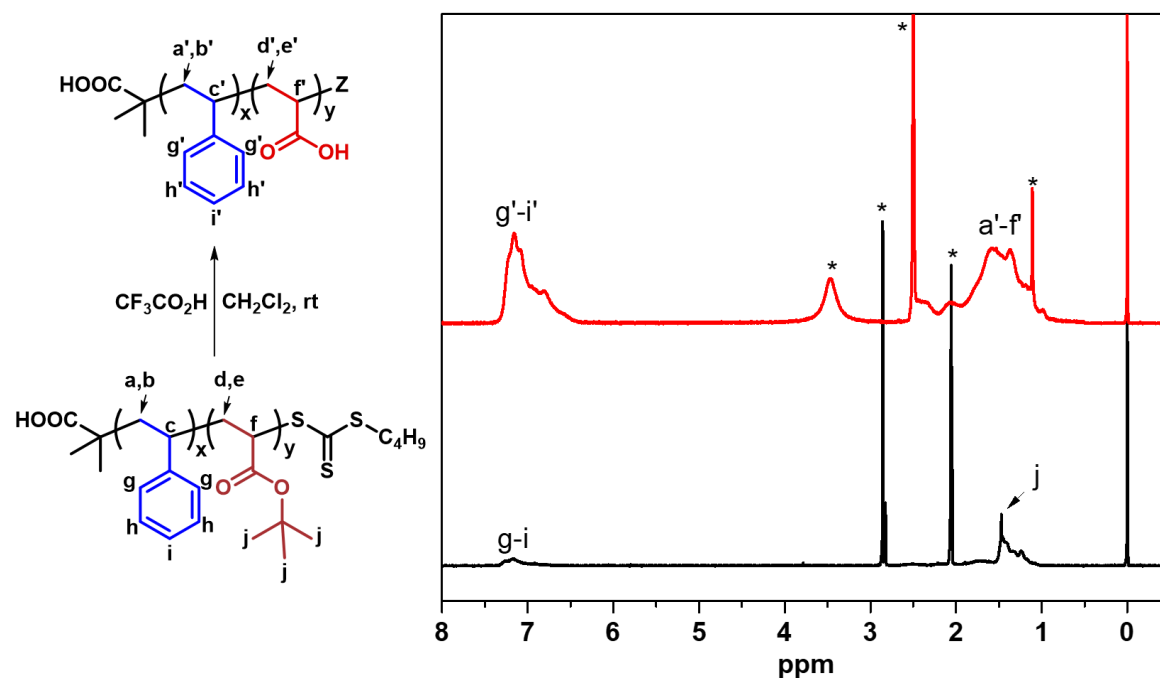
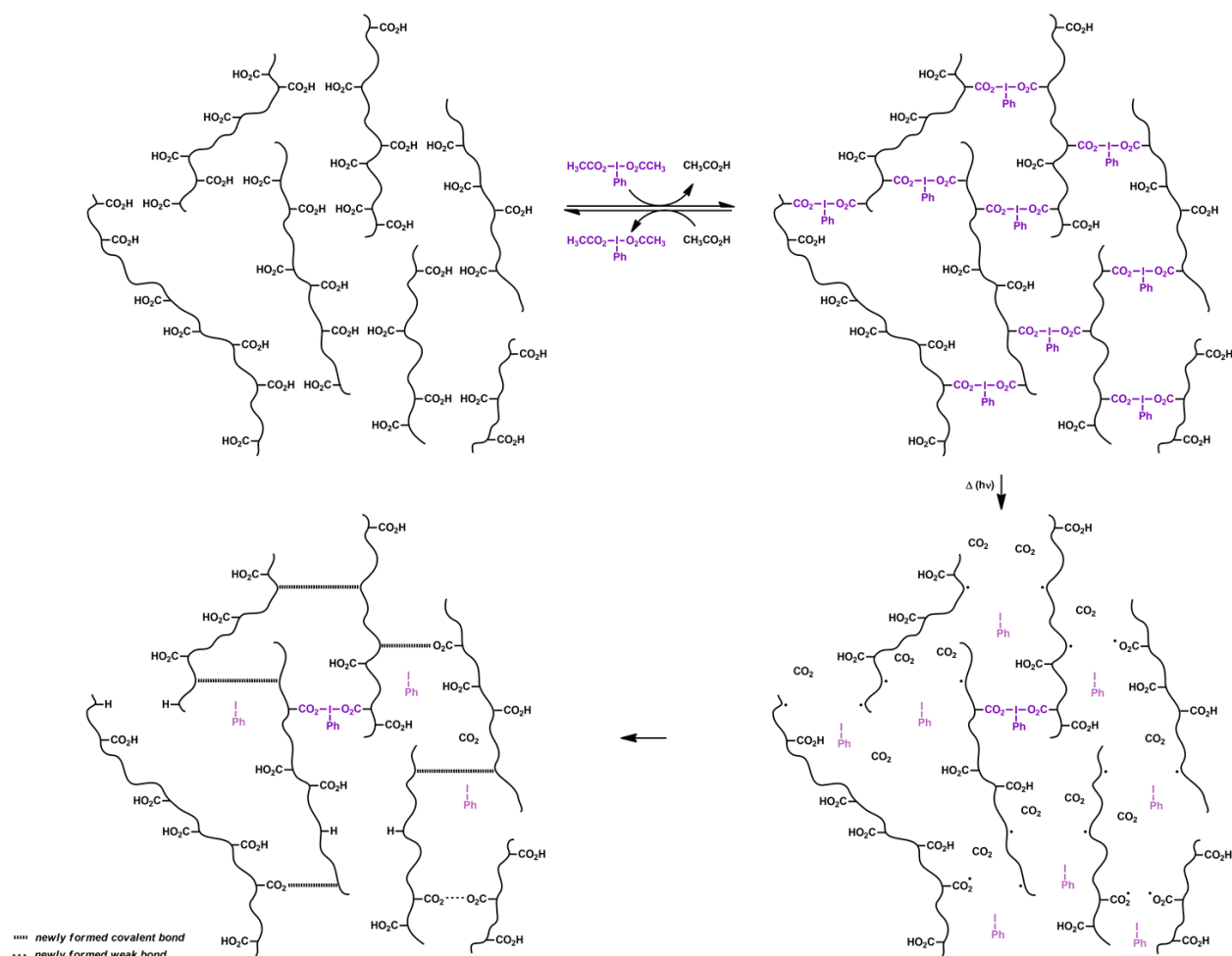


Figure II-3 ^1H NMR spectra of poly(Sty-co-tBA) (bottom) and poly(Sty-co-AA) (top) in acetone- d_6 and DMSO- d_6 , respectively. The peaks marked with asterisks belong to residual solvents.

II.2.1.1 Preparation of dynamic gels

(Diacyloxyiodo)arenes can participate in ligand-exchange reactions with nucleophiles, including carboxylates. In this work, $\text{PhI}(\text{O}_2\text{CCH}_3)_2$ was used to prepare dynamic network utilizing the ligand exchange reaction between pendant carboxylate groups in poly(Sty-co-AA) and the acetoxy ligands attached to the HV iodine atom in $\text{PhI}(\text{O}_2\text{CCH}_3)_2$ as shown in Scheme II-2. First, three different poly(Sty-co-AA) copolymers (designated Sty₁AA_{0.9}, Sty₁AA_{0.7}, and Sty₁AA_{0.5}, as explained in Scheme II-1) were prepared by removal of the *tert*-butyl ester groups in the poly(Sty-co-tBA) precursors by treatment with $\text{CF}_3\text{CO}_2\text{H}$. A dynamic gel was then prepared by mixing 200 μL of $\text{PhI}(\text{O}_2\text{CCH}_3)_2$ (0.15 M) and 300 μL of Sty₁AA_{0.9} (0.73 M with respect to carboxylate groups) solutions prepared in DMAc, with or without addition of trace amounts of Co Blue (added to distinguish the line where two pieces of gels were joined together in the self-healing

experiments). Once the gel was formed, the HV iodine center could exchange ligands with unreacted carboxylate acid groups, or external nucleophiles. The Sty₁AA_{0.5} copolymer did not form a gel with PhI(O₂CCH₃)₂, most likely due to insufficient amount of accessible carboxylate pendant groups in the copolymer. The formation of network polymers and their transformations in the presence of monocarboxylic acids, or upon irradiation or heating are presented in Scheme II-2.



Scheme II-2 Preparation of dynamic gels via carboxylate ligand-exchange reactions with PhI(O₂CCH₃)₂, curing of the gels using light or heat, and conversion of the dynamic to permanent network following the coupling of some of the radicals formed during the curing step.

To confirm the dynamic nature of the network polymers, a small amount of $\text{CH}_3\text{CO}_2\text{H}$ (100 μL , 1.75 mmol) was added after washing the gel twice with DMAc and, as expected, the gel completely disintegrated in 12 h to yield the initial copolymer and $\text{PhI}(\text{O}_2\text{CCH}_3)_2$, as shown in Figure II-4.

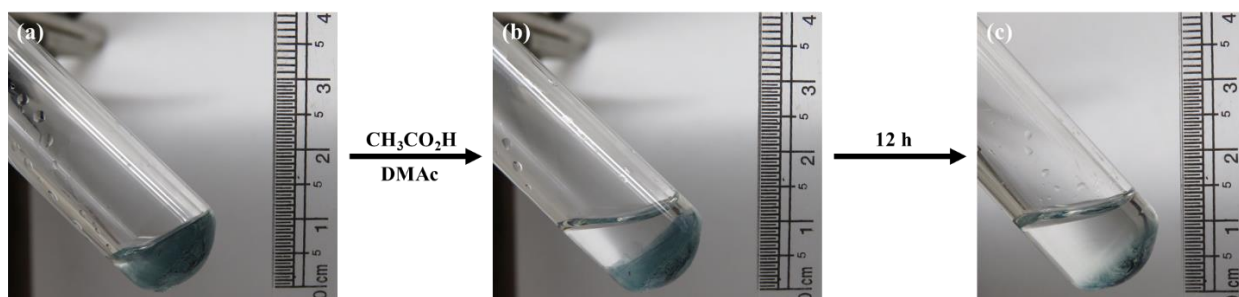


Figure II-4 Dynamic gel 15 min after mixing copolymer $\text{Sty}_1\text{AA}_{0.9}$ (300 μL , 0.73 M with respect to carboxylate groups) and $\text{PhI}(\text{O}_2\text{CCH}_3)_2$ (200 μL , 0.15 M) solutions (a), gel immediately after addition of DMAc and $\text{CH}_3\text{CO}_2\text{H}$ (600 μL , 5:1 (v/v)) (b), and degraded gel 12 h after the addition of $\text{CH}_3\text{CO}_2\text{H}$ (c). The precipitate on the bottom of the tube consists of Co Blue.

The same experiment was repeated with azide as a nucleophile, and again the gel disintegrated as shown in Figure II-5. This reaction yields the very unstable $\text{PhI}(\text{N}_3)_2$,⁶⁷ which degrades readily with the formation of iodobenzene PhI and the highly reactive azide radicals.⁶⁸ The dynamic gel also degraded upon addition of reducing agent, Bu_3P , which reduces iodine(III) to iodine(I),⁶⁹ *i.e.*, PhI , leading to gel degradation (Figure II-5). This reductive degradation in the presence of Bu_3P was recently demonstrated to occur in closely-related branched polymers with (diacyloxyiodo)benzene groups at the branching points.⁷⁰

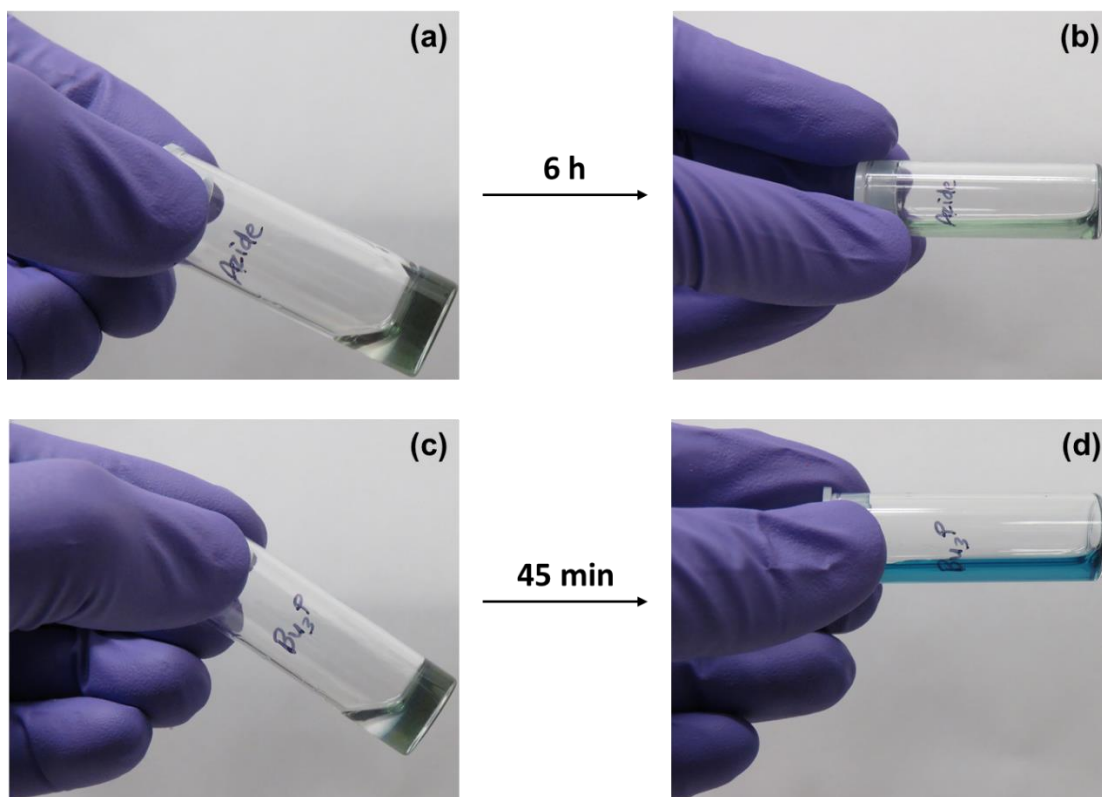


Figure II-5 Gels with (diacyloxyiodo)benzene-type groups at the crosslinks treated with NaN_3 solution (a, b) or Bu_3P (c, d). The first picture in each case shows the gel right after the addition of the reagent, and the second picture shows the degraded gel after the specified time.

II.2.1.2 Self-Healing and Rheological Properties of Dynamic Gels

After establishing the dynamic nature of the gels, their ability to self-heal was examined. As a preliminary experiment, two circular disk-shaped gels were prepared by mixing 400 μL of $\text{Sty}_1\text{AA}_{0.7}$ (0.35 M) solution and 100 μL of $\text{PhI}(\text{O}_2\text{CCH}_3)_2$ (0.15 M) solution prepared in DMAc, one of which contained a minuscule amount of indigo carmine dye to provide color difference, in a round plastic vial cap. Gelation occurred within ca. 10 min and the gels were transparent in appearance (Figure II-6). Then, the disk-shaped gels were cut in halves and the pieces were swapped and kept in contact for 30 min without any external pressure. The free carboxylate groups and HV crosslinks present on the surface of one piece of cut gel could participate in ligand-

exchange with HV iodine centers on the other piece, which led to the re-formation of the network. As expected, the cut between the two original semicircular pieces became invisible after 30 min and the healed gel did not break at the conjoining line even upon stretching, which demonstrated the self-healing ability of the dynamic gel. The self-healing was also monitored under an optical microscope and a time-lapse video showing healing of the cut was recorded.

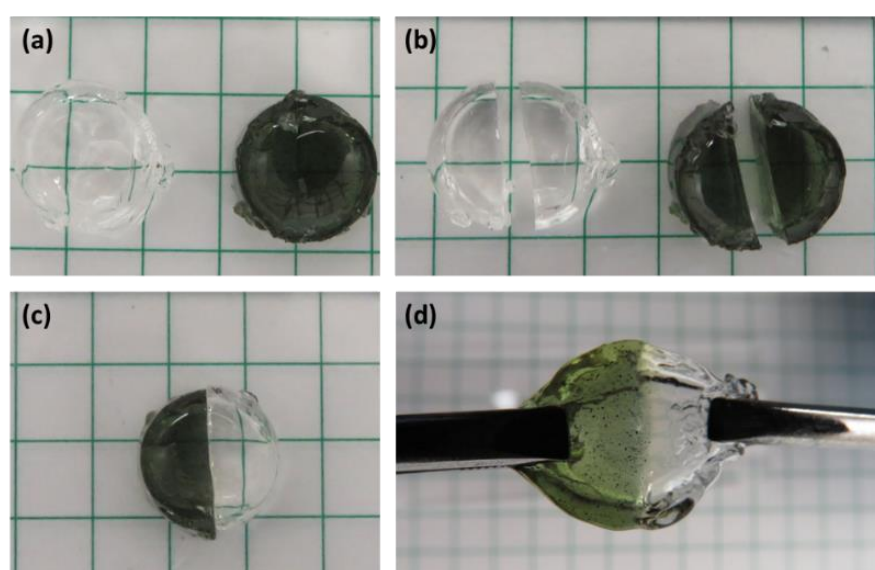


Figure II-6 Gels prepared by mixing solutions of Sty₁AA_{0.7} (400 μ L, 0.73 M with respect to carboxylate groups) and PhI(O₂CCH₃)₂ (100 μ L, 0.15 M) in DMAc with trace amount of indigo carmine present in one of the gels (a); the gels cut into two pieces (b); reattached semicircular segments taken from the two pieces of gels after 30 min (c); and effect of stretching on the self-healed gel (d).

The self-healing was then quantified by rheological measurements. The elastic response of the crosslinked network was analyzed first by strain amplitude sweep to determine the linear viscoelastic regime of the gel. In this experiment (Figure II-7), the storage and loss moduli (G' and G'' , respectively) were recorded as a function of the strain (γ) at a constant angular frequency

($\omega = 10$ rad/s). It was noticed that, in the viscoelastic region, *i.e.* 0.1% to ca. 500% strain, G' was constant and greater than G'' , but above a critical strain ($\gamma_c \approx 500\%$), it rapidly began to decline, which suggested the collapse of the crosslinked network. When the strain was increased to over 1200%, the values of G' became lower than G'' (Figure II-7a), which suggested that virtually no crosslinking between the polymer chains had been retained. At this point, the gel behaved like a viscoelastic liquid rather than a solid. In another experiment, the rheological behavior of the gel was assessed by subjecting it to increasing angular frequency ($\omega = 0.1$ -100 rad/s) at a constant strain (1%), which was in the viscoelastic regime. The G' values (ca. 230 Pa) were independent of ω and larger than the G'' values over the entire range of angular frequencies (Figure II-7b), which reaffirmed the formation of gel.^{71, 72}

After the preliminary rheological experiments, self-healing was confirmed by time-dependent strain sweep and continuous step-strain measurements. In the time-dependent strain sweep experiment, at first the strain was increased gradually, from 0.1 to 1300%, to break the network and then the strain was reduced to 1% for 300 s at a constant angular frequency ($\omega = 10$ rad/s), as shown in Figure II-7c. Interestingly, the gel exhibited a swift recovery of the mechanical strength after large amplitude oscillatory breakdown. The gel recovered ca. 85% of its original G' values in less than 20 s, which demonstrated efficient and rapid self-healing. Furthermore, continuous step-strain measurements were conducted to quantify the reproducibility of the self-healing. In this experiment, the gel was subjected to 1300% strain for 30 s and then the strain was decreased to 1% for 120 s. This cycle was repeated three times. When nonlinear, large amplitude oscillations ($\gamma = 1300\%$ at $\omega = 10$ rad/s) were applied to the gel, the values of G' decreased to ca. 10 Pa, resulting in viscoelastic fluid-like behavior ($\tan \delta (G''/G') \approx 1.5$). However, when the strain was decreased to 1%, the values of G' recovered promptly (within 20 s) to ca. 100 Pa and G' values

became greater than G'' values, showing quasi-solid-like behavior (Figure II-7d). Although the G' values were not completely restored after each cycle, the recovery of the gel was reproducible for at least three cycles. This was the conclusive evidence of self-healing nature of the gel.

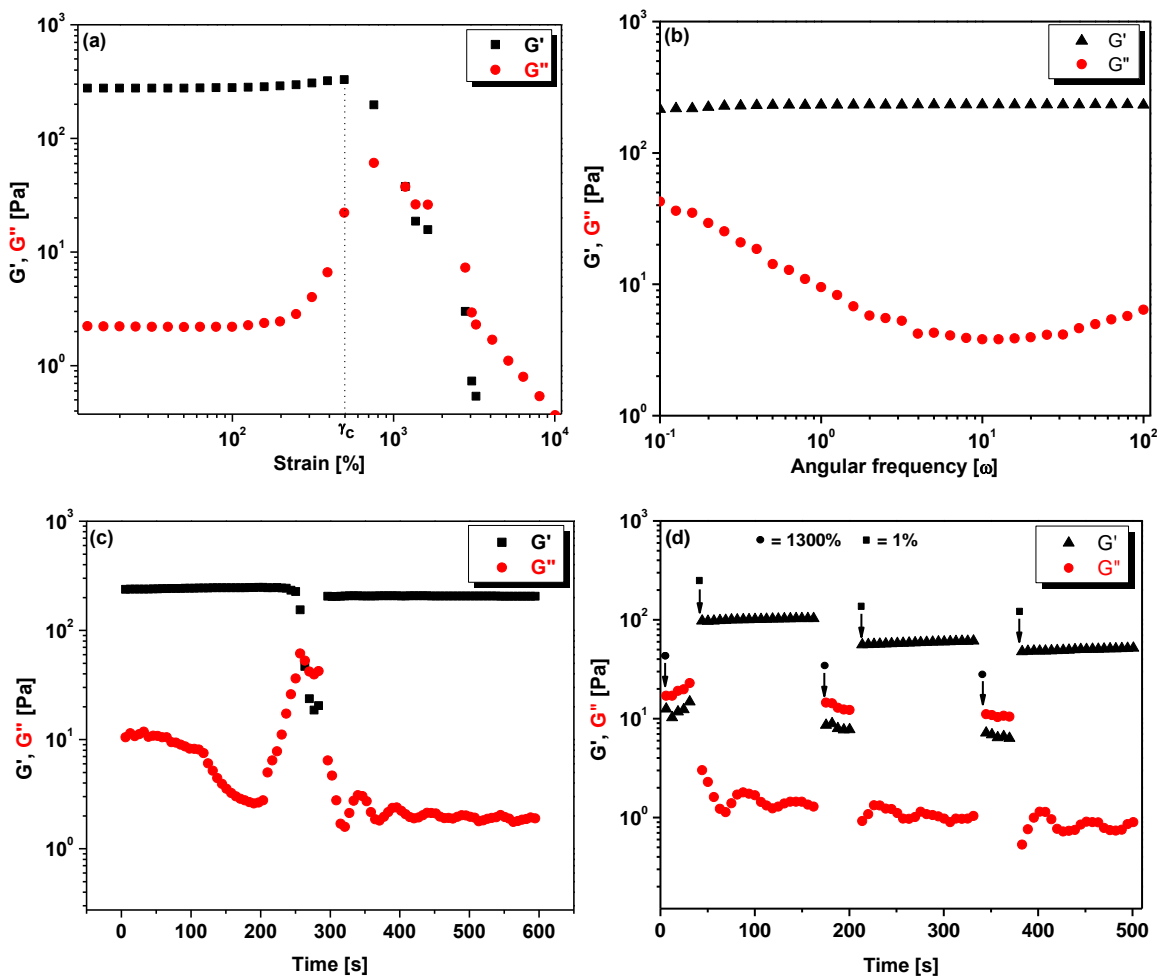


Figure II-7 G' and G'' values of a gel prepared by using $\text{Sty}_1\text{AA}_{0.7}$ and $\text{PhI}(\text{O}_2\text{CCH}_3)_2$ in DMAC (a) on strain amplitude sweep; (b) on angular frequency sweep; (c) in time-dependent strain sweep measurement, in which, strain was gradually increased from 0.1% to 1300% and then back to 1% strain for 300 s; (d) in continuous step strain measurement, gel was subjected to 1300% strain for 30 s, then go back to 1% strain in the linear regime for 120 s, and 3 cycles were carried out.

II.2.1.3 Conversion of Dynamic to Permanent Gels

The HV I-O bonds in $\text{ArI}(\text{O}_2\text{CR})_2$ can dissociate homolytically upon irradiation or heating to yield acyloxy radicals (RCO_2^\bullet) or the products of their decarboxylation (R^\bullet), along with iodoarene ArI. This property of the HV bonds was taken advantage of to convert the dynamic to permanently crosslinked gel by exposing the former to UV light or heat. Upon irradiation, some of the acyloxy and alkyl radicals attached to the polymer chains coupled to form permanent crosslinking, *i.e.*, non-dynamic network (Scheme II-2). The efficiencies of formation of the weak O-O bonds (via coupling of carboxylate radicals), which can be cleaved homolytically again to carboxylate radicals, and of the stable C-C or C-O bonds, responsible for the formation of permanent network, all depend on the flexibility of the polymer chains in the medium and the ease of diffusion of the macromolecular radicals. If these radicals cannot diffuse fast enough to couple, transfer reactions with the solvent are likely to occur, which will minimize and may even completely prevent the formation of permanent crosslinks.

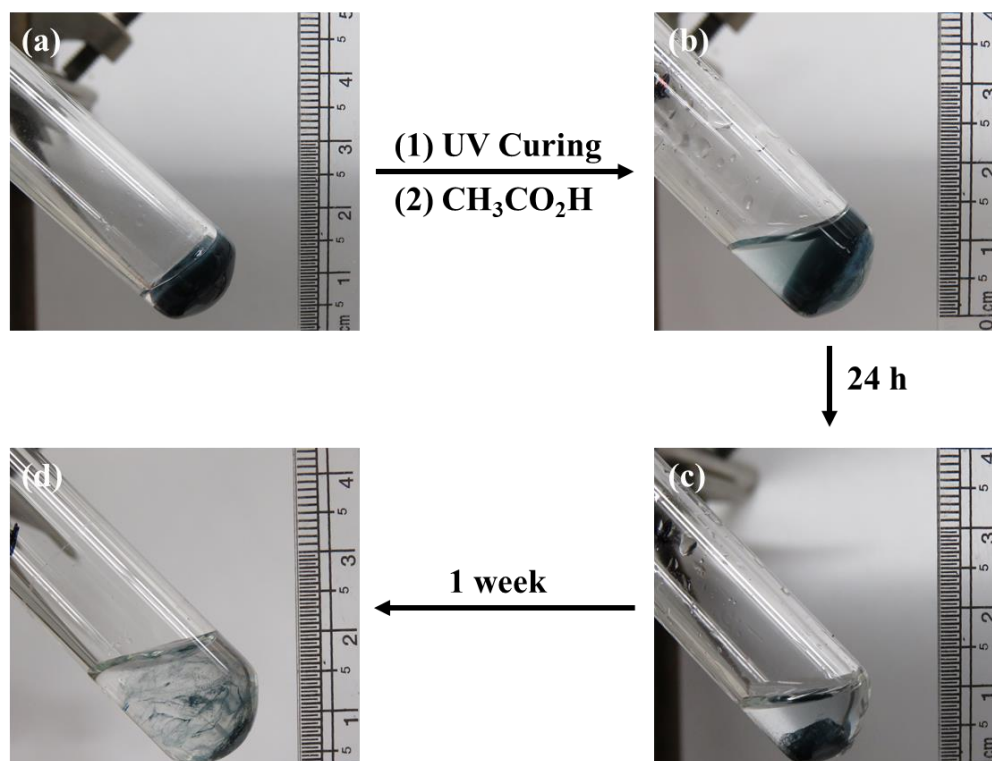


Figure II-8 a) Gel 15 mins after mixing of Sty₁AA_{0.9} (300 μ L, 0.73 M with respect to carboxylate groups) and PhI(O₂CCH₃)₂ (200 μ L, 0.15 M) solutions in DMAc. b) Gel after 30 mins of UV curing and addition of CH₃CO₂H in DMAc (600 μ L, 1:5 (v/v)). c) Washed gel 24 h after the addition of CH₃CO₂H and DMAc, and d) the same swollen gel after 1 week.

To show the conversion of dynamic to set, non-dynamic, network, an experiment was carried out by exposing the dynamic gel, prepared by mixing 200 μ L of PhI(O₂CCH₃)₂ (0.15 M) solution and 300 μ L of Sty₁AA_{0.9} (0.73 M with respect to carboxylate groups) solution in DMAc along with trace amount of Co Blue, to UV light (365 nm) for 30 min in a glass tube. After curing, 500 μ L of DMAc was added to the tube along with 100 μ L of glacial CH₃CO₂H. It was noticed that although some fraction of the gel degraded, a significant portion remained intact even after 24 h. This suggested that the dynamic gel was at least partially converted to permanently crosslinked network. Due to the moderate efficiency of radical coupling, and inconsistent curing throughout the gel, not all the dynamic linkages were converted to permanent bonds. In addition,

transfer reactions to the solvent could have occurred. The gel was then washed again with DMAc until all the side products and extra Co Blue was removed. Then, 1 mL of DMAc was added again to the tube, followed by 100 μ L of glacial $\text{CH}_3\text{CO}_2\text{H}$ and the gel was left for 1 week. Even after that period, the gel did not degrade but swelled to a larger degree than the original dynamic precursor, owing to low crosslinking density after the curing, as shown in Figure II-8d.

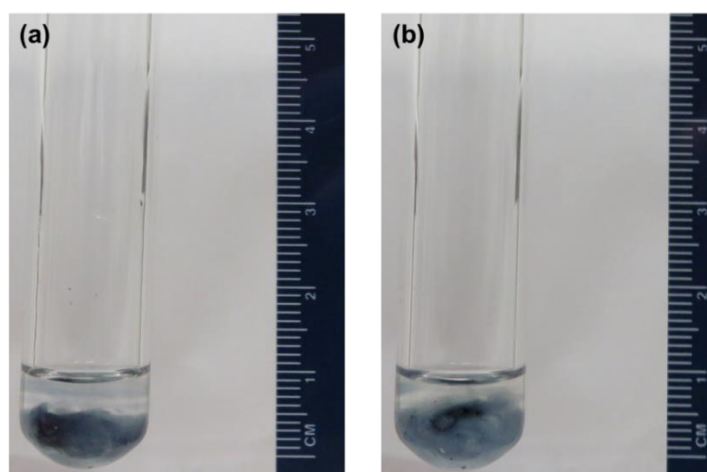


Figure II-9 Set gel prepared by microwave heating of dynamic gel just after the addition of $\text{CH}_3\text{CO}_2\text{H}$ (a) and 72 h later (b).

Similar conversion to permanent gel was conducted by microwave heating, but the gel was either completely degraded or not properly cured even after trying several different conditions. This is due to the high dielectric constant of DMAc,⁷³ because of which, it attains a high temperature at low power in a short time, when subjected to microwave. The steep increase in temperature does not give the gel enough time to set. Therefore, 1,4-dioxane was chosen since it has lower dielectric constant than DMAc⁷³ and it dissolved well both $\text{PhI}(\text{O}_2\text{CCH}_3)_2$ and the Sty-

AA copolymers. The gels prepared in 1,4-dioxane were cured efficiently by microwave as shown in Figure II-9.

To confirm the formation of permanently crosslinked network, continuous step-strain measurements were carried out on the UV-light-cured gel. In this experiment, a dynamic gel was formed by mixing 400 μL of $\text{PhI}(\text{O}_2\text{CCH}_3)_2$ (0.15 M) solution with 1600 μL of $\text{Sty}_1\text{AA}_{0.7}$ (0.35 M) solution in DMAc. Subsequently, the gel was cured by using two UV lamps (254 nm, 21 W) for 90 min, followed by continuous step-strain measurement. The gel was subjected to high-amplitude oscillations ($\gamma = 1300\%$, $\omega = 10$ rad/s) for 30 s, resulting in an increase in the $\tan \delta$ value, which showed quasi-liquid-like behavior. Moreover, G' did not recover to even close to its original value of 230 Pa. The average G' value measured under low amplitude oscillations ($\gamma = 1\%$, $\omega = 10$ rad/s) was only 33 Pa, which clearly suggested the scarcity of dynamic bonds, as expected. The data indicated that the major fraction of dynamic HV bonds were converted to permanent crosslinks (since the gel did not degrade in the presence of $\text{CH}_3\text{CO}_2\text{H}$). The self-healing efficiency was significantly decreased after the second and third cycle of high-amplitude oscillations due to unrecoverable damage to the dynamic bonds and crosslinked network during the first damage.

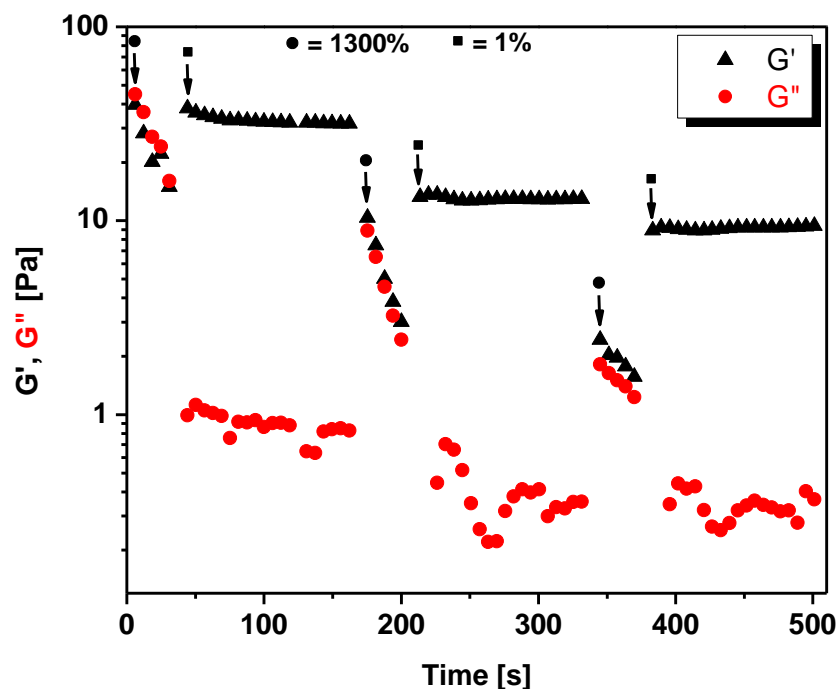


Figure II-10 Continuous step-strain measurement of the UV cured gel, in which, gel was subjected to 1300% strain for 30 s, then go back to 1% strain in the linear regime for 120 s, and 3 cycles were done.

Although the conversion of dynamic into permanent networks has been reported previously,¹⁴ the approach presented here has the advantage of using readily accessible monomers and crosslinkers. In principle, any polymer containing carboxylate groups can be employed to prepare dynamic networks, which can be readily converted into permanent ones by simple irradiation or thermal treatment.

II.2.2 HV Iodine-Based Star Polymers

In this section, another pathway is explored to prepared new polymeric species with covalently incorporated HVI building blocks based on the self-assembly of preformed anionic block copolymer in the presence of $\text{PhI}(\text{O}_2\text{CCH}_3)_2$. When the anionic block copolymers, such as

the well-defined polystyrene-block-poly(acrylic acid) (polySty-b-polyAA) and polymethyl methacrylate-block-poly(acrylic acid) (polyMMA-b-polyAA), were mixed with the $\text{PhI}(\text{O}_2\text{CCH}_3)_2$ in DMF (a good solution for both blocks), a mono-dispersed star-like copolymers were produced in situ through a self-assembling process driven by ligand exchange reactions.

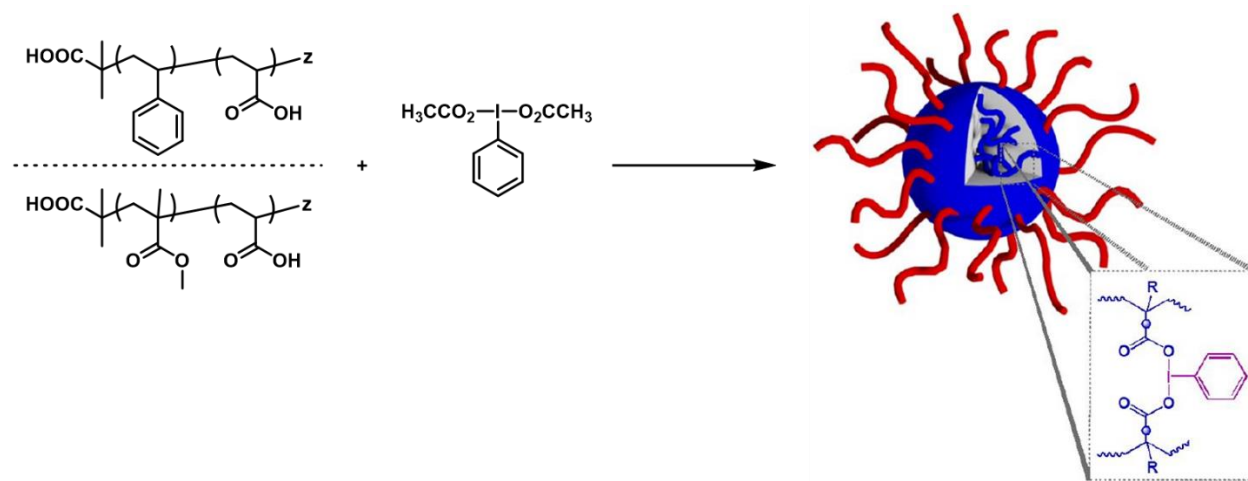
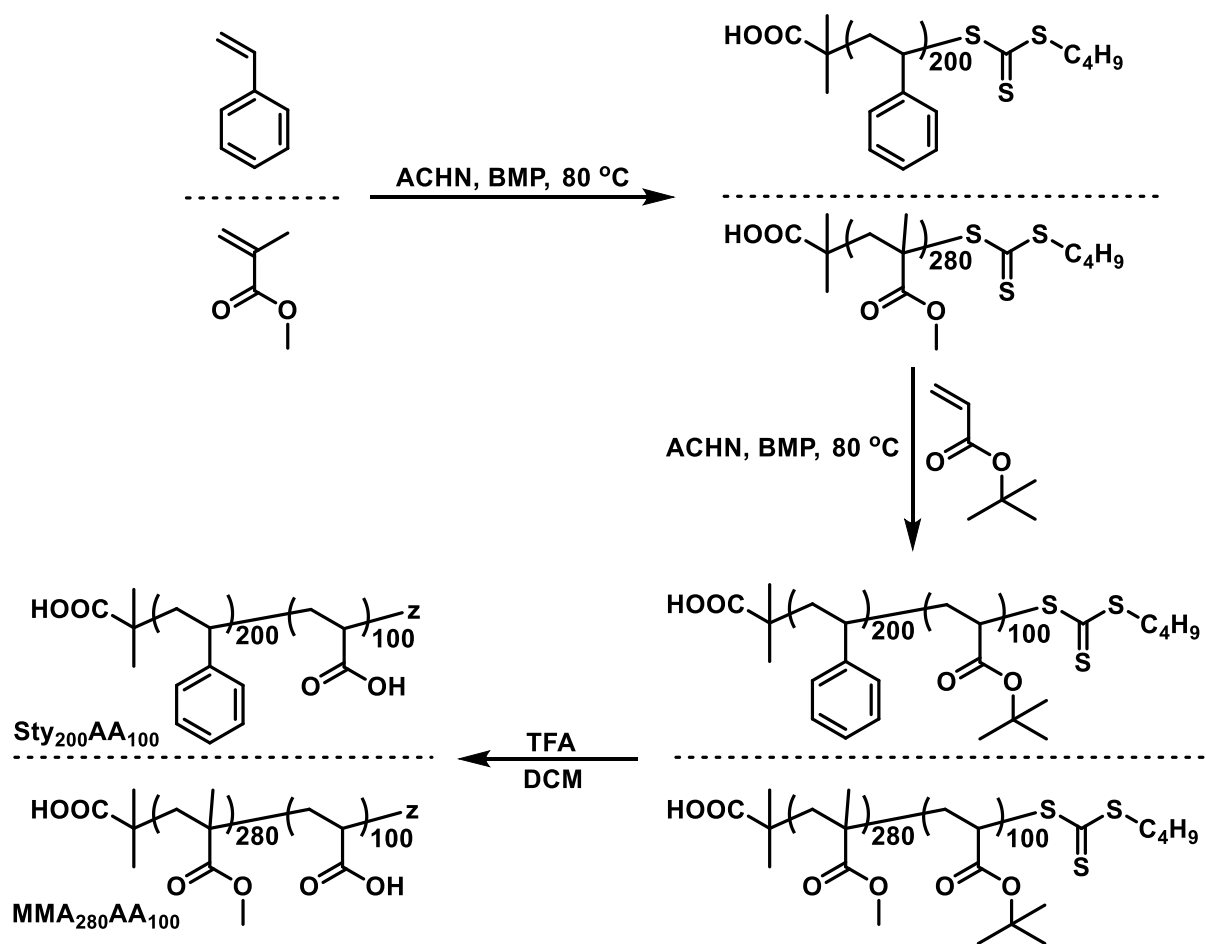


Figure II-11 Schematic representation of star polymers prepared by mixing solutions of block copolymers and $\text{PhI}(\text{O}_2\text{CCH}_3)_2$.

II.2.2.1 Synthesis of block copolymers

To synthesize block copolymers, first homopolymers of Sty (DP = 200) and MMA (DP = 280) were prepared using RAFT polymerization. The chain length of homopolymers were kept different to distinguish the size of resulting star polymers. The RAFT polymerization was carried out using BMP as chain transfer agent and ACHN as initiator at 80 °C as shown in Scheme II-3. BMP was chosen since it works well with Sty, MMA, and tBA. The polymerization kinetics was monitored using NMR (for conversion) and SEC (for molecular weight) as shown in Figure II-12. As the polymer reached required molecular weight, the polymerization was quenched by exposing

the reaction mixture to air. The polymers were purified by precipitating in methanol solution. To remove the impurities completely, polymer was again dissolved in CH_2Cl_2 and then precipitated again in methanol. This process was repeated three times. After purification, these polymers were used macro chain transfer agents to prepare block copolymers with tBA.



Scheme II-3 Synthesis of block copolymers Sty₂₀₀AA₁₀₀ and MMA₂₈₀AA₁₀₀

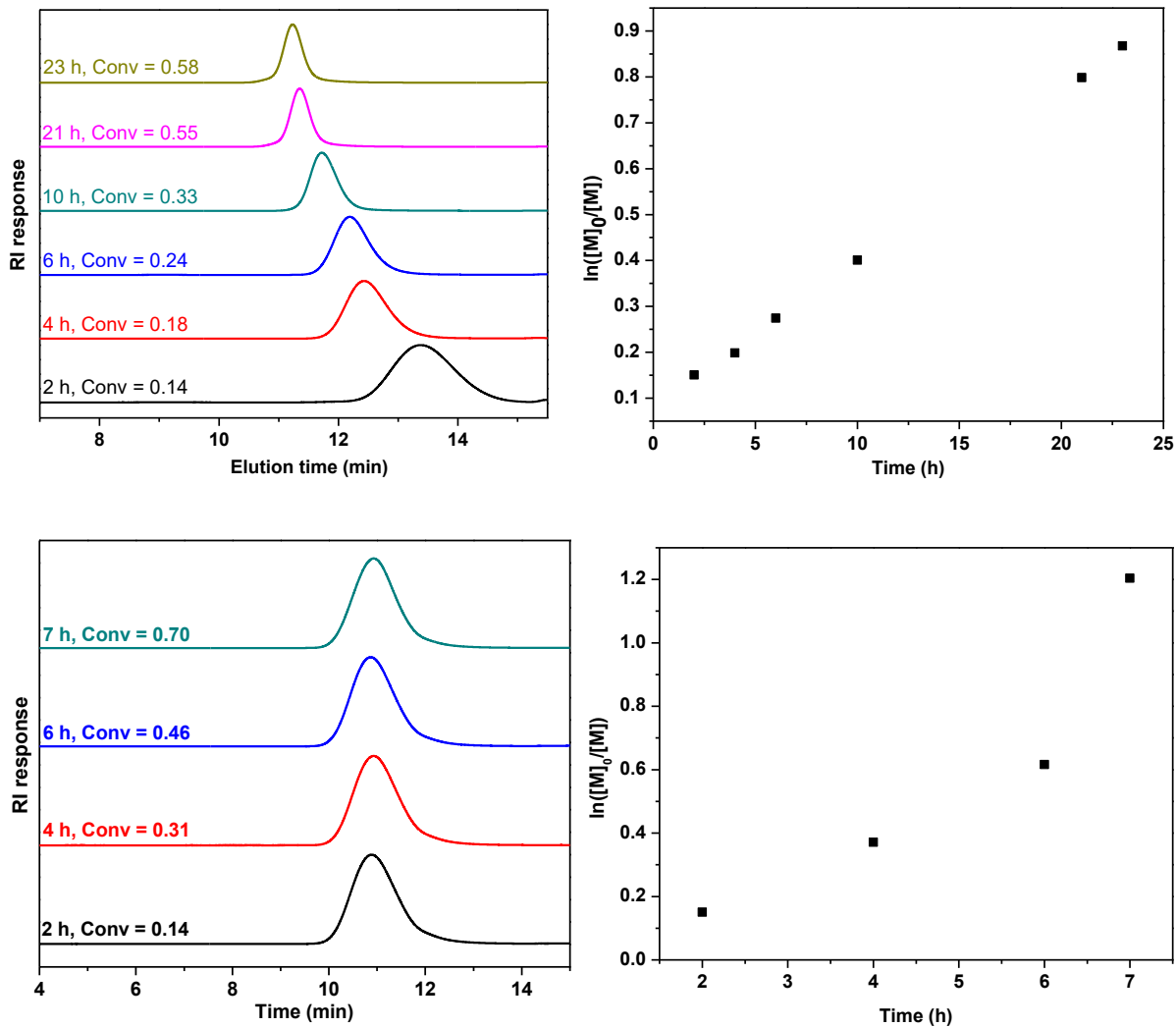


Figure II-12 Kinetics of homopolymerization of Sty and MMA.

Similar procedure was repeated to prepare the block copolymers (Sty₂₀₀tBA₁₀₀ and MMA₂₈₀tBA₁₀₀) with tBA. The number of repeating units for tBA were kept constant (DP = 100) to compare the results of star polymers. The kinetics of polymerization was monitored, and reaction was stopped after reaching desired molecular weight. After following the above-mentioned procedure, the final polymers were precipitated in methanol and vacuum dried.

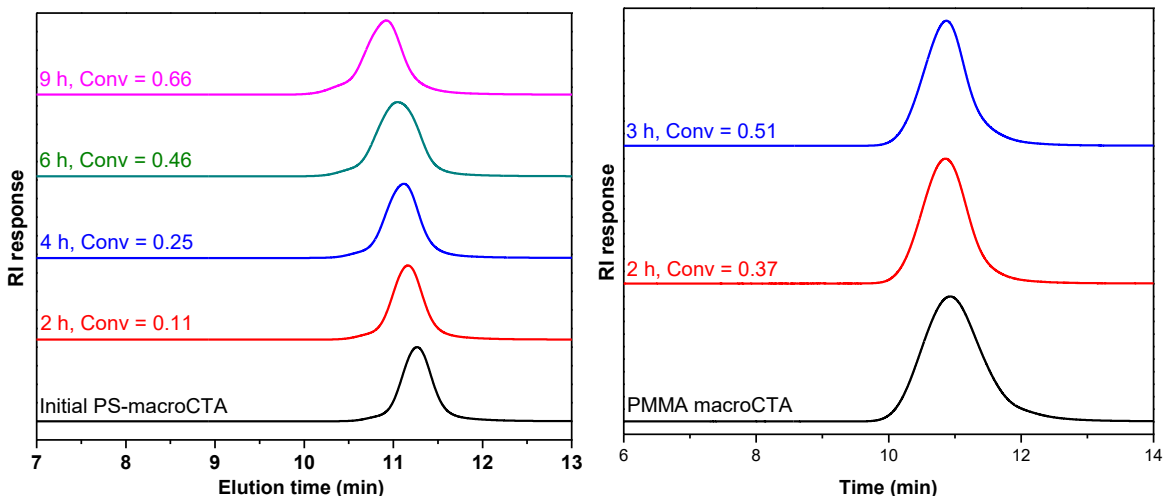


Figure II-13 Evolution of GPC traces during the synthesis of block copolymers.

II.2.2.2 Hydrolysis of Sty₂₀₀tBA₁₀₀ and MMA₂₈₀tBA₁₀₀

Hydrolysis of block copolymers was performed using TFA to hydrolyze the ester bond in DCM at room temperature. Reaction was monitored by NMR and after the methyl proton present in the tert-butyl groups were not visible in the NMR, the reaction was stopped, and polymers were precipitated in cold methanol to get block copolymers Sty₂₀₀AA₁₀₀ and MMA₂₈₀AA₁₀₀. The purified polymers were characterized by NMR.

II.2.2.3 Preparation and characterization of star polymers

The star polymers were prepared in-situ by mixing solutions of Sty₂₀₀AA₁₀₀ (or MMA₂₈₀AA₁₀₀) and PhI(O₂CCH₃)₂ (20 eq with respect to -COOH groups) prepared in DMF. DMF was chosen as solvent since it dissolves both polymer and HV iodine compound. The resulting solution was analyzed by dynamic light scattering (DLS) after 5 min of mixing. It was observed that the star polymers were formed immediately as shown in Figure II-14.

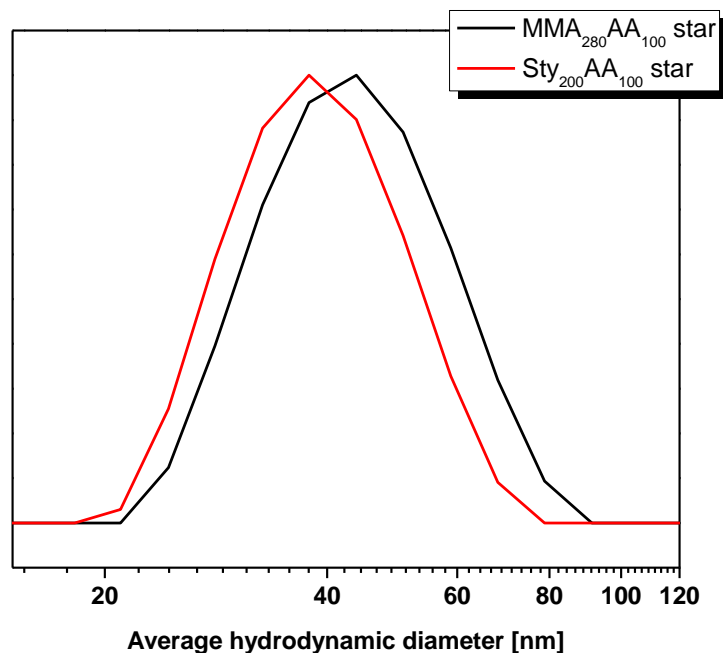


Figure II-14 DLS measurement of star polymers.

The DLS measurements were performed at constant temperature (25 °C) for every sample to maintain the viscosity of the solvent for better results. It was found that both polymers Sty₂₀₀AA₁₀₀ and MMA₂₈₀AA₁₀₀ formed similar size particles with hydrodynamic radius of 40 nm (PDI = 0.048) and 42 nm (PDI = 0.053), respectively.

Besides DLS, block copolymers and star polymers were characterized by diffusion ordered NMR spectroscopy (DOSY NMR) to measure and compare the diffusion coefficients. The parameters (gradient strength (g), gradient length (δ), and diffusion time (Δ)) for DOSY NMR were changed for each sample to get the best gradient. The DOSY NMR of all the polymers is shown in Figure II-15Figure II-18.

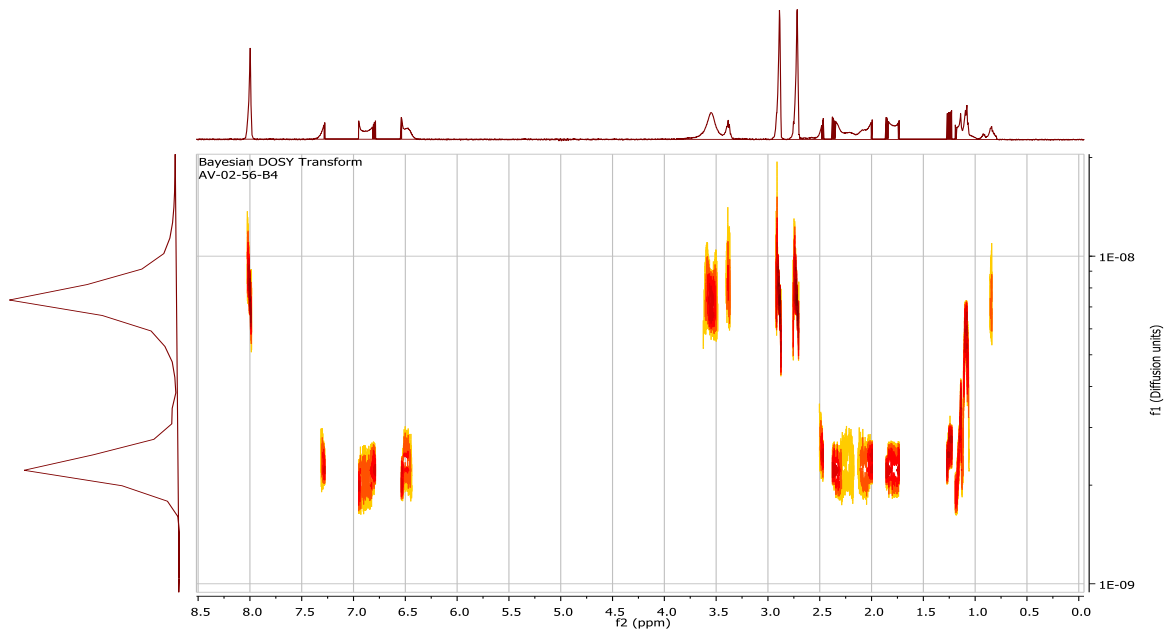


Figure II-15 . DOSY spectra of Sty₂₀₀AA₁₀₀. $\Delta = 0.2$ s; $\delta = 2$ ms; g was varied from 27 mT/m to 0.27 T/m.

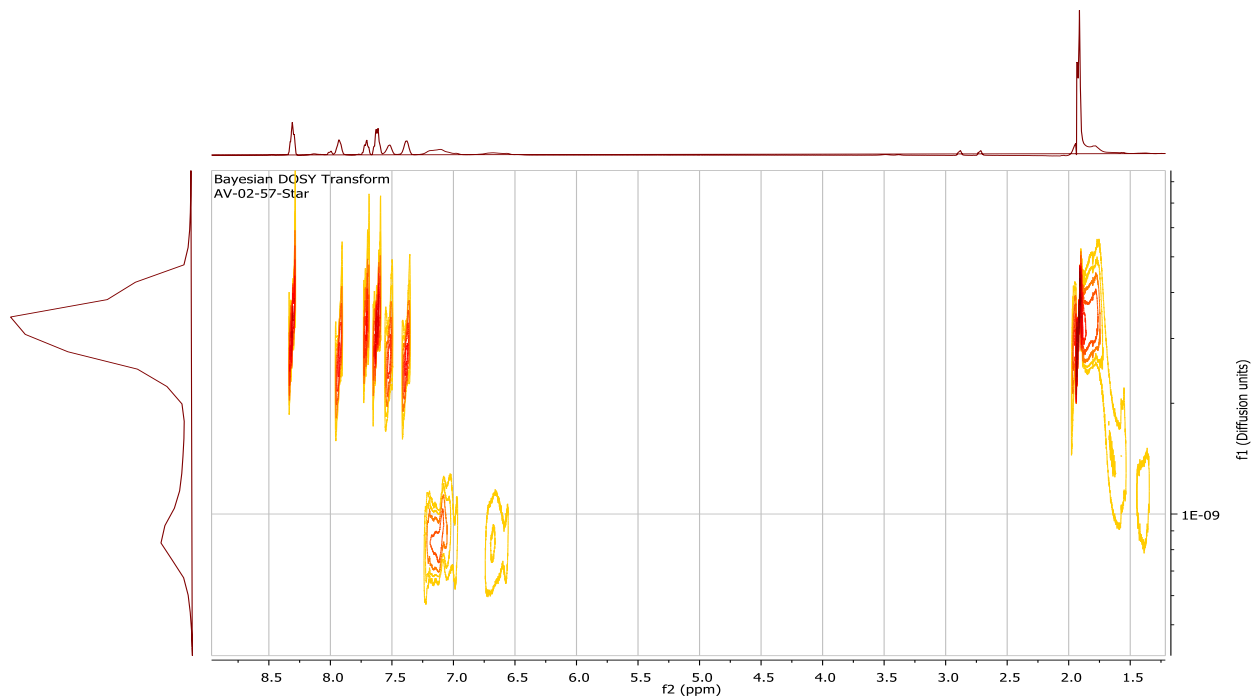


Figure II-16 DOSY spectra of star polymer prepared by using Sty₂₀₀AA₁₀₀. $\Delta = 0.2$ s; $\delta = 3$ ms; g was varied from 27 mT/m to 0.27 T/m,



Figure II-17 DOSY spectra of MMA₂₈₀AA₁₀₀. $\Delta = 0.2$ s; $\delta = 2$ ms; g was varied from 27 mT/m to 0.27 T/m.

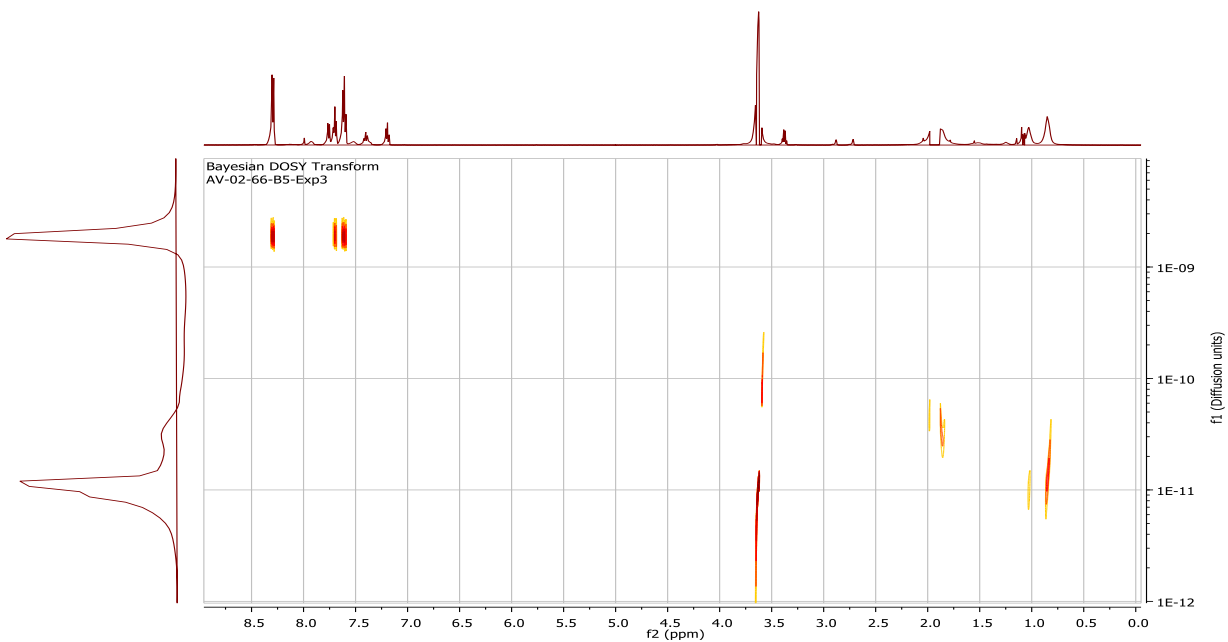


Figure II-18 DOSY spectra of star polymer prepared by using MMA₂₈₀AA₁₀₀. $\Delta = 0.2$ s; $\delta = 3$ ms; g was varied from 27 mT/m to 0.27 T/m,

Table II-1 Diffusion coefficients of block and star polymers.

Polymer	Diffusion Coefficient (cm ² s ⁻¹)
Sty ₂₀₀ AA ₁₀₀	2.22×10 ⁻⁹
Sty ₂₀₀ AA ₁₀₀ (star)	8.20×10 ⁻¹⁰
MMA ₂₈₀ AA ₁₀₀	1.31×10 ⁻¹⁰
MMA ₂₈₀ AA ₁₀₀ (star)	1.11×10 ⁻¹¹

The diffusion coefficients of block copolymers and star polymers is shown in Table II-1. The diffusion coefficient of Sty₂₀₀AA₁₀₀ was determined as 2.22×10⁻⁹ cm²s⁻¹ which was lower than the diffusion coefficient (8.20×10⁻¹⁰ cm²s⁻¹) of the corresponding star polymer. This is due the higher molecular weight of star polymer which was responsible for slower diffusion in the solvent. As expected, similar results were observed in case of MMA₂₈₀AA₁₀₀. The diffusion coefficient for MMA₂₈₀AA₁₀₀ and the corresponding star polymer was observed to be 1.31×10⁻¹⁰ cm²s⁻¹ and 1.11×10⁻¹¹ cm²s⁻¹, respectively. The lower diffusion coefficients after adding PhI(O₂CCH₃)₂ confirmed the formation of star polymers.

II.3 Experimental Section

II.3.1 Materials

Styrene (Sty, 99%, Alfa Aesar) and *tert*-butyl acrylate (tBA, 98%, Aldrich) were purified before the polymerizations by passing through a column filled with basic alumina to remove the inhibitor. The radical initiator, 1,1'-azobis(cyclohexanecarbonitrile) (ACHN, 98%, Aldrich), anisole (99%, Acros), CF₃CO₂H (99%, Aldrich), PhI(O₂CCH₃)₂ (98%, Acros), indigo carmine (>

80%, Fisher), glacial $\text{CH}_3\text{CO}_2\text{H}$ (99.7%, Fisher), NaN_3 (99.5%, Aldrich), tri-*n*-butylphosphine (Bu_3P , 95%, Alfa Aesar), *N,N*-dimethylacetamide (DMAc, 99%, Alfa Aesar), 1,4-dioxane (99.8%, Alfa Aesar), dichloromethane (99%, Fisher), methanol (MeOH , 99%, Fisher), and tetrahydrofuran (THF, 99.5%, EMD Milipore) were used as received. (2-(((butylthio)carbonothioyl)thio)-2-methylpropanoic acid (BMP) was synthesized by following a reported method.⁷⁴ Cobalt Blue was prepared by first drying a mixture of cobalt(II) and aluminum hydroxides (1:2 molar ratio) at 120 °C for 40 h and then calcining the obtained material at 1000 °C for 6 h.⁷⁵ The deuterated solvents, acetone- d_6 (99.9% D, Cambridge Isotope Laboratories) and DMSO- d_6 (99.9% D, Cambridge Isotope Laboratories), contained a small amount of tetramethylsilane (TMS) as the chemical shift reference.

II.3.2 Analyses and characterization methods

Molecular weights and molecular weight distribution (MWD) dispersities ($\mathcal{D} = M_w/M_n$) were determined by size exclusion chromatography (SEC) on a Tosoh EcoSEC system equipped with a series of 4 columns (TSK gel guard Super HZ-L, Super HZM-M, Super HZM-N, and Super HZ2000) and using refractive index (RI) and UV detectors. THF was used as an eluent at a flow rate of 0.35 mL min^{-1} (40 °C). The SEC calibration was based on linear polystyrene standards. Monomer conversions were determined by ^1H NMR spectroscopy using a Bruker Avance DRX (400 MHz) or a JEOL ECCA (500 MHz) spectrometer, by monitoring the decrease of the sums of intensities of the vinyl peaks (from Sty and tBA) relative to the intensity of the methoxy protons of anisole (internal standard present in the reaction mixtures). Rheological data was obtained by using a Discovery Hybrid HR-3 rheometer (TA instruments) with cone plate geometry (diameter of 40 mm, cone angle $2^\circ 00' 32''$, truncation gap was 53 μm). All rheological measurements were

carried out at 25 °C, which was controlled with a Peltier thermo-module unit. The entire plate (with diameter of 40 mm) was covered with sample for consistent results and the measurements were performed 30 min after mixing of the components of the gel. Photochemical curing was conducted by either UVP CL-1000L UV crosslinker (365 nm) or Ushio G20T10 low pressure mercury arc UV lamps (254 nm, 21 W). Thermal curing was carried out in a CEM Discover SP microwave reactor (300 W). The time-lapse video of gel healing was taken by using AmScope optical microscope and MD600E camera.

II.3.3 Synthetic procedures

Synthesis and characterization of poly(Sty-*co*-tBA). Random copolymer of Sty and tBA with equal monomer feed ratio was synthesized by preparing a solution of Sty (15 mL, 0.131 mol), tBA (19.16 mL, 0.131 mol), BMP (0.0264 g, 1.05×10^{-4} mol), ACHN (0.0128 g, 5.24×10^{-5} mol), and anisole (internal standard for determination of monomer conversion by NMR spectroscopy, 2 mL) in a round bottom flask equipped with magnetic stir bar. The flask was sealed with a rubber septum and was placed in an ice-water cooling bath in order to minimize evaporation of the reaction components during the following purging with nitrogen. The reaction mixture was deoxygenated by purging with nitrogen for 20 min. The flask was then immersed in an oil bath at 85 °C and samples were withdrawn from the mixture at timed intervals with a nitrogen-purged syringe for ^1H NMR analysis (after dilution with acetone-*d*₆) or for SEC analysis (after dilution with THF). After reaching the targeted molecular weight, the polymerization was quenched by exposing the mixture to air and the reaction mixture was diluted with CH₂Cl₂ and precipitated in methanol. The reprecipitation was repeated two additional times, and the polymer was dried. In other experiments, the molar ratio of Sty and tBA were changed to 1:3 and 3:1, keeping the same total

monomer to chain transfer agent (BMP) ratio. Polymerization kinetics as well as the evolution of molecular weights and MWD dispersities with conversion, and individual SEC traces are shown in Figure S1 in the Supporting Information (SI).

Conversion of poly(Sty-co-tBA) to poly(Sty-co-AA) (AA = acrylic acid). The Sty-tBA copolymer (0.06 mol with respect to *tert*-butyl groups, i.e., 15-20 g depending on copolymer composition) was dissolved in CH₂Cl₂ (50 mL) and CF₃CO₂H (15 mL, 0.2 mol) was added to convert the *tert*-butyl ester into carboxylic acid groups. The reactions were monitored by ¹H NMR spectroscopy and after 4 h, when the methyl proton peak from the *tert*-butyl groups (at ca. 1.5 ppm) was no longer discernable (Figure S2), the mixture was diluted with acetone (25 mL) and the polymer was precipitated in methanol and water mixture (2:1 (v/v)). The reprecipitation procedure was repeated once again. The polymers were then dried under vacuum for one day.

Preparation of gels with (diacyloxyiodo)benzene-type crosslinking groups. The gels were prepared by three different methods for different purposes. First, Sty₁AA_{0.9} (0.73 M with respect to carboxylate groups) and PhI(O₂CCH₃)₂ (0.15 M) solutions were prepared in DMAc. The PhI(O₂CCH₃)₂ solution was kept away from light to prevent the photochemical dissociation of the HV I-O bonds. Then, 300 μL of the copolymer solution was mixed with 200 μL of the PhI(O₂CCH₃)₂ solution in a vial. Gelation occurred almost instantaneously and yielded a heterogeneous gel. Although the dynamic nature of the network thus prepared could be studied visually, it was not suitable for the following rheological studies due to its heterogeneity. Therefore, to study the self-healing process further, 100 μL of 0.15 M solution of PhI(O₂CCH₃)₂

was mixed with 400 μL of 0.35 M (with respect to carboxylate groups) solution of $\text{Sty}_1\text{AA}_{0.7}$ in DMAc. After mixing, a homogeneous gel was formed in ca. 10 min. The same procedure was repeated but a miniscule amount of indigo carmine was added as colorant for the visual inspection of the self-healing (Figure 2). For rheological measurements, it was important that the entire plate was covered by the studied material and therefore larger volume (2 mL) of the gel was prepared by keeping the same ratio of $\text{PhI}(\text{O}_2\text{CCH}_3)_2$ and $\text{Sty}_1\text{AA}_{0.7}$ solutions but increasing the amounts four-fold.

In some cases, to achieve better visibility of the gels, a small amount of indigo carmine was added, but due to the tendency of this dye to change color and fade over time in the presence of the components of the gels, most of the colored gels were prepared using Co Blue (selected due to its stability in the presence of many reagents, including oxidants⁷⁵).

Conversion of dynamic to non-dynamic (permanent, “set”) networks by irradiation with UV light. The gels were prepared by mixing 300 μL of $\text{Sty}_1\text{AA}_{0.9}$ solution (0.73 M with respect to carboxylate groups) with 200 μL of $\text{PhI}(\text{O}_2\text{CCH}_3)_2$ solution (0.15 M) in DMAc in a glass tube. After 10 min, the glass tube was inserted into a UV chamber (UVP CL-1000L UV crosslinker), and the gel was exposed to UV light (365 nm) for 30 min. Subsequently, 500 μL of DMAc was added to the tube along with 100 μL of glacial $\text{CH}_3\text{CO}_2\text{H}$ to check the stability of the network.

Larger amounts of gels were prepared by mixing 400 μL of $\text{PhI}(\text{O}_2\text{CCH}_3)_2$ (0.15 M) solution with 1600 μL of $\text{Sty}_1\text{AA}_{0.7}$ (0.35 M) solution in DMAc in a 10 mL glass beaker. After 10 min of mixing, the gel was cured by exposing it to two low pressure mercury arc UV lamps (254 nm, 21 W) from top for 90 min. The light source was kept ca. 5 inches above the surface of the

gel. After curing, the gel was washed twice with 1 mL of DMAc to remove the byproducts (e.g., iodobenzene and the products of its photochemical decomposition) and the gel was subjected to rheological examination.

Conversion of dynamic to non-dynamic (permanent, “set”) networks by thermal curing. Gels were prepared by mixing 300 μL of Sty₁AA_{0.9} solution (0.21 M with respect to carboxylate groups) with 200 μL of freshly-prepared PhI(O₂CCH₃)₂ solution (0.10 M) in 1,4-dioxane in a microwave tube, which was then kept in a microwave reactor at 200 °C for 2 min. The power was set to 300 W and the timer was started when the temperature reached 200 °C. The total reaction time (including heating and cooling) was 40 min. At the end of the procedure, the gel was washed two times with 500 μL of 1,4-dioxane, which was discarded and then 100 μL of CH₃CO₂H along with 500 μL of 1,4-dioxane were added to the tube. The stability of the gel in the presence of CH₃CO₂H was inspected visually just after the addition of the acid and 72 h later.

Synthesis of polySty. Polystyrene was synthesized by preparing a stock solution of St (110 mL, 0.960 mol), BMP (0.484 g, 1.92×10^{-3} mol), ACHN (0.234 g, 9.60×10^{-4} mol) and anisol (11 mL, 0.096 mol) in a round bottom flask equipped with a magnetic stirrer and sealed with a rubber septum. Anisol was used as internal standard. The stock solution was stirred and purged with nitrogen for 20 min to remove air. After that, the flask was placed in an oil bath at 80 °C. Samples were withdrawn from the mixture at timed intervals with a nitrogen-purged syringe, part of which were diluted with acetone-*d*₆ (for NMR analysis) and part-with THF (for SEC analysis). After reaching the required molecular weight, the polymerization was quenched by exposing the mixture

to air. Subsequently, the polymer was precipitated in methanol twice from DCM to remove the impurities.

Synthesis of Sty₂₀₀tBA₁₀₀. Sty₂₀₀tBA₁₀₀ was synthesized by preparing a stock solution of tBA (22 mL, 0.15 mol), polySty macroCTA (15 g, 7.5×10^{-4} mol), ACHN (0.092 g, 3.75×10^{-4} mol) and anisol (25 mL, 0.096 mol) in a round bottom flask equipped with a magnetic stirrer and sealed with a rubber septum. Anisol was used as internal standard. The stock solution was stirred and purged with nitrogen for 20 min to remove air. After that, the flask was placed in an oil bath at 80 °C. Samples were withdrawn from the mixture at timed intervals with a nitrogen-purged syringe, part of which were diluted with acetone-*d*₆ (for NMR analysis) and part-with THF (for SEC analysis). After reaching the required molecular weight, the polymerization was quenched by exposing the mixture to air. Subsequently, the polymer was precipitated in methanol (and deionized water if necessary) twice from DCM to remove the impurities.

Synthesis of polyMMA. PolyMMA was synthesized by preparing a stock solution of MMA (22 mL, 0.200 mol), BMP (0.126 g, 5.00×10^{-4} mol), ACHN (0.030 g, 1.25×10^{-4} mol) and anisol (2.2 mL, 0.020 mol) in a round bottom flask equipped with a magnetic stirrer and sealed with a rubber septum. Anisol was used as internal standard. The stock solution was stirred and purged with nitrogen for 20 min to remove air. After that, the flask was placed in an oil bath at 80 °C. Samples were withdrawn from the mixture at timed intervals with a nitrogen-purged syringe, part of which were diluted with acetone-*d*₆ (for NMR analysis) and part-with THF (for SEC analysis). After reaching the required molecular weight, the polymerization was quenched by exposing the mixture

to air. Subsequently, the polymer was precipitated in methanol twice from DCM to remove the impurities.

Synthesis of MMA₂₈₀tBA₁₀₀. MMA₂₈₀tBA₁₀₀ was synthesized by preparing a stock solution of polyMMA macroCTA (8 g, 3.80×10^{-4} mol), ACHN (0.023 g, 9.52×10^{-5} mol), anisol (0.83 mL, 0.008 mol) and DMF (25 mL) in a round bottom flask equipped with a magnetic stirrer and sealed with a rubber septum. DMF was used as a solvent. *t*-BA (11 mL, 0.076 mol) was added to the stock solution after complete dissolution of PMMA-macroCTA. The stock solution was stirred and purged with nitrogen for 20 min to remove air. After that, the flask was placed in an oil bath at 80 °C. Samples were withdrawn from the mixture at timed intervals with a nitrogen-purged syringe, part of which were diluted with acetone-*d*₆ (for NMR analysis) and part-with THF (for SEC analysis). After reaching the required molecular weight, the polymerization was quenched by exposing the mixture to air. Subsequently, the polymer was precipitated in cold methanol (and deionized water if necessary) twice from DCM to remove the impurities.

Hydrolysis of Sty₂₀₀tBA₁₀₀ and MMA₂₈₀tBA₁₀₀. After precipitation, polymers were dissolved in minimum amount of DCM followed by an addition of TFA to hydrolyze the tertiary butyl ester groups in a round bottom flask for 15 h. The reaction was monitored by NMR and polymer was reprecipitated twice in diethylether from DCM after the methyl proton peak from the tert-butyl groups (1.5 ppm) had disappeared in the NMR spectrum. Subsequently, polymers were dried under vacuum for one day to get the final block copolymers.

Preparation of star polymers. Star polymers were prepared by mixing 500 μL of 1 mM solution (with respect to carboxylate groups) of block copolymers Sty₂₀₀AA₁₀₀ and MMA₂₈₀AA₁₀₀ in DMF with 1.66 mM solution (1.5 mL) of $\text{PhI}(\text{O}_2\text{CCH}_3)_2$ in DMF. After 5 mins of mixing, the stars were characterized by DLS.

II.4 Conclusions

Dynamic gels were prepared using ligand exchange reaction between $\text{PhI}(\text{O}_2\text{CCH}_3)_2$ and the free pendant carboxylate groups in copolymers of Sty and AA. The gels exhibited self-healing, were confirmed by rheological measurements. The dynamic gel prepared by mixing 4:1 volume ratio Sty₁AA_{0.7} (0.35 M) and $\text{PhI}(\text{O}_2\text{CCH}_3)_2$ (0.15 M) solutions in DMAc, respectively, showed 85% recovery even after 1300% strain in less than 20 s over several cycles. Furthermore, the conversion of dynamic to permanent gels following exposure to UV light or microwave heating was demonstrated. The conversion of dynamic gel to permanent crosslink network was visually confirmed by adding $\text{CH}_3\text{CO}_2\text{H}$ to the gel, which did not degrade the network even after a week. The formation of permanent gel was confirmed by continuous step-strain measurements, during which the gel showed poor recovery due to conversion of majority of dynamic bonds to permanent bonds by irreversible radical coupling reaction between the macromolecular carboxylate radicals and/or the alkyl radicals, which are product of their decarboxylation, produced by the photochemical or thermal cleavage of the (diacyloxyiodo)benzene bridging groups. Star polymers were also prepared by mixing the Sty-b-AA and $\text{PhI}(\text{O}_2\text{CCH}_3)_2$ solutions. The star polymers were characterized by DLS and DOSY NMR.

II.5 Acknowledgements

The authors gratefully acknowledge financial support provided by National Science Foundation, (NSF Award Career 1455200). The authors also thank to Prof. Danieli Rodrigues and Mr. Danyal Siddiqui from University of Texas at Dallas for providing help with the rheological measurements.

II.6 References

- 1 Lehn, J. M. *Proc. Natl. Acad. Sci. U.S.A* **2002**, *99*, 4763.
- 2 Stuart, J. R. *Angew. Chem. Int. Ed.* **2002**, *41*, 899.
- 3 Lehn, J.-M. *Aust. J. Chem.* **2010**, *63*, 611.
- 4 Roy, D.; Cambre, J. N.; Sumerlin, B. S. *Prog. Polym. Sci.* **2010**, *35*, 278.
- 5 Stuart, M. A. C.; Huck, W. T. S.; Genzer, J.; Müller, M.; Ober, C.; Stamm, M.; Sukhorukov, G. B.; Szleifer, I.; Tsukruk, V. V.; Urban, M.; Winnik, F.; Zauscher, S.; Luzinov, I.; Minko, S. *Nat. Mater.* **2010**, *9*, 101.
- 6 Wojtecki, R. J.; Meador, M. A.; Rowan, S. J. *Nat. Mater.* **2011**, *10*, 14.
- 7 Bowman, C. N.; Kloxin, C. J. *Angew. Chem. Int. Ed.* **2012**, *51*, 4272.
- 8 Stuparu, M. C.; Khan, A.; Hawker, C. J. *Polym. Chem.* **2012**, *3*, 3033.
- 9 Lehn, J.-M. *Angew. Chem. Int. Ed.* **2013**, *52*, 2836.
- 10 Lehn, J.-M. In *Dynamers: From Supramolecular Polymers to Adaptive Dynamic Polymers*; Springer, Cham :, 2013; Vol. 261. pp 155.
- 11 Roy, N.; Bruchmann, B.; Lehn, J.-M. *Chem. Soc. Rev.* **2015**, *44*, 3786.
- 12 Brooks, W. L. A.; Sumerlin, B. S. *Chem. Rev.* **2016**, *116*, 1375.
- 13 Schmidt, B. V. K. J.; Barner-Kowollik, C. *Angew. Chem. Int. Ed.* **2017**, *56*, 8350.

- 14 Sun, H.; Kabb, C. P.; Dai, Y.; Hill, M. R.; Ghiviriga, I.; Bapat, A. P.; Sumerlin, B. S. *Nat. Chem.* **2017**, *9*, 817.
- 15 Frisch, H.; Marschner, D. E.; Goldmann, A. S.; Barner-Kowollik, C. *Angew. Chem. Int. Ed.* **2018**, *57*, 2036.
- 16 García, F.; Smulders, M. M. J. *Journal of Polymer Science Part A: Polymer Chemistry* **2016**, *54*, 3551.
- 17 Burattini, S.; Greenland, B. W.; Chappell, D.; Colquhoun, H. M.; Hayes, W. *Chem. Soc. Rev.* **2010**, *39*, 1973.
- 18 Murphy, E. B.; Wudl, F. *Prog. Polym. Sci.* **2010**, *35*, 223.
- 19 Billiet, S.; Hillewaere, X. K. D.; Teixeira, R. F. A.; Du Prez, F. E. *Macromol. Rapid Commun.* **2012**, *34*, 290.
- 20 Phadke, A.; Zhang, C.; Arman, B.; Hsu, C.-C.; Mashelkar, R. A.; Lele, A. K.; Tauber, M. J.; Arya, G.; Varghese, S. *Proc. Natl. Acad. Sci. U.S.A* **2012**, *109*, 4383.
- 21 Urban, M. W. *Nat. Chem.* **2012**, *4*, 80.
- 22 Fiore, G. L.; Rowan, S. J.; Weder, C. *Chem. Soc. Rev.* **2013**, *42*, 7278.
- 23 Wei, Z.; Yang, J. H.; Zhou, J.; Xu, F.; Zrínyi, M.; Dussault, P. H.; Osada, Y.; Chen, Y. M. *Chem. Soc. Rev.* **2014**, *43*, 8114.
- 24 Barner-Kowollik, C.; Georg Schmidt, F. *Macromol. Chem. Phys.* **2012**, *213*, 129.
- 25 Urban, M. W. *Prog. Polym. Sci.* **2015**, *49-50*, 1.
- 26 Yang, Y.; Urban, M. W. *Adv. Mater. Interfaces* **2018**, *5*, 1800384.
- 27 Bergman, S. D.; Wudl, F. *J. Mater. Chem.* **2008**, *18*, 41.
- 28 Hager, M. D.; Greil, P.; Leyens, C.; van der Zwaag, S.; Schubert, U. S. *Adv. Mater.* **2010**, *22*, 5424.

- 29 Michal, B. T.; Jaye, C. A.; Spencer, E. J.; Rowan, S. J. *ACS Macro Lett.* **2013**, *2*, 694.
- 30 Yang, Y.; Urban, M. W. *Chem. Soc. Rev.* **2013**, *42*, 7446.
- 31 Urban, M. W. *Angew. Chem. Int. Ed.* **2014**, *53*, 3775.
- 32 Yang, Y. *Polym. Chem.* **2013**, *5*, 126.
- 33 Cash, J. J.; Kubo, T.; Bapat, A. P.; Sumerlin, B. S. *Macromolecules* **2015**, *48*, 2098.
- 34 Yang, Y.; Ding, X.; Urban, M. W. *Prog. Polym. Sci.* **2015**, *49-50*, 34.
- 35 Stukalin, E. B.; Cai, L.-H.; Kumar, N. A.; Leibler, L.; Rubinstein, M. *Macromolecules* **2013**, *46*, 7525.
- 36 Wu, D. Y.; Meure, S.; Solomon, D. *Prog. Polym. Sci.* **2008**, *33*, 479.
- 37 Urban, M. W.; Davydovich, D.; Yang, Y.; Demir, T.; Zhang, Y.; Casabianca, L. *Science* **2018**, *362*, 220.
- 38 Yoshimura, A.; Zhdankin, V. V. *Chem. Rev.* **2016**, *116*, 3328.
- 39 Georgiev, G.; Kamenska, E.; Christov, L.; Sideridou-Karayannidou, I.; Karayannidis, G.; Varvoglis, A. *Eur. Polym. J.* **1992**, *28*, 207.
- 40 Yoshimura, A.; Yusubov, M. S.; Zhdankin, V. V. *Org. Biomol. Chem.* **2016**, *14*, 4771.
- 41 Maity, A.; Powers, D. C. *Synlett* **2019**, *30*, 257.
- 42 Crivello, J. V. *Adv. Polym. Sci.* **1984**, *62*, 1.
- 43 Crivello, J. V. *J. Polym. Sci.* **1999**, *37*, 4241.
- 44 Vaish, A.; Tsarevsky, N. V. *Main Group Strategies towards Functional Hybrid Materials* **2017**.
- 45 Georgiev, G.; Spyroudis, S.; Varvoglis, A. *Polym. Bull.* **1985**, *14*, 523.
- 46 Georgiev, G. S. *Polym. Bull.* **1999**, *43*, 223.

- 47 Georgiev, G. S.; Kamenska, E. B.; Tsarevsky, N. V.; Christov, L. K. *Polym. Int.* **2001**, *50*, 313.
- 48 Kumar, R.; Cao, Y.; Tsarevsky, N. V. *The Journal of Organic Chemistry* **2017**, *82*, 11806.
- 49 Hach, R. J.; Rundle, R. E. *J. Am. Chem. Soc.* **1951**, *73*, 4321.
- 50 Pimentel, G. C. *J. Chem. Phys.* **1951**, *19*, 446.
- 51 Musher, J. I. *Angew. Chem. Int. Ed.* **1969**, *8*, 54.
- 52 Akiba, K.-y.; Yamamoto, Y. *Heteroat. Chem.* **2007**, *18*, 161.
- 53 Fox, A. R.; Pausacker, K. H. *J. Chem. Soc.* **1957**, 295.
- 54 Kumar, R.; Vaish, A.; Runčevski, T.; Tsarevsky, N. V. *J. Org. Chem.* **2018**, *83*, 12496.
- 55 Han, H.; Tsarevsky, N. V. *Polym. Chem.* **2012**, *3*, 1910.
- 56 Han, H.; Tsarevsky, N. V. *Chem. Sci.* **2014**, *5*, 4599.
- 57 Muraki, T.; Togo, H.; Yokoyama, M. *Rev. Heteroatom Chem.* **1997**, *17*, 213.
- 58 Togo, H.; Katohgi, M. *Synlett* **2001**, 565.
- 59 Asandei, A. D.; Adebolu, O. I.; Simpson, C. P.; Kim, J.-S. *Angew. Chem. Int. Ed.* **2013**, *52*, 10027.
- 60 Vaish, A.; Tsarevsky, N. V. In *Hypervalent Iodine Compounds in Polymer Science and Technology*; Wiley, 2018. pp 483.
- 61 Kumar, R.; Cao, Y.; Tsarevsky, N. V. *J. Org. Chem.* **2017**, *82*, 11806.
- 62 Moad, G.; Chiefari, J.; Chong, Y. K.; Krstina, J.; Mayadunne, R. T. A.; Postma, A.; Rizzardo, E.; Thang, S. H. *Polym. Int.* **2000**, *49*, 993.
- 63 Perrier, S.; Takolpuckdee, P. *J. Polym. Sci.: Part A: Polym. Chem.* **2005**, *43*, 5347.
- 64 Barner-Kowollik, C. In *Handbook of RAFT Polymerization*; Wiley-VCH, Weinheim, 2008. p xi + 543.

- 65 Moad, G.; Rizzardo, E.; Thang, S. H. In *Fundamentals of RAFT Polymerization*; RSC, Cambridge, 2013. pp 205.
- 66 Denisov, E. T.; Denisova, T. G.; Pokidova, T. S. *Handbook of Free Radical Initiators*; Wiley, Hoboken, 2003.
- 67 Cech, F.; Zbiral, E. *Tetrahedron* **1975**, *31*, 605.
- 68 Tsarevsky, N. V. *J. Polym. Sci.: Part A: Polym. Chem.* **2010**, *48*, 966.
- 69 Makowiec, S.; Rachon, J. *Heteroat. Chem.* **2003**, *14*, 352.
- 70 Han, H.; Kumar, R.; Tsarevsky, N. V. *Macromol. Rapid Commun.* **2019**, *0*, 1900073.
- 71 Vaish, A.; Roy, S. G.; De, P. *Polymer* **2015**, *58*, 1.
- 72 Shaw, M. T. *Introduction to Polymer Rheology*; Wiley, 2012.
- 73 Reichardt, C.; Welton, T. In *Appendix A. Properties, Purification, and Use of Organic Solvents*; Wiley, 2010. pp 549.
- 74 Gody, G.; Roberts, D. A.; Maschmeyer, T.; Perrier, S. *J. Am. Chem. Soc.* **2016**, *138*, 4061.
- 75 Roy, A. In *Cobalt Blue*; National Gallery of Art, Washington, 2007; Vol. 4. p 151.

CHAPTER III
SYNTHESIS, CHARACTERIZATION AND REACTIVITY OF OLIGOMERIC
HYPERVALENT IODINE(III) COMPOUNDS
WITH TETRAZOLE LIGANDS

III.1. Introduction

The organic compounds of polyvalent iodine have been known since 1886 when several (dichloroiodo)arenes ArICl_2 were prepared by Willgerodt¹ by the reaction of iodoarenes ArI with chlorine. This discovery was followed, in a swift succession during the following decade, by other organic compounds of iodine(III) such as iodosylarenes ArIO^{2-4} and (diacyloxyiodo)arenes $\text{ArI}(\text{O}_2\text{CR})_2$ (and other, e.g., nitric and chromic, acid derivatives),^{3,5} as well as some of iodine(V), notably iodylarenes ArIO_2 .⁴⁻⁶ By 1914, when the first monograph⁷ summarizing the knowledge about organic polyvalent iodine compounds was published, hundreds of them had been reported and studied. The nature of bonding in the molecules of these and in many other compounds containing polyvalent (i.e., exceeding the valency expected from the octet rule) main group elements was a subject of debate for several decades. In 1951, Hach and Rundle,⁸ and Pimentel⁹ reasoned that in polyhalide anions (and, as it was soon realized, by extension – in the molecules of many of the other aforementioned compounds¹⁰), delocalized 3-center-4-electron bonds are formed exclusively with the participation of p-orbital(s) of the central polyvalent atom. This idea was applied more broadly to describe theoretically the bonding in many molecules containing

polyvalent main group elements in 1969 by Musher¹¹ who dubbed the bonds in question *hypervalent* (HV). The molecules of ArIL₂ compounds (L represents a ligand with electronegative atom(s), such as carboxylate or (pseudo)halide), which are the subject of this work, are T-shaped and contain the almost linear L-I-L fragment. The presence of the relatively weak, compared to the “classical” covalent (2-center-2-electron), and highly polar HV bonds I-L determines the rich reactivity of HV iodine compounds, i.e., their ability to participate in various electron transfer, ionic (e.g., ligand exchange with nucleophiles), and radical reactions. A number of monographs or edited books^{7, 12-15} and review papers¹⁶⁻²⁷ deal with all aspects of organic HV iodine compounds, including the methods of their preparation, structures, spectral and other physical as well as chemical properties, and uses in synthetic chemistry and materials science.

HV iodine(III) reagents can serve as efficient electrophiles and have found numerous applications in synthetic organic chemistry in this capacity, for instance in C-H bond functionalization reactions with trifluoromethyl,²⁸ cyano,²⁹ azido,³⁰ and many other functional groups. Radical reactions involving HV iodine(III) compounds have found synthetic utility as well.^{22, 31, 32} Heterocyclic compounds with a HV iodine(III) atom as part of the ring such as Togni's and Zhdankin's reagents have gained significant popularity due to their increased stability (compared to their acyclic analogues) at ambient conditions.^{28, 33, 34} Acyclic compounds of the type ArIL₂ are easily prepared by ligand exchange reactions between commercially available compounds such as PhI(O₂CCH₃)₂ or PhI(O₂CCF₃)₂ and either sources of the anions L⁻ (salts) or the silicon compounds Me₃SiL. An alternative approach is to employ the reaction between iodosylarenes ArIO and the acid HL or Me₃SiL. Some ArIL₂ compounds are rather unstable (e.g., when L = N₃) and are prepared *in situ* to afford, upon decomposition, the monovalent iodine compound ArI and the radicals L[•], which can functionalize substrates (e.g., unsaturated

compounds) or initiate radical polymerization, yielding end- and in some cases backbone-functionalized polymers.^{35, 36} In other words, ligand exchange reactions at HV iodine(III) centers with the nucleophiles L^- followed by homolytic decomposition of the newly-formed compound $ArIL_2$ – a reaction that is formally identical to oxidation of the anion L^- to the radical L^\bullet – is a convenient route to functional radicals from readily accessible precursors.

Out of many oxidative ligand transfer reactions, those that allow for the direct transformation of C-H to C-N bonds are of great interest, as the products of these reactions are often the building blocks of various pharmaceuticals and biologically active natural compounds. Such transformations are often conveniently carried out using HV iodine(III) reagents with I-N bonds but unfortunately, these compounds, especially the acyclic ones, are comparatively unstable and difficult to store, which limits the range of synthetically useful reactions that can be developed. These compounds are also usually hydrolytically unstable, which imposes a further restriction on their utility. The formation of acyclic HV iodine(III) compounds with I-N bonds derived from cyclic imides¹⁹ or azoles³⁷ was first reported by Varvoglis. Over the following years, several other structural classes were demonstrated including heterocyclic and iodonium salts with I-N bonds. For instance, azidoiodanes,^{33, 34, 38, 39} benziodazoles,^{40, 41} and iminoiodanes⁴²⁻⁴⁶ were investigated as efficient reagents for C-N bond-forming reactions. These reagents have been used in direct azidation,^{39, 47-49} amination,^{43, 47, 50-55} aziridination,^{44, 45} and C-H insertion reactions.^{49, 56} The discovery of reactions in which the HV iodine(III) reagents with I-N bonds were formed *in situ* using iodoarenes (typically, iodobenzene) as catalysts,^{50, 57} was a major advancement due to the relatively inexpensive setup and the markedly reduced negative environmental impact compared to C-H to C-N transformations mediated by transition metal compounds. Nevertheless, the need remains to isolate and characterize structurally and determine the reactivity of more, especially

acyclic, HV iodine(III) compounds with N-based ligands, both from fundamental and applied chemistry viewpoint.

Among the many N-based nucleophiles that can potentially serve as ligands in HV iodine compounds, tetrazoles⁵⁸⁻⁶³ are of interest, due to properties such as complex-formation ability, biological activity, and especially their highly positive enthalpy of formation,⁶⁴ which makes them attractive as effective propellants and explosives producing molecular nitrogen as the dominating gaseous product of decomposition. C-(5-)substituted tetrazoles RCN_4H resemble structurally carboxylic acids RCO_2H and are often characterized by similar (typically, within an order of magnitude) values of K_a ,⁶⁵ which is why they are often referred to as tetrazolic acids. For instance, pK_a of 5-methyltetrazole $\text{CH}_3\text{CN}_4\text{H}$ is around 5.6,⁶⁵ while pK_a of $\text{CH}_3\text{CO}_2\text{H}$ is 4.8.⁶⁶ Likewise, the pK_a values of 5-phenyltetrazole and benzoic acid are respectively 4.8⁶⁵ and 4.2.⁶⁶ It was therefore to be expected that tetrazoles or tetrazolate anions can be used in the place of carboxylic acids or carboxylate anions to prepare the compounds $\text{ArI}(\text{N}_4\text{CR})_2$, which are formally analogues of the corresponding dicarboxylates $\text{ArI}(\text{O}_2\text{CR})_2$.

As mentioned, HV iodine compounds are used frequently in organic synthesis as highly selective and environment friendly oxidizing agents. Among these reagents, iodosyl benzene, $(\text{PhIO})_n$, is extremely important as oxygen transfer agent that is extensively used in catalytic oxygenation reaction. Besides that, PhIO is particularly important as precursor to new HV iodine (III) compounds. Despite its usefulness as an oxidant, practical applications of iodosylbenzene are hampered by its low solubility in nonreactive media, as well as low thermal stability and explosive properties upon moderate heating.⁶⁷ The low solubility of iodosylbenzene is explained by a zigzag polymeric, asymmetrically bridged structure, in which monomeric units of PhIO are linked by intermolecular I---O secondary bonds. The polymeric structure of iodosylbenzene was also

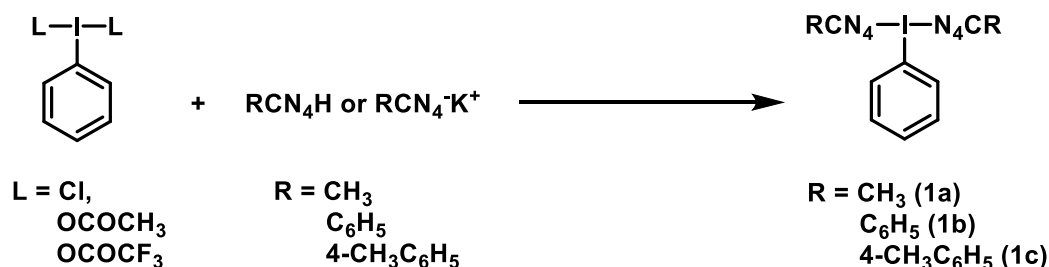
theoretically analyzed by density functional theory computations at the B3LYP level and, in particular, the importance of the presence of a terminal hydration water in its zigzag polymeric structure $\text{HO-I(Ph)(PhIO)}_n\text{(Ph)I-OH}$ was established⁶⁸ confirming the earlier suggestion⁶⁹.

This chapter primarily focus on the synthesis, characterization, and reactivity of oligomeric HV iodine(III) compounds with tetrazole ligands using PhIO. Besides that, synthesis of non-oligomeric HV compounds is discussed briefly along with their electrochemical properties.

III.2. Results and Discussion

III.2.1. Tetrazole Containing Oligomeric HV Iodine(III) Compounds

Tetrazole containing HV iodine(III) compounds, $\text{PhI(N}_4\text{CR)}_2$ ($\text{R} = \text{CH}_3$ (**1a**), C_6H_5 (**1b**), and $4\text{-CH}_3\text{C}_6\text{H}_5$ (**1c**)), were synthesized reacting PhIL_2 ($\text{L} = \text{Cl}$, OCOCH_3 , and OCOCF_3) with either RCN_4H ($\text{R} = \text{CH}_3$, C_6H_5 , $4\text{-CH}_3\text{C}_6\text{H}_5$) or their potassium salts in different solvents. as shown in Scheme III-1. The desired compounds were formed in decent yield. Although, the use of potassium salts was preferred due to the precipitation of byproduct which drove the reaction forward and simplified the purification.



Scheme III-1 Synthesis of $\text{PhI(N}_4\text{CR)}_2$ using PhIL_2 and RCN_4H (or RCN_4K^+) at room temperature in different solvents.

After synthesis and isolation of three symmetric HV iodine(III) compounds **1a-c**, they were further characterized by cyclic voltammetry (CV) to examine their oxidizing ability. The CV measurements were performed in dry and deoxygenated DMF (good solvent for all compounds **1a-c**) using glassy carbon electrode. In addition to that, the reduction potential of $\text{PhI}(\text{O}_2\text{CCH}_3)_2$ was measured in the same solvent and it was found that $\text{PhI}(\text{O}_2\text{CCH}_3)_2$ was harder to reduce than the tetrazole-based HV iodine(III) compounds. It was confirmed that the electrolyte used in CV measurements, $(n\text{-Bu})_4\text{NPF}_6$, does not interact with the HV iodine(III) compounds (Figure III-1). $(n\text{-Bu})_4\text{NPF}_6$ does not have any effect on the spectrum of compound **1c** even after 2h, which suggested that $(n\text{-Bu})_4\text{NPF}_6$ was a suitable electrolyte for the CV experiments.

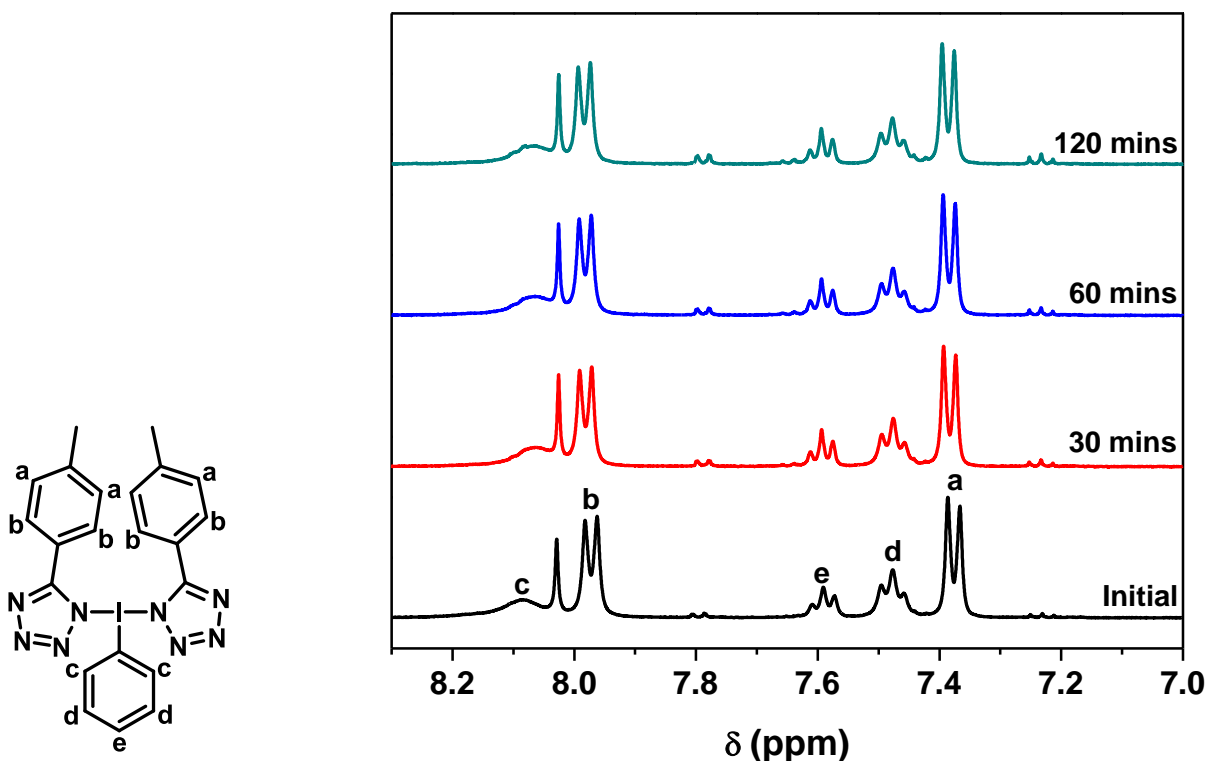


Figure III-1 ^1H NMR spectra of mixture of compound **1c** (20 mM) and $(n\text{-Bu})_4\text{NPF}_6$ (400 mM) on regular interval.

To make the comparison, redox potential of ferrocene ($\text{Fc}^+|\text{Fc}$) was measured and all the reduction potentials were also reported with respect to $\text{Fc}^+|\text{Fc}$. The cyclic voltammogram and the redox potential of ferrocene is shown below.

Table III-1 Redox potential of ferrocene at different scan rates

Scan Rate	E_{Red}	E_{Ox}	E_{Redox}
0.02	0.010	0.124	0.067
0.04	-0.007	0.142	0.067
0.06	-0.016	0.153	0.068
0.08	-0.024	0.158	0.067
0.1	-0.029	0.168	0.069

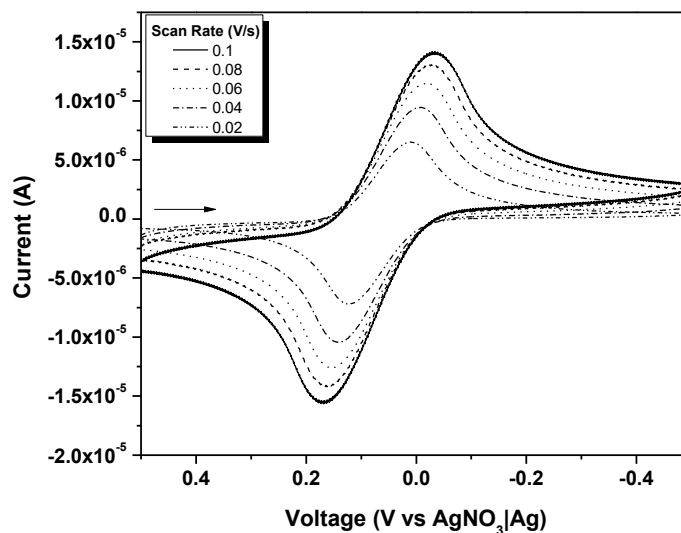


Figure III-2 Cyclic voltammogram of ferrocene (1 mM) in anhydrous DMF containing 0.1 M (*n*-Bu)₄NPF₆ (vs. AgNO₃/Ag) at different scan rates using glassy carbon electrode.

Table III-2 Reduction potential of various HV iodine(III) compounds (1 mM) in anhydrous DMF containing 0.1 M (n-Bu)₄NPF₆ (vs. AgNO₃/Ag) at different scan rates using glassy carbon electrode.

Entry	Compound	Scan Rate (V/s)	E _{red} vs. AgNO ₃ Ag (V)	E _{red} vs. Fc ⁺ Fc (V)
1	1b	0.02	-0.249	-0.316
2		0.04	-0.248	-0.315
3		0.06	-0.264	-0.332
4	1c	0.02	-0.377	-0.444
5		0.04	-0.312	-0.379
6		0.06	-0.344	-0.412
7	1a	0.02	-0.433	-0.5
8		0.04	-0.472	-0.539
9		0.06	-0.520	-0.588
10	PhI(O ₂ CCH ₃) ₂	0.02	-1.156	-1.223
11		0.04	-1.303	-1.37
12		0.06	-1.292	-1.36

The cyclic voltammogram of PhI(O₂CCH₃)₂ showed an irreversible wave with two-electron reduction peak ranging from -1.223 V to -1.360 V (vs. Fc⁺/Fc), depending on the scan rates (Table III-2, entries 10-12 and Figure III-3).

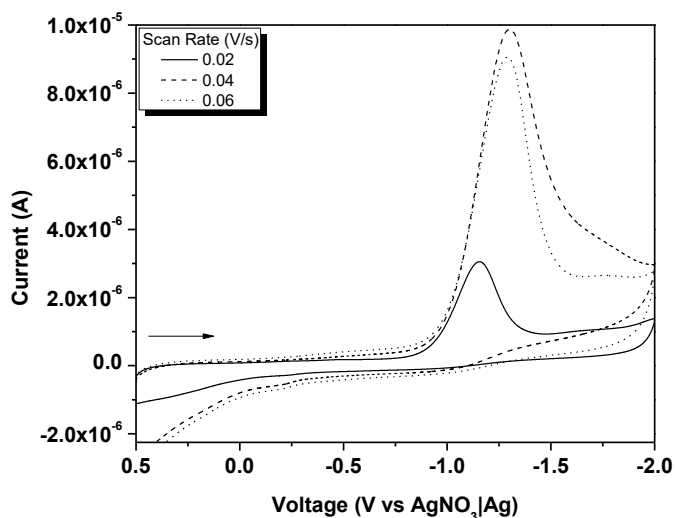


Figure III-3 Cyclic voltammogram of PhI(O₂CCH₃)₂ (1 mM) in anhydrous DMF containing 0.1 M (n-Bu)₄NPF₆ (vs. AgNO₃/Ag) at different scan rates using glassy carbon electrode.

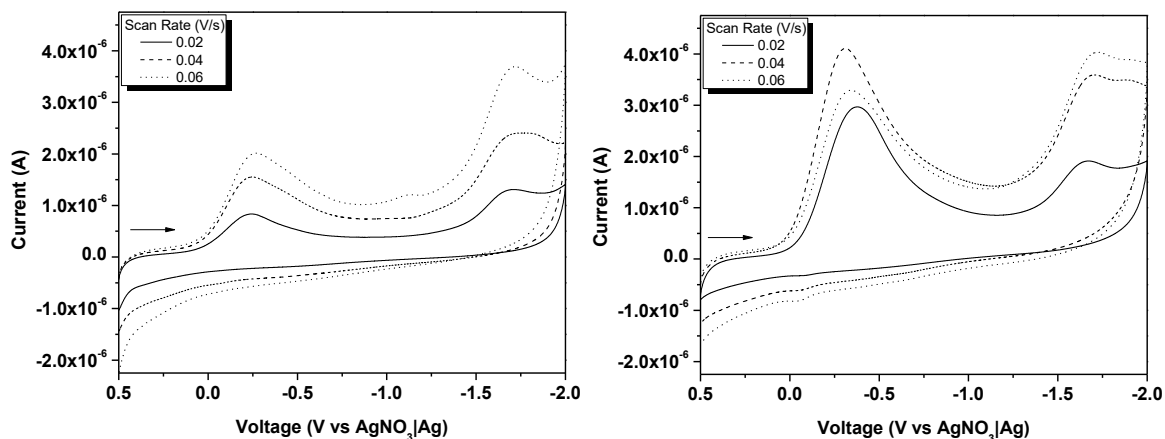


Figure III-4 Cyclic voltammogram of $\text{Phi}(\text{N}_4\text{CC}_6\text{H}_5)_2$ (1 mM, on left) and $\text{Phi}(\text{N}_4\text{C}(4\text{-CH}_3\text{C}_6\text{H}_4))_2$ (1 mM, on right) in anhydrous DMF containing 0.1 M $(\text{n-Bu})_4\text{NPF}_6$ (vs. AgNO_3/Ag) at different scan rates using glassy carbon electrode.

Compounds **1a-c** were better electron-acceptors with a less negative reduction potential than $\text{Phi}(\text{O}_2\text{CCH}_3)_2$ at any scan rate (Table III-2). Compound **1b** had the least negative reduction potential ranging from -0.316 V to -0.332 V (vs. Fc^+/Fc) at various scan rates (Table III-2, entries 1-3 and Figure III-4). The oxidizing power of compounds **1a-c** followed the expected trend based on the electron donating ability of the R group in the tetrazole ligand, i.e., compound **3c** was more oxidizing than compound **3a** but less than **1b** with reduction potential from -0.444 V to -0.412 V (vs. Fc^+/Fc) at different scan rates (Table III-2, entries 4-6 and Figure III-4). The reduction potential of compound **1a** varied from -0.500 V to -0.588 V (vs. Fc^+/Fc) upon altering the scan rates (Table III-2, entries 7-9 and Figure III-5).

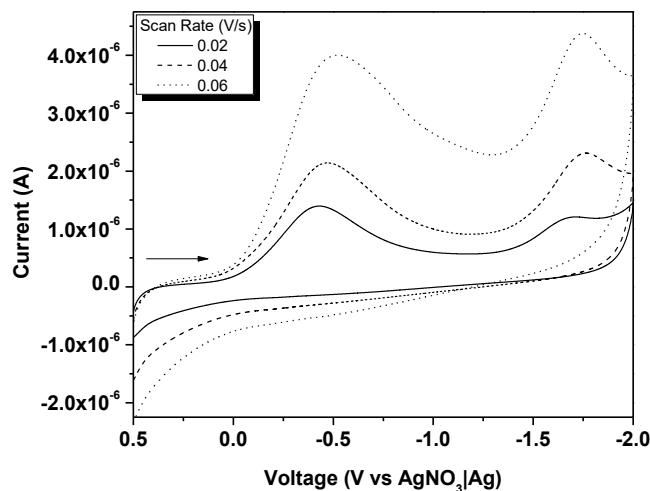
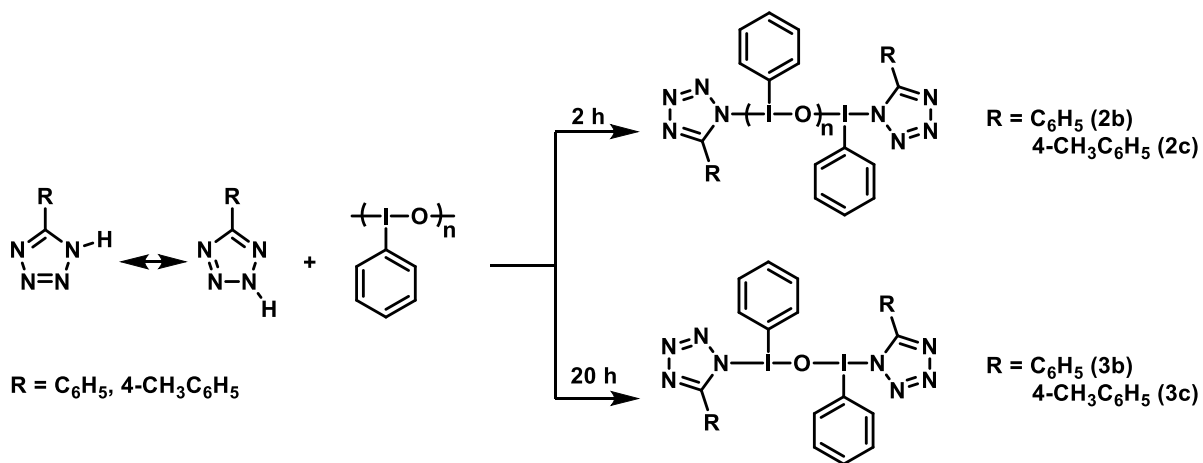


Figure III-5 Voltammogram for $\text{PhI}(\text{N}_4\text{CCH}_3)_2$ (vs. AgNO_3/Ag) in anhydrous DMF (1mM) + 0.1 M $(n\text{-Bu})_4\text{NPF}_6$, glassy carbon electrode at different scan rates.



Scheme III-2 Reaction of RCN_4H ($\text{R} = \text{C}_6\text{H}_5, 4\text{-CH}_3\text{C}_6\text{H}_5$) with PhIO .

The same reaction of PhIO was then conducted using RCN_4H ($\text{R} = \text{C}_6\text{H}_5, 4\text{-CH}_3\text{C}_6\text{H}_5$). The reaction mixtures when using 2 eq. of the tetrazoles vs PhIO in CH_3CN were heterogeneous, and the products, isolated by filtration, were obtained as off-white solids and were found to be insoluble in most organic solvents with the notable exception of CH_3OH . The reaction between PhIO and carboxylic acids such as $\text{CH}_3\text{CO}_2\text{H}$ and $\text{CF}_3\text{CO}_2\text{H}$ usually generates oligomeric HV iodine(III)

compounds with I and O atoms in the backbone.⁷⁰ Similarly, it was ascertained that the compounds obtained from the reactions of PhIO and tetrazoles were oligomeric compounds – **2b** and **2c** (instead of the expected compounds **3b** and **3c**). The structural data (*vide infra*) revealed that **2b** exists as oligomeric HV iodine(III) compound, containing three I atoms linked through two bridging O atoms, and the N2-atoms of 5-phenyl tetrazole were coordinated to the two terminal HV iodine(III) centers. The reason the reactions of PhIO with RCN₄H (R = C₆H₅, 4-CH₃C₆H₅) afforded oligomers could plausibly be attributed to the poor solubility of those oligomers, which, as soon as formed, precipitated, and were not accessible to react with the still present unreacted tetrazole. In contrast, as mentioned, compound **1a** is much more soluble and is formed as the main product (possibly via the reaction of initially formed oligomers **2a** (not observed) with CH₃CN₄H). The contact time of PhIO and RCN₄H (2 eq.) in CH₃CN was increased to 20 h in order to allow the unreacted tetrazole to cleave the I-O-I bridges in the poorly soluble oligomers. The increased reaction time resulted in off-white solids in both cases and the products were found to be soluble in polar solvents such as DMF. ¹H NMR analysis in DMF-*d*₇ revealed that both products were μ-oxo compounds **3b** and **3c**. This suggested that by varying the reaction time between PhIO and RCN₄H (2 eq.) and/or the excess amount of tetrazole, the molecular weights of obtained HV iodine(III) species could be controlled to some degree. It was observed that compounds **3b** and **3c**, while soluble in DMSO, reacted with it and oxidized it.

The formation of oligomeric HVI compound was confirmed by diffusion ordered NMR spectroscopy (DOSY NMR). The molecular weight based DOSY NMR was performed for PhI, **1c**, **2c**, and **3c**. CD₃OD was used as NMR solvent since all four compounds were soluble in this solvent (it was not a suitable choice which will be explained later). As shown in Table III-3, the

highest diffusion coefficient (D) is for PhI ($7.33 \times 10^{-9} \text{ m}^2 \text{ s}^{-1}$) since it has the lowest molecular weight among all four compounds as shown in Figure III-6.

Table III-3 Diffusion coefficients of PhI and various tetrazole containing HV iodine(III) compounds

Compound	Diffusion Coefficient ($\times 10^{-9}$) [$\text{m}^2 \text{ s}^{-1}$]
PhI	7.33
1c	4.26
3c	4.11
2c	1.99

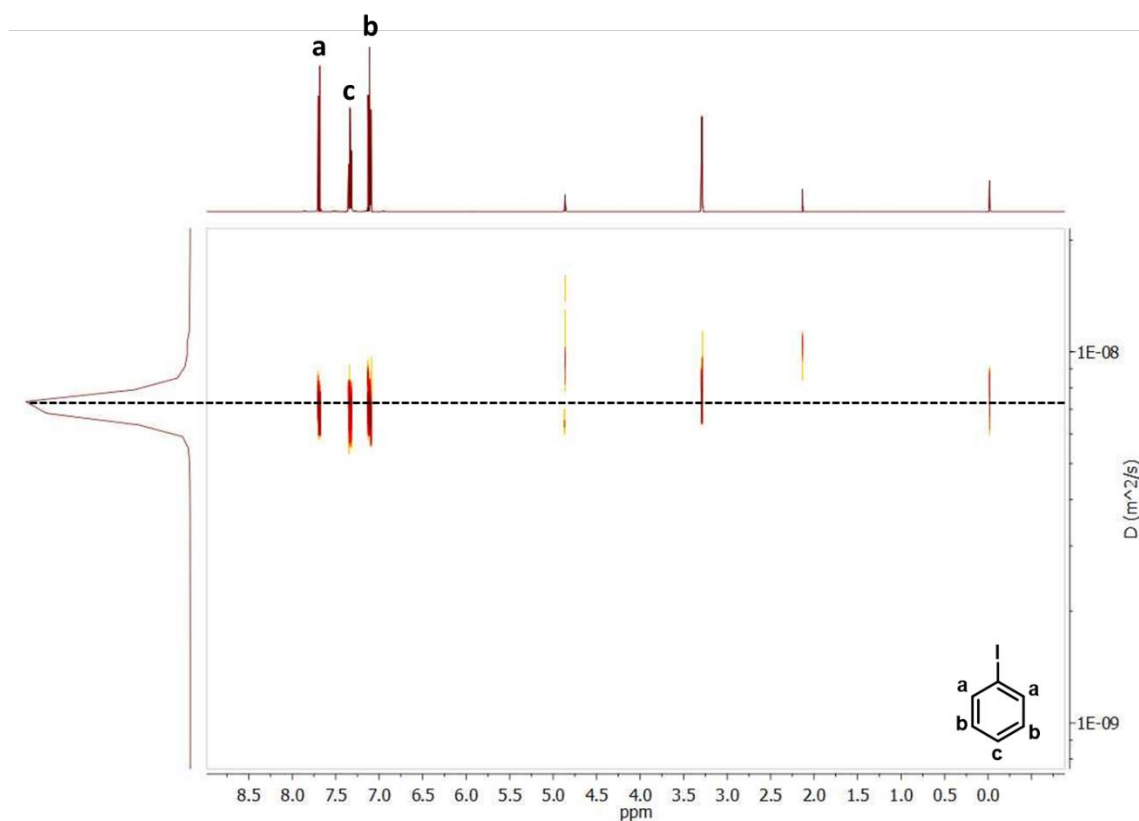


Figure III-6 DOSY NMR spectrum of PhI in CD₃OD.

Between compounds **1c** and **3c**, the μ -oxo compound **3c** had slightly lower D which was expected. The lowest D is for **2c** ($1.99 \times 10^{-9} \text{ m}^2 \text{ s}^{-1}$) since it has the highest molecular weight. The large difference between the diffusion coefficient of **3c** and **2c** demonstrated the formation of oligomeric HV iodine compound.

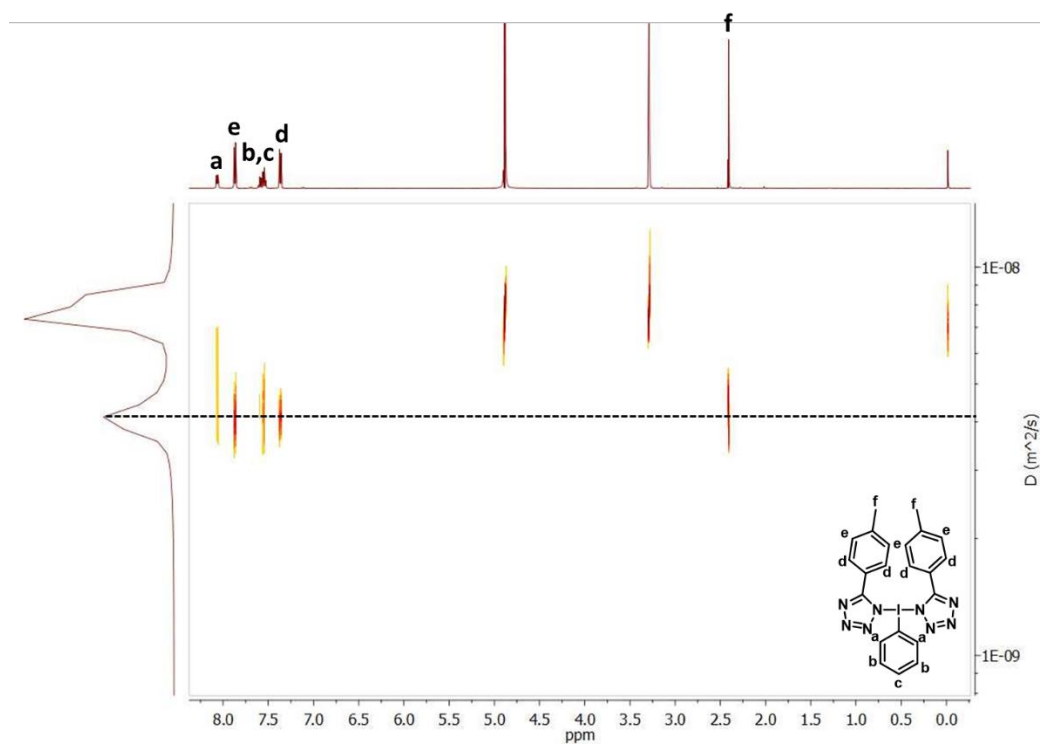


Figure III-7 DOSY NMR spectrum of **1c** in CD_3OD .

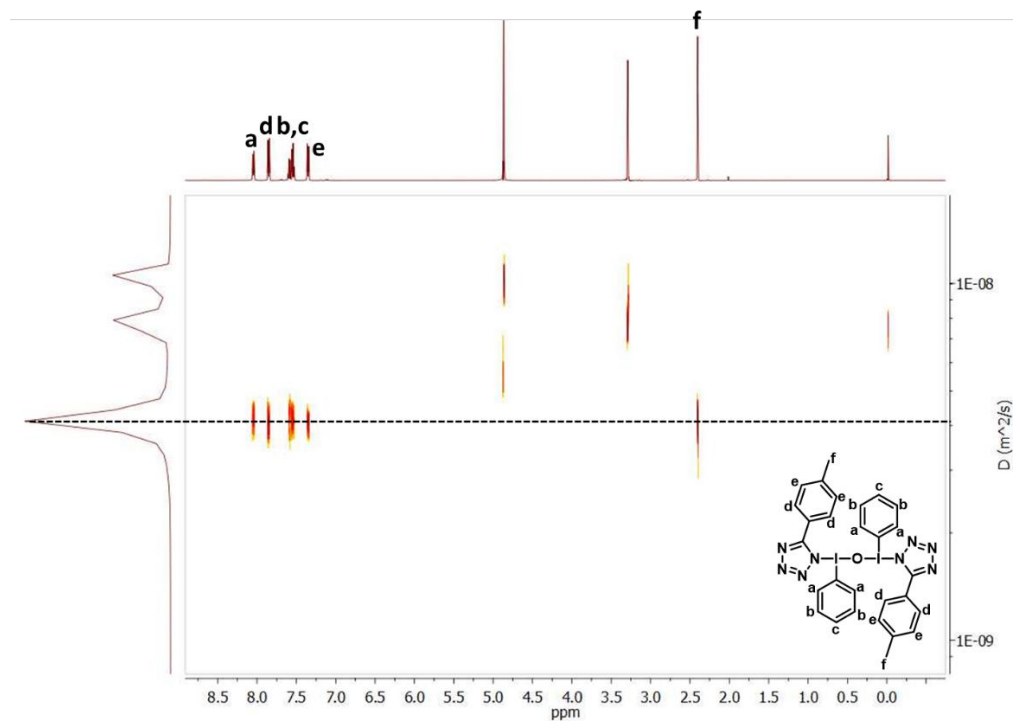


Figure III-8 DOSY NMR spectrum of **3c** in CD₃OD.

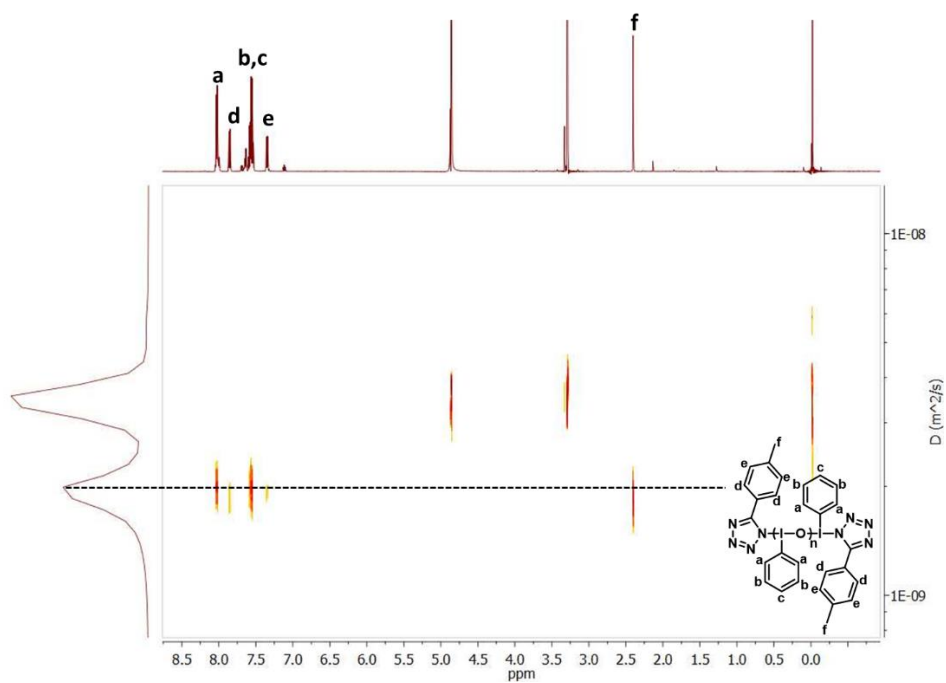


Figure III-9 DOSY NMR spectrum of **2c** in CD₃OD.

Unfortunately, while doing the reactivity study it was realized that the tetrazole containing HV iodine compounds can exchange ligand with CH₃OH to form PhI(OCH₃)₂ which makes the DOSY NMR data unreliable.

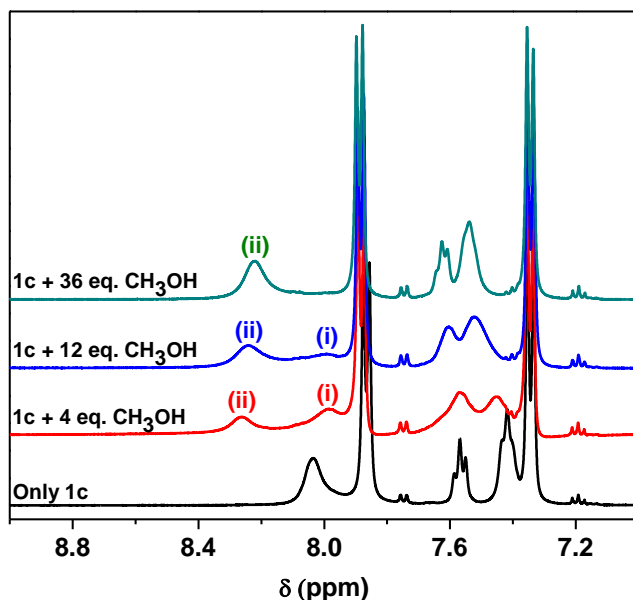
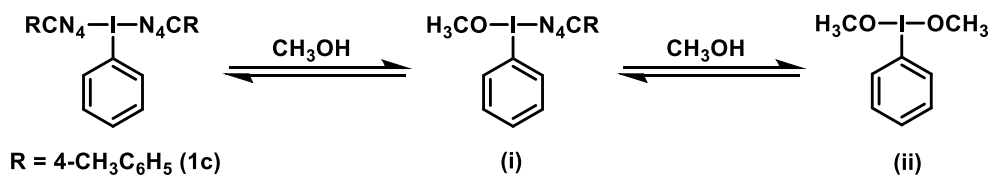


Figure III-10 ¹H NMR spectra of compound **1c** (80 mM) in DMSO-*d*₆ after adding 4 eq, 12 eq, and 36 eq of CH₃OH.

After that, detailed kinetic study was done to understand the ligand exchange between compound **1c** and CH₃OH. The reaction between **1c** and increasing amounts of MeOH was examined by ¹H NMR in DMSO-*d*₆ and the results suggested that the exchange reaction indeed occurred (Figure III-10). It was observed that CH₃OH reacts rapidly with **1c** to form mono- and di-

methoxy HV iodine(III) products (shown as (i) and (ii) in Figure III-10). In the first NMR tube (4 eq. of MeOH), both mono- and di- methoxy compounds were clearly visible at 7.99 ppm and 8.26 ppm, respectively. On the other hand, as the amount of CH₃OH was increased (12 eq.), the intensity of the peak associated with mono-substituted compounds HV iodine compound decreased and eventually disappeared in the presence of excess CH₃OH (36 eq.) as shown in the Figure III-10.

Growing single crystals of the studied compounds, suitable for single crystal X-ray diffraction, proved to be a challenging task. However, **2b** was obtained as a polycrystalline powder with an excellent crystallinity. Therefore, the crystal structure was analyzed using powder X-ray diffraction data, collected with synchrotron radiation. The structure was solved using the Simulated Annealing algorithm, and refined by the Rietveld method. The molecule of **2b** consists of three iodine atoms (Figure III-11a), linked through bridging oxygen atoms, with I–O distances ranging between 1.95 and 2.08 Å. The two terminal iodine atoms are coordinated by the nitrogen atoms (N2) of the 5-phenyl tetrazole units, with I–N bond distances of 2.443(1) Å and 2.401(1) Å, respectively. The N–I–O–I–O–I–N fragment of the structure adopts a characteristic zigzag geometry, because of the almost linear (with maximum deviation from linearity of 11 °) arrangement of the structural motif L–I–L, where L is either bridging O atom or the N2 atom of the terminal tetrazole ligands, combined with the valent angles of about 131.7(1)° and 120.7(1)° in the I–O–I fragments. This geometry is similar to other HV iodine(III) compounds.⁷¹ As mentioned, the N–I–O and O–I–O angles were refined to be close to linear. Each iodine atom is coordinated to a phenyl group, with I–C bond distances ranging between 2.00 and 2.12 Å. The three phenyl groups are positioned perpendicularly to the zigzag motif of the oligomer backbone, and aligned in almost parallel fashion one to another, with an average π – π distance of 3.8 Å. The crystal packing of **2b** is

made of infinite, one-dimensional molecular chains, connected with relatively strong intermolecular I...N bonds (2.99(1) Å and 3.12(1) Å), as shown in Figure III-11b.

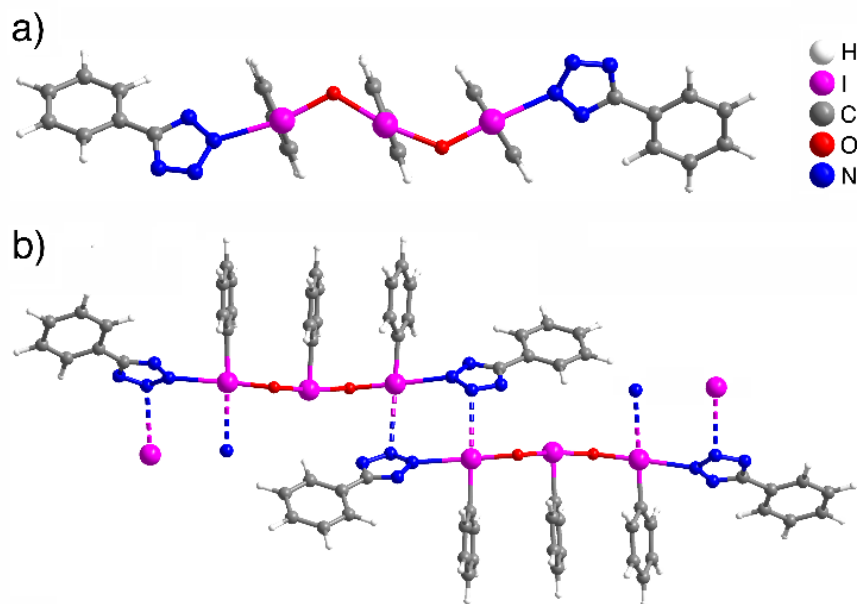


Figure III-11 a) One molecule of **2b** featuring three HV iodine(III) atoms, linked by bridging oxygen atoms and terminal nitrogen (N2) atoms of the 5-phenyltetrazole units in a zigzag motif. b) Intermolecular I...N interactions between two neighbouring molecules in the crystal packing of **2b**.

We noticed that the lone pair of N3 of the tetrazole groups was not directed exactly as one would expect. However, all attempts to model the orientation resulted in worse fit to the Rietveld plot. Considering that the orientation deviates by only few degrees (and the I...N is relatively weak bonding), we decided to present the structure as freely refined (as it is customary for solving crystal structures from powder diffraction data). This observation might be a result from local disorder, *i.e.*, it can be assumed that the tetrazole ring is rotationally disordered and the presented structure is an average of all positions. Due to severe limitations of the powder X-ray diffraction method, it

is not possible to address this potential disorder issue in much greater detail. Less likely, this observation might be due to steric effects in the solid state, where the crystal packing “forces” the tetrazole ligand in a slightly deviated angle with respect to the I atom. A close inspection of difference Fourier electron density map did not indicate the presence of solvent molecules. However, we cannot exclude the possibility of disordered solvent molecules in close contacts with the **2b** molecule in the solid-state. Unfortunately, even if present, these solvent molecules would be difficult to detect even with single crystal diffraction, due to (potentially) low occupancies and disorder.

III.2.1.1. Reactivity

In the above discussion, the preparation of HV iodine(III) compounds with two tetrazole terminal groups, containing only one HV iodine(III) atom (compounds **1a-c**), two HV iodine(III) atoms connected through an oxo-bridge (the μ -oxo compounds **3a-c**), and more than two iodine(III) atoms and several oxo-bridges (the oligomeric compounds **2b-c**) was demonstrated. Tetrazoles are commonly used as propellants and explosives and it was interesting to test and compare the thermal stability of a series of HV iodine(III) compounds with two identical tetrazole ligands at both ends of molecules with different chain lengths. Four compounds (several milligrams) were charged in four test tubes, namely 5-(p-tolyl)tetrazole, and compounds with the general formula $4\text{-CH}_3\text{C}_6\text{H}_4\text{CN}_4\text{-I(Ph)-[O-I(Ph)]}_n\text{-N}_4\text{CC}_6\text{H}_4(4\text{-})\text{CH}_3$ with $n = 0$ (i.e., compound **1c**), $n = 1$ (i.e., the μ -oxo compound **3c**), and $n = 2\text{-}3$ (mixture of oligomers **2c**). The test tubes were immersed in an oil bath, the temperature of which was gradually increased and monitored. The lowest molecular weight HV iodine(III) compound, which contained the largest molar fraction of tetrazole groups, decomposed explosively at ca. 135 °C, and it was followed by the next higher

molecular weight (μ -oxo) compound at ca. 145 °C. Eventually, the oligomer exploded at ca. 178 °C, at which point the experiment was stopped. The parent tetrazole was stable up to the end of the heating (i.e., up to ca. 180 °C). The experiment was recorded and can be found as a video file at this [web address](#). It can be expected that control over the degree of polymerization in oligomers of type **2** would allow for control over the temperatures of explosive degradation. More detailed studies related to the thermal properties of tetrazole-containing HV iodine(III) compounds are underway.

Suarez and coworkers^{72, 73} demonstrated the use of $\text{PhI}(\text{O}_2\text{CCH}_3)_2\text{-I}_2$ in the acetoxylation of various substrates, and the reaction was further implemented to the iodoacetoxylation of olefins.⁷⁴ In this context, compounds **3b-c** were reacted with cyclohexene and styrene in the presence of I_2 in different solvents, leading to the formation to iodotetrazolylation (addition) products. All reactions were performed in dark at 25 °C for 1 h as shown in Table 3.

Table III-4 Iodotetrazolylation reaction of cyclohexene.

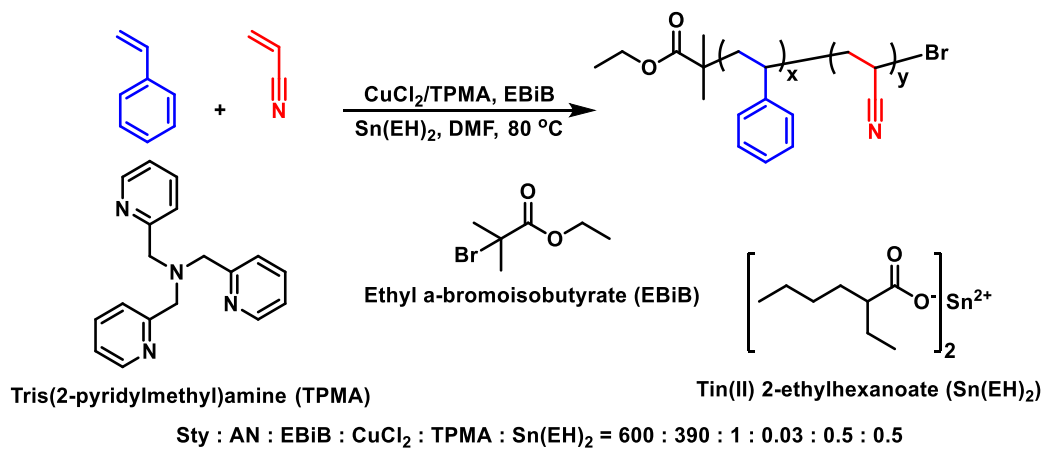
Entry	Reactant	Solvent	Yield (%)
1	3b	DCM	82
2	3c	DCM	72

III.2.2. Preparation of Network Polymers Using Tetrazole Containing HV Iodine(III) Compounds

To take advantage of tetrazole based HV iodine compounds, this chemistry was translated and applied to polymers to prepare tetrazole based polymer networks. In the following work, random copolymer of styrene (Sty) and acrylonitrile (AN) was prepared by controlled radical polymerization and the pendant nitrile groups present in the random copolymer were converted to tetrazole (or tetrazolate) groups. This tetrazole (or tetrazolate) groups were used to replace ligands in various HV iodine(III) compounds to form a polymer network.

III.2.2.1. Synthesis of random copolymer of Sty and AN (SAN)

The random copolymer of Sty and AN (SAN) is synthesized using Activators ReGenerated by Electron Transfer Atom Transfer Radical Polymerization (ARGET ATRP). Sty was chosen as comonomer since it forms an azeotrope with AN when the ratio of two monomers was kept 1.53:1 (Sty:AN) and copolymerize well. ARGET ATRP was performed since it uses low concentration of catalyst, tolerant to air, and works well with above mentioned monomers. ARGET ATRP was conducted with ethyl 2-bromoisobutyrate (EBiB) as an initiator and Tris(2-pyridylmethyl)amine (TPMA)/CuBr₂ as the catalyst. Tin(II) ethylhexanoate (Sn(EH)₂) was used as reducing agent to reduce Cu(II) to Cu(I). The polymerization was carried out at 80 °C in DMF as shown in Scheme III-3.



Scheme III-3 ARGET ATRP of Sty and AN.

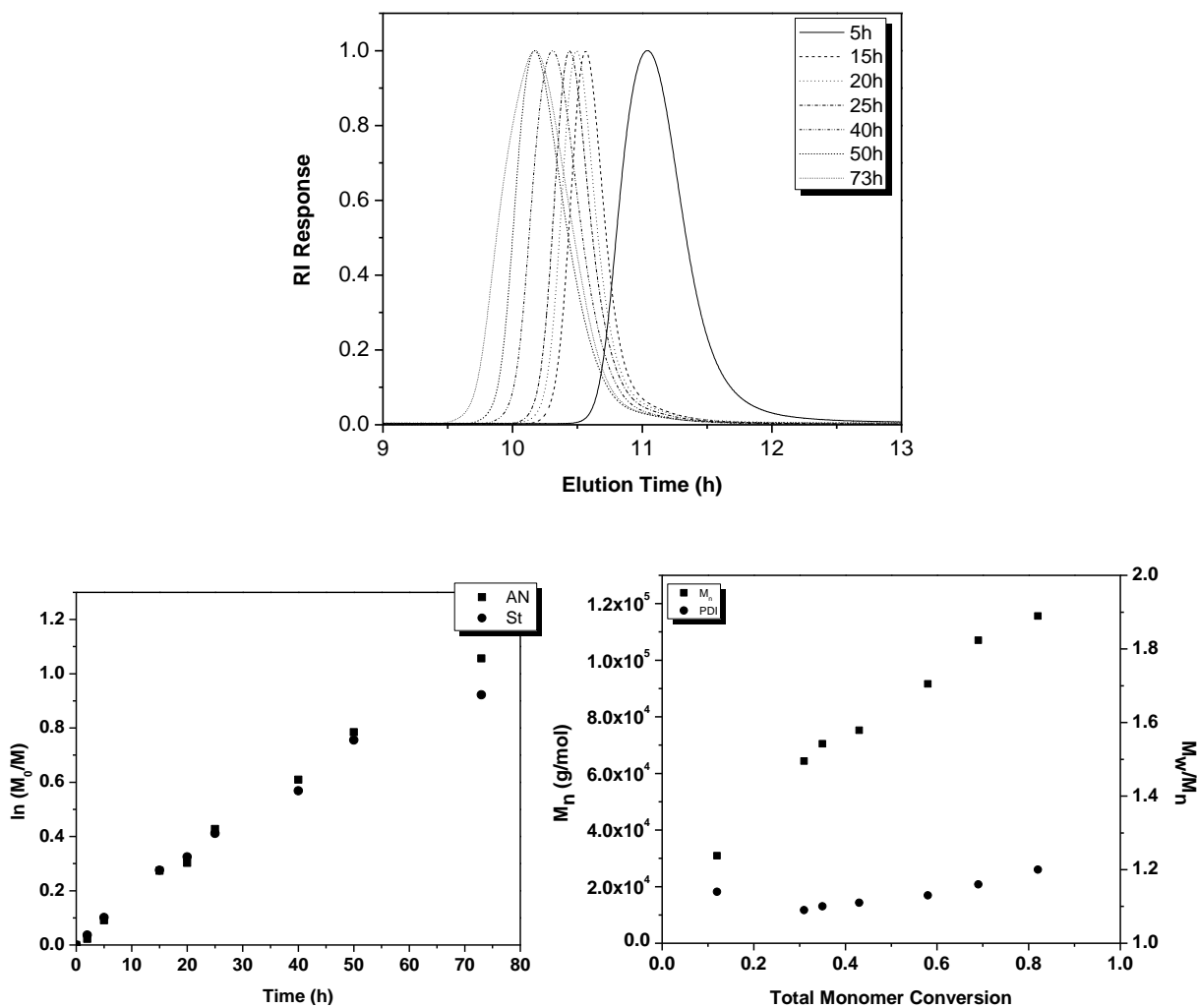
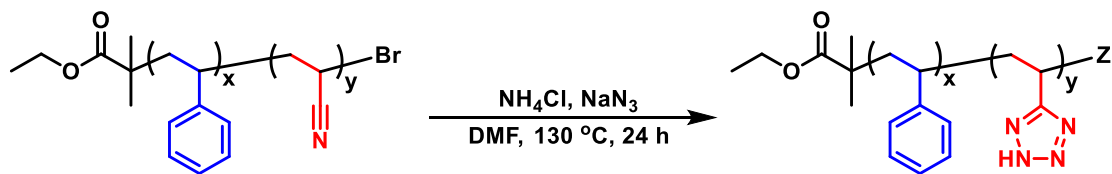


Figure III-12 Molecular weight evolution with time (on top) and kinetics of polymerization of Sty and AN (bottom).

The polymerization kinetics was monitored by ^1H NMR (for conversion) and SEC (for molecular weight) as shown in Figure III-12. The molecular weight of polymer increased and PDI decreased constantly with the conversion. After reaching the target DP, the polymerization was quenched by exposing the reaction mixture to air. After the reaction mixture reached room temperature, the polymer was precipitated in hexane to remove the impurities.

III.2.2.2. Conversion of nitrile groups to tetrazole groups.

After preparing SAN, the pendant nitrile groups were converted to tetrazole groups by reaction the polymer with NaN_3 and NH_4Cl in DMF at $130\text{ }^\circ\text{C}$ for 24 h (Scheme III-4). After the reaction was complete, polymer was precipitated in 0.5 N HCl solution to protonate the tetrazole groups completely. The final polymer (SVT) was characterized by FT-IR and compared with SAN. As expected, the characteristic nitrile peak (at 2240 cm^{-1}) present in SAN was not visible in the spectrum of SVT (Figure III-15), which showed the complete conversion of nitrile groups to tetrazoles.



Scheme III-4 Conversion of SAN to SVT.

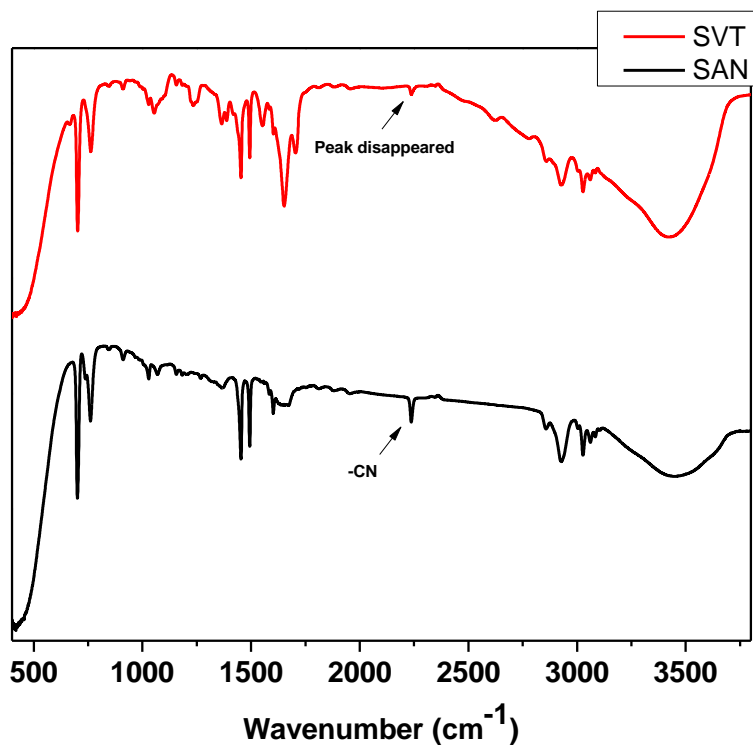
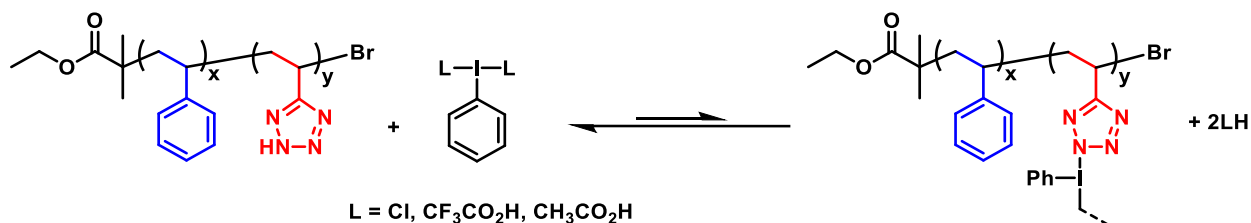


Figure III-13 FT-IR spectra of SAN and SVT.

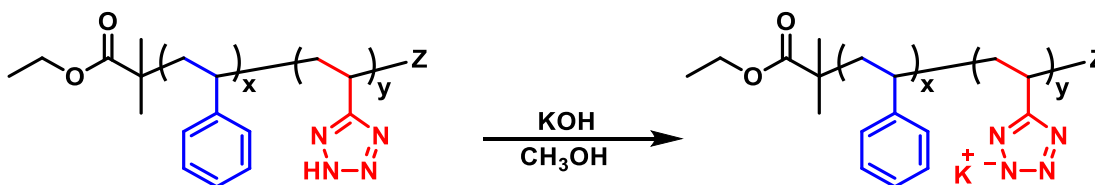
III.2.2.3. Preparation of network polymers using SVT and HV iodine(III) compounds

To prepare the gel, solutions (10 wt% and 8 wt%) of SVT was made DMF and these solutions were mixed with solutions of various HV iodine(III) compounds ($\text{PhI}(\text{O}_2\text{CCH}_3)_2$, $\text{PhI}(\text{O}_2\text{CCF}_3)_2$, and PhICl_2) with different concentrations (1 M, 0.8 M, 0.6 M, 0.4 M, and 0.2 M) as shown in Scheme III-5.



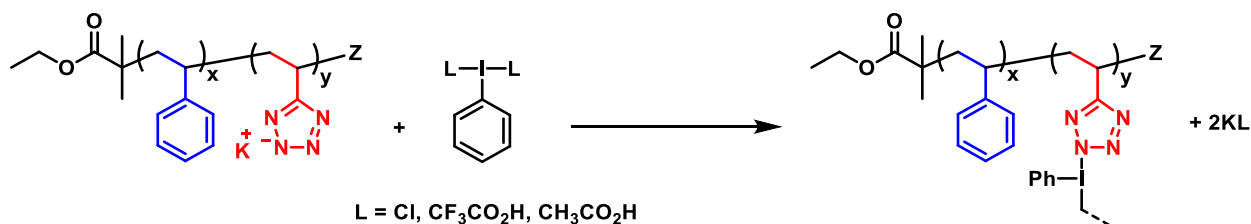
Scheme III-5 Preparation of polymer network using SVT.

The formation of gels was observed in several cases, but the formed networks were quickly disintegrated to yield initial polymer. This was due to the high affinity of acid byproducts ($\text{CH}_3\text{CO}_2\text{H}$, $\text{CF}_3\text{CO}_2\text{H}$, and HCl) towards the HV iodine crosslink bonds which shifted the reaction equilibrium to the left to give initial HV iodine compound and SVT.



Scheme III-6 Deprotonation of SVT.

To solve this issue, the tetrazole pendant groups in SVT were deprotonated and converted to corresponding potassium salts (SVT^-K^+) using KOH in CH_3OH . As mentioned above, it was observed that the potassium salts of tetrazoles were better choice to prepare tetrazole containing HV iodine(III) compounds because the poor solubility of byproducts drive the reaction forward. Similar approach was tried to prepare the polymer network.



Scheme III-7 Preparation of network polymers using SVT^-K^+ .

The gels were prepared using similar method mentioned above (with same concentration) except, in this case, SVT^-K^+ was dissolved in deionized water. Using this approach, the network was formed immediately but the insoluble byproducts ($\text{CH}_3\text{CO}_2\text{K}$, $\text{CF}_3\text{CO}_2\text{K}$, and KCl) were trapped inside the gel. As a result of this, gels were fragile, non-homogeneous, and not suitable for any further characterization.

III.3. Experimental Section

III.3.1. Materials

5-Methyl-1H-tetrazole (Alfa Aesar, 97 %), 5-phenyl-1H-tetrazole (Alfa Aesar, 99 %), 5-(p-tolyl)-1H-tetrazole (TCI, 98 %), (diacetoxyiodo)benzene ($\text{PhI}(\text{O}_2\text{CCH}_3)_2$, Acros, 98 %), [bis(trifluoroacetoxy)iodo]benzene ($\text{PhI}(\text{O}_2\text{CCF}_3)_2$, Acros, 98 %), cyclohexene (Sigma-Aldrich, 97+ %), styrene (Acros, 99 %), trans-2-[3-(4-tert-butylphenyl)-2-methyl-2-propenyldene]malononitrile (DCTB, TCI, 98 %), NaCl (Sigma-Aldrich, 99.9 %), NaNO_3 (Sigma-Aldrich, 99.9 %), (*n*-Bu) $_4\text{NPF}_6$ (TCI, 98 %), I_2 (Sigma-Aldrich, 99.8 %), $\text{Na}_2\text{S}_2\text{O}_3$ (Acros, 99.8 %), $\text{CH}_3\text{CO}_2\text{H}$ (Sigma-Aldrich, 99 %), Na_2SO_4 (Sigma-Aldrich, 99.8 %), *N,N*-dimethylaniline (Sigma-Aldrich, 99 %) were used as received. Iodosylbenzene (PhIO) was synthesized using a procedure described in the literature,⁷⁵ which is based on the hydrolysis of $\text{PhI}(\text{O}_2\text{CCH}_3)_2$ with 3 M aqueous NaOH (pellets, 97+ %, Sigma-Aldrich, were employed to prepare the solution), followed by washing with chloroform (Acros, 99 % extra pure). Dichloriodobenzene (PhICl_2) was synthesized using a procedure described in the literature.⁷⁶ The solvents, including anhydrous acetonitrile (Acros, 99.9 %), anhydrous dichloromethane (Acros, 99.9 %), 1,2-dichloroethane (Acros, 99.8 %), diethyl ether (Acros, 99 %), *n*-hexane (Acros, 99.9 %), methanol (Acros, 99.8 %) were used as received.. The deuterated solvents, $\text{DMSO-}d_6$ (Acros, 99.8 % D), $\text{DMF-}d_7$ (Alfa

Aesar, 99.5 % D), CD₃CN (Cambridge Isotope Laboratories, 99.8 % D), CDCl₃ (Cambridge Isotope Laboratories, 99.8 % D), CD₃OD (Cambridge Isotope Laboratories, 99.8 % D), contained a small amount of tetramethylsilane (TMS) as a chemical shift reference. All chemicals were used as received without further purification.

III.3.2. Analytical Procedures

NMR spectra were recorded on a Bruker Avance DRX (400 MHz) spectrometer. Compound **3b-c** were characterized by MALDI-ToF. MALDI mass spectra were acquired on a Shimadzu Axima Performance MALDI TOF-TOF (Shimadzu Biotech) in both positive and negative ion reflectron modes (100-1000 Da). For each compound, 100 profiles of 10 spectra/profile were collected at repetition rates of either 10 or 50 Hz. Laser power was optimized for each sample based on the intensity and resolution of the peaks in the spectra. Pulsed ion extraction voltages were optimized for the expected molecular weight of each compound. The matrix used was DCTB dissolved in methanol (30 mg/mL) and NaCl and NaNO₃ were used as doping agents. All spectra were baseline subtracted and Gaussian filtered for final analysis and compared with the matrix spectrum.

Electrochemical measurements were carried out in an electrochemical cell system controlled with a CHI620E electrochemical station (CH Instruments, Inc., USA) with a Pt wire as the counter electrode, AgNO₃/Ag as the reference and glassy carbon (GC) as working electrode while purging dry argon. All potential values are referenced to AgNO₃/Ag in 0.1 M (*n*-Bu)₄NPF₆ with 0.01 M AgNO₃ in DMF. Samples were prepared by dissolving 10⁻⁵ mol of the studied HV iodine(III) compounds in 10 mL of 0.1 M solution of (*n*-Bu)₄NPF₆ in dry and deoxygenated DMF. The sample (10 mL) was divided in 3 parts and CV measurements were done on each part only once at a

particular scan rate. For comparison, first, the redox potential of 1 mM ferrocene solution in DMF was measured with respect to AgNO_3/Ag at the same scan rates. All samples were prepared in glove box to avoid moisture or air.

Growing single crystals of size and quality suitable to single crystal X-ray diffraction analyses proved to be a very challenging task. However, the compound **2b** was obtained as a polycrystalline powder with an exceptionally high crystallinity (reflected in the well-resolved and sharp diffraction peaks). Therefore, the sample was amenable to analyses using the methods of powder X-ray diffraction.

To ensure high-resolution and high-quality diffraction data, the powder X-ray diffraction pattern of **2b** was collected using synchrotron radiation, at the beamline 17-BM at the Advanced Photon Source (Argonne National Laboratory). The average wavelength of X-rays was set to be 0.45236 Å, and the exposition time was in the range of minutes. No beam-damage was evidenced during data collection. Scattered intensity was recorded by a Perkin Elmer a-Si Flat Panel detector at room temperature. The experiment was performed at room temperature. Prior to diffraction data collection, the sample was manually ground with pestle in a mortar, and sealed in borosilicate glass capillary of 1 mm diameter (Hilgenberg glass No. 50). The capillary was placed on the goniometer head, and spun during data collection to ensure better particle statistics, and mitigate possible preferred orientation of the particles. The sample handling was done under minimal exposure to light to prevent possible photolysis.

The analysis of the data (pattern indexing, profile fitting, crystal structure solution and refinement) was performed with the program TOPAS 4.1. The pattern indexing was done with the singular value decomposition method, resulting in monoclinic unit cell. The space group was assumed to be either Cc or $C2/c$, and later the Rietveld refinement (Figure III-14) indicated the Cc

as more suitable space group. Precise lattice and peak profile parameters were determined by a structureless Pawley fitting, and later used in the crystal structure solution process. The crystal structure of **2b** was solved by the global optimization method of simulated annealing (SA) in real space. Considering the calculated unit cell volume ($\sim 3279.4 \text{ \AA}^3$), the general site multiplicity of the *Cc* space group (4), and the average volume occupied by a non-hydrogen atom, it was assumed that the asymmetric unit counts ~ 50 non-hydrogen atoms. Informed by chemical analyses and synthetic conditions, it was assumed that the asymmetric unit is composed of three iodobenzene and two 5-phenyl-tetrazole fragments, and two oxygen atoms (total of 51 non-hydrogen atoms). To decrease the number degrees of freedom and ease the global optimization process, the iodobenzene and phenyl-tetrazole structural fragments were introduced in form of independent rigid bodies. For the definition of the connectivity between the atoms within the rigid bodies *z* matrix notation was used. The SA process was initiated using a total of five rigid bodies and two oxygen atoms. During the SA runs three rotation and three translation parameters for each rigid body and oxygen atom were set flexible. In addition, the torsion angle within each phenyl-tetrazole was independently refined. An overall temperature factor for each atom type was included in the SA process.

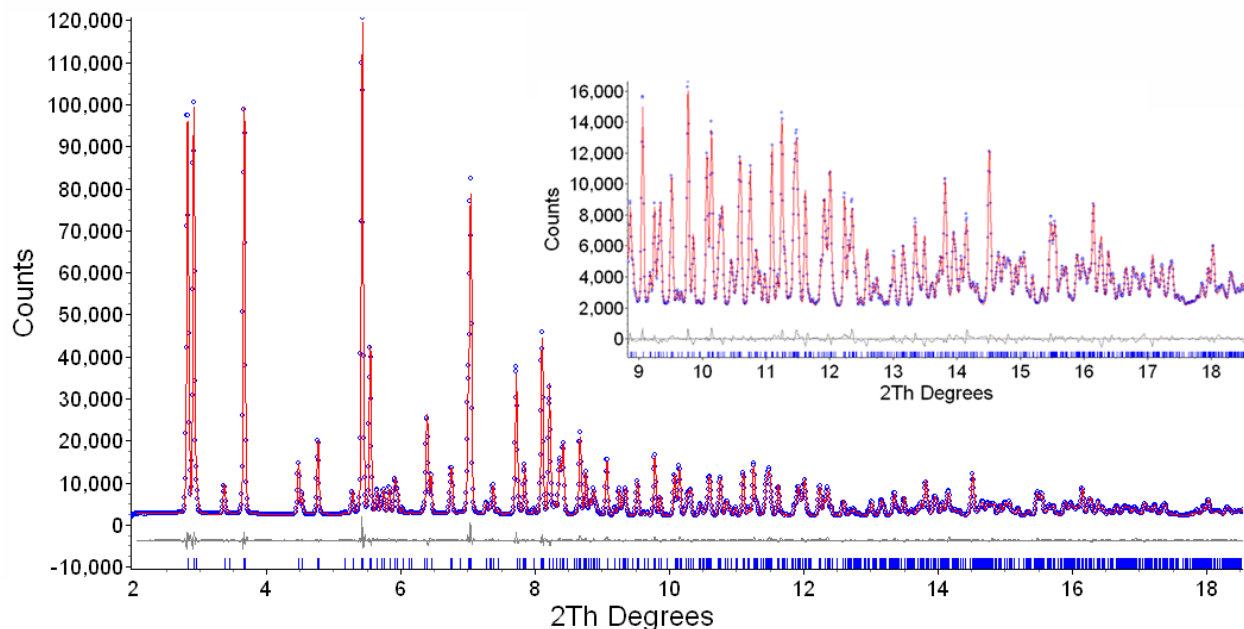


Figure III-14 Rietveld refinement plot of **2b**. Measured scattered intensity is presented with blue dots; the best fit with read line and the corresponding difference plot with gray line. The Bragg reflections are given with blue bars.

Once a global minimum was found, the crystal structures were subjected to Rietveld refinement, in which bond lengths and angles were refined within the rigid bodies, together with free refinement of all profile and lattice parameters. The refinement converged quickly with a reasonable figures-of-merit. The final Rietveld plot is presented in Figure III-14, and the crystallographic and structural data in the appendix. Hydrogen atoms were added at calculated positions by the program Mercury. Further crystallographic details are provided in the deposited CIF. It should be mentioned that the structure could be also described in the $C2/c$ space group and the molecule could be idealized to have a center of symmetry.

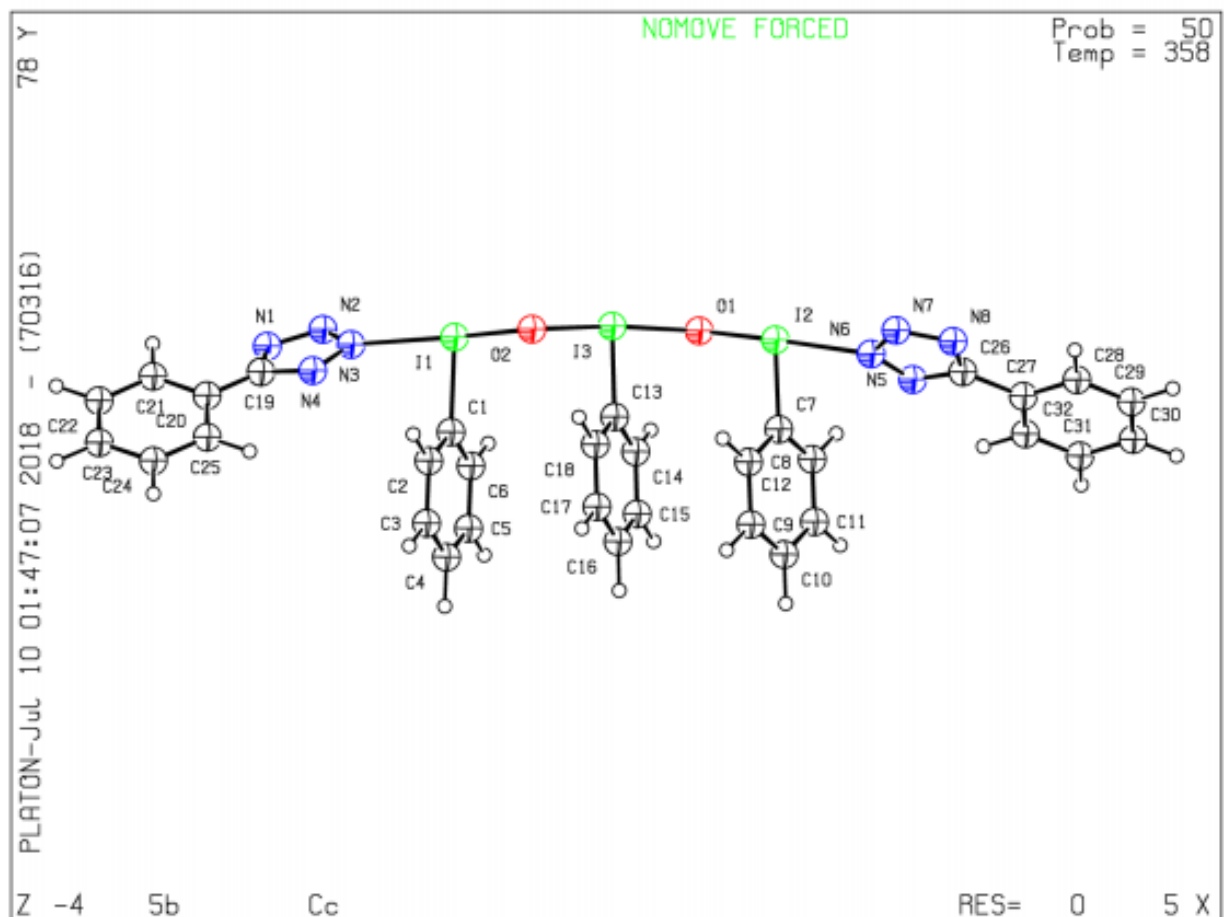


Figure III-15 Thermal ellipsoid plot for compound **2b**.

III.3.3. Synthetic Procedures

General procedure for the synthesis of HV iodine (III) compounds **2b-c** and **3b-c**

In a 10 mL dry reaction tube, a magnetic stir bar was placed followed by PhIO (2.0 mmol, 1 eq.) and tetrazoles (4.0 mmol, 2 eq.). The tube was capped with a rubber septum and wrapped with aluminum foil to prevent exposure of the contents to light. Then, dry solvent (2.0 mL) was injected, the tube was immersed in a water bath at 25 °C for two different time intervals: 2 h and 20 h. When the reaction time was 2 h, the products were **2b** or **2c**, whereas, when contact time was

increased to 20 h, mixture of oligomers **3b** or **3c** were obtained. Due to the poor solubility of both **2b** and **2c**, the spectroscopic characterizations were not performed.

*μ -Oxo-bis(5-phenyltetrazolyl)iodobenzene (**3b**)*. Following the general procedure, PhIO (0.44 g, 2.0 mmol) and **1b** (0.58 g, 4.0 mmol) were added in a vial followed by the addition of anhydrous CH₃CN (20.0 mL) and then removal of solvent in 20 h yielded **4b** (0.80 g, 60 %) as an off-white solid; ¹H NMR (400 MHz, DMF-*d*₇): δ 7.41 (m, 12H), 7.54 (m, 8H); ¹³C{¹H}NMR (400 MHz, DMF-*d*₇): δ 21.1, 126.6, 127.0, 128.0, 130.0, 131.0, 131.1, 133.7, 137.7 ppm; MALDI-ToF: calculated m/z for C₁₉H₁₅I₂N₄O⁺ [M-N₄CC₆H₅]⁺: 568.9335; found: 568.8090.

*μ -Oxo-bis(5-*p*-tolyltetrazolyl)iodobenzene (**3c**)*. Following the general procedure, PhIO (0.44 g, 2.0 mmol) and **1c** (0.64 g, 4.0 mmol) were added in a vial followed by the addition of anhydrous CH₃CN (20.0 mL) and then removal of solvent in 20 h yielded **4c** (0.83 g, 56 %) as an off-white solid; ¹H NMR (400 MHz, DMF-*d*₇): δ 2.35 (s, 6H), 7.31 (d, *J* = 7.75 Hz, 4H), 7.44 (t, *J* = 7.5 Hz, 4H), 7.55 (t, *J* = 7.9 Hz, 2H), 7.92 (d, *J* = 7.8 Hz, 4H), 8.03 (b, 4H); ¹³C{¹H}NMR (400 MHz, DMF-*d*₇): δ 21.1, 126.6, 127.0, 128.0, 130.0, 131.0, 131.1, 133.7, 137.7 ppm; MALDI-ToF: calculated m/z for C₂₈H₂₃I₂N₈O⁻ [M-H]⁻: 741.0084; found: 740.9355.

Reaction of PhI(N₄RC)₂ and RCN₄-I(Ph)-[O-I(Ph)]_n-N₄CR with cyclohexene in the presence of I₂

In a 10 mL reaction tube, a stir bar was placed followed by **3b** (0.37 g, 1.0 mmol) and the tube was wrapped with aluminum foil to protect the contents from light. Then, anhydrous DCM (2.0 mL) was added and the tube was immersed in a water bath at 25 °C and stirred until the solution became clear (ca. 30 min). Then, I₂ (0.26 g, 1.0 mmol) was added and clear solution turned

turbid white. This heterogeneous solution was stirred for another 5 min. and cyclohexene (0.11 mL, 1.0 mmol) was added using a micropipette. It was noted that upon the addition of cyclohexene the color turned brown and the solution remained heterogeneous. After 1 h, the reaction was quenched using 10 % Na₂S₂O₃ and the contents were extracted with CH₂Cl₂ (5×10 mL). All the CH₂Cl₂ layers were collected and washed with distilled water (3×10 mL), dried over Na₂SO₄, and then the solvent was evaporated using rotovap to obtain a yellow oil as the crude product. The crude product was dissolved in CH₂Cl₂ (1.0 mL) and hexane (20.0 mL) was added. Subsequently, the mixture was left at room temperature for about an hour to obtain crystals of pure product (0.218 g, 74.8 % yield). Similar experiments were carried out with **3c** in different solvents.

1-(2-iodocyclohexyl)-5-phenyltetrazole. Following the above procedure, product **6b** was obtained as colorless crystalline compound (0.30 g, 85 %); ¹H NMR (400 MHz, CD₃CN): δ 7.80–7.40 (m, 5H), 4.70 (ddd, J = 12.4, 10.9, 4.2 Hz, 1H), 4.64–4.50 (m, 1H), 2.64–2.55 (m, 1H), 2.39–2.04 (m, 4H), 1.75–1.12 (m, 3H); ¹³C{¹H}NMR (400 MHz, CD₃CN): δ 155.6, 132.2, 130.3, 130.3, 125.1, 65.3, 40.2, 35.1, 33.9, 28.2, 25.0 ppm; GC-MS: calculated m/z for C₁₃H₁₅IN₄: 354.19; found: 354.0. ¹H NMR spectrum is in agreement with that reported.⁸⁵

1-(2-iodocyclohexyl)-5-(p-tolyl)tetrazole. Following the above procedure, product **6c** was obtained as colorless crystalline compound (0.29 g, 80 %); ¹H NMR (400 MHz, CD₃CN): δ 7.80–7.40 (m, 5H), 4.70 (ddd, J = 12.4, 10.9, 4.2 Hz, 1H), 4.64–4.50 (m, 1H), 2.64–2.55 (m, 1H), 2.39–2.04 (m, 4H), 1.75–1.12 (m, 3H); ¹³C{¹H}NMR (400 MHz, CD₃CN): δ 155.5–152.8, 141.3, 129.5, 128.7, 120.4, 117.2, 63.8, 33.7, 32.7, 26.8, 23.6, 20.2 ppm; HRMS: calculated for C₁₄H₁₇IN₄ [M+H]⁺: 369.0566; found: 369.0571.

Interaction of (*n*-Bu)₄NPF₆ with **1c** in DMF

To monitor the effect of (*n*-Bu)₄NPF₆ on compound **3c** in DMF, 9.4 mg (0.018 mmol) of **1c** was dissolved in 0.9 mL of DMF-*d*₇ to prepare a 20 mM solution. The solution was then transferred into NMR tube and an initial ¹H NMR spectrum was collected. Then, (*n*-Bu)₄NPF₆ (0.1394 g, 0.359 mmol, 400 mM, 20 equiv with respect to compound **1c**) was added and the evolution of the NMR spectrum was monitored. No changes were observed even after 120 min (longer than the time needed for the CV measurements described in the next section), indicating that (*n*-Bu)₄NPF₆ does not react with **1c**, i.e., the salt was found to be a suitable electrolyte for the CV experiments.

Ligand exchange between **1c** and CH₃OH

Compound **1c** (0.0626 g, 0.119 mmol, 80 mM) was dissolved in DMSO-*d*₆ (1.5 mL) and the solution was divided into three equal parts. Then, CH₃OH (7 μL, 0.173 mmol, 4 equiv relative to **1c** or 20 μL, 0.495 mmol, 12 equiv relative to **1c**, or 58 μL, 1.435 mmol, 36 equiv relative to **1c**) was added to the first, second and third NMR tubes, respectively. Each reaction reached equilibrium (the relative peaks intensities remained constant) in less than 10 min but all spectra shown in Figure S8 were collected 30 min after the addition of CH₃OH.

Preparation of SAN

Styrene (20.0 mL, 0.1745 mol), acrylonitrile (7.43 mL, 0.1135 mol), and DMF (5 mL) were added to a dry Schlenk flask. Then, an initiator EBiB (0.0567 g, 0.291 mmol) and a solution of CuCl₂ complex (0.0012 g, 8.73 μmol)/TPMA (0.0025 g, 8.73 μmol) in DMF (2 mL) were added.

The resulting mixture was degassed by four freeze-pump-thaw cycles. After melting the mixture, a solution of $\text{Sn}(\text{EH})_2$ (0.0589 g, 0.146 mmol) and TPMA (0.0422 g, 0.146 mmol) in DMF (8 mL) was added. An initial sample was taken, and the sealed flask was placed in an oil bath set at 80 °C. Samples were taken at timed intervals and analyzed by NMR and gel permeation chromatography (GPC) to follow the progress of the reaction. The polymerization was stopped after 73 h by opening the flask and exposing the catalyst to air. The polymer was precipitated in hexane twice to yield the final polymer.

Conversion of SAN to SVT

First, SAN (3.9 g) was dissolved in 50 mL of DMF in a round bottom flask. Subsequently, NaN_3 (4.8 g) and NH_4Cl (5.1 g) was added to the solution and the flask was kept at 130 °C for 24 h. After stopping the reaction polymer was precipitated in 0.5 N HCl solution. The obtained polymer (PVT) was washed with acetone and dried under vacuum.

Conversion of SVT to SVT^+K^-

SVT was dissolved in basic solution of methanol (4 g in 50 mL) and kept for 2 h. Subsequently, ionic polymer was precipitated in ether and stirred until the solution became clear. The obtained polymer was dried under vacuum and characterized by FT-IR.

III.4. Conclusions

In conclusion, novel symmetric HV iodine(III) reagents containing different 5-substituted tetrazoles were prepared and were found to be reasonably stable under ambient conditions in both the solid and solution states. The compounds proved to be strong oxidants which was confirmed by CV measurements. An oligomer with I-O-based backbone and tetrazole end groups was characterized by X-ray diffraction. The use of these reagents allowed oxidative iodotetrazolylations of styrene and cyclohexene as well as radical transfer of tetrazole groups to *N,N*-dimethylaniline. An attempt was made to prepare tetrazole based polymer network. Further investigations focused on expanding the utility of the HV iodine(III) reagents is currently in progress.

III.5. Acknowledgments

The authors gratefully acknowledge financial support by the National Science Foundation through a CAREER grant (CHE-1455200) to NVT. Professor Isaac Garcia-Bosch, Khashayar Rajabimoghadam, and Rachel Trammell are acknowledged for helping with the electrochemical measurements. Thanks to Dr. Tomce Runcevski for performing Powder X-ray diffraction. Powder X-ray diffraction data were collected on the 17-BM Beamline at the Advanced Photon Source, a U.S. Department of Energy Office of Science User Facility operated by Argonne National Laboratory.

III.6. References

- 1 Willgerodt, C. *J. Prakt. Chem.* **1886**, 33, 154.

- 2 Meyer, V.; Wachter, W. *Chem. Ber.* **1892**, 25, 2632.
- 3 Willgerodt, C. *Chem. Ber.* **1892**, 25, 3494.
- 4 Willgerodt, C. *Ber.* **1893**, 26, 357.
- 5 Willgerodt, C. *Ber.* **1893**, 26, 1307.
- 6 Hartmann, C.; Meyer, V. *Ber.* **1893**, 26, 1727.
- 7 Willgerodt, C. *Die Organischen Verbindungen mit Mehrwertigem Jod*; Ferdinand Enke, Stuttgart, 1914.
- 8 Hach, R. J.; Rundle, R. E. *J. Am. Chem. Soc.* **1951**, 73, 4321.
- 9 Pimentel, G. C. *J. Chem. Phys.* **1951**, 19, 446.
- 10 Rundle, R. E. *Survey Chem. Prog.* **1963**, 1, 81.
- 11 Musher, J. I. *Angew. Chem. Int. Ed.* **1969**, 8, 54.
- 12 Varvoglis, A. *Organic Compounds of Polycordinated Iodine*; Wiley-VCH, Weinheim, 1992.
- 13 Varvoglis, A. *Hypervalent Iodine in Organic Synthesis*; Academic Press, San Diego, 1997.
- 14 Wirth, T. *Hypervalent Iodine Chemistry: Modern Developments in Organic Synthesis*; Springer, Berlin, 2003.
- 15 Zhdankin, V. V. *Hypervalent Iodine Chemistry: Preparation, Structure and Synthetic Applications of Polyvalent Iodine Compounds*; Wiley, Chichester, 2014.
- 16 Sandin, R. B. *Chem. Rev.* **1943**, 32, 249.
- 17 Banks, D. F. *Chem. Rev.* **1966**, 66, 243.
- 18 Koser, G. F. In *Ch. 18: Hypervalent Halogen Compounds*; Wiley, Chichester, 1983; Vol. 1. p 721.
- 19 Varvoglis, A. *Synthesis* **1984**, 709.

- 20 Moriarty, R. M.; Prakash, O. *Acc. Chem. Res.* **1986**, *19*, 244.
- 21 Stang, P. J.; Zhdankin, V. V. *Chem. Rev.* **1996**, *96*, 1123.
- 22 Muraki, T.; Togo, H.; Yokoyama, M. *Rev. Heteroatom Chem.* **1997**, *17*, 213.
- 23 Zhdankin, V. V.; Stang, P. J. *Chem. Rev.* **2002**, *102*, 2523.
- 24 Zhdankin, V. V.; Stang, P. J. *Chem. Rev.* **2008**, *108*, 5299.
- 25 Zhdankin, V. V.; Protasiewicz, J. D. *Coord. Chem. Rev.* **2014**, *275*, 54.
- 26 Yoshimura, A.; Zhdankin, V. V. *Chem. Rev.* **2016**, *116*, 3328.
- 27 Vaish, A.; Tsarevsky, N. V. In *Hypervalent Iodine Compounds in Polymer Science and Technology*; Wiley, 2018. pp 483.
- 28 Eisenberger, P.; Gischig, S.; Togni, A. *Chem. Eur. J* **2006**, *12*, 2579.
- 29 Wang, Y.-F.; Qiu, J.; Kong, D.; Gao, Y.; Lu, F.; Karmaker, P. G.; Chen, F.-X. *Org. Biomol. Chem* **2015**, *13*, 365.
- 30 Vita, M. V.; Waser, J. *Org. Lett.* **2013**, *15*, 3246.
- 31 Togo, H.; Katohgi, M. *Synlett* **2001**, 565.
- 32 Wang, X.; Studer, A. *Acc. Chem. Res.* **2017**, *50*, 1712.
- 33 Zhdankin, V. V.; Kuehl, C. J.; Krasutsky, A. P.; Formanek, M. S.; Bolz, J. T. *Tetrahedron Lett.* **1994**, *35*, 9677.
- 34 Akai, S.; Okuno, T.; Egi, M.; Takada, T.; Tohma, H.; Kita, Y. *Heterocycles* **1996**, *42*, 47.
- 35 Han, H.; Tsarevsky, N. V. *Chem. Sci.* **2014**, *5*, 4599.
- 36 Kumar, R.; Cao, Y.; Tsarevsky, N. V. *J. Org. Chem.* **2017**, *82*, 11806.
- 37 Papadopoulou, M.; Varvoglis, A. *J. Chem. Res. (S)* **1983**, *3*, 66.
- 38 Fan, Y.; Wan, W.; Ma, G.; Gao, W.; Jiang, H.; Zhu, S.; Hao, J. *Chem. Commun.* **2014**, *50*, 5733.

- 39 Rabet, P. T. G.; Fumagalli, G.; Boyd, S.; Greaney, M. F. *Org. Lett.* **2016**, *18*, 1646.
- 40 Zhdankin, V. V.; Arbit, R. M.; McSherry, M.; Mismash, B.; Young, V. G. *J. Am. Chem. Soc.* **1997**, *119*, 7408.
- 41 Zhdankin, V. V.; Arbit, R. M.; Lynch, B. J.; Kiprof, P.; Young, V. G. *J. Org. Chem.* **1998**, *63*, 6590.
- 42 Díaz-Requejo, M. M.; Belderraín, T. R.; Nicasio, M. C.; Trofimenko, S.; Pérez, P. J. *J. Am. Chem. Soc.* **2003**, *125*, 12078.
- 43 Chang, J. W. W.; Chan, P. W. H. *Angew. Chem. Int. Ed.* **2008**, *47*, 1138.
- 44 Llaveria, J.; Beltrán, Á.; Díaz-Requejo, M. M.; Pérez, P. J.; Matheu, M. I.; Castellón, S. *Angew. Chem. Int. Ed.* **2010**, *49*, 7092.
- 45 Meprathu, B. V.; Protasiewicz, J. D. *Tetrahedron* **2010**, *66*, 5768.
- 46 Yoshimura, A.; Nemykin, V. N.; Zhdankin, V. V. *Chem. Eur. J.* **2011**, *17*, 10538.
- 47 Brand, J. P.; González, D. F.; Nicolai, S.; Waser, J. *Chem. Commun.* **2011**, *47*, 102.
- 48 More, A. A.; Pathe, G. K.; Parida, K. N.; Maksymenko, S.; Lipisa, Y. B.; Szpilman, A. M. *J. Org. Chem.* **2018**, *83*, 2442.
- 49 Tsarevsky, N. V. *J. Polym. Sci., Part A: Polym. Chem.* **2010**, *48*, 966.
- 50 Katak, A. A.; Potavathri, S.; Barham, R. A.; Romano, K. M.; Deboef, B. *J. Am. Chem. Soc.* **2011**, *133*, 19960.
- 51 Katak, A. A.; Marchetti, L.; DeBoef, B. *Chem. Commun.* **2015**, *51*, 3574.
- 52 Kiyokawa, K.; Kosaka, T.; Kojima, T.; Minakata, S. *Angew. Chem. Int. Ed.* **2015**, *54*, 13719.
- 53 Yoshimura, A.; Koski, S. R.; Fuchs, J. M.; Saito, A.; Nemykin, V. N.; Zhdankin, V. V. *Chem. Eur. J.* **2015**, *21*, 5328.

- 54 Ciesielski, J.; Dequirez, G.; Retailleau, P.; Gandon, V.; Dauban, P. *Chem. Eur. J* **2016**, *22*, 9338.
- 55 Souto, J. A.; Martínez, C.; Velilla, I.; Muñoz, K. *Angewandte Chemie - International Edition* **2013**, *52*, 1324.
- 56 Liu, D.; Bielawski, C. W. *Poly. Int.* **2016**, *66*, 70.
- 57 Kim, H. J.; Kim, J.; Cho, S. H.; Chang, S. *J. Am. Chem. Soc.* **2011**, *133*, 16382.
- 58 Benson, F. R. *Chem. Rev.* **1947**, *41*, 1.
- 59 Butler, R. N. *Adv. Heterocyclic Chem.* **1977**, *21*, 323.
- 60 Butler, R. N. In *Ch. 4.13: Tetrazoles*; Pergamon, Oxford, 1984; Vol. 5. pp 791.
- 61 Koldobskii, G. I.; Ostrovskii, V. A. *Russ. Chem. Rev.* **1994**, *63*, 797.
- 62 Butler, R. N. In *Ch. 4.17: Tetrazoles*; Elsevier, Oxford, 1996; Vol. 4. pp 621.
- 63 Ostrovskii, V. A.; Koldobskii, G. I.; Trifonov, R. E. In *Ch. 6.07: Tetrazoles*; Elsevier, Oxford, 2008; Vol. 4. pp 257.
- 64 Singh Rajendra, P.; Verma Rajendar, D.; Meshri Dayal, T.; Shreeve Jean'ne, M. *Angew. Chem. Int. Ed.* **2006**, *45*, 3584.
- 65 Trifonov, R. E.; Ostrovskii, V. A. *Russ. J. Org. Chem.* **2006**, *42*, 1585.
- 66 Vanysek, P. In *Handbook of Chemistry and Physics*; CRC Press, Boca Raton, 1994.
- 67 McQuaid, K. M.; Pettus, T. R. R. *Synlett* **2004**, *2004*, 2403.
- 68 Barea, G.; Maseras, F.; Lledós, A. *New Journal of Chemistry* **2003**, *27*, 811.
- 69 Richter, H. W.; Cherry, B. R.; Zook, T. D.; Koser, G. F. *Journal of the American Chemical Society* **1997**, *119*, 9614.
- 70 Varvoglis, J. G.; Anastasios *J. Chem. Soc., Perkin Trans. 1* **1985**, *1985*, 757.

- 71 Nemykin, V. N.; Kopusov, A. Y.; Netzel, B. C.; Yusubov, M. S.; Zhdankin, V. V. *Inorg. Chem.* **2009**, *48*, 4908.
- 72 Jose I. Concepción Rosendo Herndndez, J. A. S.; Ernesto Suárez, C. G. F. *Tetrahedron Lett.* **1984**, *25*, 1953.
- 73 de Armas, P.; Carrau, R.; Concepción, J. I.; Francisco, C. G.; Hernández, R.; Suárez, E. *Tetrahedron Lett.* **1985**, *26*, 2493.
- 74 Achar, T. K.; Maiti, S.; Mal, P. *Org. Biomol. Chem* **2016**, *14*, 4654.
- 75 Saltzman, H. S., J. G. *Org. Synth.* **1973**, *5*, 658.
- 76 Karele, B. Y.; Neiland, O. Y. *Latv. PSR Zin. Akad. Vest.* **1970**, 587.

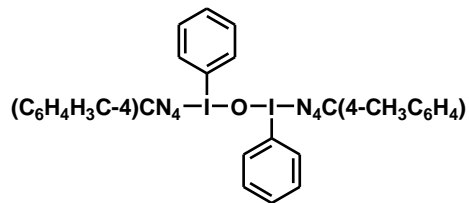
III.7. Appendix

III.7.1. Crystallographic Data

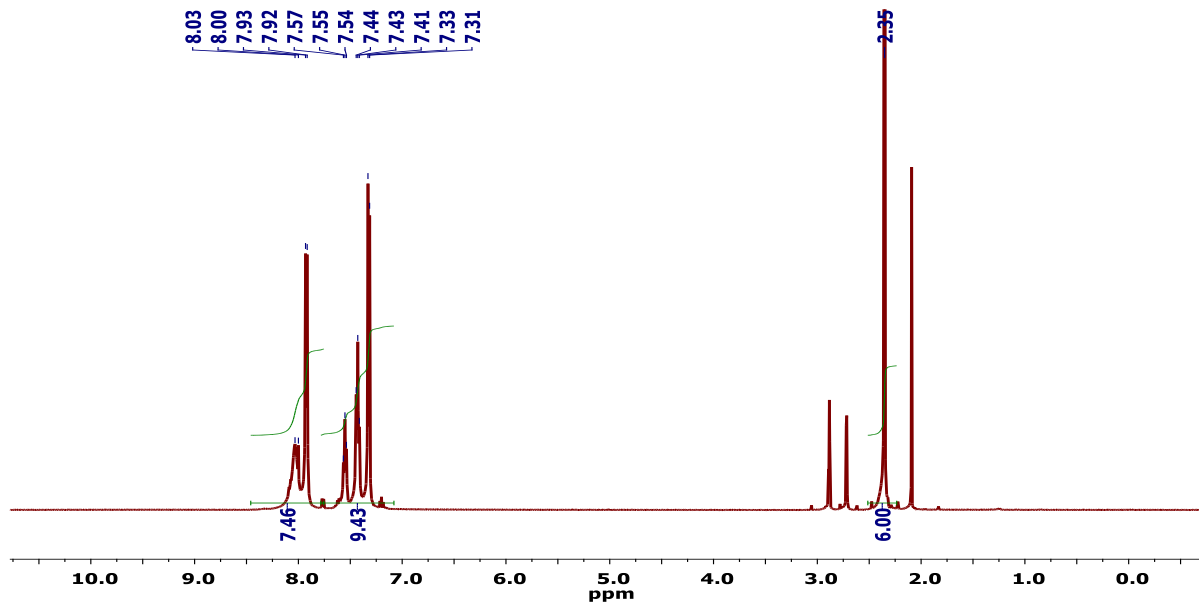
Sample	2b		
Wavelength / Å	0.45236		
X-ray source	Synchrotron radiation		
Temperature / K	358		
Crystal system	Monoclinic		
Space group	Cc		
<i>a</i> / Å	16.33100(11)		
<i>b</i> / Å	11.444378(86)		
<i>c</i> / Å	18.61358(15)		
β / °	70.50625(58)		
<i>R</i>_{exp}	1.328		
<i>R</i>_{wp}	3.169		
<i>R</i>_p	2.458		
<i>R</i>_{Bragg}	1.795		
<i>GOF</i>	2.386		
No. refined parameters	69		
Fractional coordinates			
Atom	x	y	z
I1	0.1901(2)	0.6162(7)	0.2139(2)
I2	0.4424(2)	0.6176(6)	-0.1850(2)
I3	0.3064(5)	0.6411(1)	0.0165(8)
C1	0.1906(2)	0.4303(7)	0.2176(2)
C2	0.2362(2)	0.3720(7)	0.2585(2)
C3	0.2364(2)	0.2497(7)	0.2608(2)
C4	0.1910(2)	0.1858(7)	0.2221(2)
C5	0.1454(2)	0.2441(7)	0.1812(2)
C6	0.1452(2)	0.3663(7)	0.1789(2)
C7	0.4436(2)	0.4427(6)	-0.1910(2)
C8	0.4738(2)	0.3767(6)	-0.1421(2)
C9	0.4745(2)	0.2545(6)	-0.1461(2)
C10	0.4451(2)	0.1983(6)	-0.2000(2)
C11	0.4150(2)	0.2642(6)	-0.2491(2)
C12	0.4143(2)	0.3864(6)	-0.2451(2)
C13	0.3168(5)	0.4635(1)	0.0138(8)
C14	0.2736(5)	0.3977(1)	-0.0259(8)
C15	0.2804(5)	0.2757(1)	-0.0277(8)
C16	0.3303(5)	0.2196(1)	0.0102(8)
C17	0.3736(5)	0.2854(1)	0.0499(8)

C18	0.3668(5)	0.4074(1)	0.0517(8)
C19	0.0103(2)	0.545(1)	0.4479(2)
C20	-0.0054(2)	0.497(1)	0.5205(2)
C21	-0.0778(2)	0.534(1)	0.5814(2)
C22	-0.0935(2)	0.485(1)	0.6540(2)
C23	-0.0368(2)	0.401(1)	0.6656(2)
C24	0.0356(2)	0.366(1)	0.6046(2)
C25	0.0513(2)	0.414(1)	0.5321(2)
C26	0.6377(3)	0.557(1)	-0.4080(2)
C27	0.6553(3)	0.512(1)	-0.4900(2)
C28	0.7318(3)	0.544(1)	-0.5490(2)
C29	0.7476(3)	0.503(1)	-0.6231(2)
C30	0.6870(3)	0.431(1)	-0.6391(2)
C31	0.6105(3)	0.399(1)	-0.5810(2)
C32	0.5947(3)	0.440(1)	-0.5070(2)
N1	-0.0489(2)	0.5973(1)	0.4263(2)
N2	-0.0124(2)	0.6315(1)	0.3558(2)
N3	0.0694(2)	0.6008(1)	0.3339(2)
N4	0.0834(2)	0.5477(1)	0.3908(2)
N5	0.5653(3)	0.5423(1)	-0.3530(2)
N6	0.5726(3)	0.5905(1)	-0.2921(2)
N7	0.6495(3)	0.6354(1)	-0.3100(2)
N8	0.6897(3)	0.6151(1)	-0.3821(2)
O1	0.3336(9)	0.635(1)	-0.1009(4)
O2	0.3027(5)	0.632(1)	0.1292(4)
Selected bond distances			
I2 – N6 / Å			2.401(1)
I2 – O1 / Å			1.947(1)
I3 – O1 / Å			2.08(1)
I3 – O2 / Å			2.08(2)
I1 – O2 / Å			1.991(1)
I1 – N3 / Å			2.443(1)
Selected angles			
N6 – I2 – O1 / °			177.07(1)
O1 – I3 – O2 / °			168.87(1)
O2 – I1 – N3 / °			168.74(1)

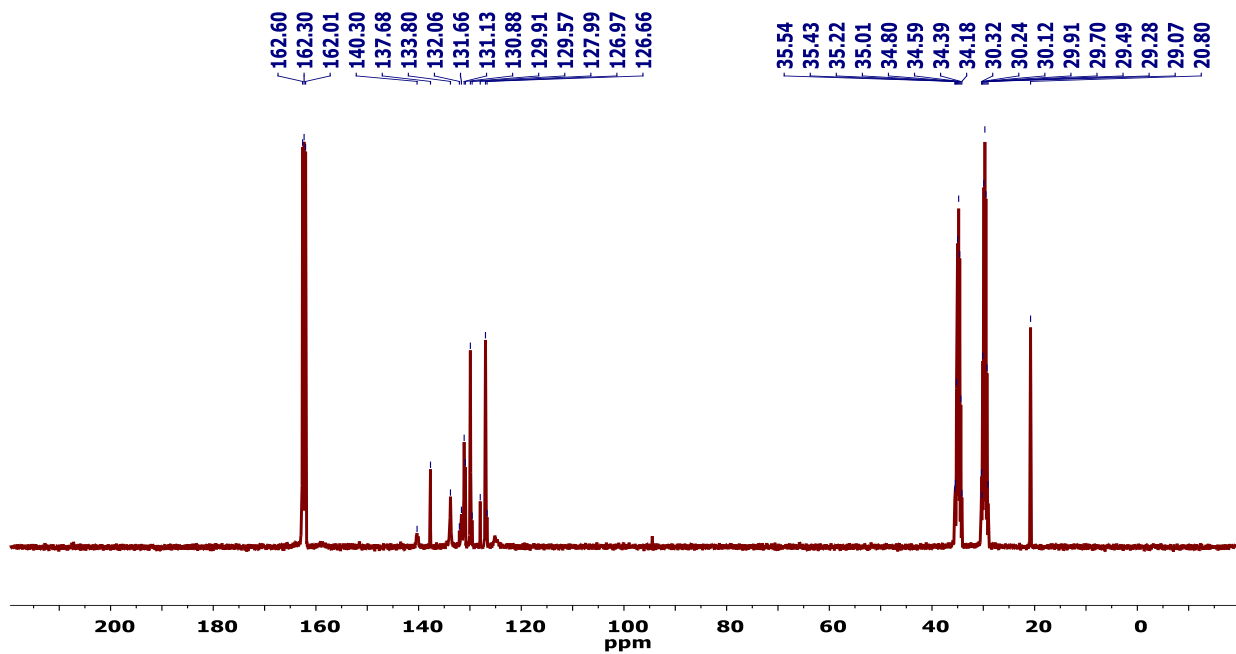
III.7.2. NMR Spectra

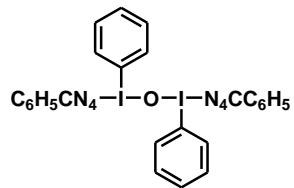


¹H NMR: (400 MHz, DMF-*d*₇)

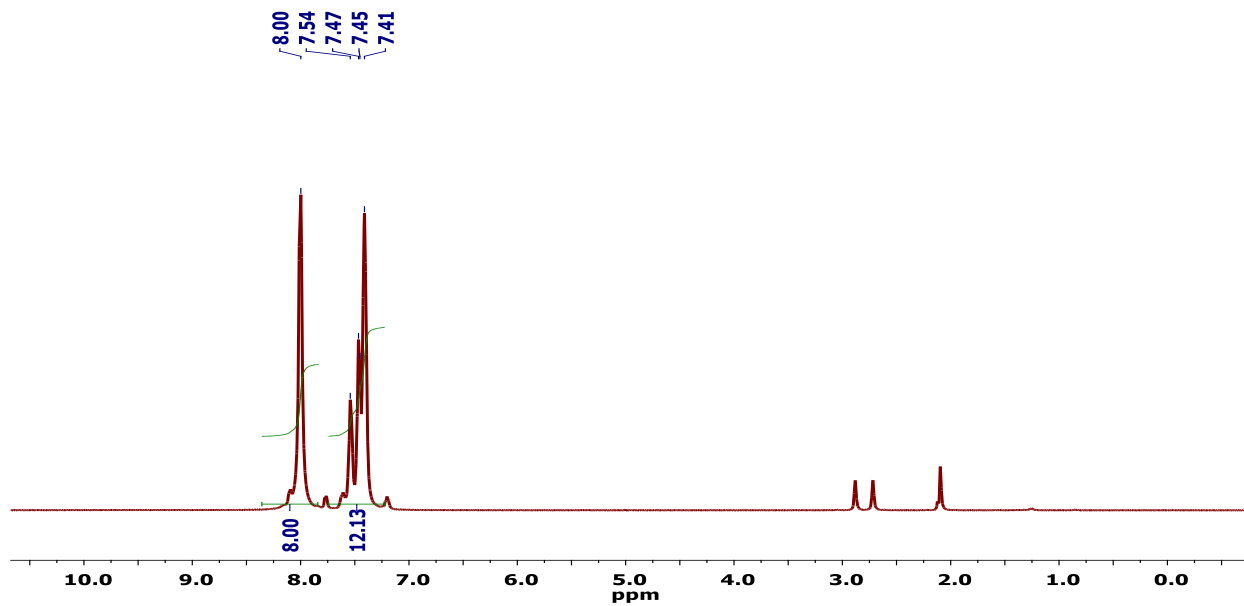


¹³C NMR: (400 MHz, DMF-*d*₇)

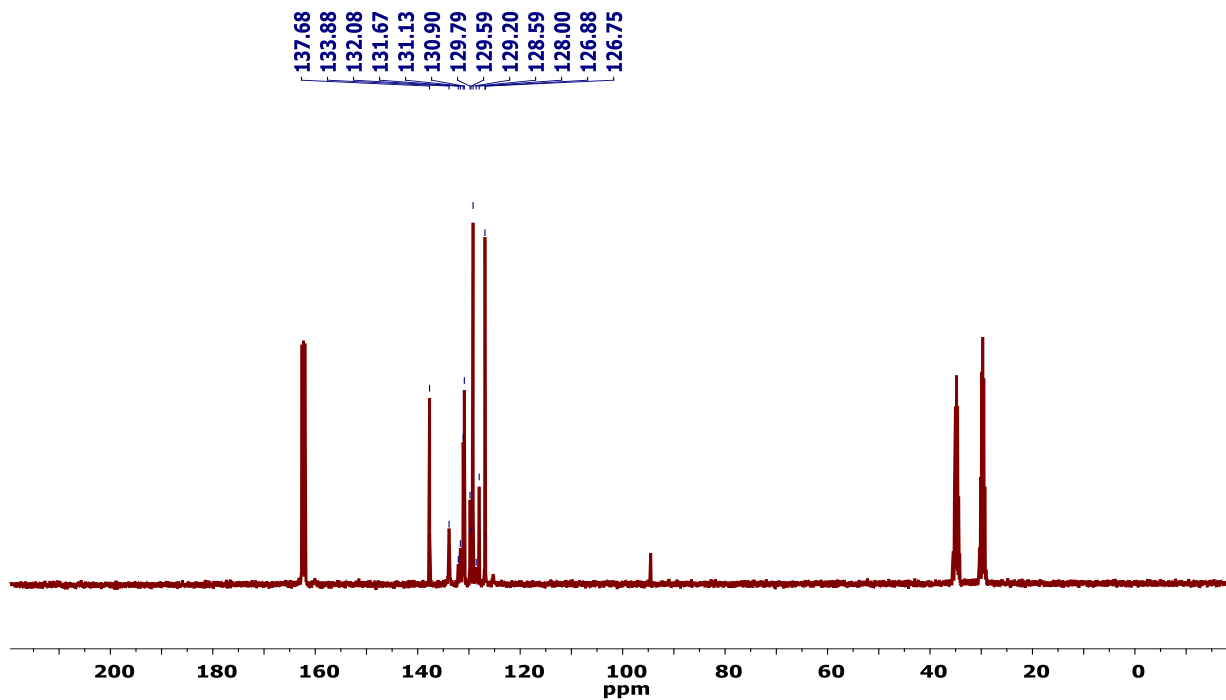


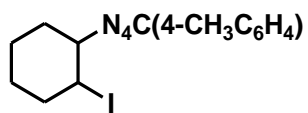


1H NMR: (400 MHz, DMF- d_7)

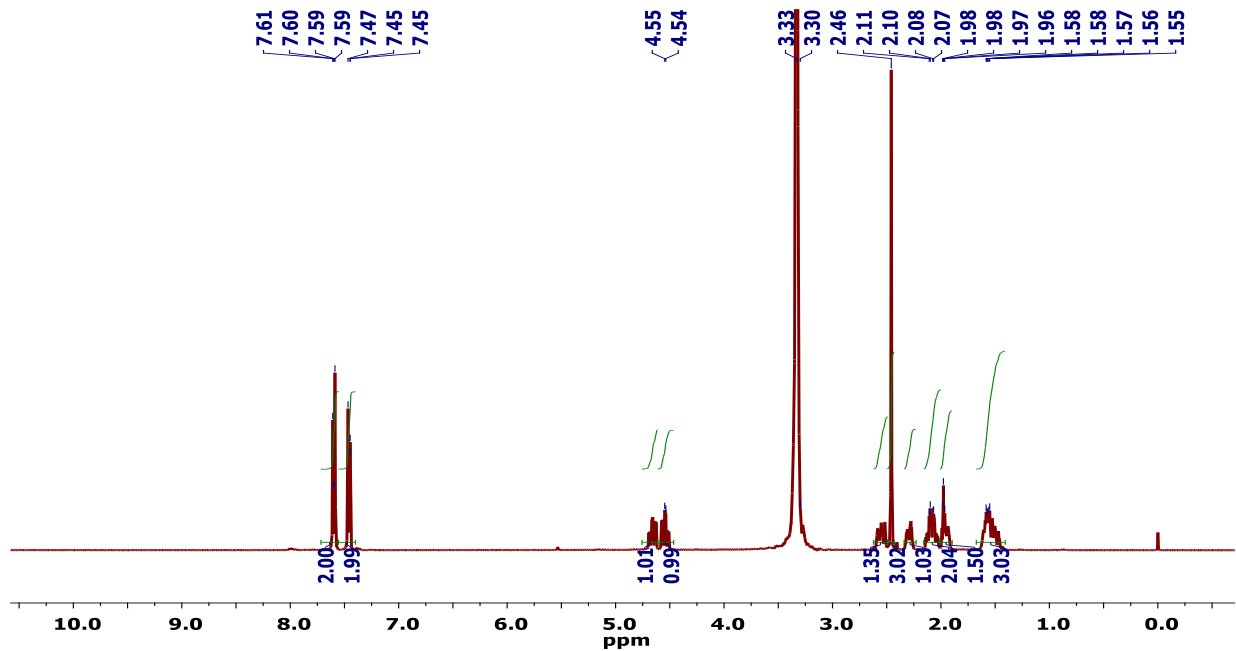


^{13}C NMR: (400 MHz, DMF- d_7)

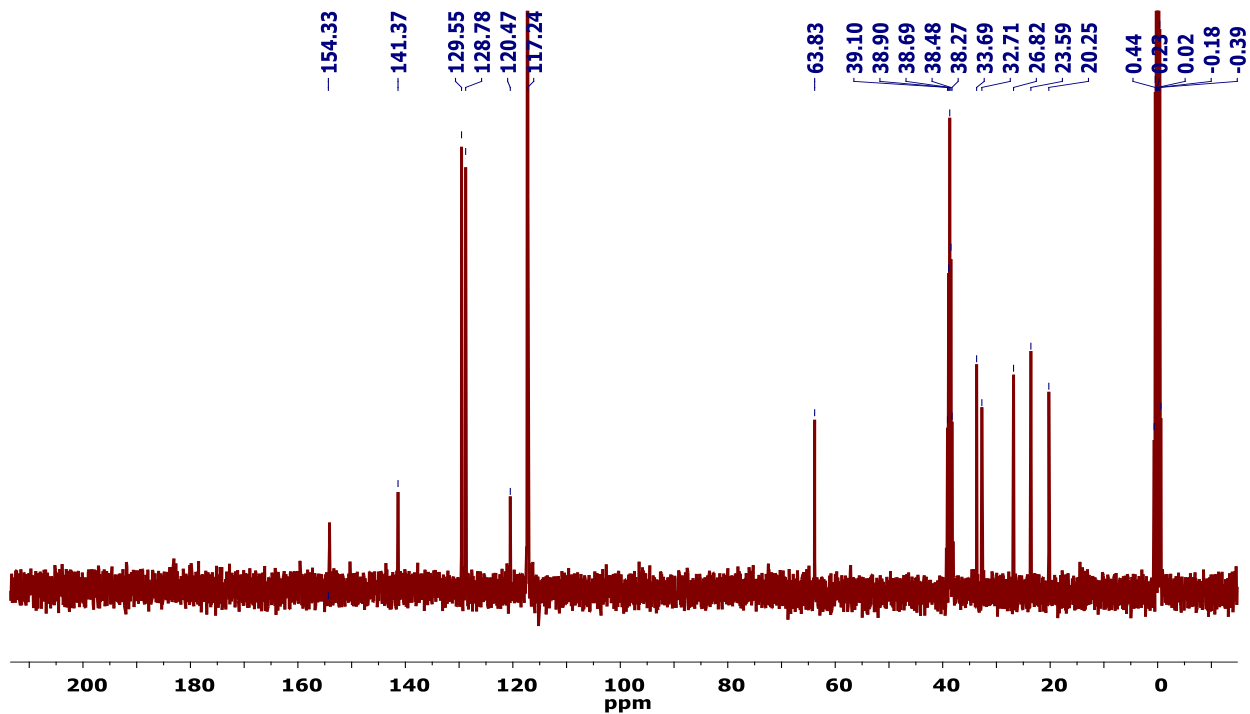


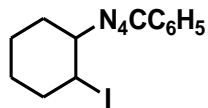


1H NMR: (400 MHz, $CD_3CN + DMSO-d_6$)

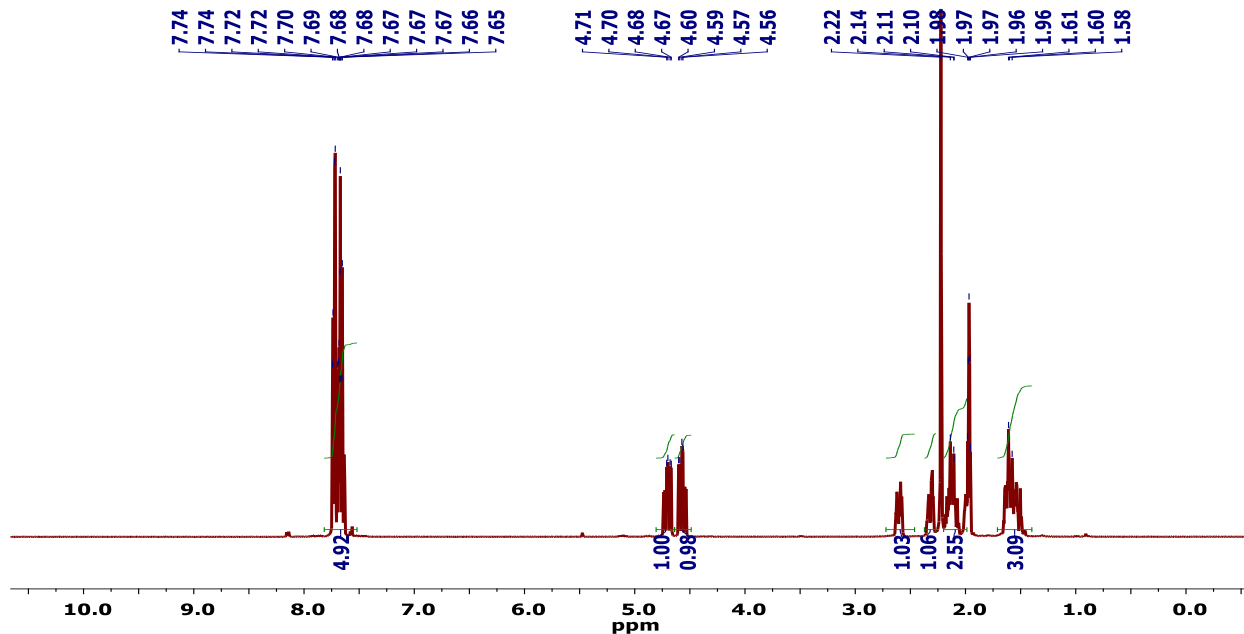


^{13}C NMR: (400 MHz, $CD_3CN + DMSO-d_6$)

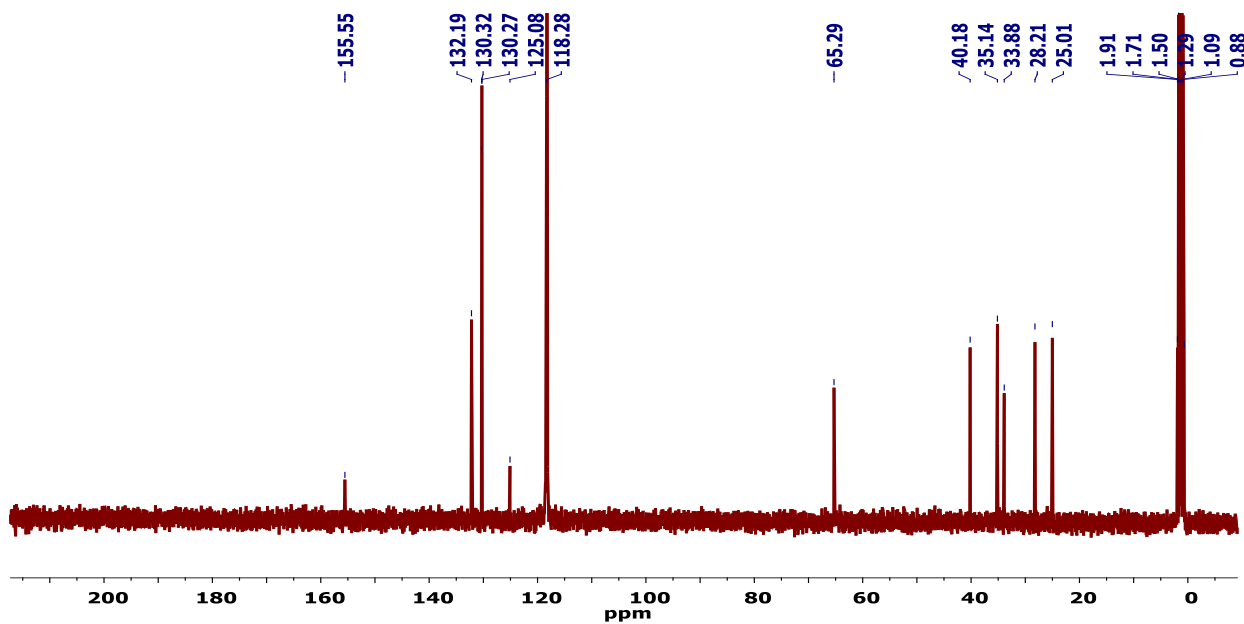




^1H NMR: (400 MHz, CD_3CN)



^{13}C NMR: (400 MHz, CD_3CN)



CHAPTER IV

N-HETEROCYCLE (TETRAZOLE)-STABILIZED PSEUDOCYCLIC λ^3 -IODANE: SYNTHESIS, STRUCTURE, AND REACTIVITY

IV.1. Introduction

Organic hypervalent (HV) iodine compounds have emerged as efficient, versatile and environmentally benign reagents for a plethora of synthetically useful oxidative transformations.¹⁻¹⁴ including oxidation and electrophilic group transfer reactions. Early examples of HV iodine-based oxidants such as iodosyl benzene (PhIO) had critical drawbacks including poor solubility and short bench lifetime. In a pioneering work, Carmalt and co-workers demonstrated that the extensive secondary intermolecular I \cdots O interactions of unstabilized λ^3 -iodanes produces highly insoluble and thermally labile polymeric networks.¹⁵ To overcome this problem, Protasiewicz et al. developed stable and soluble ortho-sulfonyl- substituted iodosylbenzene (**4**) and ortho-phosphoryl- substituted iodylbenzene (**5**), which possess improved reactivity toward organic substrates.¹⁶⁻¹⁹ Subsequently, Zhdankin and co-workers reported the first example of the pseudocyclic benziodoxole triflate and tosylate (**6**).^{20, 21} Furthermore, several pseudocyclic *O*-donor-stabilized λ^3 -iodanes with ether (**7**),^{22, 23} amide (**8**)²⁴ and nitro (**9**)²⁵ groups interacting with the I(III) centers were described. In 2017, Muniz reported first *N*-heterocycle-stabilized pseudocyclic HV iodine reagent (**10**) with an ortho-pyridinyl group.²⁶ Recently, Nachtsheim et al.

reported a series of *N*-heterocycle stabilized pseudocyclic HV iodine reagents with different atoms in the ring (**11**) and showed that their reactivity can be easily tuned by altering the heterocycle.²⁷

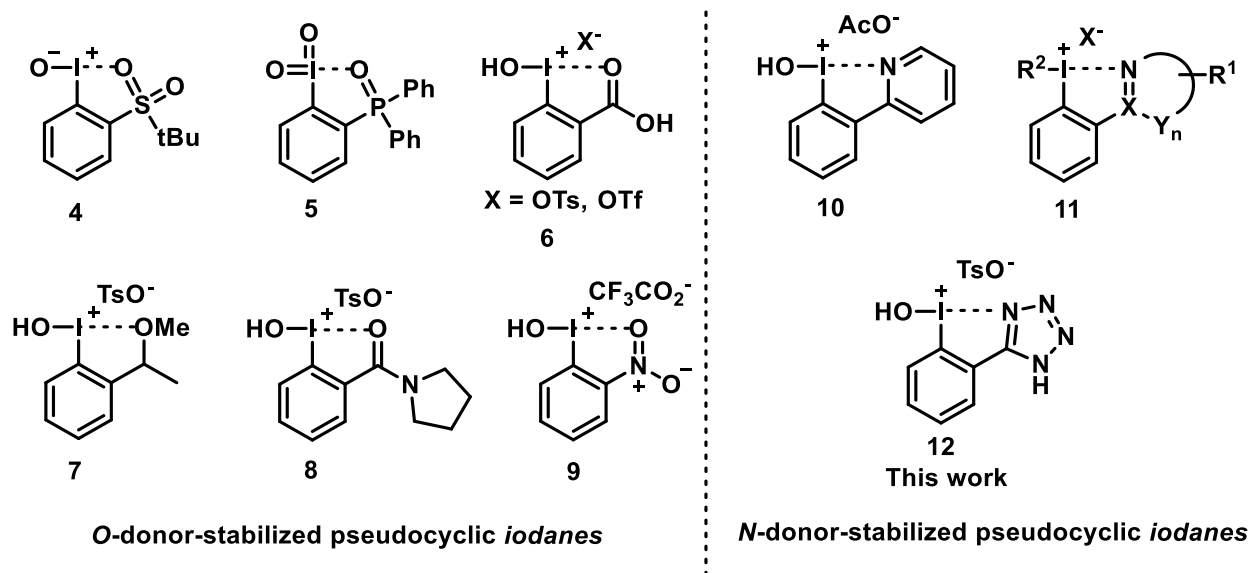
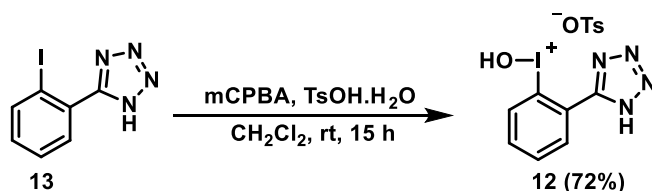


Figure IV-1 O- and N-stabilized pseudocyclic λ^3 -iodanes.

We recently reported that tetrazolates RCN_4^- , similar to carboxylates RCO_2^- , can serve as ligands that bind to HV iodine(III) centers, and described the synthesis, structural characterization, thermal degradation, electrochemical behavior, and reactivity of a number of tetrazole-containing HV iodine(III) compounds with the general formula $\text{RCN}_4-[\text{I}(\text{Ar})-\text{O}]_n-\text{I}(\text{Ar})-\text{N}_4\text{CR}$ ($\text{R} = \text{CH}_3$, C_6H_5 , or $4\text{-CH}_3\text{C}_6\text{H}_4$, and $n = 0, 1, \geq 2$; the compounds with $n = 0$ being the tetrazole analogues $\text{ArI}(\text{N}_4\text{CR})_2$ or (diacyloxyiodo)arenes $\text{Ar}(\text{O}_2\text{CR})_2$).²⁸ As a continuation of our studies, this chapter discusses the synthesis and properties of an *N*-tetrazole-stabilized pseudocyclic HV iodine(III) reagent, namely (2-(1H-tetrazol-5-yl)phenyl)(hydroxy)iodonium tosylate (**12**).

IV.2. Results and Discussion

The precursor of the title compound, 5-(2-iodophenyl)-1H-tetrazole **13**, was synthesized in good yield (75%) by the reaction of 2-iodobenzonitrile with sodium azide in the presence of a protic acid (ammonium chloride) in *N,N*-dimethylformamide at 130 °C for 20 h using a simplified literature²⁹ procedure. The monovalent iodine compound was then oxidized with meta-chloroperoxybenzoic acid (mCPBA) in the presence of *p*-toluenesulfonic acid monohydrate (TsOH.H₂O) in CH₂Cl₂ at room temperature for 15 h to afford **12** in good yield (72%), as shown in Scheme IV-1. The pseudocyclic HV iodine(III) compound with a single tetrazole ligand **12** was obtained in an analytically pure form as off-white powder after washing with diethyl ether (all starting materials are well soluble in excess of diethyl ether) and was found to be stable at room temperature for several weeks when kept in a vacuum desiccator.



Scheme IV-1 Synthesis of (2-(1H-tetrazol-5-yl)phenyl)(hydroxy)iodonium tosylate **12**.

The thermal stability of the λ^3 -iodane **12** was examined by simultaneous thermogravimetric analysis (TGA) and differential scanning calorimetry (DSC). Samples were heated from 25 °C to 550 °C at a rate of 5 °C/min under nitrogen. Both **12** and **13** were analyzed twice, and the averaged thermal decomposition curves are shown in Figure IV-1. The TGA curve of **12** exhibits a two-step degradation profile with a T_d (onset degradation temperature, at which 5% weight loss has taken place) of 142 °C, and steep weight loss between 127 °C and 152 °C, with an exothermic signal in

the DSC curve, due to the dissociation of the weak HV bond. Compound **13**, which also contains the thermally labile tetrazole group but no HV bonds, was more stable than **12** and started to degrade at 183 °C without showing any prominent exothermic peak in the DSC curve save for a small peak at 210 °C. The enthalpies of degradation (ΔH_d) were calculated by integrating the mentioned exothermic peaks and the average ΔH_d for compound **12** was -548 ± 86 J/g, which was about 20-fold higher than that of compound **13** (-27.5 ± 7.5 J/g). This shows that compound **12** can be used as energetic material. Similarly, linear tetrazole-containing HV iodine(III) compounds were shown to degrade explosively at elevated temperatures,²⁸ although their enthalpies of thermolysis were not measured.

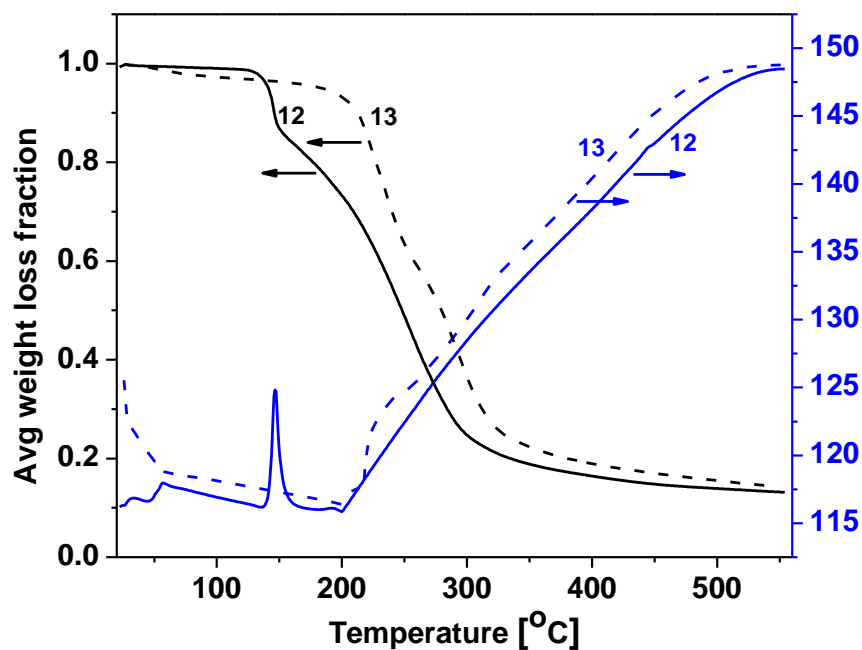


Figure IV-2 Simultaneous TGA and DSC analysis of compounds **12** (solid lines) and **13** (dashed lines).

HV iodine compounds are often used as oxidizing agents. Therefore, newly synthesized compound **12** was further analyzed by cyclic voltammetry (CV) to examine its oxidizing power. The starting materials used to prepare **12**, namely the tetrazole **13** and TsOH.H₂O were also analyzed to understand the origin of all the peaks in the cyclic voltammogram of **12**. The CV measurements (0.5 V to -1.5 V) were performed in dry and deoxygenated dimethyl sulfoxide (DMSO) (a good solvent for all compounds), using a glassy carbon electrode at a scan rate of 0.02 V/s using 0.1 M (*n*-Bu)₄NPF₆ as the electrolyte. The CV of DMSO containing only the electrolyte was studied also in the same voltage range to check its redox stability. DMSO did not show any peak in the above-mentioned region and hence it was concluded to be appropriate to use as solvent for the electrochemical studies.

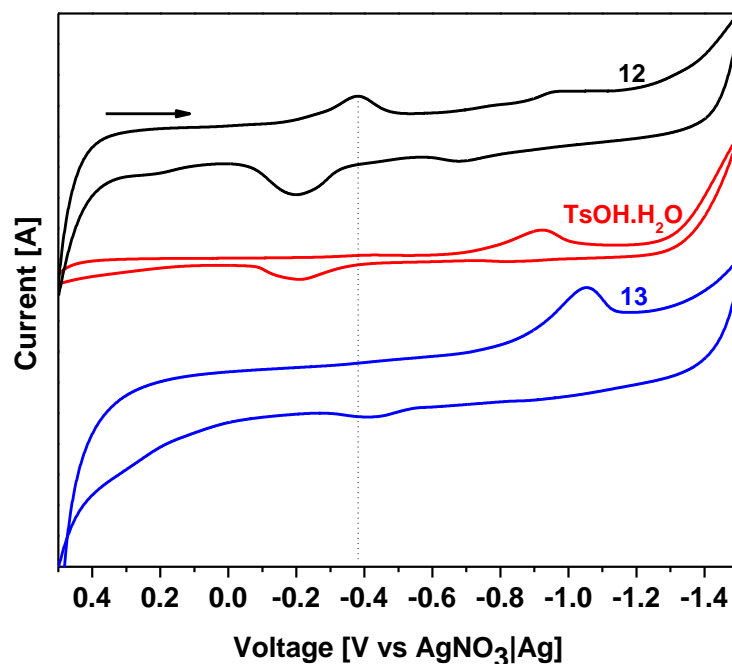
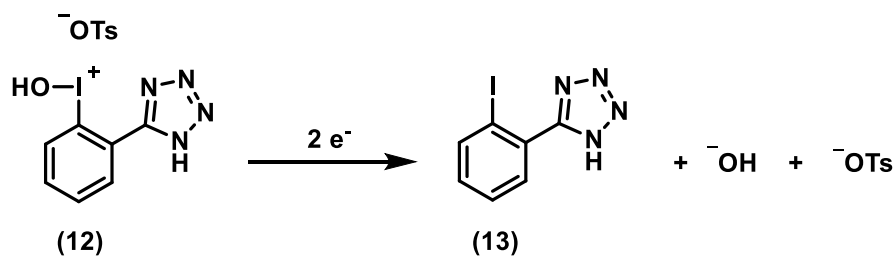


Figure IV-3 Cyclic voltammograms of 1 mM solutions of compound **12**, **13**, and TsOH in anhydrous DMSO containing 0.1 M (*n*-Bu)₄NPF₆ at scan rate of 0.02 V/s using a glassy carbon electrode.

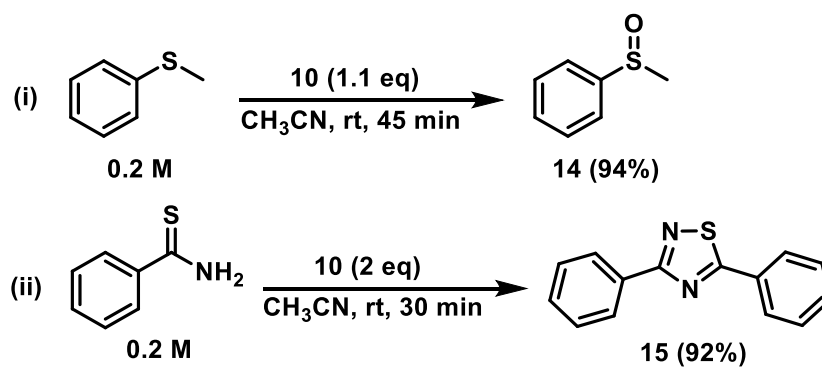
The cyclic voltammogram of **12** showed two main reduction peaks and several oxidation peaks (Figure IV-3). The first reduction peak at -0.38 V was due to the two-electron reduction of iodine(III) in **12** to iodine(I), i.e. formation of **13** as shown in Scheme IV-2. Formation of **13** is also observed in chemical reductions of **12** e.g. by thioanisole. This reaction is described in more detail below. The wide reduction peak observed at more negative voltages (in the range from 0.95 V to 1.05 V) is likely the result of overlap of the reduction peaks seen in the individual CV traces of **13** and TsOH (also shown in Figure IV-3). The nature of products of reduction of TsOH and/or TsO⁻ is difficult to ascertain. Mechanism of reduction of aromatic sulfonic acids and/or sulfonate anions is complex and it depends upon the composition of the solvent, and it often involves the cleavage of carbon-sulfur bonds. CV has been employed previously to study the reduction potential of various λ³-iodanes.^{28, 30-32} HV iodine compounds show irreversible reduction peak, like compound **12**, due to the formation of iodine(I) compounds, typically iodoarenes. The reduction potentials of various HV iodine(III) compounds with tetrazole ligands were between -0.25 V to -0.43 V, i.e., comparable to the reduction potential of compound **12**.²⁸



Scheme IV-2 Proposed pathway of electrochemical reduction of **13**.

Compound **12** was then employed to oxidize thioanisole to the corresponding sulfoxide **14**. First, the preliminary reaction was carried out in DMSO-d₆ and after confirming the formation of

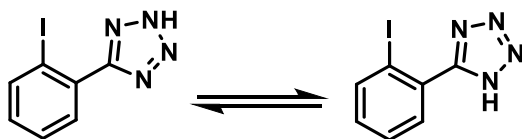
14, the reaction was then conducted in CH₃CN at room temperature for 45 min to simplify the workup and to increase the conversion by taking advantage of poor solubility of **13** in CH₃CN. Indeed, under these conditions the product was isolated in excellent yield (94%). Compound **12** was proved very useful in the synthesis of *N,S*-heterocycles as well. For instance, the oxidative dimerization of thiobenzamide in the presence of reagent **12**, conducted in CH₃CN at room temperature for 30 min, afforded 3,5-diphenyl-1,2,4-thiadiazole (**14**) in high isolated yield (92%). Both reactions are presented in Scheme IV-3.



Scheme IV-3 (i) Oxidation of thioanisole, (ii) oxidative rearrangement of thiobenzamide in the presence of λ^3 -iodane **12**.

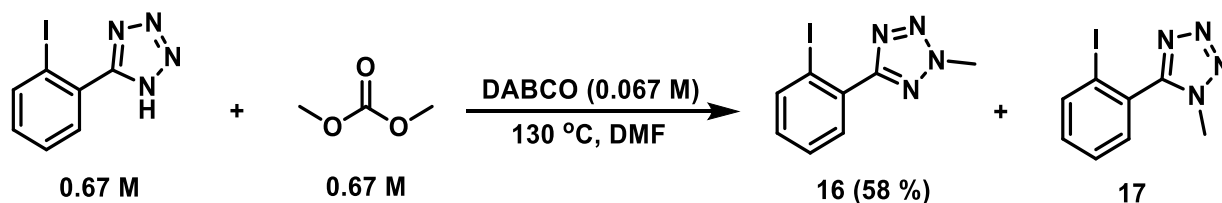
Several failed attempts were made to crystallize the pseudocyclic compound **12**. The powder of pure compound **12** was also analyzed by power X-ray diffraction. Although the powder showed crystallinity, it was not possible to solve the structure due to the presence of huge unit cell. The failure to crystallize the compound **12** was credited to tautomerization of tetrazole group present in the pseudocyclic compound. It is well known that the proton attached to nitrogen in the

tetrazole can migrate to different nitrogen atoms to form a mixture of tautomer as shown in Scheme IV-4.



Scheme IV-4 Tautomerism in compound **13**.

Therefore, it was hypothesized to methylate the tetrazole group in compound **13** and isolate both the isomers to prepare new pseudocyclic HV iodine compounds which could be able to crystallize due lack of tautomerization.



Scheme IV-5 Synthesis of compound **16** and **17**.

The methylation of compound **13** to form 2-methyl-5-iodophenyl tetrazole (**16**) was done using dimethyl carbonate (DMC) and 1,4 - diazobicyclo[2,2,2]octane (DABCO) in dimethylformamide (DMF) at 130 °C for 20 h. The product **16** was isolated in moderate yield (58%) as a pale pink powder. The product was characterized by NMR and GC-MS. To confirm

the position of methyl group, compound **16** was crystallized in acetonitrile. The crystal structure of compound **16** is shown in Figure IV-4.

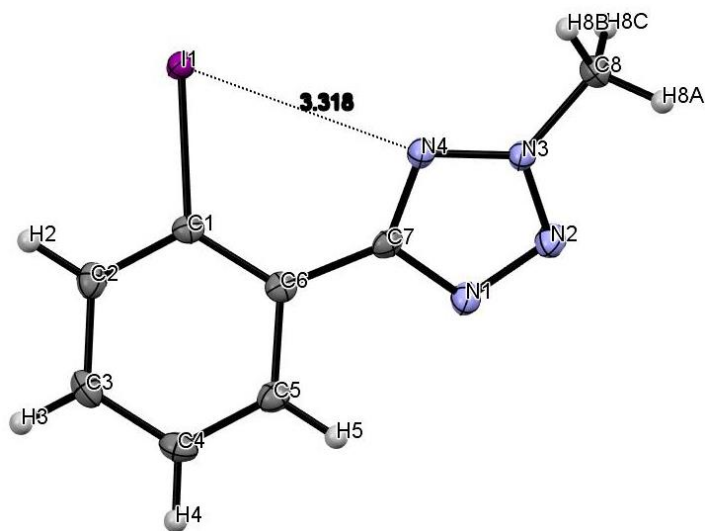
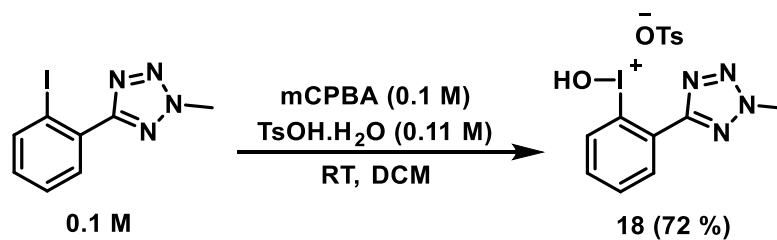


Figure IV-4 ORTEP drawing of the X-ray crystal structure of compound **16** at 50% ellipsoid probabilities.

The crystal structure of **16** revealed that the methyl is connected to the nitrogen on 2-position (N3 in the structure). The structure did not show any bond between iodine atom (I1) and N4 and the distance between mentioned atoms was measured as 3.318 Å. Inter- and intramolecular secondary interactions were also observed between I1 and N4 atoms.

After confirming the crystal structure of compound **16**, it was converted to pseudocyclic HV iodine compound **18** by oxidizing the iodine in presence of mCPBA and TsOH.H₂O. The reaction was performed in CH₂Cl₂ for 16 h at room temperature as shown in Scheme IV-6. The product was insoluble in DCM which drove the reaction in the forward direction and helped in the

purification process as well. The compound **18** was isolated in good yield (72 %) as off-white powder and characterized by ^1H and ^{13}C NMR.



Scheme IV-6 Synthesis of compound **18**.

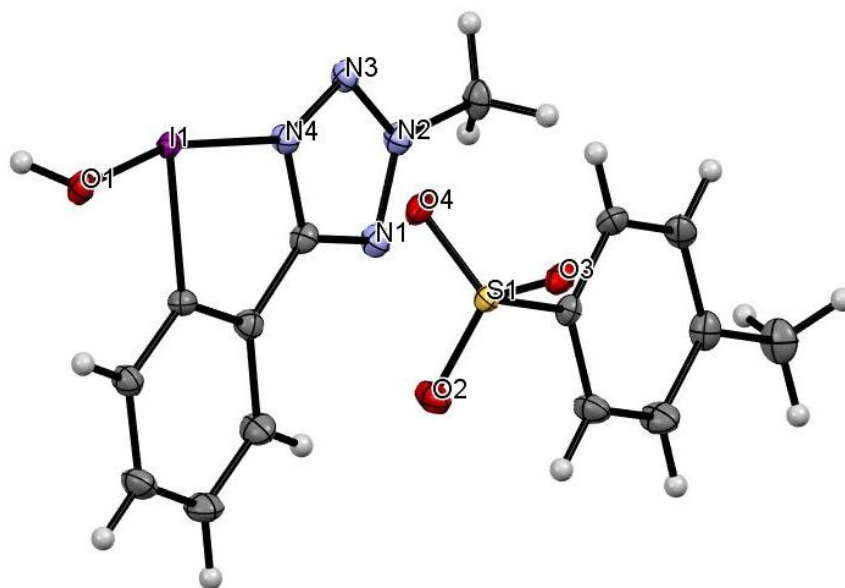


Figure IV-5 ORTEP drawing of the X-ray crystal structure of compound **18** at 50% ellipsoid probabilities.

After synthesizing compound **18**, crystallization of pure product was attempted by dissolving in methanol and slowly evaporating the solvent at 4 °C. After a week, beautiful crystals were formed which proved our hypothesis. X-ray crystallographic study of a single crystal of **18** revealed a complex structure characterized by numerous intramolecular and intermolecular secondary contacts in the solid state (Figure IV-5 and Figure IV-6).

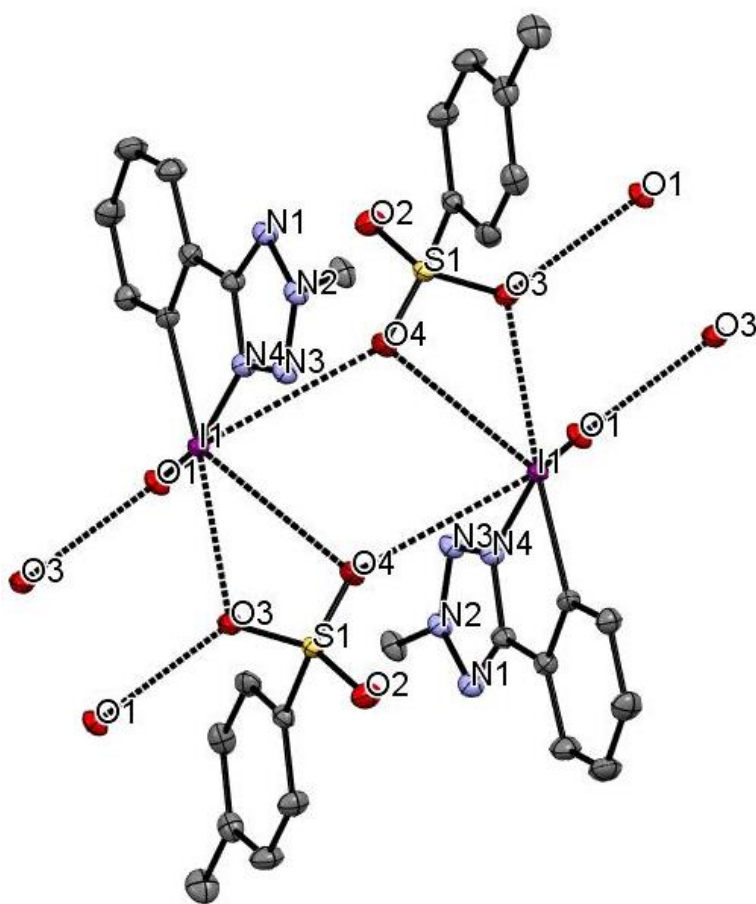


Figure IV-6 Secondary interactions found in the crystal structure of **18** (at the 50% probability level).

X-ray crystal data of **18** (Figure IV-5) demonstrates the presence of one short (1.945 Å) iodine (I1)–oxygen (O1) covalent bond and one relatively long (2.477 Å) dative bond. Besides that, long distance (3.323 Å) intramolecular hydrogen bond interaction between I1 and O4 and intermolecular hydrogen bond interaction between I1-O4 (3.294 Å) and I1-O3 (2.826 Å) was found. The intramolecular geometry around iodine(III) center of hydroxy(aryl)iodonium ion in **18** can be described as distorted T-shaped with observed N4-I1-O1 angle of 165.6°.

The crystal structure proved that tautomerization plays an important role in the chemistry of tetrazole based HV iodine compounds. In the future, this work will be extended by isolating compound **17**, synthesizing corresponding pseudocyclic compound, and comparing its reactivity with compound **18**.

IV.3. Experimental Section

IV.3.1. Materials

2-Iodobenzonitrile (98%, Oakwood Chemicals), NH₄Cl (99%, Acros Organics), NaN₃ (99%, Acros Organics), 3-chloroperoxybenzoic acid (*m*CPBA, 70-75%, Acros Organics), *p*-toluenesulfonic acid monohydrate (*p*-TsOH.H₂O, 98%, Sigma-Aldrich), thioanisole (99%, Sigma-Aldrich), thiobenzamide (95%, Acros Organics), Na₂S₂O₃ (99%, Alfa Aesar), NaHCO₃ (99%, Acros Organics), (*n*-Bu)₄NPF₆ (98%, TCI). The solvents, including anhydrous acetonitrile (99.9%, Acros), anhydrous dichloromethane (99.9%, Acros), *N,N*-dimethylformamide (99.8%, Acros), dimethyl sulfoxide (99.8%, Acros), diethyl ether (99%, Acros), *n*-hexane (99.9%, Acros), ethyl acetate (99.9%, Acros) and methanol (99.8%, Acros) were used as received. The deuterated solvents, (CD₃)₂SO (99.8% D, Acros), CDCl₃ (99.8% D, Cambridge Isotope Laboratories) used

for NMR analysis contained a small amount of tetramethylsilane (TMS) as a chemical shift reference.

IV.3.2. Analytical Procedures

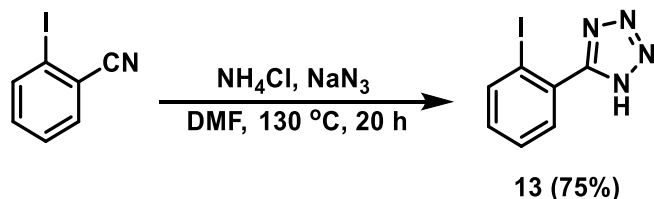
NMR spectra were recorded on a Bruker Avance DRX (400 MHz) spectrometer. Mass spectrometric analysis were conducted by Shimadzu LCMS-IT-ToF mass spectrometer (for HRMS) and Agilent 5975B gas chromatograph/mass spectrometer (for GC-MS) using default methods. Electrochemical measurements were carried out in an electrochemical cell system controlled with a CHI620E electrochemical station (CH Instruments, Inc., USA) with a Pt wire as the counter electrode, AgNO₃/Ag as the reference, and glassy carbon (GC) as the working electrode. All potential values are referenced to AgNO₃/Ag in 0.1 M (*n*-Bu)₄NPF₆ with 0.01 M AgNO₃ in DMSO. Samples were prepared by dissolving 0.01 mmol of the studied compound in 10 mL of 0.1 M solution of (*n*-Bu)₄NPF₆ in dry and deoxygenated DMSO. All samples were prepared in a glovebox to prevent exposure to moisture or air. During the acquisition of the data, the solutions were purged with dry argon. The thermal analyses of samples were carried out with an SDT Q600 thermal analyzer (TA Instruments Co., Ltd., America). The samples (1-2 mg) were placed in an alumina crucible. The tests were performed under heating rate of 5 °C min⁻¹ from 25 to 550 °C under flow (50 mL min⁻¹) of high-purity nitrogen.

All reflection intensities were measured at 110(2) K using a SuperNova diffractometer (equipped with Atlas detector) with Mo *K*α radiation ($\lambda = 0.71073 \text{ \AA}$) under the program CrysAlisPro (Version CrysAlisPro 1.171.39.29c, Rigaku OD, 2017). The same program was used to refine the cell dimensions and for data reduction. The structure was solved with the program SHELXS-2018/3 (Sheldrick, 2018) and was refined on F^2 with SHELXL-2018/3 (Sheldrick, 2018). Numerical absorption correction based on gaussian integration over a multifaceted crystal

model was applied using CrysAlisPro. The temperature of the data collection was controlled using the system Cryojet (manufactured by Oxford Instruments). The H atoms were placed at calculated positions (unless otherwise specified) using the instructions AFIX 43 or AFIX 137 with isotropic displacement parameters having values 1.2 or 1.5 U_{eq} of the attached C atoms. The H atom attached to O3 was found from difference Fourier map, and its coordinates were restrained pseudofreely using the DFIX instruction in order to keep the O–H bond distance within an acceptable range. The structure is ordered.

IV.4. Synthetic Procedures

IV.4.1. Synthesis of 2-iodophenyl tetrazole (13)



A modified literature procedure was employed.²⁹ In a 500 mL round bottom flask equipped with magnetic stir bar, 2-iodobenzonitrile (10.0 g, 0.0436 mol), NH_4Cl (4.67 g, 0.0872 mol) and NaN_3 (5.67 g, 0.0872 mol) were added, followed by DMF (200 mL). Subsequently, the flask was sealed with a glass stopper and submerged in an oil bath at $130\text{ }^\circ\text{C}$. The reaction mixture was stirred vigorously for 20 h and the flask was allowed to cool down to ambient temperature. Then, distilled water (150 mL) was added to the reaction mixture, followed by 10% (v/v) aqueous HCl solution, until pH reached the value of 1-2. The product and unreacted 2-iodobenzonitrile precipitated, and was filtered, and washed with water several times. Then, 0.1 N NaOH (500 mL) was added to the precipitate to get a suspension. This suspension was filtered to remove the unreacted 2-

iodobenzonitrile and the filtrate was collected. Subsequently, 10% (v/v) aqueous HCl solution was added to the filtrate until pH reached the value of 1-2 and the product precipitated. The precipitate was filtered, and washed with water several times, and then with diethyl ether. The obtained product was dried under vacuum at 40 °C for 24 h and the yield was determined (8.9 g, 75%). ¹H NMR (400 MHz, (CD₃)₂SO): δ 8.10 (d, *J* = 7.9 Hz, 1H), 7.60 (d, *J* = 4.1 Hz, 2H), 7.42 – 7.30 (m, 1H). ¹³C{¹H} NMR (101 MHz, (CD₃)₂SO): δ 156.97, 140.26, 132.87, 131.73, 131.01, 128.94, 98.11.

IV.4.2. Synthesis of (2-(1H-tetrazol-5-yl)phenyl)(hydroxy)iodonium tosylate (12)

In a 1 L round bottom flask equipped with a magnetic stir bar, 2-iodophenyl tetrazole (8.0 g, 29.4 mmol), TsOH.H₂O (5.592 g, 29.4 mmol), and *m*CPBA (70-75% purity, 7.794 g) were added followed by CH₂Cl₂ (500 mL). The reaction mixture was stirred for 15 h at room temperature. Then the solvent was evaporated under reduced pressure and diethyl ether (1 L) was added. The mixture was stirred for 30 min. The product was filtered and washed with diethyl ether again. The final product was dried under vacuum to obtain an off-white solid in a good yield (11.2 g, 82%). ¹H NMR (400 MHz, (CD₃)₂SO): δ 8.27 (d, *J* = 7.3 Hz, 1H), 7.98 (d, *J* = 8.2 Hz, 1H), 7.80 (dt, *J* = 21.9, 7.4 Hz, 2H), 7.51 (d, *J* = 7.9 Hz, 2H), 7.14 (d, *J* = 7.8 Hz, 2H), 2.30 (s, 3H); ¹³C{¹H} NMR (101 MHz, (CD₃)₂SO): δ 160.45, 145.49, 138.53, 132.63, 131.66, 128.66, 127.95, 127.74, 126.24, 125.97, 121.77, 21.26. HRMS calculated for C₇H₆IN₄O⁺ ([M-OTs]⁺): 288.9581 found: 288.9559.

IV.4.3. Oxidation of thioanisole

In a 20 mL round bottom flask equipped with a magnetic stir bar, thioanisole (0.1242 g, 1 mmol) and **12** (0.5062 g, 1.1 mmol) were added along with CH₃CN (5 mL). The heterogeneous reaction mixture was stirred at room temperature. To optimize the reaction time, consumption of thioanisole was monitored by ¹H NMR spectroscopy. Within 30 min, the thioanisole was completely consumed. After optimizing the reaction time, the reaction was repeated in exact same conditions with same amount of reactants to get accurate yield. The stirring was stopped after 45 mins and reaction was quenched using 5 mL of 5% (w/v) aqueous solution of Na₂S₂O₃. Then, 5 mL saturated solution of NaHCO₃ was added to neutralize the acidic byproducts, *i.e.* TsOH and compound **13**, and the contents were extracted with CH₂Cl₂ (3 × 15 mL). The combined CH₂Cl₂ layers were washed with distilled water (3 × 10 mL) and dried over anhydrous Na₂SO₄. The solvent was evaporated under reduced pressure to obtain a yellow oil as the crude product. The crude product was dissolved in CH₂Cl₂ (1.0 mL) and was purified by preparative TLC using hexane : ethyl acetate (1 : 3 (v/v)) as the eluent. The pure product as pale-yellow oil was obtained in excellent yield (0.132 g, 94%). ¹H NMR (400 MHz, CDCl₃): δ 7.65 (d, *J* = 6.5 Hz, 2H), 7.60 – 7.44 (m, 3H), 2.72 (s, 3H). ¹³C{¹H} NMR (101 MHz, CDCl₃): δ 145.52, 130.93, 129.25, 123.36, 43.82. GC-MS calculated for C₇H₈OS [M⁺]: 140.02 found: 140.00.

IV.4.4. Oxidative dimerization of thiobenzamide

In a 20 mL round bottom flask equipped with stir bar, thiobenzamide (0.1372 g, 1 mmol) and **12** (0.9206 g, 2 mmol) were added along with CH₃CN (5 mL). The heterogeneous reaction mixture was stirred at room temperature and the consumption of thiobenzamide was monitored by ¹H NMR spectroscopy. The reaction was complete after 15 min (thiobenzamide was completely consumed).

After optimizing the reaction time, the reaction was repeated in exact same conditions with same amount of reactants to get accurate yield. The stirring was stopped after 30 mins and reaction was quenched using 10 mL of 5% (w/v) solution of $\text{Na}_2\text{S}_2\text{O}_3$. Subsequently, 20 mL saturated solution of NaHCO_3 was added to neutralize the acidic byproducts, *i.e.* TsOH and compound **13**. The product was extracted with ethyl acetate (3×20 mL). All ethyl acetate layers were collected and dried over anhydrous Na_2SO_4 , and then the solvent was evaporated under reduced pressure to obtain orange-yellow solid. The crude product was dissolved in CH_2Cl_2 (1.0 mL) and pure product was isolated by column chromatography using silica as absorbent and hexane : ethyl acetate (9 : 1 (v/v)) as eluent. The product was vacuum dried, and yield was determined (0.110 g, 92%). ^1H NMR (400 MHz, CDCl_3): δ 8.38 (d, $J = 6.0$ Hz, 2H), 7.97 (d, $J = 5.5$ Hz, 2H), 7.44 (s, 6H). $^{13}\text{C}\{^1\text{H}\}$ NMR (101 MHz, CDCl_3): δ 188.06, 173.75, 132.91, 131.88, 130.66, 130.37, 129.23, 128.70, 128.39, 127.46. GC-MS calculated for $\text{C}_{14}\text{H}_{10}\text{N}_2\text{S}$ [M^+]: 238.05 found: 238.00.

IV.4.5. Synthesis of compound 16

Compound **13** (2.72 g, 10 mmol) and dimethyl carbonate (0.90 g, 10 mmol) were taken in a round bottom flask along with DABCO (0.112 g, 1 mmol). Reactants were dissolved in DMF (15 mL) and flask was immersed in an oil bath set at 130 °C for 20 h. Reaction was monitored using GC-MS. After completion, reaction was quenched by adding 5N NaOH solution (20 mL). The reaction mixture was allowed to cool down to room temperature. Subsequently, reaction mixture was extracted with ethyl acetate (3×15 mL) and then washed with water (2×10 mL). The organic layer was collected and solvent of evaporated under reduced pressure. The product **16** was isolated by column chromatography using hexane : ethyl acetate (1:4) as solvent. The product was isolated in moderate yield (58%) as pale pink powder. It was crystallized by dissolving in CH_3CN and

slowly evaporating the solvent at room temperature. ^1H NMR (400 MHz, CDCl_3) δ 8.04 (d, $J = 7.8$ Hz, 1H), 7.74 (d, $J = 7.7$ Hz, 1H), 7.47 (t, $J = 7.4$ Hz, 1H), 7.17 (t, $J = 7.5$ Hz, 1H), 4.46 (s, 3H). GC-MS calculated for $\text{C}_8\text{H}_7\text{IN}_4$ [M^+] = 286.07 found = 286.00. Crystal structure shown in Figure IV-4.

IV.4.6. Synthesis of compound 18

In a 250 mL round bottom flask equipped with a magnetic stir bar, compound **16** (1.0 g, 3.49 mmol), $\text{TsOH}\cdot\text{H}_2\text{O}$ (0.6 g, 3.49 mmol), and *m*CPBA (70-75% purity, 0.857 g) were added followed by CH_2Cl_2 (100 mL). The reaction mixture was stirred for 15 h at room temperature. Then the solvent was evaporated under reduced pressure and diethyl ether (200 mL) was added. The mixture was stirred for 30 min. The product was filtered and washed with diethyl ether again. The final product was dried under vacuum to obtain an off-white solid in a good yield (82%). ^1H NMR (400 MHz, DMSO-d_6) δ 8.27 (d, $J = 3.3$ Hz, 6H), 7.99 – 7.78 (m, 10H), 7.49 (d, $J = 7.9$ Hz, 8H), 7.12 (d, $J = 7.8$ Hz, 7H), 4.58 (s, 9H), 2.28 (s, 10H). ^{13}C NMR (101 MHz, DMSO-d_6) δ 166.54 (s), 163.08 (s), 138.35 (s), 134.24 (s), 133.80 (s), 133.11 (d, $J = 17.0$ Hz), 131.15 (s), 130.03 (s), 129.28 (s), 128.60 (s), 128.39 (s), 125.96 (s), 121.61 (s), 21.26 (s). Crystal structure is shown in Figure IV-5.

IV.5. Conclusions

Tetrazole is demonstrated to serve as a suitable *N*-donor to stabilize pseudocyclic λ^3 -iodane, (2-(1H-tetrazol-5-yl)phenyl)(hydroxy)iodonium tosylate, which was stable at room temperature for weeks. The identity of the tetrazole-containing HV iodine(III) compound was proved by NMR spectroscopy and high-resolution mass spectrometry. Although stable at ambient temperatures, the compound decomposed with the release of significant amount of heat at temperatures exceeding

140 °C. The oxidative power of the iodonium salt was quantified by cyclic voltammetry and it was taken advantage of in the high-yield oxidation of thioanisole to sulfoxide and the oxidative dimerization of thiobenzamide to 3,5-diphenyl-1,2,4-thiadiazole.

IV.6. Acknowledgements

The authors gratefully acknowledge financial support by the National Science Foundation through a CAREER grant (CHE-1455200) to N.V.T. Professor Isaac Garcia-Bosch and Khashayar Rajabimoghadam are acknowledged for helping with the electrochemical measurements.

IV.7. References

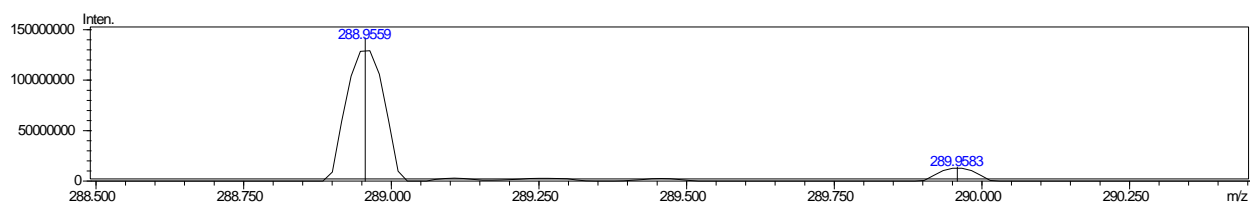
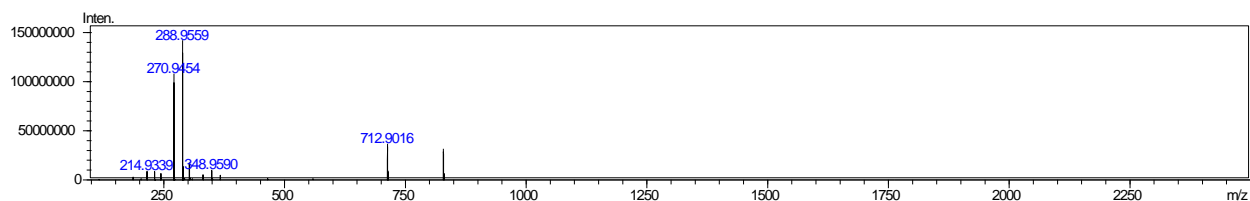
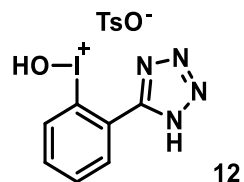
- 1 Brand, J. P.; Waser, J. *Chem. Soc. Rev.* **2012**, *41*, 4165.
- 2 Brown, M.; Farid, U.; Wirth, T. *Synlett* **2013**, *24*, 424.
- 3 Charpentier, J.; Früh, N.; Togni, A. *Chem. Rev.* **2015**, *115*, 650.
- 4 Dohi, T.; Kita, Y. *Chem. Commun.* **2009**, 2073.
- 5 Mekhman, S. Y.; Viktor, V. Z. *Curr. Org. Synth.* **2012**, *9*, 247.
- 6 Parra, A.; Reboredo, S. *Chem. Eur. J.* **2013**, *19*, 17244.
- 7 Romero, R. M.; Wöste, T. H.; Muñiz, K. *Chem. Asian J.* **2014**, *9*, 972.
- 8 Samanta, R.; Matcha, K.; Antonchick, A. P. *Eur. J. Org. Chem.* **2013**, *2013*, 5769.
- 9 Singh, F. V.; Wirth, T. *Chem. Asian J.* **2014**, *9*, 950.
- 10 Uyanik, M.; Ishihara, K. *Chem. Commun.* **2009**, 2086.
- 11 Wirth, T. *Hypervalent Iodine Chemistry*; Springer International Publishing, 2016.
- 12 Yoshimura, A.; Zhdankin, V. V. *Chem. Rev.* **2016**, *116*, 3328.

- 13 Zhdankin, V. V. *Wiley* **2013**, pp. i.
- 14 Vaish, A.; Tsarevsky, N. V. *Main Group Strategies towards Functional Hybrid Materials* **2017**.
- 15 Carmalt, C. J.; Crossley, J. G.; Knight, J. G.; Lightfoot, P.; Martín, A.; Muldowney, M. P.; Norman, N. C.; Orpen, A. G. *J. Chem. Soc., Chem. Commun.* **1994**, 2367.
- 16 Macikenas, D.; Skrzypczak-Jankun, E.; Protasiewicz, J. D. *J. Am. Chem. Soc.* **1999**, *121*, 7164.
- 17 Macikenas, D.; Skrzypczak-Jankun, E.; Protasiewicz, J. D. *Angew. Chem. Int. Ed.* **2000**, *39*, 2007.
- 18 Meprathu, B. V.; Justik, M. W.; Protasiewicz, J. D. *Tetrahedron Lett.* **2005**, *46*, 5187.
- 19 Meprathu, B. V.; Protasiewicz, J. D. *Tetrahedron* **2010**, *66*, 5768.
- 20 Yoshimura, A.; Klasen, S. C.; Shea, M. T.; Nguyen, K. C.; Rohde, G. T.; Saito, A.; Postnikov, P. S.; Yusubov, M. S.; Nemykin, V. N.; Zhdankin, V. V. *Chem. Eur. J.* **2017**, *23*, 691.
- 21 Yoshimura, A.; Nguyen, K. C.; Klasen, S. C.; Saito, A.; Nemykin, V. N.; Zhdankin, V. V. *Chem. Commun.* **2015**, *51*, 7835.
- 22 Hirt, Urs H.; Schuster, Martin F. H.; French, Andrew N.; Wiest, Olaf G.; Wirth, T. *Eur. J. Org. Chem.* **2001**, *2001*, 1569.
- 23 Yudasaka, M.; Maruyama, T.; Yamaguchi, E.; Tada, N.; Itoh, A. *Eur. J. Org. Chem.* **2018**, *2018*, 550.
- 24 Guilbault, A.-A.; Legault, C. Y. *ACS Catalysis* **2012**, *2*, 219.
- 25 Nikiforov, V. A.; Karavan, V. S.; Miltsov, S. A.; Selivanov, S. I.; Kolehmainen, E.; Wegelius, E.; Nissinen, M. *ARKIVOC (Gainesville, FL, U.S.)* **2003**, 191.

- 26 Aertker, K.; Rama, R. J.; Opalach, J.; Muñiz, K. *Adv. Synth. Catal.* **2017**, 359, 1290.
- 27 Boelke, A.; Lork, E.; Nachtsheim, B. J. *Chem. Eur. J.* **2018**, 24, 18653.
- 28 Kumar, R.; Vaish, A.; Runčevski, T.; Tsarevsky, N. V. *J. Org. Chem.* **2018**, 83, 12496.
- 29 Finnegan, W. G.; Henry, R. A.; Lofquist, R. *J. Am. Chem. Soc.* **1958**, 80, 3908.
- 30 Colomer, I.; Batchelor-McAuley, C.; Odell, B.; Donohoe, T. J.; Compton, R. G. *J. Am. Chem. Soc.* **2016**, 138, 8855.
- 31 Kiyokawa, K.; Kosaka, T.; Kojima, T.; Minakata, S. *Angew. Chem. Int. Ed.* **2015**, 54, 13719.
- 32 Kokkinidis, G.; Hatzigrigoriou, E.; Sazou, D.; Varvoglis, A. *Electrochim. Acta* **1991**, 36, 1391.

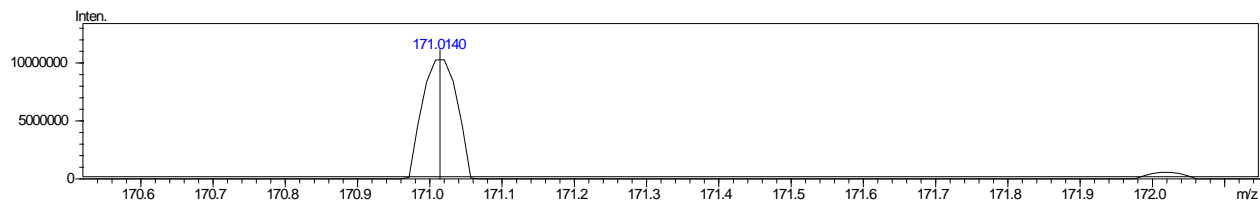
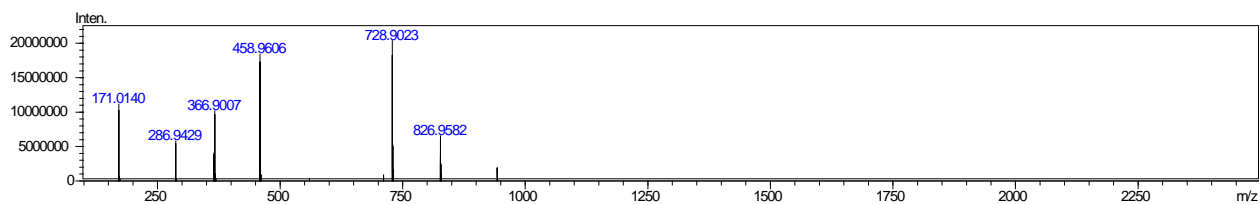
IV.8. Appendix

IV.8.1. HRMS Spectra



Calculated for $C_7H_6IN_4O^+$ ([M-OTs]⁺): 288.9581 found: 288.9559

Figure 1. Positive mode high resolution mass spectrum of **12**.



Calculated for $C_7H_7O_3S^-$ (TsO⁻): 171.0121 found: 171.0140

Figure 2. Negative mode high resolution mass spectrum of **12**.

IV.8.2. NMR Spectra

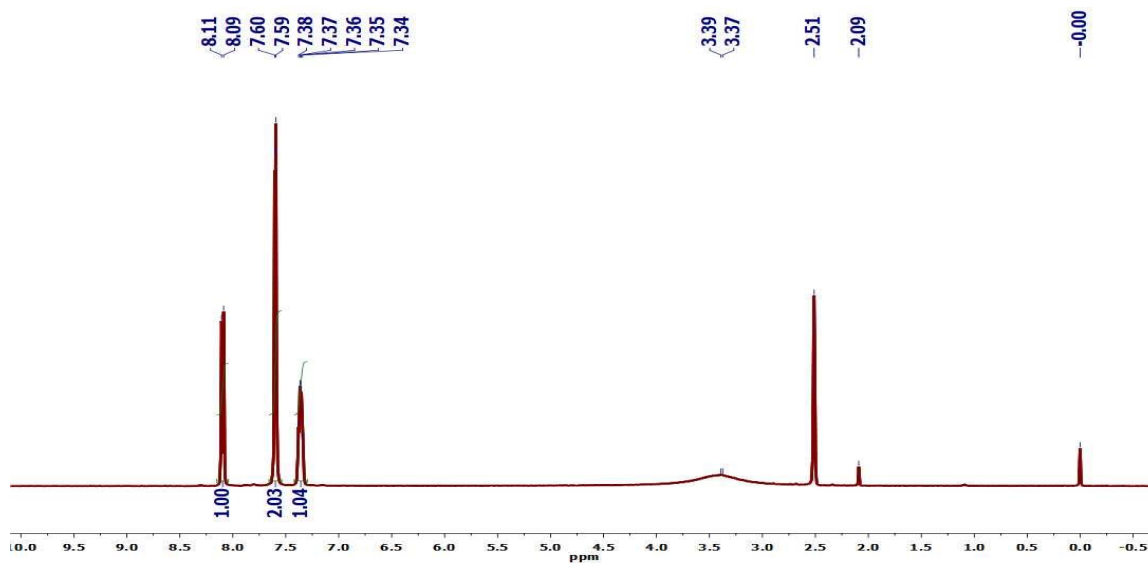
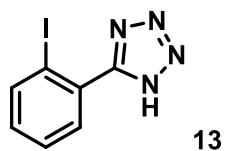


Figure 3. ^1H NMR spectrum of compound **13** in $(\text{CD}_3)_2\text{SO}$.

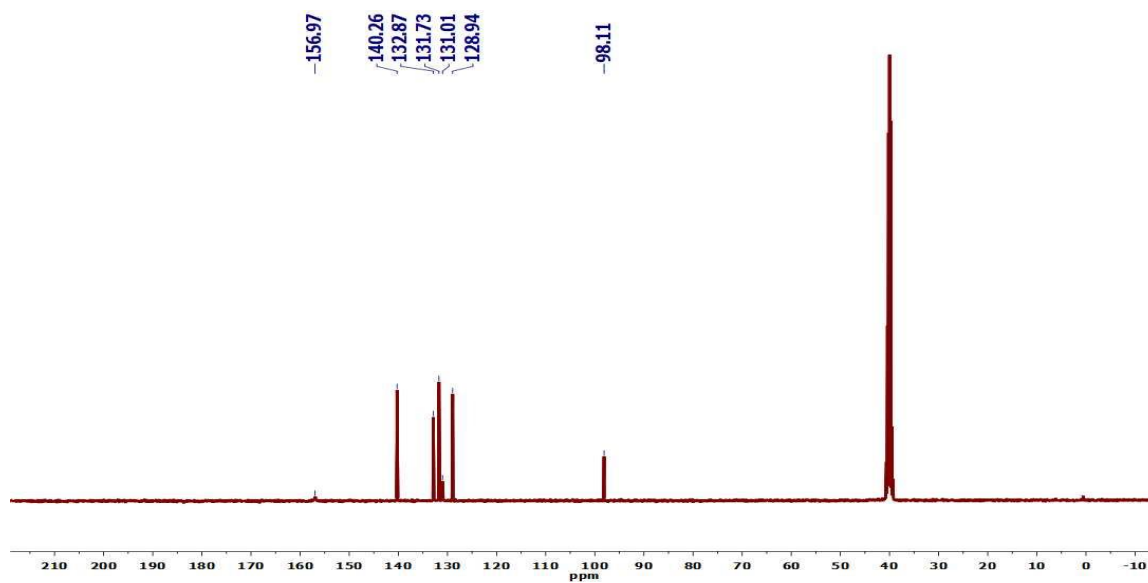


Figure 4. ^{13}C NMR spectrum of compound **13** in $(\text{CD}_3)_2\text{SO}$.

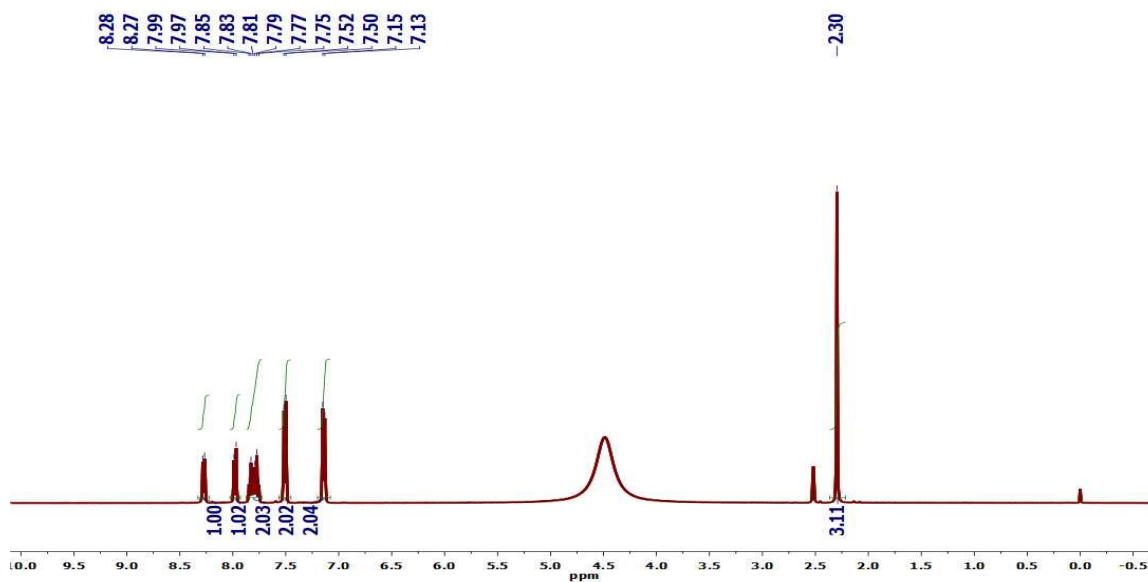
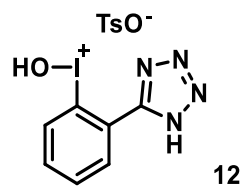


Figure 5. ^1H NMR spectrum of compound **12** in $(\text{CD}_3)_2\text{SO}$.

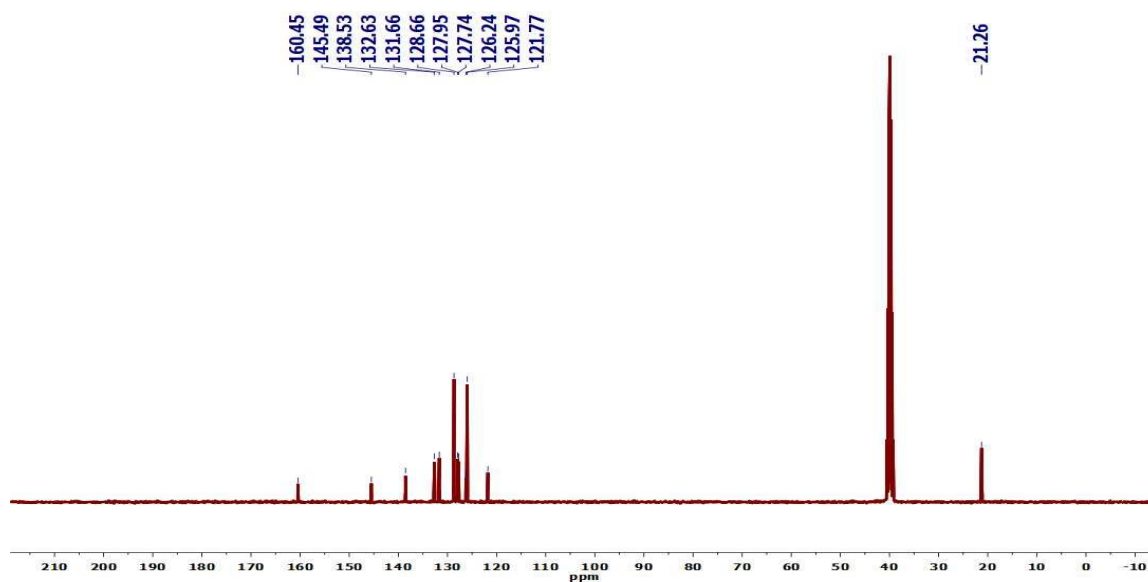


Figure 6. ^{13}C NMR spectrum of compound **12** in $(\text{CD}_3)_2\text{SO}$.

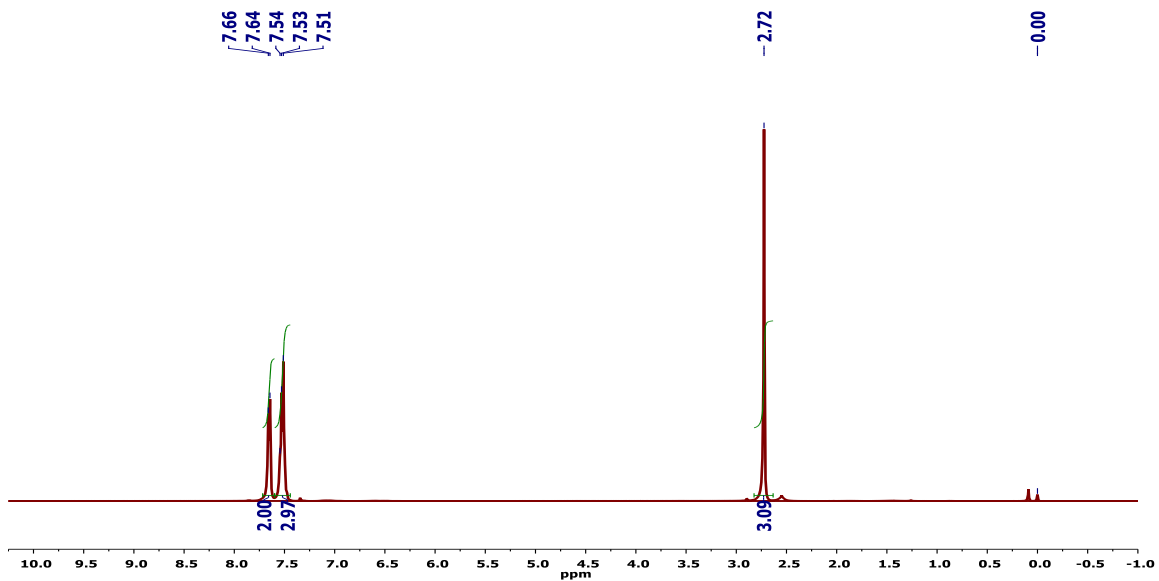
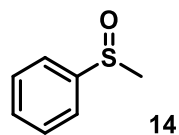


Figure 7. ^1H NMR spectrum of compound **14** in CDCl_3 .

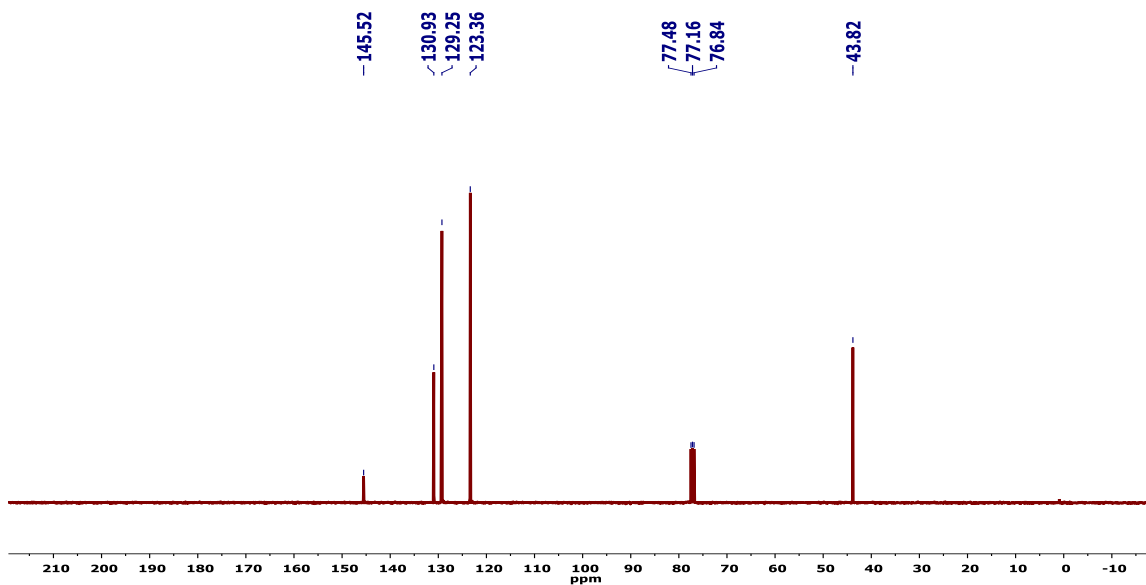


Figure 8. ^{13}C NMR spectrum of compound **14** in CDCl_3 .

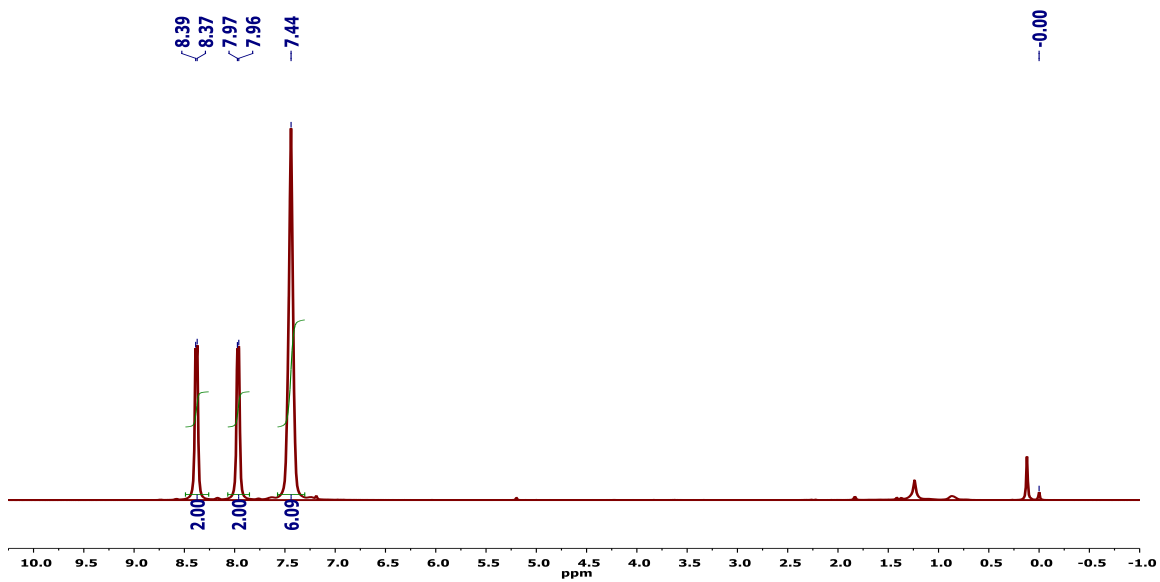
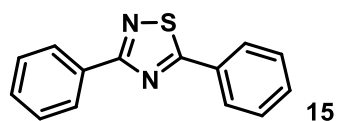


Figure 9. ^1H NMR spectrum of compound **15** in CDCl_3 .

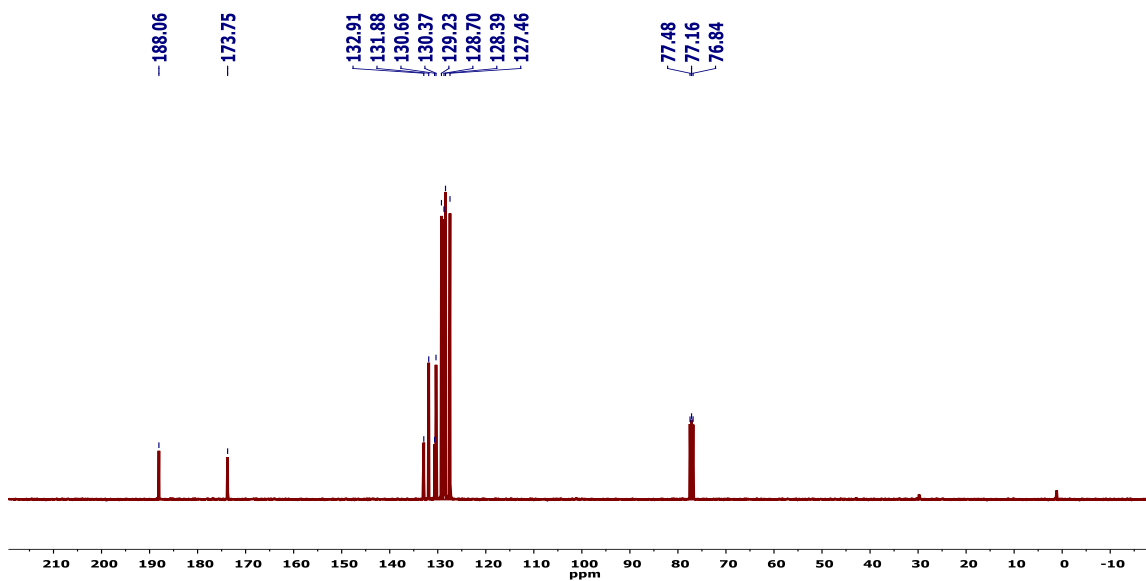


Figure 10. ^{13}C NMR spectrum of compound **15** in CDCl_3 .

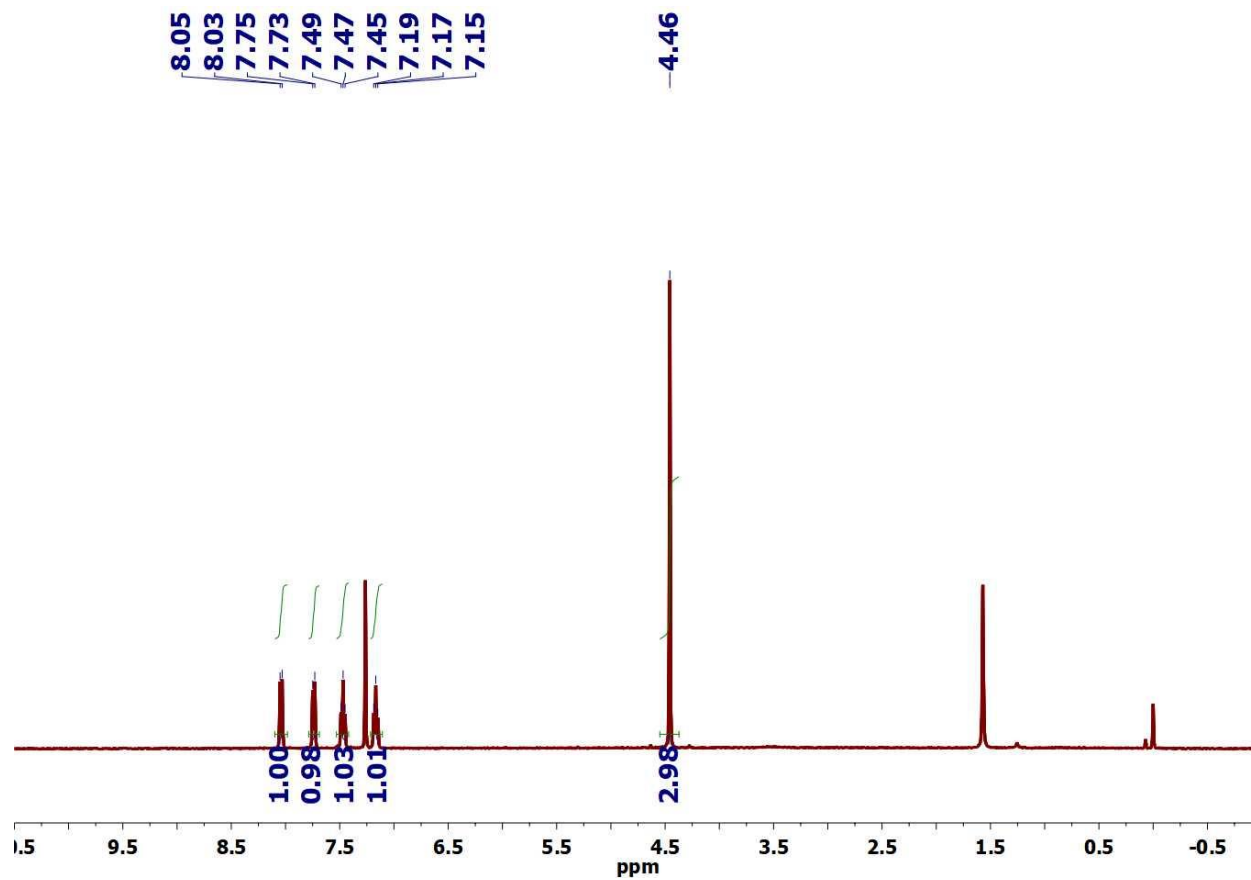
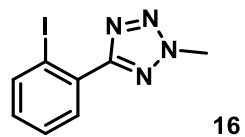


Figure 11. ¹H NMR spectrum of compound 16 in CDCl₃.

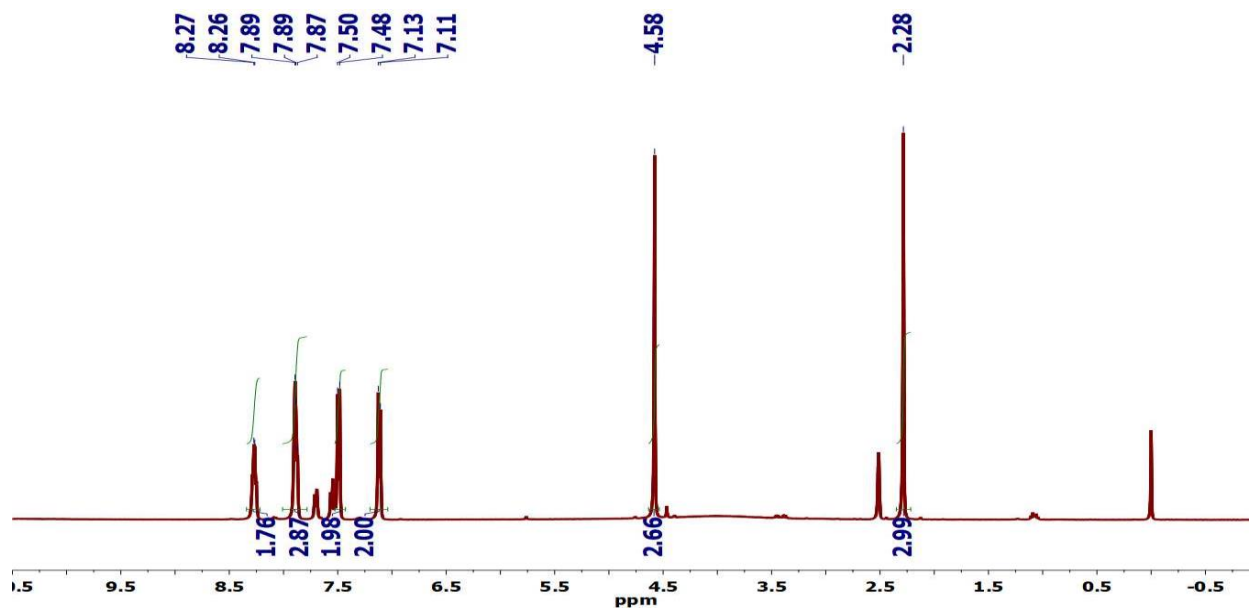
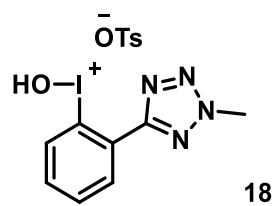


Figure 12. ^1H NMR spectrum of compound **18** in $(\text{CD}_3)_2\text{SO}$.

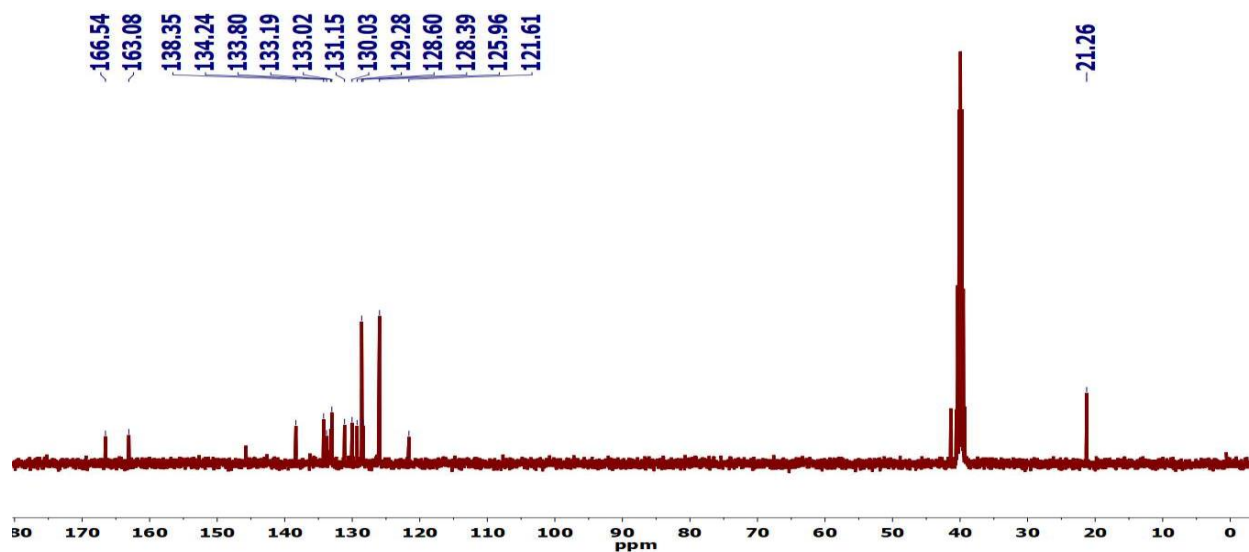
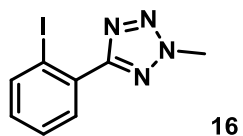


Figure 13. ^{13}C NMR spectrum of compound **18** in $(\text{CD}_3)_2\text{SO}$.

IV.8.3. Crystallographic Data



Crystal Morphology



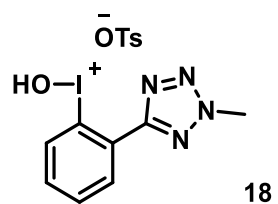
Experimental Report

	xs2237a
Crystal data	
Chemical formula	C ₈ H ₇ IN ₄
<i>M_r</i>	286.08
Crystal system, space group	Monoclinic, <i>P</i> 2 ₁ / <i>c</i>
Temperature (K)	110
<i>a</i> , <i>b</i> , <i>c</i> (Å)	14.6505 (3), 4.16813 (9), 14.8815 (3)
∠ (°)	93.2108 (19)
<i>V</i> (Å ³)	907.32 (3)
<i>Z</i>	4
Radiation type	Mo <i>K</i> ∅
∠ (mm ⁻¹)	3.49

Crystal size (mm)	0.31 × 0.30 × 0.25
Data collection	
Diffractometer	SuperNova, Dual, Cu at zero, Atlas
Absorption correction	Gaussian <i>CrysAlis PRO</i> 1.171.39.29c (Rigaku Oxford Diffraction, 2017) Numerical absorption correction based on gaussian integration over a multifaceted crystal model Empirical absorption correction using spherical harmonics, implemented in SCALE3 ABSPACK scaling algorithm.
T_{\min}, T_{\max}	0.422, 1.000
No. of measured, independent and observed [$I > 2\sigma(I)$] reflections	17669, 2073, 1979
R_{int}	0.041
$(\sin \theta/\lambda)_{\text{max}}$ (\AA^{-1})	0.650
Refinement	
$R[F^2 > 2\sigma(F^2)], wR(F^2), S$	0.015, 0.035, 1.08
No. of reflections	2073
No. of parameters	120
H-atom treatment	H-atom parameters constrained
$\rho_{\text{max}}, \rho_{\text{min}}$ (e \AA^{-3})	0.36, -0.36

Number	Atom1	Atom2	Cyclicity	Length	SybylType
1	C7	C6	acyclic	1.469(2)	un
2	C7	N4	cyclic	1.335(2)	un
3	C7	N1	cyclic	1.356(2)	un
4	C5	H5	acyclic	0.95	1
5	C5	C6	cyclic	1.404(3)	un
6	C5	C4	cyclic	1.379(3)	un
7	C8	H8A	acyclic	0.98	1
8	C8	H8B	acyclic	0.98	1
9	C8	H8C	acyclic	0.98	1
10	C8	N3	acyclic	1.457(2)	1
11	C1	C6	cyclic	1.397(3)	1

12	C1	C2	cyclic	1.397(3)	1
13	C1	I1	acyclic	2.098(2)	1
14	C3	H3	acyclic	0.95	1
15	C3	C4	cyclic	1.388(3)	un
16	C3	C2	cyclic	1.386(3)	un
17	C4	H4	acyclic	0.95	1
18	C2	H2	acyclic	0.95	1
19	N2	N3	cyclic	1.317(2)	1
20	N2	N1	cyclic	1.319(2)	un
21	N4	N3	cyclic	1.333(2)	1



Crystal Morphology



Experimental Report

	xs2236a
Crystal data	
Chemical formula	$C_8H_8IN_4O \cdot C_7H_7O_3S$
M_r	474.27
Crystal system, space group	Triclinic, $P-1$
Temperature (K)	110
a, b, c (Å)	8.25785 (19), 8.8309 (2), 11.9974 (3)
α, β, γ (°)	93.3151 (18), 97.4706 (18), 99.6468 (19)
V (Å ³)	852.37 (4)
Z	2
Radiation type	Mo $K\alpha$

λ (mm ⁻¹)	2.03
Crystal size (mm)	0.35 × 0.24 × 0.18
Data collection	
Diffractometer	SuperNova, Dual, Cu at zero, Atlas
Absorption correction	Gaussian <i>CrysAlis PRO</i> 1.171.39.29c (Rigaku Oxford Diffraction, 2017) Numerical absorption correction based on gaussian integration over a multifaceted crystal model Empirical absorption correction using spherical harmonics, implemented in SCALE3 ABSPACK scaling algorithm.
T_{\min}, T_{\max}	0.420, 1.000
No. of measured, independent and observed [$I > 2\sigma(I)$] reflections	23573, 3926, 3745
R_{int}	0.030
$(\sin \theta/\lambda)_{\text{max}}$ (Å ⁻¹)	0.650
Refinement	
$R[F^2 > 2\sigma(F^2)]$, $wR(F^2)$, S	0.016, 0.038, 1.05
No. of reflections	3926
No. of parameters	231
No. of restraints	1
H-atom treatment	H atoms treated by a mixture of independent and constrained refinement
ρ_{max} , ρ_{min} (e Å ⁻³)	0.47, -0.38

Number	Atom1	Atom2	Cyclicity	Length	SybylType
1	C1	C2	cyclic	1.381(3)	1
2	C1	C6	cyclic	1.399(2)	1
3	C1	I1	cyclic	2.121(2)	1
4	C2	H2	acyclic	0.95	1
5	C2	C3	cyclic	1.390(2)	un
6	C3	H3	acyclic	0.95	1
7	C3	C4	cyclic	1.388(3)	un
8	C4	H4	acyclic	0.95	1

9	C4	C5	cyclic	1.376(3)	un
10	C5	H5	acyclic	0.95	1
11	C5	C6	cyclic	1.396(2)	un
12	C6	C7	cyclic	1.452(3)	un
13	C7	N1	cyclic	1.332(2)	un
14	C7	N4	cyclic	1.347(2)	1
15	C8	H8A	acyclic	0.98	1
16	C8	H8B	acyclic	0.98	1
17	C8	H8C	acyclic	0.98	1
18	C8	N2	acyclic	1.462(2)	1
19	N1	N2	cyclic	1.337(2)	1
20	N2	N3	cyclic	1.317(2)	1
21	N3	N4	cyclic	1.320(2)	1
22	N4	I1	cyclic	2.477(1)	1
23	O1	H1O	acyclic	0.84(2)	1
24	O1	I1	acyclic	1.945(1)	1
25	C9	H9A	acyclic	0.98	1
26	C9	H9B	acyclic	0.98	1
27	C9	H9C	acyclic	0.98	1
28	C9	C10	acyclic	1.507(3)	1
29	C10	C11	cyclic	1.385(3)	un
30	C10	C15	cyclic	1.399(3)	un
31	C11	H11	acyclic	0.95	1
32	C11	C12	cyclic	1.389(3)	un
33	C12	H12	acyclic	0.95	1
34	C12	C13	cyclic	1.383(2)	1
35	C13	C14	cyclic	1.390(3)	1
36	C13	S1	acyclic	1.773(2)	1
37	C14	H14	acyclic	0.95	1
38	C14	C15	cyclic	1.386(2)	un
39	C15	H15	acyclic	0.95	1
40	S1	O2	acyclic	1.443(1)	un
41	S1	O3	acyclic	1.485(1)	un
42	S1	O4	acyclic	1.448(1)	un